Raw Material Encapsulating Microsphere-Based Scaffolds For Osteochondral Regeneration

By

Vineet Gupta

B.Sc. (Honors School), Biophysics, Panjab University, India, 2009

Submitted to the Bioengineering program
and the Graduate Faculty of the University of Kansas
in partial fulfillment of the degree requirements for the degree of
Doctor of Philosophy

Committee Members:

Dr. Michael Detamore, Committee Chair

Dr. Cory Berkland

Dr. Vincent Key

Dr. Neethu Mohan

Dr. Prasad Kulkarni

Dr. Laird Forrest

December 10, 2015
Date Defended

The Dissertation Committee for Vineet Gupta certifies that this is the approved version of the following dissertation:

Raw Material Encapsulating Microsphere-Based Scaffolds For Osteochondral Regeneration

Committee Chair

Dr. Michael Detamore, Committee Chair

December 10, 2015

Date Approved

ABSTRACT

The current thesis describes the evaluation of a microsphere-based scaffold that may be used as an early intervention therapy for treating focal cartilage and bone-cartilage interface defects. This scaffold is comprised of extracellular matrix materials, which serve as 'raw materials,' encapsulated in a biodegradable polymer for differentiation of progenitor or resident cells into bone and cartilage. The work in the thesis initially evaluated the *in vitro* performance of raw material encapsulating microsphere-based scaffolds fabricated using a high molecular weight polymer as a first step to establish their clinical efficacy. Subsequently, concentrations of raw materials were increased in microsphere-based scaffolds to stimulate *in vitro* osteogenesis and chondrogenesis in stem cells. Lastly, a novel combination of raw materials, demineralized bone matrix (DBM) and decellularized cartilage (DCC), encapsulated in a continuously graded scaffold design was tested for *in vivo* regeneration potential in a rabbit model. Results from the body of *in vitro* studies suggested that raw material encapsulation in microsphere-based scaffolds can potentially facilitate neo-tissue synthesis. The encapsulated raw materials readily enhanced biochemical production, stimulated gene expression, and tissue synthesis. Additionally, biochemical and gene expression evidence highlighted the benefits of using gradient-based strategies for regenerating bone and cartilage. The *in vivo* study demonstrated the feasibility and applicability of DBM and DCC gradient microsphere-based scaffolds in the New Zealand White rabbit knee defect. The results of the study indicated toward some benefits of using DCC and DBM and emphasized on the need to further refine the technology. The important next steps would be to investigate polymer degradation rate and its effect on tissue regeneration, and further attune raw material concentrations to augment osteochondral regeneration. Ultimately, this thesis demonstrated the benefits of raw material encapsulation in microsphere-based scaffolds, in

addition to opening new areas of investigation with regard to transitioning this technology for clinical use.

ACKNOWLEDGMENTS

I gratefully acknowledge the funding from National Institutes of Health (NIH R01 AR056347), the Kansas Bioscience Authority Rising Star Award, and the University of Kansas School of Engineering. I would also like to acknowledge Drs. Michael Detamore, Cory Berkland, Vincent Key, Neethu Mohan, Prasad Kulkarni, and Laird Forrest for serving on my dissertation committee and for providing valuable guidance with regard to development of this thesis and my scientific research. I would also like to acknowledge those who have provided guidance and assistance toward this dissertation project over the years: Dr. Prem Thapa for training and assistance with SEM and EDS, Alan Walker for assistance in developing custom stage for indentation testing, Dr. Gerard Ateshian for guidance in the analysis of compression indentation data and assistance with FEBio software, Michael Ponticiello for supplying with human demineralized bone matrix, Dr. Qiang Ye for providing access to, and data acquisition from a μCT and DSC facility, and Dr. Richard Galbraith for insightful training on histological techniques. I would like to thank Drs., Joshua Bunch, Donna Pacicca, Jeremiah Easley, Ross Palmer, and Vincent Key for their collaborative efforts during *in vivo* studies. A special recognition goes out to the past and current staff at University of Kansas Animal Care facility, including Heidi Lewis and Allison Tajchman and Drs. William Hill and Keith Anderson for assisting with animal surgeries.

Many thanks to the several undergraduate students who made my graduate experience more exciting and rewarding: Dina Lyne, Kevin Tenny, Towne Walston, Clinton Herman, Gelareh Samandi, and Shawn Briley. Additionally, I would like to give a special thank you to Marilyn Barragan, Amy Laflin, and Taylor Zabel for their many hours of help as I completed the last portions of my research. I acknowledge current and former graduate students and post-

doctorate fellows in the KU Biomaterials and Tissue Engineering lab for their support in tackling challenging research problems and assisting with continual lab maintenance. I would like to recognize Drs. Nathan Dormer, Neethu Mohan, and Emily Beck for their tenacious work ethic and extraordinary patience in training me on all the techniques in the lab, and Dr. Milind Singh for his scientific insight while answering my research related queries. A special thank you to Peggy Keefe for being an exceptionally skillful and caring laboratory manager. I also thank my industry mentors, Maria Flynn, Drs. Cory Berkland and Nathan Dormer at Orbis Biosciences Inc. for broadening my scientific experience.

I will forever be indebted to my advisor, Michael Detamore, for his continuous support, encouragement and guidance over the course of my graduate studies. His advice in professional and personal matters has been instrumental in shaping my scientific career. He is undeniably an exceptional mentor and continues to make significant contributions in the lives of many young researchers. I would also like to acknowledge the faculty and staff of Bioengineering Graduate Program for giving me the opportunity to pursue my passion in biomaterials, tissue engineering, and regenerative medicine.

Lastly, I want to thank my parents, Rakesh and Usha, for their unconditional love and support that has made me the person I am today. I thank my elder brother, Vivek, for endowing me with the inspiration to achieve my dreams. I am also thankful to my sister-in-law, Ruchi, my niece, Ruvishka, and my extended family. Finally, I thank my girlfriend, Kawaljit, for giving me the motivation and a reason to look forward to the future.

TABLE OF CONTENTS

LIST OF FIGURES

CHAPTER 1
No Figures

CHAPTER 2

CHAPTER 3

CHAPTER 4

CHAPTER 5

CHAPTER 6

CHAPTER 7
No Figures

LIST OF TABLES

CHAPTER 1: INTRODUCTION TO THESIS

The overall goal of this thesis is to evaluate a novel microsphere-based scaffold consisting of extracellular matrix (ECM) components encapsulated in a biodegradable polymer that can be used to treat small cartilage and bone-cartilage defects. The ECM materials were selected to serve as 'raw materials,' providing both bioactive signals and building blocks, thus enhancing the differentiation of surrounding progenitor cells toward bone- and cartilage-like cells. The overall progression was to first investigate *in vitro* response of encapsulating ECM materials (or raw materials) in clinically relevant microsphere-based scaffold systems, refine concentrations of raw materials for *in vitro* osteogenesis and chondrogenesis, and finally to evaluate preliminary *in vivo* performance of a gradient microsphere-based scaffold consisting of a unique combination of raw materials. Therefore, this thesis included three specific aims: (1) evaluate *in vitro* potential of gradients of raw materials in microsphere-based scaffolds of relevance to large animal models or human patients, (2) refine composition of raw materials for stimulating *in vitro* osteogenesis and chondrogenesis in homogenous microsphere-based scaffolds, and (3) assess the *in vivo* performance of a novel microsphere-based gradient scaffold incorporating opposing gradients of raw materials.

The first aim evaluated the *in vitro* potential of two raw materials, chondroitin sulfate (CS) and β-tricalcium phosphate (β-TCP), encapsulated in microsphere-based scaffolds comprised of high molecular weight poly(D,L-lactic acid-co-glycolic acid) (PLGA). The second aim was divided into two parts, with the goal being to identify raw material combinations for future iterations of continuously graded microsphere-based scaffold design. The first part of the second aim investigated the use of calcium phosphate mixtures of β-tricalcium phosphate (β-TCP) and hydroxyapatite (HAp) to enhance osteogenesis *in vitro*. The second part compared the

use of DCC and CS in driving chondrogenesis *in vitro*. The third and final aim evaluated the *in vivo* efficacy of a novel microsphere-based scaffold consisting of opposing gradients of decellularized cartilage (DCC) and demineralized bone matrix (DBM) in rabbit osteochondral knee defects. The subsequent chapters reflect the chronological progression of these aims, which provided valuable information that guided the direction of subsequent phases of the work. The organization of these chapters is as follows:

Chapter 2 provides a historical context on microsphere-based scaffolds for tissue engineering and regenerative medicine, highlights the different methods for microsphere fabrication and sintering, and discusses how these methods influence the microsphere and overall scaffold properties. This chapter emphasizes the versatility of the microsphere-based scaffolds regarding fabrication materials, encapsulated factors, and abilities to provide physicochemical gradients and shape-specific grafts, with the goal of enticing the researchers across the regenerative medicine field toward microsphere-based scaffolds. Chapter 2 thus lays the foundation for this thesis, and provides the motivation for developing a clinically relevant biomimetic scaffold for treating focal cartilage and bone-cartilage defects.

Chapter 3 addresses the first aim of investigating whether the encapsulated raw materials (CS and TCP) in high molecular weight PLGA scaffolds can provide building blocks and facilitate differentiation of the seeded cells simultaneously in the direction of bone- and cartilage-like cells. The outcome analyses included morphological analysis, osteogenic and chondrogenic gene expression, biochemical output, and mechanical properties of constructs cultured with rat bone marrow stromal cells (rBMSCs). The findings of this chapter provided validation for the use of raw materials in microsphere-based scaffolds.

Chapter 4 addresses the first part of the second aim by employing TCP and HAp mixtures to stimulate osteogenesis in homogenous microsphere-based scaffolds. Mechanical, biochemical output, gene expression, and histological data evaluated as a function of scaffolds with 30 wt% TCP and HAp encapsulated in two different ratios (7:3 and 1:1, TCP:HAp), seeded with rBMSCs. The results of this chapter yielded vital information on how to use TCP/HAp combinations in future iterations of gradient microsphere-based scaffolds.

Chapter 5 addresses the second part of the second aim i.e., comparing CS and DCC for influencing chondrogenesis in microsphere-based scaffolds. Homogenous microsphere-based scaffolds were fabricated either encapsulating CS or DCC at a concentration of 30 wt%. Biochemical content, gene expression, and histological results of engineered constructs suggested that incorporation of CS and DCC could enhance cellularity and have a modulatory effect on seeded rBMSCs thus, highlighting the benefits of employing ECM materials for driving chondrogenesis in microsphere-based scaffolds.

Chapter 6 further addresses the third aim by evaluating the *in vivo* regeneration potential of a microsphere-based scaffold incorporating of opposing gradients of decellularized cartilage (DCC) and demineralized bone matrix (DBM). Scaffolds were implanted into the medial femoral condyles of New Zealand White rabbits. After sacrificing the animals at 12 weeks, gross morphological, mechanical, and histological analyses were performed to evaluate bone and cartilage tissue regeneration. The results of this study provided an insight into parameters that can have profound implications during subsequent *in vitro* and *in vivo* experiments.

Chapter 7 serves as the conclusion for this thesis. It summarizes key internal findings from a global perspective, and provides recommendations with regard to future generations of

experiments, which attempt to address the limitations of the physicochemical microsphere-based scaffold design.

Altogether, the work conducted in this thesis proposed a translational and clinically relevant solution for treating focal cartilage (chondral) and bone/cartilage (osteochondral) defects that can be implanted in a single surgery, which avoids a three-stage approach for autologous chondrocyte graft harvest, cell isolation and culture, and reimplantation, or the two-incision approach of mosaicplasty with osteochondral plug harvest site morbidity. Other treatments available are products such as Arthrex's Biocartilage® and Cartiform® that are composed of living, human chondral or osteochondral tissue. These treatments not only require viable donated tissues, of which availability of donors is a concern, but they still lack the ability to regenerate fully functional tissue. Therefore, using biodegradable polymers combined with ECM materials that can act as raw materials for the regenerating tissue is an attractive solution. The work within this thesis not only highlights the benefits in efficacy of using raw materials alone, but also imparts tremendous clinical significance to microsphere-based scaffolds, as scaffolds that do not include growth factors may be strategically positioned for a more streamlined regulatory approval. Moreover, avoidance of high cost associated with the growth factors will translate into higher profit margins for investors; thus furthering the prospects of the raw material microsphere-based scaffolds for translation to the clinic.

CHAPTER 2: MICROSPHERE-BASED SCAFFOLDS IN TISSUE ENGINEERING AND REGENERATIVE MEDICINE†

ABSTRACT

Microspheres have long been used in drug delivery applications because of their controlled release capabilities. Recently, they have started to gain attention for fabricating tissue-engineering scaffolds because of their other structural attributes like rigidity in shape, ability to provide porous network, and uniform mechanical properties. Moreover, they offer versatility in terms of methods for fabrication and sintering thus, further warranting their use as scaffolds for regenerating tissues. Furthermore, the microspheres can provide physicochemical gradients via spatio-temporal release of bioactive factors and nano-phase ceramics thereby making them suitable candidates for engineering complex tissues and biological interfaces. Lastly, these microspheres can be injected through most clinical needles and can be assembled into intricate geometries to treat irregular- and complex-shaped defects. Hence, these microspheres have the ability to provide patient-specific biological grafts for clinical utilities. Therefore, it is essential to study the factors that affect the properties of the microspheres and microsphere-based scaffolds. This review describes various methods for microsphere fabrication and sintering, and discusses how these methods influence the microsphere and scaffold properties. Furthermore, key applications of the microspheres and microsphere scaffolds in regenerating different tissue types will also be reviewed. By summarizing the methods for microsphere fabrication and

† To be submitted as **Gupta V**, Khan Y, Berkland CJ, Laurencin CT, Detamore MS, Microspheres As Scaffolds In Tissue Engineering And Regenerative Medicine, *Annual Review of Biomedical Engineering*, 2015

sintering and highlighting their use in tissue engineering, our goal is to inspire researchers to use microspheres as tissue engineering scaffolds so that their full potential could be realized.

INTRODUCTION

In the last few decades, the field of tissue engineering and regenerative medicine has come into limelight because of its ability to provide patient specific biological substitutes overcoming limitations, like donor shortage and graft rejection, posed by conventional methods for treating damaged tissue or organs. The main tissue engineering approach involves transplantation of cells onto engineered matrices, called scaffolds. These scaffolds provide a temporal and spatial environment for cellular in-growth and are also capable of supporting the regenerating tissue. An ideal scaffold: (a) provides a three-dimensional architecture with a desired volume, shape, and mechanical strength, (b) has a highly porous and well interconnected open pore structure to allow high cell seeding density and tissue in-growth (c) possesses chemical compositions such that its degradation products are biocompatible causing minimal immune or inflammatory response, and (d) its degradation rate is tuned in a pattern that it provides sufficient support until the full re-growth of impaired tissues has occurred.[43] Many scaffold fabrication techniques such as solvent casting, particulate leaching, phase separation, electrospinning, fiber mesh, fiber bonding, etc. are employed for tissue engineering applications[192, 221] but recently microsphere-based scaffold fabrication techniques have gained importance because these scaffolds provide excellent initial mechanical properties and also allow for controlled release of bioactive molecules to promote tissue regeneration.[206]

Microspheres (aka microparticles) are organic or inorganic spherical free flowing particles of size range 1-1000 mm with drugs or bioactive molecules either entrapped or

encapsulated in them. They have been extensively used in drug delivery/targeting applications because of their ability to enhance the efficacy of the encapsulated drug by providing a large surface area to volume ratio for its release and exerting a spatial and temporal control over its release.

Besides their ability to serve as excellent controlled release vehicles, these microspheres are rigid in shape and can be packed together alone or in combination with other materials to yield porous three-dimensional structures that can serve as tissue engineering scaffolds. The microsphere-based tissue engineering scaffolds can broadly be divided into two categories: - *i) microsphere encompassing scaffolds (MESs) and ii) microsphere scaffolds (MSs)*. In MESs, microspheres act either as controlled release/delivery vehicles[15, 20, 31, 33, 48, 52, 95, 100, 104, 109, 111, 112, 119, 129-131, 133, 143-148, 153, 159, 165, 182, 194, 195, 197, 198, 219, 220, 236, 241, 243, 244, 248, 259, 264, 265] or pore generating entities (porogens).[49, 53, 54, 92, 231, 232] As delivery vehicles in scaffolds (Table 2.1), microspheres are used for encapsulating peptides/proteins[15, 20, 31, 33, 48, 52, 100, 104, 109, 111, 129-131, 143-148, 159, 182, 194, 195, 198, 220, 236, 241, 243, 244, 248, 259, 264], hormones or antimicrobials[119, 153, 165, 219] and nucleotides[95, 112, 133, 197] to direct fate of the transplanted (or seeded) cells. It has been shown that the release profile of encapsulated bioactive molecules from the microspheres depends on the properties of scaffolding materials as well as on the properties of the microspheres themselves[52, 265]. Moreover, the release profile from these microspheres exhibits a three-stage profile: an initial burst period, a lag period and an increased release period afterwards. During the initial phases, the release profile is primarily governed by diffusion from within the microsphere matrix and afterwards by degradation of the microsphere materials[264]. Additionally, it has been shown that the biological activity of the encapsulated molecule is not significantly altered during the microencapsulation process[130]. Furthermore, multiple bioactive molecules have been released

simultaneously from MESs via the use of different microsphere systems. The loading and release profiles from these multiple systems were distinct and depend on the nature of the carrier matrices used and also on the microencapsulation process[244]. Another way of incorporating microspheres into MESs for controlled release is to apply them as surface coatings[78, 265]. Francis *et al.* (Table 2.1) developed a multi-functional Bioglass-based ceramic scaffold for bone tissue engineering that could deliver an antimicrobial, gentamycin, via the immobilization of gentamycin encapsulating poly(3-hydroxybutyrate) microspheres on the scaffold surface[78].

Microspheres in MESs also serve to act as porogens, generating a network of pores into the interior of a scaffold that would facilitate cellular in-growth and transportation of nutrients and wastes in and out of the scaffold. Certain scaffold fabrication techniques like solvent casting, phase separation, rapid prototyping, etc. are limited in their ability to create pores within the scaffold; therefore, microspheres are incorporated into such scaffolds to create macro- or micro-sized pores. Dellinger *et al.*[53, 54] incorporated polymethylmethacrylate (PMMA) microspheres into hydroxyapatite (HA) scaffolds, which burnt out during subsequent calcination process thus, creating macro- and micro-sized pores in the scaffolds. Using microspheres as porogens an ordered, uniform and interconnected network of pores could be created within the scaffolds with porosity values as high as 95%[231, 232]. Moreover, generated pores influence the physical and mechanical properties of the scaffolds that could in turn affect the cell growth kinetics within a scaffold[92].

Microsphere encompassing scaffolds possess some inherent advantages over scaffolds fabricated via conventional techniques in the sense that they allow control over the release of the encapsulated molecules and structural properties (porosity and mechanical) of the fabricated scaffold. However, they also suffer from some limitations. Fabrication of a MES is a multi-step

tedious process involving creation of a scaffold matrix, microspheres, and then combining them into a single structure. Moreover, the matrix and microspheres are usually fabricated from different materials leading to difference in mechanical properties at the microsphere-matrix interface that in turn may cause undesirable results. Therefore, to overcome problems associated with MESs, microspheres are themselves used as building blocks for fabricating scaffolds. Such scaffolds known as microsphere scaffolds (MSs) are advantageous in terms that they possess uniform mechanical properties, provide porous network, allow for controlled release or surface modifications via bioactive factors, can be assembled into different shapes, and can also be injected via small incisions in minimally invasive surgeries. The MSs can further be classified as sintered microsphere scaffolds (SMSs) and injectable microsphere scaffolds (IMSs). In SMSs, microspheres are sintered or bonded together to form a three-dimensional structure whereas in IMSs the microspheres are not sintered and only act as cell growth substrates or cell/cell-matrix carriers.

Borden *et al.*[25] first reported the use of MSs (SMSs) in 2002 for bone tissue engineering applications. Since then, a lot of research groups have started employing MSs for regenerating a variety of tissues and rapid progress has been made in the field of MSs especially in the past 5-6 years (Figure 2.1). In a review, Shi *et al.* discussed the use of SMSs fabricated via heat and solvent sintering for drug delivery and tissue engineering applications [206]. Huang *et al.* in an another review examined the use of these scaffolds in bone tissue engineering applications where they discussed different material approaches being applied to fabricate such scaffolds[101].

The objective of this review is to recapitulate the use of the microsphere scaffolds (MSs) in the tissue-engineering field with emphasis on the methods and materials used for microsphere fabrication and sintering. Moreover, the influence of these parameters on scaffold properties will

also be discussed. Lastly, the use of MSs in regenerating different tissue types will be reviewed and some key emerging applications will also be highlighted.

MICROSPHERE FABRICATION METHODS

Microspheres are fabricated via a variety of methods (Figure 2.2) for use in MSs. The type of method used for microsphere fabrication greatly influences their properties. Therefore, the following section describes the different methods used for microsphere fabrication and how they affect their size and morphology.

EMULSION BASED METHODS

The emulsion-based methods (Figures 2.3 – 2.7) are the most commonly and widely used methods for microsphere fabrication (Table 2.2) as they are relatively less time consuming, don't require complex apparatus and can be applied to multiple systems[4, 11, 14, 25, 26, 29, 39, 41, 42, 44, 46, 47, 51, 69, 70, 82, 90, 91, 94, 99, 100, 105-109, 112, 115-118, 121-125, 135, 137, 138, 140, 149-151, 158, 160, 168, 178-180, 183, 184, 186, 187, 190, 200, 208, 210, 228, 233, 239, 242, 246, 247, 255, 257, 260-263]. These methods can broadly be divided into a) emulsion solvent evaporation, b) emulsion gas foaming, c) emulsion microgel fabrication, and d) cryogenic double emulsion methods.

EMULSION SOLVENT EVAPORATION

Microsphere fabrication by emulsion solvent evaporation/extraction (ESE) consists of four major steps (Figures 2.3 & 2.4): - (A) dissolution or dispersion of the bioactive compound often in an organic solvent containing the microsphere matrix (usually a polymer); (B) emulsification of this organic phase in a second continuous (frequently aqueous) phase immiscible with the first one;

(C) extraction of the solvent from the dispersed phase by the continuous phase, which is optionally accompanied by solvent evaporation, either one transforming the droplets into solid microspheres; (D) harvesting and drying of the microspheres[79]. Based on the number of emulsions used in the fabrication, the ESE method can be classified either as a) a single emulsion solvent evaporation (SESE) or b) a double emulsion solvent evaporation (DESE). In SESE, the microsphere matrix (containing either dissolved or dispersed bioactive molecule) is emulsified into the aqueous phase followed by microsphere hardening through solvent evaporation and polymer precipitation (Figure 2.3). On the other hand, in DESE an aqueous solution of the bioactive compound is first dispersed in the matrix solution forming primary emulsion, which is then further emulsified to form secondary emulsion followed by microsphere hardening (Figure 2.4).

Microspheres with smooth, rough and porous surface morphologies can be fabricated via ESE methods. Smooth morphology is obtained when a homogenous organic phase is emulsified into the aqueous phase during microsphere fabrication. Jiang *et al.* fabricated smooth poly(lactic acid-glycolic acid) (PLAGA) microspheres using a SESE method. However, they observed that addition of chitosan to the PLAGA organic phase led to formation of microspheres with a rough morphology, which was due to the presence of chitosan particles on the microsphere surface. During solvent evaporation and microsphere hardening, only a small amount of loaded chitosan particles got incorporated into the interior of the microspheres because of chitosan's tendency to disperse in water and partition onto the microsphere surface thereby imparting a rough appearance[115]. Moreover, addition of inorganic minerals such as hydroxyapatite or titanium dioxide[107, 160, 246] also led to fabrication of rough microspheres. Microspheres with minute pores on their surface could be fabricated when an aqueous inner phase was first dispersed in the

organic phase during microsphere fabrication. The pores form due to water leaching from the inner aqueous phase amid microsphere hardening via solvent evaporation. Additionally, pores could also be generated with the use of a porogen in microsphere matrix material. Hong *et al.*[94] prepared novel microspheres of polycaprolactone (PCL) with a porous surface by introducing camphene as a porogen in the organic phase. PCL and camphene were first dissolved in the co-solvent chloroform. In the course of solidification, camphene and PCL phases separated to form an interconnected structure. Since camphene sublimes (below 40^0C) easily, the camphene part disappeared leaving a porous structure within the PCL microspheres. Microsphere morphology and porosity are also influenced by rate and conditions of drying process used to obtain a free-flowing powder as it is responsible for removal of the continuous phase, wash fluid adhering to the microspheres' surface, and traces of solvents and continuous phase from the interior of the microparticles.

In emulsion solvent extraction methods the factors that influence the size of the fabricated microspheres include: - (a) matrix/polymer concentration in the organic phase, (b) concentration of the stabilizer/surface active agent used, (c) shear forces produced either by homogenizer, sonicator or whirl mixer during the emulsification step and lastly, (d) rate of solvent evaporation during microsphere hardening. Increasing the viscosity of the bioactive molecule/matrix dispersion increases the diameter of the microspheres, as higher shear forces are needed to break the dispersed phase into droplets. Such increase in the dispersion viscosity, typically caused by higher concentration or molecular weight of the matrix material, may be desirable to improve the encapsulation of the bioactive molecule. To prevent coalescence of the bioactive molecule/matrix dispersion droplets, a surface-active or viscosity-enhancing stabilizer such as polyvinyl alcohol (PVA) is generally added to the continuous phase and it has been

observed that increasing the stabilizer concentration frequently leads to decrease in size of the fabricated microspheres. Higher stabilizer concentrations yield an excess of material that adsorbs on the surface of newly formed droplets, thus preventing coalescence. Moreover, with increase in concentration of stabilizers, the viscosity of the continuous phase also increases, amplifying (for a given stirring rate) the shear forces acting upon the bioactive molecule/matrix dispersion droplets and thus minimizing their size. Furthermore, it is observed that increasing the shear forces by increasing the mixing speed generally also results in decreased microsphere mean size as it produces smaller emulsion droplets through stronger shear forces and increased turbulence. In addition to a smaller mean diameter, more rapid mixing also resulted in lower microsphere polydispersity. The ideal rate of solvent evaporation depends on a variety of factors like the type of matrix material, encapsulated bioactive molecule and solvent as well on the desired release profile of the microspheres. Increasing the temperature can lead to higher solvent evaporation rates thus producing larger microspheres because of rapid microsphere solidification with insufficient mixing time to reduce droplet size. As an alternative to elevated temperatures, reduced pressure also has a similar effect on the size of the microspheres[79]. The parameters affecting the microsphere size in ESE methods offer limited control over the microsphere size; therefore fabricated microspheres are largely polydisperse. In other words, microspheres fabricated via ESE methods have varied sizes that could be undesirable in certain tissue engineering applications where a tight control over microsphere size is required.

EMULSION GAS FOAMING

The emulsion gas foaming method (Figure 2.5) is similar to the DESE method with the exception that an effervescent salt is dissolved in the organic phase. The dissolved salt acts as a gas

foaming agent, generating gas bubbles when the primary emulsion contacts the secondary aqueous phase, thereby creating open porous morphology within the microspheres [41, 42, 122, 123, 136, 168, 257]. Kim *et al.*[136] fabricated porous poly(lactic-co-glycolic acid) (PLGA) microspheres using ammonium bicarbonate in the inner aqueous phase as the gas foaming agent. An aqueous solution containing ammonium bicarbonate was homogenized into an organic phase of PLGA-dissolved methylene chloride. The primary emulsion solution was re-emulsified into an aqueous solution of PVA for a double emulsion and subsequent solvent evaporation. The inner aqueous phase containing ammonium bicarbonate gradually generated carbon dioxide and ammonia gas, blowing up their droplet volumes within the embryonic PLGA microspheres during the solvent removal process. As a result, porous microspheres with highly inter-connected, open pore channels were produced. Moreover, the evolved gas bubbles also stabilized the primary emulsion droplets against coalescence during solvent evaporation. Furthermore, it was observed that increasing amount of ammonium bicarbonate not only led to a more porous structure but also increased the diameter of the microspheres themselves. This was due to internal gas foaming effect that expanded the dimension of gas evolving primary aqueous droplets in the solidifying polymer phase. The generation of gas within the primary aqueous droplets caused the surrounding solidifying PLGA phase to enlarge its original volume during solvent evaporation in the second emulsification step.

EMULSION MICROGEL FABRICATION

Emulsion microgel fabrication involves production of micron or sub-micron sized gel spheres (microgels) using hydrophilic materials via ionic crosslinking[14], chemical crosslinking[90, 100, 247, 262] and co-precipitation[39, 179] in an emulsion (Figure 2.6). Barrias *et al.* fabricated alginate

microgels encapsulating calcium titanium phosphate (CTP) to drive the osteogenic differentiation of human osteoblastic cells. CTP was first mixed at a ratio of 0.4 with 2% w/v sodium alginate aqueous solution and homogenized to form a paste. Afterwards, this CTP-alginate paste was extruded drop-wise into a 0.1*M* $CaCl_2$ crosslinking solution, in which spherical-shaped particles instantaneously formed. The size of the microspheres was controlled by regulating the extrusion flow rate using a syringe pump and also by applying a coaxial air stream. At completion of the gelling period, microspheres were recovered, dried and heated at 1100°C for 1 h to burn off the polymer causing the CTP granules to become associated. It was observed that the CTP microspheres retained their spherical morphology and possessed a rough surface[14]. In an another type of gelation method, Zhu *et al.*, Habraken *et al.*, Watanabe *et al.*, and Huang *et al.* fabricated gelatin microgels using a water-in-oil emulsion process followed by chemical (glutaraldehyde) crosslinking[90, 100, 247, 262]. They noticed that the swelling ratio (ratio between wet and dry volumes) of microgels was influenced by the concentration of the crosslinker used however; it did not affect their size. Lastly, Chesnutt *et al.* and Nguyen *et al.* produced composite microgels from chitosan and hydroxyapatite (HA) by employing a co-precipitation gelation method. Deacetylated chitosan powder was first dissolved in 2 wt % acetic acid and then ten milliliter of 1M $CaCl_2$ in 2% acetic acid and 6 mL of 1M NaH_2PO_4 in 2% acetic acid was added to the chitosan solution. The final solution was then extruded through a syringe fitted with a needle and placed on a syringe pump into a precipitation solution consisting of 20% sodium hydroxide, 30% methanol, and 50% water (pH=13). The precipitation solution caused the chitosan drops to precipitate into solid beads that were left in the basic solution to allow crystalline HA to develop from unstable brushite and amorphous calcium phosphate. Finally, the fabricated beads were washed with DI water until they reached a neutral pH of 7.0–

7.5. Scanning electron microscopy (SEM) revealed that the fabricated beads were approximately spherical with a textured surface, which could be attributed to the presence of nano-scale calcium phosphate particles on the surface of the microspheres.

The emulsion microgel fabrication method differs from other emulsion-based methods in the aspect that it involves the use of hydrophilic materials as microsphere matrices whereas the other methods primarily use relatively hydrophobic materials as matrices. However, it is similar to them in the fact that the size of the microspheres is majorly controlled by the emulsion parameters as observed in the other emulsion-based methods as well.

CRYOGENIC DOUBLE EMULSION

Cryogenic double emulsion or cryopreparation is a method commonly employed for preparing DNA or nucleotide encapsulating microspheres[5, 112]. The use of conventional DESE method to encapsulate DNA causes it to lose its native supercoiled state thus, resulting in loss of its bioactivity. Therefore, cryopreparation was developed as an improvement over the DESE method to encapsulate DNA into the microspheres.

Cryopreparation involves lowering the temperature of the DNA-containing primary emulsion below the freezing point of the aqueous inner phase resulting in a solid particulate suspension prior to homogenization to form the secondary emulsion (Figure 2.7). Homogenization can cause shear stress induced DNA degradation. The shear stress within a solid is zero; therefore, plasmid DNA frozen in the inner phase is exposed to minimum shear stress during homogenization, thus preserving the supercoiled state of the plasmid DNA. Furthermore, cryopreparation also enhances the overall encapsulation efficiency of the plasmid DNA by preventing its diffusion out of the microsphere during homogenization.

Similar to DESE, the size of microspheres fabricated via cryopreparation is governed by parameters such as concentration of the organic phase, stabilizer or surface-active agent, mixing speed and rate of solvent evaporation. Moreover, the morphology of the fabricated microspheres is also similar to those fabricated via DESE. Cryopreparation differs from other emulsion-based methods using temperature as a variable parameter in regard that it involves only selective freezing of the aqueous inner emulsion whereas other methods freeze or gel the entire microsphere.

Emulsion based methods were among the first methods to be used for microsphere fabrication. Although they have evolved a lot in terms of number of systems to which these can be applied yet they are limited in certain aspects. These methods offer minimal control over microsphere size; resulting in low encapsulation efficiency of the encapsulated molecule and also can lead to its denaturation during the encapsulation process. Therefore, to overcome these limitations new methods have been developed that offer better control over microsphere size and lead to high encapsulation efficiencies of encapsulated molecules without the loss of their bioactivity.

THERMALLY INDUCED PHASE SEPARATION (TIPS)

Before being applied to fabricate microspheres, thermally induced phase separation (TIPS) was used for making monoliths for tissue-engineering purposes. In TIPS, a solvent with a low boiling point that easily sublimes is used. Solvent dissolved matrix material (usually a polymer) droplets are either preformed via an emulsion or directly dropped (via a syringe or sprayed through a nozzle) into the cooling solution to generate porous microspheres (Figure 2.8). When the temperature of the polymer solution gets below the freezing point of the solvent, it separates into

a polymer-rich phase and a polymer-lean phase due to crystallization of the solvent. The polymer is expelled from the crystallization front to form a continuous polymer-rich phase and the solvent is sublimed to leave the pores, which are a three-dimensional fingerprint of the geometry of the solvent crystals[21]. The droplet forming parameters control the size of the microspheres fabricated by TIPS whereas the polymer concentration, solvent and the quenching temperature control the microstructure of the pores and walls.

TIPS offers certain advantages over other microsphere fabrication techniques (particularly emulsion based) such as versatility, repeatability, and simplicity. Moreover, it also allows control over pore morphology and porosity within the microspheres. Furthermore, it permits the inclusion of drug and particulates with high encapsulation efficiency, as the encapsulation process is rapid. Additionally, the encapsulated molecules are not exposed to solvent phase for prolonged time thereby preventing their degradation. Lastly, the fabricated microspheres are exposed to an aqueous continuous phase for a short period thus only a small concentration of the encapsulated molecule diffuses out of the microsphere matrix.

PROLEASE

Originally described by Gombotz *et al.*[32], in this process microspheres are produced by first dissolving a polymer/matrix in a solvent together with an active agent that can either be dissolved in the solvent or dispersed in it. The polymer/active agent mixture is then atomized into a vessel containing a liquid non-solvent, alone or frozen and overlaid with a liquefied gas, at a temperature below the freezing point of the polymer/active agent solution. When the combination with the liquefied gas is used, the atomized droplets freeze into microspheres upon contacting the cold liquefied gas, then sink onto the frozen non-solvent layer. The frozen non-

solvent is then thawed. As the non-solvent thaws, the microspheres that are still frozen sink into the liquid non-solvent. The solvent in the microspheres then thaws and is slowly extracted into the non-solvent, resulting in hardened microspheres containing active agent either as a homogeneous mixture of the polymer and the active agent or as a heterogeneous two phase system of discrete zones of polymer and active agent. If a cold solvent is used alone, the atomized droplets freeze upon contacting the solvent, and sink to the bottom of the vessel. As the non-solvent for the polymer is warmed, the solvent in the microspheres thaws and is extracted into the non-solvent, resulting in hardened microspheres (Figure 2.9). Microspheres with different sizes can be made by either using nozzles with different diameters or by changing the viscosity of the polymer solution. An advantage of this method is that it doesn't require the use of surface-active agents, as required in the most other processes for making microspheres that could interfere with release of encapsulated molecule or cause an undesirable reaction. Moreover, it results in minimal loss of the bioactive molecule during encapsulation (high encapsulation efficiency) and also preserves its biological activity.

PRECISION PARTICLE FABRICATION

Precision particle fabrication (PPF) is another method that offers better control on microsphere size as compared to other fabrication methods. In PPF, a solution containing the microsphere matrix, and any other molecule to be encapsulated, is passed through a small nozzle to form a smooth cylindrical jet. A piezoelectric transducer driven by a wave generator at a frequency tuned to match the flow rate and the desired drop size vibrates the nozzle. The mechanical excitation launches a wave of acoustic energy along the liquid jet generating periodic instabilities that, in turn, breaks the liquid jet into a train of uniform droplets. To further control the sphere

size, an annular flow of a non-solvent phase around the matrix jet is employed that is pumped at a linear velocity greater than that of the matrix stream. The frictional contact between the two streams generates an additional downward force that effectively pulls the microsphere solution away from the orifice of the nozzle. The microsphere matrix stream is accelerated by this force and, therefore, thinned to a degree depending on the difference in linear velocities of the two streams. The emanated microspheres are flowed into a beaker containing non-solvent phase with a surfactant to prevent them from coalescing (Figure 2.10). To extract the solvent, incipient microspheres are stirred for 3–4 hours and subsequently, the hardened microspheres are filtered and lyophilized[18, 19, 59, 60, 62, 64, 66, 114, 169, 171, 213, 215, 216].

PPF allows a user to control the microsphere size by varying the process parameters that include: (a) the nozzle diameter, (b) flow rate of matrix material, (c) flow rate of non-solvent phase, (d) frequency, and (e) amplitude of acoustic energy employed. Using PPF, predetermined mono-disperse microspheres can be fabricated within 10-20% range of the set target size. Such a precise control over microsphere size can have critical implications in the field of tissue engineering. The ability to fabricate mono-disperse microspheres can lead to improved systems to explore the effects of microsphere size on microsphere-based scaffolds. Scaffolds made of uniform microspheres can be employed to study the influence of microsphere size on the degradation patterns and rates within scaffolds. In addition, uniform size microspheres can pack closely compared to randomly sized microspheres, providing better control over the pore sizes and porosity of the scaffold, and may considerably aid the mechanical integrity of the scaffolds. Moreover, local release of molecules from the microspheres in a bulk scaffold is related to size of an individual microsphere and its material properties. Reproducibility and predictability associated with uniform microsphere-based scaffolds can make them suitable for a systematic

study of physical and chemical effects in order to achieve control over local release of growth factors within such a scaffold[215].

FLAME SPHEROIDIZATION

Lakhkar *et al.* demonstrated the successful production of titanium phosphate glass microspheres using an inexpensive, efficient and easily scalable process called flame spheroidization. The microsphere fabrication apparatus comprised of: - (a) a blowtorch, (b) feed and (c) collectors (Figure 2.11). The blowtorch assembly consisted of a gas torch fitted to a gas cylinder. The blowtorch assembly was positioned such that the flame of the gas torch was horizontal. The feed assembly comprised of an aluminum trough with the edge of one end positioned ~10 mm above the outlet of torch at a slight angle to the horizontal. A DC motor was attached to the other end of the trough and was connected to a programmable power supply. A metal screw connected to the axle of the motor served as an offset to generate vibration when the motor was in operation so that the particle feed for microsphere production was distributed over the surface of the trough before the particles entered the flame. The collectors consisted of four rectangular glass boxes with their longer edges in contact with each other. The first collector was placed directly below the flame so as to collect particles that did not pass through the flame. During operation, glass microparticles placed at one end of the trough travelled to the other end under the influence of vibratory forces exerted by the DC motor. At the other end, the particles passed into the flame and then travelled along the flame axis. As they passed through the flame, they underwent spheroidization due to surface tension forces and were then collected in the glass boxes placed one after the other below the flame.

Flame temperature and the particle residence time in the flame are the only factors that affect the size of the microspheres in flame spheroidization process[142]. The advantages of the method include that it is: - (a) inexpensive, (b) efficient as the microspheres can be produced very quickly, and (c) easily scalable to make kilograms of microspheres. All of these attributes are highly desirable from the standpoint of developing viable commercial applications.

Summary Of Microsphere Fabrication Methods

In summary, there are merits and demerits associated with each microsphere fabrication method. Emulsion based methods are relatively simple and can be used to fabricate microspheres from a variety of materials however; they yield particles with non-uniform size and broad size distribution. On the other hand, processes like Prolease, PPF and Flame spheroidization can fabricate uniform size with narrow size distribution but they are complex and require special apparatus. Moreover, the processing parameters involved in the microsphere fabrication hugely impact the microspheres' characteristics. Therefore, the choice of method for microsphere fabrication will largely depend on the desired characteristics, composition, and amount of microspheres; on the release profile of the encapsulated protein; and lastly on the intended application of the microspheres.

METHODS OF MICROSPHERE SINTERING

Once fabricated, microspheres can either be used as cell/cell-matrix delivery vehicles (IMSs) or packed and joined to create three-dimensional structures (SMSs), which can provide mechanical support to the regenerating tissue and can also present the surrounding cells with differentiation cues to go down a specific lineage. The injectable scaffolds will be discussed separately along

with the applications of the MSs in regenerating different type of tissues. In this section, various methods used for coupling (aka sintering) microspheres will be described in detail highlighting the effects of sintering process parameters on scaffold properties (porosity, mechanical characteristics, etc.). Furthermore, merits and demerits of each sintering process will also be listed.

HEAT SINTERING

Heat sintering is the most widely used method to sinter microspheres (Table 2.2) for fabricating SMSs[4, 11, 25, 26, 44, 46, 47, 105-108, 115-117, 137, 138, 140, 151, 158, 160, 190, 228, 239, 242, 246, 255]. Briefly, prefabricated dried polymeric microspheres are poured into a mold and heated to a specific temperature above the glass transition temperature (T_g) of the polymeric matrix for several hours resulting in the melting of the surface layer on the microspheres and thus inducing them to bond with their adjacent neighbors forming a three-dimensional porous scaffold (Figure 2.12).

Microspheres are the building blocks of SMSs therefore; their characteristics in turn govern the properties of the fabricated scaffolds irrespective of the method used to fabricate scaffolds. Borden *et al.*[26] fabricated PLAGA microspheres heat sintered scaffolds and observed that decreasing the microsphere size increased the compressive modulus of the sintered scaffolds. This phenomenon was due to the increase in surface area that further increased the number of fusion points between the spheres thereby leading to stronger bonding between the spheres. Moreover, decreasing the size led to smaller pore size but did not affect the overall porosity of the scaffolds. Other than microsphere size, sintering temperature and sintering time are recognized as two crucial factors influencing the mechanical properties and porosities of the heat sintered scaffolds. A higher sintering temperature and a longer sintering time have equivalent

effects on the properties of the scaffolds. In general, a higher sintering temperature results in an elevated compressive modulus and compressive strength, a greater median pore size, and decreased pore volume. This is because elevated sintering temperature results in greater fusion between the microspheres, which contributes to the increase in the compressive properties of the scaffolds. At the same time, greater fusion between microspheres results in possible closure of pores among three or more microspheres in contact, which decreases the overall pore volume of the scaffolds. On the contrary, lower sintering temperature and shorter sintering time induce weaker coalescent bonds among the adjacent microspheres that results in lower capability of SMSs to resist outside forces.

The heat sintering method has several advantages compared to other sintering methods especially solvent-based methods. Heat sintering method is simple and efficient, as it requires moderate temperatures whereas methods like solvent vapor sintering requires an organic solvent and also in some cases high temperatures as well. Moreover, heat sintering offers flexible time constraints (on the order of several minutes) that make fabricating scaffolds with consistent mechanical properties relatively easy. On the other hand, time constraints offered by solvent-based methods are more stringent (on the order of a few seconds). If a scaffold is left for too long during solvent sintering, it could result in significantly reduced porosity of the structure thus, simultaneously compromising the mechanical properties of the scaffold. Lastly, a large number of scaffolds can be fabricated via heat sintering (in an oven) at one particular time whereas methods like solvent sintering requires exposure of the scaffolds to solvent (or its vapors) in a confined space thereby limiting the number of scaffolds that can be sintered at any given time [253]. The biggest drawback of using heat sintering for fabricating SMSs is that it makes encapsulation of bioactive molecules difficult. The sintering temperatures and durations of heat exposure used

in some previous studies were 65^0C for 4 h, 70^0C for 4 h and 62^0C for varied times of 4, 24, 48, and 72 h[215]. Such high temperatures for extended durations may lead to reduction or complete loss in bioactivity of the encapsulated proteins. Furthermore, properties such as T_g, viscosity, crystallinity and surface tension of the polymer, as well as heating conditions (heating temperature and heating time), must be taken into consideration when fabricating SMSs utilizing heat sintering therefore; it is not applicable across a broad spectrum of polymer types due to its dependence on those parameters.

SOLVENT BASED METHODS

Solvent-based sintering strategy is another widely used approach for fabricating SMSs (Table 2.2) because only two factors must be taken into account in solvent based strategies: (i) species of solvent and (ii) sintering time. Solvent-based sintering methods can further be divided into three categories: - (a) solvent vapor sintering [109, 110], (b) poor solvent sintering [39, 59, 60, 62, 64, 66, 169, 171, 179, 208, 213, 215], and (c) solvent/non-solvent sintering [29, 30, 184, 186, 200].

SOLVENT VAPOR SINTERING

In solvent vapor sintering, the scaffold fabrication process relies on diffusion of solvent vapors into the microspheres, which lowers the polymer glass transition temperature, thus softening the microspheres and allowing them to fuse (Figure 2.12). Jaklenec *et al.*[110] fabricated bovine serum albumin (BSA) loaded PLGA SMSs via dichloromethane (DCM) vapor sintering and studied the effects of sintering time and protein loading on the extent of fusion. They observed that the rate-limiting step in scaffold fusion was the saturation of fusion chamber with DCM vapors. Once the chamber reached the saturation vapor pressure for DCM, the further reaction was rather fast.

After 4 min, the microspheres started to fuse together and after 4 min and 30 s the scaffold was over fused, finally turning into a film after 5 min. At that point, the dichloromethane had sufficiently penetrated throughout the entire microsphere matrix reducing the polymer T_g, whereas at earlier time stages only the microsphere surface was affected. Additionally, it was observed that the fusion time increased with scaffold mass. This was because the fusion process was governed by dichloromethane vapor diffusion and added mass generally indicated longer diffusion time. Furthermore, microspheres containing the least amount of BSA fused the most while those with the highest amount of BSA fused the least, showing that when fusion time and mass were held constant, the fusion process was more pronounced for samples with less BSA. This phenomenon was a function of BSA, which acted as reinforcement for the soft microspheres, thus requiring more vapors for fusion.

The biggest advantage of solvent vapor sintered microsphere scaffolds is that growth factors or proteins can be encapsulated and released from these scaffolds in bioactive form. Jaklenec *et al.*[109] showed that both insulin growth factor-I (IGF-I) and transforming growth factor-β_1 (TGF-β_1) were released in bioactive form for up to 70 days from PLGA SMSs sintered via DCM vapors. Moreover, the method allows control over scaffold morphology, composition, spatial distribution, pore size, and protein release kinetics. Changing the process parameters can vary these scaffold attributes. However, it can be argued that presence of residual solvent can potentially have deleterious effects. Furthermore, stringent time constraints and consistency issues add to the limitations of the technique.

POOR SOLVENT SINTERING

With the use of poor solvent sintering technique, bioinductive microsphere scaffolds can be fabricated consisting of growth factor or protein encapsulating microspheres. In this technique, a poor solvent for microsphere matrix is used as the sintering agent. The stacked microspheres are treated with the poor solvent causing T_g of the matrix material to drop, which results in softening of the microspheres near the surface generating a skin layer around them. These skin layers then adjoin resulting in formation of sintering junctions among the adjacent microspheres (Figure 2.12).

Singh *et al.*[215] fabricated PLGA microsphere scaffolds employing poor solvent ethanol for PLGA sintering. They observed that the duration of the ethanol soak was an important process parameter, as longer durations led to increase in the extent of interconnection between the microspheres due to increased thicknesses of the surface film layer formed by the diffusion of ethanol into the microspheres. Moreover, it was observed that increased durations of ethanol exposure led to increased deformation of the microspheres from spherical morphology. In addition to ethanol soak time, polymer properties such as molecular weight and crystallinity also affected the extent of sintering between the microspheres. Furthermore, mechanical test results indicated that the average elastic modulus of scaffolds soaked with ethanol for 60min was significantly higher than the moduli of the scaffolds soaked for 30min and 240min. The observed phenomenon was due to the fact that scaffolds prepared by a 30min soak did not have well-integrated microspheres resulting in poor mechanical properties whereas, the reduction in mechanical integrity for scaffolds sintered for 240min might be because of increased morphological distortion of the microspheres from a spherical shape resulting in a poor packing of the microspheres. On the other hand, changing the ethanol soak time resulted in only slight

variation in the overall porosity of the scaffold. The mean theoretical porosities of scaffolds soaked for 30min, 60min, 120min and 240min were 41.1%, 38.8%, 32.8%, and 40.4%, respectively. The porosity for the 240min group was higher than that for the 60min and 120mi groups; however, no statistically significant differences were noticed among the groups. In addition to affecting the scaffold properties, ethanol treatment was found to affect the polymer properties[215] and the release of the encapsulated proteins[60]. The ethanol treatment during the fabrication of scaffolds resulted in a drop of 14% in Tg of the PLGA when compared to the raw polymer[215]. This was due to the plasticization effect of ethanol on PLGA. Dormer *et al.*[60] noticed considerable differences in protein release from microspheres treated with ethanol. It was observed that the ethanol-treated groups released more proteins from PLGA microspheres because of a pre-solubilization effect of ethanol on the polymer that allowed for diffusion of proteins from the innermost layers of the microspheres towards the perimeter. When placed in release medium, the outermost layers of the microspheres were primed with proteins, hence dumping large quantities of proteins in the first week of release.

In contrast to solvent vapor sintering method, poor solvent sintering employs a relatively milder organic solvent that can be easily removed via subsequent processing methods like freeze-drying thus preventing any deleterious effects caused by the residual solvent. The poor solvent sintering method requires long exposure to the solvent (due to use of a poor solvent) thereby increasing the time required for scaffold fabrication. However, the time required for scaffold fabrication is still comparable (often less) to the time required in heat sintering thus making it a widely used method for microsphere sintering [39, 59, 60, 62, 64, 66, 169, 171, 179, 208, 213, 215].

SOLVENT/NON-SOLVENT SINTERING

Solvent/non-solvent sintering is similar to the poor solvent sintering method except for that it involves the use of a solvent and a non-solvent, which are selected based on the following parameters: the solvent is more volatile (higher vapor pressure at room temperature and pressure) than the non-solvent, the solvent and non-solvent are miscible, and there exists no azeotropes across the range of solvent/non-solvent ratio. The solvent/non-solvent sintering method sinters a range of different polymers based on Flory–Huggins solution theory, which states that a greater affinity between the solvent and polymer will allow the solvent to dissolve progressively longer chains of the polymer. The solvent in the solvent/non-solvent mixture allows polymer chains on the surface of the microspheres to swell and intertwine with each other. The sintering is completed when the more volatile solvent begins to evaporate at a greater rate than the less volatile non-solvent, which decreases the affinity of solvent/non-solvent mixture for the surface chains and causes polymer precipitation resulting in bonding between the microspheres[29].

Parameters such as solvent/non-solvent sintering solution composition and submersion time affect the sintering process. If the solvent concentration becomes too high, dissolution will occur freeing the smaller surface chains and leading to the occlusion of the pores and flattening of the resulting scaffold. The submersion time appears to affect the bonding region only slightly and has a more profound effect on the morphology of the microspheres. Presumably this slight correlation between submersion time and bonding region is caused by quickly reaching a steady state between the solvent/non-solvent sintering solution and the microsphere surface. The long submersion time allows diffusion of the sintering solution throughout the microsphere allowing interior polymer chains to move in relation to each other resulting in a change in the spherical morphology of the microsphere[29].

Brown *et al.*[29] studied the versatility of the solvent/non-solvent sintering process with six different biodegradable polymers and compared it to heat sintering. They observed that the microsphere scaffolds fabricated via solvent/non-solvent sintering exhibited porosities similar to those observed with heat sintered scaffolds and produced average pore diameters that are in the range necessary for *in vitro* cell culture as well as *in vivo* scaffold implantation. The porosities and pore diameters of the poly[bis(ethyl alaninato)phosphazene] (PNEA) and poly[bis(ethyl phenylalaninato) phosphazene] (PNEPhA) scaffolds showed a significant dependence on the solvent/non-solvent sintering solution composition with the overall trend being a decrease in porosity and pore diameter at high solvent compositions. The higher solvent compositions created a greater bonding region, which occluded some of the porosity while decreasing the diameter of the resulting pore. The poly[bis(methyl valinato)phosphazene], (PNMV) scaffolds had the opposite trend with respect to the total porosity, which was thought to be caused by an exposure of the interior porosity of the microspheres due to fracturing or dissolution of the surface chains covering the interior pores. Additionally, the compressive modulus of the PNEPhA scaffolds showed a significant correlation with solvent/non-solvent sintering solution composition. The highest modulus observed was found at the middle solvent concentration. The increase in modulus from the low to mid was expected due to increase in the bonding region. However, the decrease in modulus from the mid to the high composition was unexpected. This decrease could be attributed to dissolution of the surface chains on the porous PNEPhA scaffolds resulting in a loss of integrity of the individual microspheres leading to premature failure of the individual microspheres as opposed to failure of the bonding region between the spheres. On the other hand, the mechanical properties of PNMV microspheres showed no dependence on solvent/non-solvent sintering solution composition, which suggested that the observed modulus

corresponded with the bulk material or the individual microsphere and not the bonding region between the microspheres.

The advantages of the solvent/non-solvent sintering method include that it can be used regardless of the physiochemical properties of a polymer, and can be tailored to produce the desired degree of microsphere interconnectivity by varying the concentration of the solvent/non-solvent sintering solution, and to a lesser extent by varying the submersion time. Moreover, being a milder method, the solvent/non-solvent sintering technique could potentially allow preloading of bioactive factors within the scaffold for controlled/sustained release. Lastly, the solvent/non-solvent sintering technique does not require specific mold geometry, therefore a large number of different scaffold geometries can be fabricated[29]. The major limitation of the method is that it involves considerably large amounts of organic solvents which if not completely removed can have undesirable effects on the seeded cells and surrounding tissues. Moreover, some of the solvents used in the sintering method involve methylene chloride, chloroform, hexanes, etc., which can alter the secondary structure of encapsulated proteins and thereby affect their biological activity.

SUBCRITICAL CO_2 SINTERING

Subcritical CO_2 sintering is a straightforward method to fabricate cell-seeded, shape-specific microsphere scaffolds in a single step (Figure 2.12). These SMSs retain their advantages of spatiotemporal control for creating three-dimensional signal and stiffness gradients for interfacial tissue engineering within a single scaffold. Compared to the other methods of microsphere-based scaffold fabrication, the CO_2 sintering method is a more benign process. Moreover, it is also suitable for producing cell-containing matrices under relatively mild conditions. The ability to

create cell-loaded scaffolds and patches can have important implications in tissue engineering, where growth factor-encapsulated microspheres can be used to design cell-loaded controlled release vehicles in a single step.

The subcritical CO_2 sintering method for manufacturing SMSs is a modification of the conventional gas-foaming technique used for fabricating porous structures, where saturation of the polymer with CO_2 is performed at either supercritical pressures (≥ 7MPa) or subcritical pressures (< 7MPa) with equilibration periods of 24hrs and 2hrs respectively. Afterwards, rapid depressurization then leads to the nucleation of the gas thereby forming pores in the material. To prepare sintered microsphere scaffolds, the equilibration of CO_2 in the polymer is performed with subcritical CO_2 with significantly reduced exposure times. These conditions lead to a comparatively reduced plasticized state or a relatively less swollen state of the polymer limited to the surface of the microspheres. This state allows microspheres to retain their shape, while subsequent adhesion (and/or reptation) leads to sintering of the adjoining microspheres. The advantage of subcritical CO_2 sintering over the conventional gas foaming technique is that the subcritical sintering is less time consuming and allows for incorporation of bioactive factors and moreover, leads to open pore structures with interconnected pores.

The conditions (time and pressure) of CO_2 exposure are the primary factors responsible for promoting the mutual penetration, increasing the chain mobility at the interfaces of adjoining microspheres and the subsequent adhesion of the microspheres. In addition, the rate of depressurization is an important factor that governs the basic morphology of the scaffolds. Singh *et al.*[216] fabricated PLGA SMSs via CO_2 sintering using a pressure of 1.5 MPa and the duration

of CO_2 exposure was restricted to 1hr. They observed that a moderate rate of depressurization (0.014–0.021MPa s^{-1}) was optimal for the production of sintered matrices whereas, instantaneous depressurization (in less than 5 s) or depressurization at very slow rates (< 0.007MPa s^{-1}) led to foaming of the prepared scaffolds. Moreover, the extent of sintering also depended on the microsphere size and properties of the polymer. Jeon *et al*.[114] fabricated PLGA microsphere scaffolds using subcritical (or dense phase) CO_2 and studied the effects of polymer properties, porogen concentration and sintering process parameters on the mechanical properties and morphologies of the scaffolds. They observed that the optimal range of CO_2 pressure was 1.5–2.5MPa for fabricating scaffolds. Scaffolds prepared at 2.5MPa with lower lactic acid ratios and without porogen particles had a higher stiffness, while the constructs made at 1.5MPa, with lower glycolic acid content, and with porogen granules had lower elastic moduli. Furthermore, no statistically significant differences were observed in scaffold porosities with increase in applied CO_2 pressure and with increase in lactide:glycolide ratio. However, porogen concentration (at a given applied pressure) significantly affected the scaffold porosities with increasing concentration resulting in higher porosities.

Though subcritical CO_2 possess key advantages but it also suffers from some limitations. The process requires complex apparatus and at high pressures for long durations the technique may not be cytocompatible due to known sterilization efficacy of CO_2 caused by lowering the cytoplasmic pH by the formation of carbonic acid and by the shear forces of intercellular bubble formation upon depressurization.

SELECTIVE LASER SINTERING (SLS)

In recent years conventional microsphere sintering methods have been much improved and have been widely used for making scaffolds to regenerate a variety of tissues, however they can only produce scaffolds with simple architecture, irregular pores and pore sizes in a manual and inconsistent manner. Therefore, to overcome the limitations associated with the conventional methods, rapid prototyping (RP), also known as solid free-form fabrication (SFF), has been developed that can produce three-dimensional scaffolds with complex shapes and architecture in a layer-by-layer manner using data generated by computer-aided design (CAD) systems, by computer-based medical imaging techniques such as computer tomography (CT) or magnetic resonance imaging (MRI), and by digitizers. Among various RP technologies, selective laser sintering (SLS) has been found to be advantageous for tissue engineering scaffolds due to its ability to process a wide range of biocompatible and biodegradable materials. In the SLS process, 3D computer images are first sectioned into thin 2D layers (~0.1 mm thick) and then the scaffolds are built layer-by-layer to the required size, shape and internal structure by laser-induced (usually a CO_2 laser) fusion of microspheres (Fig. 12). The interaction of the laser beam with the microspheres elevates the polymer temperature to reach the glass-transition temperature, causing surfaces in contact to deform and fuse together.

The potential advantages of SLS in production of scaffolds include: (i) fewer design constraints, (ii) customization (patient-specific), (iii) faster manufacture speed, (iv) functionally graded materials, (v) free of toxic solvents and (vi) controllable and reproducible structures and porosity. Although SLS is a promising technology for TE scaffold fabrication, so far it is not economical to use because commercial SLS machines require large quantities of biomaterial thus, making the process very expensive. Moreover, the biomaterials are not available in the

appropriate powder form to be processed by these machines. Therefore, Zhou *et al.*[260] modified a commercial SLS system (Sinterstation® 2000) in order to produce scaffolds using small quantities of biomaterial powders. Porous scaffolds were sintered from poly(L-lactide) (PLLA) microspheres and PLLA/carbonated hydroxyapatite (CHAp) nanocomposite microspheres using the modified SLS machine. In order to reduce the consumption of biomaterial powders a miniature sintering platform consisting of a miniature build cylinder and two powder supply chambers, were designed, fabricated and installed in the build cylinder of the existing SLS machine. The miniature build cylinder had a diameter of 49mm and the movement of its base was directly linked to the base of the existing build cylinder of the Sinterstation® 2000 system. Two additional stepping motors beneath the miniature-sintering platform drove the two powder supply chambers. In the sintering processes, the original powder supply tanks of the Sinterstation® 2000 system were empty and small amounts of biomaterial powder were fed from the miniature powder supply chambers. The roller positions were sensed and the signals were fed to a control panel, which controlled the movement of stepping motors and the temperature of the small build cylinder. Other sintering parameters were controlled by the existing Sinterstation® 2000 system. Though they were able to successfully fabricate three-dimensional scaffolds using the modified SLS system, however they did not study the effects of SLS processing parameters on the properties of fabricated scaffolds. Duan *et al.* studied the effects of various SLS parameters on the properties of sintered scaffolds where they fabricated poly(hydroxybutyrate-co-hydroxyvalerate) (PHBV) and calcium phosphate (Ca–P)/PHBV nanocomposite scaffolds. They applied three-factor three-level complete factorial design to investigate the effects of the three factors (laser power, scan spacing, and layer thickness) on scaffold quality and to optimize SLS parameters for producing good-quality PHBV scaffolds and Ca–P/PHBV scaffolds. The

optimization results showed that all the three factors had significant effects on the integrated response, which was concerned with the structure and handling stability, dimensional accuracy and compressive properties of the fabricated scaffolds. Furthermore, based on the regression equation, optimized PHBV scaffolds and Ca–P/PHBV scaffolds were fabricated using the optimized values of SLS parameters[69]. The compressive strength and modulus for optimized Ca–P/PHBV scaffolds were 0.24 ± 0.02 and 3.96 ± 0.64MPa, respectively, and for PHBV scaffolds, the corresponding values were 0.19 ± 0.02 and 2.38 ± 0.29MPa. Although the compressive properties of both types of scaffolds were lower than those of human trabecular bone however, they could be potentially used to regenerate bone in non-load bearing areas, such as calvarial reconstruction.

Summary Of Microsphere Sintering Methods

To summarize, a number of microsphere sintering techniques have been developed so far to fabricate SMSs with simple shapes and architecture. An important future step from a tissue engineering perspective will be the advancement of these techniques to form 3D scaffolds with intricate geometries. Techniques like SLS and subcritical CO_2 sintering hold great promise to create shape specific scaffolds. However, their inability to create scaffolds with finer resolutions and dependence on mold geometries (subcritical CO_2 sintering) may postpone their widely accepted use in the tissue engineering community. Hence an ideal method to fabricate SMSs should: - allow control over scaffold properties, be free of organic solvents, preserve the bioactivity of encapsulated proteins, provide the ability to create scaffold with complex architectures, and allow simultaneous seeding of cells in a single step.

MICROSPHERE SCAFFOLDS IN MUSCULOSKELETAL TISSUE ENGINEERING

The musculoskeletal organ system is responsible for providing structure, stability, support and movement to the body. Thus, diseases and conditions affecting the system can severely reduce its function and effectiveness thereby, impairing the quality of life. These musculoskeletal disorders (MSDs) are an increasing healthcare issue globally and are the second leading cause of disability[13]. For instance, in the U.S. alone the total cost for treating MSDs is estimated to be more than $125 billion per year and the musculoskeletal-related procedures constituted 24.2% of all operating room procedures performed during hospital stays[81, 249]. Therefore, there is an urgent need to explore new treatment strategies for the steadily growing number of MSD patients. Tissue engineering offers an attractive alternative to treat MSDs by providing patient specific biological grafts overcoming limitations, like donor shortage and graft rejection associated with the currently employed surgical grafts. Of the various types of scaffolds employed in tissue engineering strategies microsphere scaffolds (MSs) have gained importance lately due to their ease of fabrication, ability to discretely control particle physicochemical properties and versatility for controlling the release kinetics of encapsulated bioactive molecules. Besides their ability to provide controlled release, MSs also possess excellent mechanical properties that further make them suitable candidates for regenerating musculoskeletal tissue. In the following section, various microsphere-scaffolding strategies used in regenerating different musculoskeletal tissues will be reviewed.

BONE

When trauma or a degenerative disease causes the loss of significant portion of bone, the remaining tissue may have difficulty in repairing itself. A graft/scaffold must be placed at the defect site in order to allow the adjacent bone to bridge the gap created by the defect. To date, autologous trabecular bone grafts taken from the patient's iliac crest serve as the gold standard in such bone grafting procedures. Due to its osteoconductive nature and well-organized three-dimensional pore structure, the autologous graft plays an important role in healing by serving as an effective scaffold for new bone regeneration. It allows for the infiltration of osteogenic and perivascular cells at the defect site, thus allowing healing to occur. Moreover, the graft houses growth factors that allows for differentiation of surrounding cells, initiation of osteogenesis and graft revascularization. The revascularization facilitates the migration of additional osteogenic cells to the graft site, thereby resulting in thickening of the internal structure of the graft and significant increase in its mechanical integrity. Upon union with the host bone (osteointegration) and the transfer of stress to the graft site, the internal graft structure undergoes a remodeling phase in which bone is resorbed and formed in response to mechanical stimuli[25].

As seen from the mechanism of bone regeneration within autologous trabecular bone, graft incorporation is dependent on osteoconductive bone growth and revascularization. Using tissue-engineering principles, several polymeric scaffolds have been designed specifically with the hope of supporting and promoting bone repair and regeneration. In 2001, Borden *et al.*[25] evaluated the osteoconductive properties of a PLAGA microsphere sintered matrix in an *in vitro* environment. They evaluated the cellular response of osteoblasts and fibroblasts on the structure of the matrix. It was observed that both osteoblasts and fibroblasts grew over the PLAGA matrices and were capable of bridging the gaps in the structures. Moreover, these cells exhibited

a unique behavior that helped their proliferation on the matrices. After their initial attachment, electron microscopy (EM) revealed that these cells formed extensions between adjacent microspheres. These cytoplasmic connections, along with cell–cell signaling, served as a guide-wire for additional cellular bridging. Another interesting finding of the EM was that these cells proliferated in concentric rings around the pores within the matrix. Over time, the diameter of the pores slowly decreased as the cells grew in concentric rings. In terms of clinical healing, the consequence of this type of cellular organization may be advantageous to the eventual remodeling of an implant site. The natural structure of trabecular bone consists of mineralized sheets of collagen organized in concentric rings about a central Haversian canal. By promoting cells to arrange in concentric layers throughout the pore system of the matrix, the regenerating tissue may organize in a manner similar to that of trabecular bone. Furthermore, trabecular bone typically consists of 30% bone and 70% void volume. The sintered matrices were found to have porosities (30-40%) similar to the percent bone found in trabecular bone. Due to the porous microsphere structure, the sintered matrices can serve as a negative template for trabecular bone regeneration. Lastly, with the compressive modulus ranging from 137.44 to 296.87MPa, the sintered microsphere structure appeared to be capable of sustaining loads in the mid-range of trabecular bone[26].

Though the PLAGA sintered matrices are biocompatible and possess some osteoconductive properties, the utility of these matrices for bone regeneration may be limited by the lack of functional groups to which bioactive molecules may be attached in order to improve biological performance. Therefore, Jiang *et al.*[115] fabricated chitosan encapsulating PLAGA microsphere sintered microsphere scaffolds to impart functionality to the previously developed PLGA matrices and further improve their bioactivity. It was observed that the PLAGA/chitosan

matrices had porosities and mechanical properties similar to their PLAGA counterparts. The presence of chitosan on the scaffold surface retarded the proliferation of MC3T3-E1 osteoblast like cells on composite chitosan/PLAGA scaffolds at early time points due to very high roughness of composite microsphere surface, however cell proliferation on composite scaffolds become comparable to the PLAGA scaffold at later time points. Moreover, monitoring of phenotypic expression of the MC3T3-E1 cells revealed that the composite scaffold up-regulated the expression of osteopontin (OPN) as compared to the PLAGA scaffold, which suggested that the presence of chitosan facilitates the maturation of MC3T3-E1 cells. Furthermore, the elevated expression of bone sialoprotein (BSP) on chitosan/PLAGA scaffold at days 14 and 21 suggested higher mineralized matrix formation on composite scaffold. Additionally, it was demonstrated that heparin could be immobilized onto the PLAGA/chitosan composite scaffolds due to the functionality imparted by chitosan because of its reactive amino groups. Immobilized heparin at a low dosage showed a stimulatory effect on MC3T3-E1 cell proliferation and differentiation (indicated by the enhanced osteocalcin expression) whereas high heparin loading did not show such effects[116]. The chitosan/PLAGA scaffolds were further implanted *in vivo* in a critical-sized rabbit ulnar defect to evaluate their bone regeneration capacities. New bone formation at the defect initially occurred at the distal ends of the scaffolds and on the side of the scaffold adjacent to the radius irrespective of the type of the scaffold. This was because of the fact that distal ends of the scaffold were in contact with the bone marrow, which contains bone marrow stromal cells, and the side of the scaffold adjacent to the radius was in contact with the periosteum, which contains osteoprogenitor cells. It was observed that immobilization of heparin and recombinant human bone morphogenetic protein-2 on the chitosan/PLAGA scaffold surface promoted early bone formation as evidenced by complete bridging of the defect along the radius and

significantly enhanced mechanical properties when compared to the chitosan/PLAGA scaffold. Furthermore, histological analysis suggested that chitosan/PLAGA-based scaffolds supported normal bone formation via intra-membranous ossification route[117].

Almost 70% of bone mass is composed of a mineral, primarily poorly crystalline hydroxyapatite (HA), therefore, efforts are being made to incorporate ceramics (particularly calcium phosphates) into scaffolds to enhance bone regeneration. Moreover, ceramics like HA are highly biocompatible, osteoconductive, and osteointegrative through the cyclical process of calcium phosphate dissolution and remineralization therefore; their use in scaffolds is further warranted. Additionally, the Ca^{2+} and PO_4^{2-} functional groups present in HA make it an excellent substrate for protein absorption during growth factor loading. On the other hand, crystalline calcium phosphates are known to have slow degradability, high melting temperatures, and brittle nature, which present certain difficulties when used as candidate materials for bone grafting. Therefore, to overcome these limitations ceramics are used in combination with a biodegradable polymer, thus benefitting from the structural and biodegradable properties of the polymer and from the bioactive and osteointegrative properties of the ceramic. Cushnie *et al.*[46] studied the effects of adding *in-situ* synthesized amorphous HA to the PLAGA microsphere scaffolds on their physical characteristics. Moreover, they also investigated the *in vitro* degradation mechanism of these scaffolds. Surface area of the PLAGA scaffolds was found to be significantly increased with HA addition due to the presence of small micropores (< 50μm) on the surface of the composite microspheres. Uniaxial compression testing showed that the purely polymeric scaffolds were significantly stronger than the composite ones because of the increased porosity that resulted from HA addition. Lv *et al.*[160] demonstrated that varying parameters, such as sintering temperature, sintering time, and PLAGA/nano-HA ratio, could control the physical

characteristics of the composite scaffolds. Furthermore, evaluation of human mesenchymal stem cells (hMSCs) response to the PLAGA/n-HA scaffolds that the cells showed enhanced proliferation, differentiation, and mineralization on the composite when compared with those on PLAGA scaffolds. Apart from calcium phosphates, inorganic materials like titanium dioxide (TiO_2) and hexagonal mesoporous silica (HMS) are also incorporated into microsphere scaffolds for bone regenration. TiO_2 powder has been shown to improve the osteoconductivity *in vitro* and *in vivo*. It induces apatite formation on PLGA/TiO2 composite surface in simulated body fluids (SBF), which is believed to be a prerequisite for bioactivity. Moreover, TiO_2 nanoparticles effectively enhance cell attachment and proliferation by promoting protein absorption. Wang *et al.*[246] fabricated TiO_2 encapsulating PLGA microsphere sintered scaffold and observed that these scaffolds had rougher surfaces, which promoted more protein adsorption than the PLGA SMSs. Moreover, these scaffolds exhibited mechanical properties similar to trabecular bone and promoted the proliferation and maturation of the seeded osteoblasts. Additionally, Xu *et al.*[255] demonstrated that the incorporation of HMS into PLGA SMSs significantly improved the compressive properties of the PLGA scaffold and promoted apatite deposition onto these scaffolds that further improved their cytocompatibilty. The benefits of having a ceramic or mineral on a scaffold can also be reaped by applying it as a coating on the surface of the scaffolds. Jabbarzadeh *et al.*[107] explored the feasibility of mineral formation on PLAGA SMSs via surface hydrolysis followed by incubation in simulated body fluid (SFB). In addition, they investigated the effect of mineralization on the level of protein adsorption on the surface of the coated SMSs. They observed that mineralized scaffolds displayed a rough surface with a relatively well-distributed apatite deposition. Mineral covered much of the microsphere surfaces and was comprised of nano-structured plate-like crystals. A higher protein adsorption with

hydrolyzed and mineralized PLAGA scaffolds was observed as compared to untreated PLAGA scaffolds. Moreover, the protein release behavior was not affected by the mineral coating.

Microspheres serve as excellent delivery vehicles, therefore another strategy involving SMSs for bone regeneration includes fabricating raw material (such as dexamethasone, alendronate and Vitamin D3) encapsulating microsphere scaffolds. These raw materials are cheap, have high stability and also possess capabilities for driving differentiation of the seeded cells thereby overcoming drawbacks of high administration dosage, short half-lives and ease of deactivation associated with the growth factor/protein encapsulating approaches. Shi *et al.* [208] encapsulated osteogenesis-inducing drugs (dexamethasone, ascorbic acid and β-glycerophosphate) into PLGA-SMSs and studied the osteogenesis of human MSCs (hMSCs) seeded onto these SMSs. It was observed that hMSCs cultured on a combination scaffold (encapsulating dexamethasone, ascorbic acid and β-glycerophosphate) exhibited superior osteogenic differentiation owing to significantly high phenotypic expression of typical osteogenic genes like osteocalcin (OC), alkaline phosphatase (ALP) etc., and protein secretion of bone-relevant markers such as osteoclast and type I collagen when compared with just dexamethasone encapsulating scaffolds. This phenomenon could be due to the synergistic effect of the three encapsulated raw materials in driving the osteogenesis of hMSCs. Additionally, Das *et al.* designed a PLAGA SMS system to sustain the release of FTY720, a selective agonist for sphingosine 1-phosphate (S1P) receptors and study the effect of its release in treating critical size cranial defects in a rat model. S1P receptor signaling affects the migration of osteoblast precursors and osteoclast progenitor cells and sustained release of S1P or S1P receptor-targeted compounds has been previously shown to enhance the bone regeneration in critical-size cranial defects. It was observed that the copolymer ratio of 85:15 in PLAGA led to higher initial

cumulative release of FTY720 from the microspheres that in turn led to enhanced bone regeneration for up to 9 weeks. The higher cumulative release could be attributed to the tendency of FTY720 to localize towards the surface of the relatively hydrophobic 85:15 PLAGA during microsphere fabrication thereby prolonging its release[47].

Osseous healing and integration with the surrounding tissue depends in part on new blood vessel formation within the porous structure of a scaffold and endothelial cells (ECs) play a key role in this process. Therefore, Jabbarzadeh *et al.*[106] studied human endothelial cell attachment, viability, growth, and phenotypic expression on sintered PLAGA microsphere scaffolds. It was observed that these cells proliferated on the surface of microspheres and through the pores of the scaffold by organizing their cytoskeleton. Moreover, these cells exhibited normal morphological structural and functional phenotypes. Furthermore, the potential of genetically modified adipose-derived stromal cells (ADSCs) combined with ECs to direct the formation of a vascular network on PLAGA SMSs was also studied. The purpose of using modified ADSCs was to release angiogenic growth factor (VEGF) that would drive the proliferation of ECs. Moreover, the ADSCs would also secrete other bioactive factors that would have a mitogenic effect on ECs as well. The results demonstrated that the combination of VEGF producing ADSCs and ECs resulted in marked vascular growth within the PLAGA scaffolds[108]. In a slightly different approach to direct the formation of a vascular network within a PLAGA SMS, VEGF was immobilized onto the surface of mineralized scaffold fabricated by sintering together PLAGA microspheres followed by nucleation of minerals in a SBF. It was observed that ECs attached and proliferated on the surface of microspheres and through the scaffold pore structures. The cells exhibited normal morphological, structural, and functional phenotypes with enhanced performance on mineralized VEGF-immobilizing scaffolds[105].

To more closely mimic the natural architecture of bone, in which there exists a center cavity where the bone marrow resides, a tubular composite-sintered microsphere matrix was formed using HA encapsulating PLAGA microspheres. It was observed that opening the central axis of the scaffold did not compromise mechanical properties of the PLAGA/HA SMS. The tubular design might promote accelerated healing *in vivo* when compared with the PLAGA cylindrical scaffold by providing a path for host marrow cells to migrate along the center axis of the scaffold without nutrient and oxygen limitations [137]. On the other hand, Wang *et al.*[242] fabricated a two-part scaffold to mimic the natural structure of bone. The scaffold consisted of a highly porous inner spiral part integrated with a rigid outer tubular part. The outer tubular part was made of PLGA sintered microparticles to provide support for the host tissue, and the inner spiral structured scaffolds consisted of nanofiber-coated porous thin polycaprolactone (PCL) sheets made by solvent casting/porogen leaching electrospinning technique to promote bone regeneration. The PCL insert was designed in a spiral 3D shape within thin outer walls of PLGA SMS to allow cells to grow completely across, and with open gaps to provide sufficient space for nutrient supply and waste removal. The morphological and mechanical properties of the scaffold were assessed and compared with the properties of three other types of scaffold: a PLGA cylindrical scaffold, a PLGA tubular scaffold and a PLGA tubular scaffold with the spiral insert but without the nanofiber coating. Moreover, attachment, proliferation and differentiation of human osteoblasts onto these scaffolds were also studied. The results demonstrated that the inner and outer parts were integrated well with each other as determined by pull-out testing that showed that the inner insert broke before detaching from the outer part. Moreover, it was demonstrated that integrated scaffolds provide more surface and space for cell attachment and growth compared with cylindrical and tubular scaffolds as high cell numbers were observed on

integrated cells determined via cell proliferation assay. Furthermore, it was observed that fibrous coating enhanced the differentiation potential of the seeded cells as fibrous integrated scaffolds showed significantly higher ALP activity and more calcium accumulation than the porous integrated scaffolds alone.

Microspheres offer several morphological and structural advantages as discussed previously for use in BTE. Another advantage of using microspheres is that they are robust and can withstand preservation processes like cryopreservation and lyophilization. The clinical application of a tissue engineering approach for bone regeneration involves isolation of autogenous cells, their in vitro expansion followed by seeding on a scaffold and then implantation. A time scale for this process might require weeks, during which the patient is incapacitated. An alternative approach that allows for the large-scale clinical use of the tissue engineered constructs, is to cryopreserve the constructs. Banking tissue-engineered constructs would allow for its immediate procurement upon an orthopedic surgeon's request. Therefore, to assess the durability of the microspheres Kofron *et al.*[138] tested the ability of human osteoblast like cells adhered to PLAGA microsphere matrices to withstand the stresses associated with low-temperature tissue banking in dimethylsulfoxide (DMSO), ethylene glycol and glycerol. It was observed that the DMSO solution yielded the greatest percent cell survival for the cells adhered to PLAGA matrices. Moreover, the extracellular matrix architecture was no different between the pre- and post-thaw structures. Another key advantage of using microspheres in BTE is that they can be used, as injectable scaffolds to fill irregularly shaped tissue defects. Habraken *et al.*[91] developed PLGA microsphere/calcium phosphate cements to be used as injectable scaffolds. It was demonstrated that their properties like injectability, setting time, cohesiveness and pore interconnectivity could be adjusted by changing the ratio of polymer and ceramic in the

injectable mixture. In addition, Kang *et al.*[124] demonstrated that suspension of osteoblast and apatite coated PLGA microspheres was easily injectable and led to formation of bone upon *in vivo* implantation.

CARTILAGE

Normal cartilage is an avascular tissue with an intercellular protein matrix reinforced by a three-dimensional network of collagen fibrils. Severe damage to cartilage tissue caused by developmental abnormalities, trauma, or aging-related degeneration result in extensive pain and if left untreated further lead to disability. Adult cartilage tissue has limited self-repair capacity due to the sparse distribution of highly differentiated, non-dividing chondrocytes, slow matrix turnover, low supply of progenitor cells and lack of vascular supply. Current treatment methods for cartilage damage are often not good enough to restore normal function therefore; cartilage tissue engineering is developing as a promising approach for cartilage repair[245]. One of the major thrusts in cartilage tissue engineering is to develop a minimally invasive cell transplantation system in which cells and an injectable scaffold could be injected into defect area via an arthroscopic procedure. In addition, injectable scaffolds can fill various sizes and shapes of defects more easily than preformed scaffolds. Since microspheres possess small size they can serve as ideal candidates for such minimally invasive procedures. Mercier *et al.*[166] first documented the use of biodegradable poly(lactide-co-glycolide) (PLG) microspheres as an injectable scaffold for cartilage tissue engineering. Chondrocytes were delivered via injection either in a cylindrical mold *in vitro* or to the subcutaneous space of athymic mice in the presence and absence of PLG microspheres. They observed progressive cartilage formation in samples containing microspheres. The presence of microspheres increased the quantity of tissue formed,

the amount of glycosaminoglycan that accumulated, and the uniformity of type II collagen deposition. Moreover, microsphere composition influenced the growth of the tissue-engineered cartilage. Higher molecular weight PLG resulted in a larger mass of cartilage formed and a higher content of proteoglycans. Microspheres comprised PLG with methyl ester end groups yielded increased tissue mass and matrix accumulation, but did not display homogenous matrix deposition. The microencapsulation of $Mg(OH)_2$ had negative effects on tissue mass and matrix accumulation suggesting that buffer release might be a contributing factor in poor tissue growth[166, 167].

Kang *et al.*[121] tested whether PLGA microspheres along with chondrocytes could be used to regenerate hyaline cartilage in rabbit knees. Histological scores indicating the extent of the cartilaginous tissue repair and the absence of degenerative changes were significantly higher in the experimental group than in the control groups consisting of no treatment and cell-alone injection. Moreover, the transplanted group with microspheres showed thicker and better-formed cartilage compared to the control groups as determined by Alcain blue, Masson's trichrome and Collagen II (IHC) staining.

Conventional cell culture methodologies using PLGA microspheres for the manufacturing of engineered cartilage tissue products are hampered by the well-known behavior of chondrocytes or mesenchymal stem cells (MSCs) cultured on PLGA microspheres, which undergo a prompt loss of their cartilage-specific phenotype and become fibroblastic. Therefore, to make a neocartilage using PLGA microsphere matrix, specific drug is needed for inducing chondrogenesis on PLGA microspheres. To meet this goal, Park *et al.*[187] fabricated nanostructured three-dimensional scaffolds onto which growth factor (TGF-β_3) loaded heparin/poly(L-lysine) nanoparticles (NP) were physically attached via tapping the ionic

interaction between the positively charged surface of PLGA microspheres and poly(ethyleneimmine) (PEI). It was observed that the PLGA microsphere constructs coated with NP loaded TGF-β_3 showed significantly higher GAG content than those coated with NP alone or uncoated ones. Moreover, MSCs cultivated in the NP TGF-β_3 PLGA microspheres synthesized higher amount of total collagen than those in the PLGA microspheres without TGF-β_3. Furthermore, after 4 weeks TGF-β_3 containing PLGA microsphere constructs were filled with hyaline cartilage cells, lacunae, and specific expression of extracellular matrix components.

OSTEOCHONDRAL INTERFACE

Osteochondral defects are a type of articular cartilage defects that extend deep into the subchondral bone. If untreated, they do not heal and osteoarthritis (OA) may develop over time. Yet, such osteochondral defects are difficult to treat because the subchondral bone and the articular cartilage possess very dissimilar intrinsic healing capacities. Structural changes in the subchondral bone resulting from inferior subchondral bone repair translate into altered biomechanical properties of the entire osteochondral unit thus, influencing the long-term performance of the cartilaginous repair tissue. For osteochondral repair, highly specialized scaffolds mimicking the hierarchical anatomical architecture of the natural osteochondral unit are needed[155]. Classically approaches to engineer osteochondral interface have largely focused on creating graded-structures (e.g., biphasic, triphasic) in cellular/biomaterial composition, which do not closely mimic the continuous transitions of native cartilage to bone, a design limitation that leads to stress concentrations at each interface and eventual failure of the implants[213]. A continuously graded osteochondral construct that simultaneously regenerates both cartilage and

bone in addition to promoting proper integration at the interface is a promising approach to firmly anchor a cartilage substitute to surrounding tissues.

Dormer *et al.*[64] fabricated protein-loaded microsphere scaffolds to achieve spatially and temporally controlled delivery of bioactive signals. Bone morphogenetic protein-2 (BMP-2) and transforming growth factor-β_1 (TGF-β_1) loaded PLGA microspheres were utilized with a gradient scaffold fabrication technology to produce microsphere scaffolds containing opposing gradients of these signals. Constructs were then seeded with either hBMSCs or human umbilical cord mesenchymal stromal cells (hUCMSCs), and osteochondral tissue regeneration was assessed in gradient scaffolds and compared to multiple control groups. The results demonstrated that the gradient scaffolds produced regionalized extracellular matrix, and outperformed the blank control scaffolds in cell number, glycosaminoglycan production, collagen content, alkaline phosphatase activity, and in some instances, gene expression of major osteogenic and chondrogenic markers suggesting that engineered signal gradients are beneficial for osteochondral tissue engineering. Moreover, Singh *et al.*[213] demonstrated that the microsphere gradient technology could be employed to create scaffolds containing a continuous macroscopic gradient in composition that further yielded a stiffness gradient along the axis of the scaffold. PLGA, and composite microspheres encapsulating a higher stiffness nano-phase material (PLGA encapsulating $CaCO_3$ or TiO2 nanoparticles) were used for the construction of microsphere scaffolds. The extent of sintering, composition of the microspheres and the relative content of the two microsphere types can be selectively varied to alter the stiffness of the matrix to create regular and inverse-gradients in mechanical properties. Furthermore, the performance of the novel microsphere gradient scaffolds was evaluated in regenerating osteochondral defects in the rabbit mandibular and femoral condyles. BMP-2 and TGF-β_1 loaded microsphere scaffolds were

implanted in mandibular and medial femoral condyles and evaluated for osteochondral repair *in vivo* for 6 weeks. The results demonstrated that the gradient design led to more uniform neotissue synthesis than in unfilled defects and also to thicker cartilage layers. Moreover, it was also observed that incorporation of hydroxyapatite (in the bone part) along with the growth factors led to formation of a tissue that more closely resembled the native cartilage in terms of glycosoaminoglycan content and cartilage thickness. It also led to higher bone filling and better edge integration with surrounding bone[59, 169]. Thus, these microsphere scaffolds with continuous gradients in both tissue-specific signals and material composition may be a beneficial approach for treating osteochondral defects in clinical settings.

MUSCLE

Skeletal muscles are composed of bundles of highly oriented and dense muscle fibers, each a multinucleated cell derived from myoblasts. These muscle fibers are closely packed together in an extracellular three-dimensional matrix to form an organized tissue with high cell density and cellular orientation. After muscle injuries, myofibers become necrotic and are removed by macrophages. A specialized myoblast sub-population called satellite cells present below the basal lamina of myofibers gets activated thus initiating muscle regeneration. These cells enter the mitotic circle in response to specific local factors released by the macrophages. This induces proliferation and fusion of myoblasts to form multinucleated and elongated myotubes, which self-assemble to form a more organized structure, namely muscle fiber. However, the number of satellite cells in skeletal muscle is very low (1%–5%) and also depends on age and muscle fiber composition. Furthermore, satellite cells themselves can migrate to the injured area and proliferate forming a scar tissue that leads to loss of functionality[10]. Therefore, there is a critical

need to develop tissue-engineering strategies for reconstructing highly organized and complex skeletal tissue.

Lorrez *et al.*[233] explored the use of biodegradable porous, gas-foamed PLG microsphere scaffolds as a substrate to which primary human myoblasts could be attached using clinical grade extracellular matrix (ECM) carriers and differentiated into myofibers, which could be maintained under tension. An immunodeficient non-obese diabetic/severe combined immunodeficiency (NOD/SCID) animal model was used to assess the *in vivo* characteristics of the constructs. It was demonstrated that human myoblasts could be efficiently seeded and differentiated into post mitotic myofibers on gas-foamed PLG SMSs and maintained under tension when implanted subcutaneously. The PLG scaffolds improved human myofiber viability *in vivo* relative to non-scaffold implants and therefore might be useful for future clinical applications.

Summary Of Microsphere Scaffolds In Musculoskeletal Tissue Engineering

Microsphere scaffolds have the potential to enhance the repair of musculoskeletal tissues because of their excellent mechanical properties. Moreover, gradient microsphere constructs providing opposing gradients of tissue-specific signals and mechanical properties are an attractive strategy to treat musculoskeletal tissue interfaces like osteochondral interface, cortical-cancellous bone interface, and ligament/tendon-bone interface. In this regard, *in vivo* comparison of these gradient microsphere constructs with other conventionally fabricated constructs will provide more insight regarding the usefulness of graded microsphere structures.

MICROSPHERE SCAFFOLDS IN OTHER TISSUE ENGINEERING APPLICATIONS

Besides their unique ability to encapsulate growth factors with a known and controllable delivery profile, one promising feature of microspheres as scaffolds is that they provide three-dimensional environments that can better preserve the phenotypes of the cells. The following section will review some of the applications of microspheres as scaffolds in fields like skin, heart, liver, and nerve regeneration and also in developing *in vitro* models for studying cancers/tumors.

SKIN REGENERATION

The skin is the largest organ of the body and is critical to survival of an organism. It acts as a barrier to the environment and is also responsible for thermal regulation and hydration retention. In order to serve these critical functions, the skin is constantly undergoing renewal and possesses limited capacity for repair of wounds. Therefore, engineered skin substitutes have a critical medical application especially to patients with extensive burn wounds and chronic ulcers. However, current skin substitutes (like epidermal sheet grafts) do not restore the normal skin anatomy, lacking the normal appendages of skin including hair follicles, sebaceous glands, and sweat glands as well as the normal mechanical properties of the skin[252].

Kim *et al.*[135] demonstrated the feasibility of using PLGA microspheres as both cell culture substrate and transplantation vehicle for skin cells (keratinocytes and dermal fibroblasts) to regenerate full thickness skin defects on the back of athymic mice. Histological and immunohistochemical analysis showed dermal regeneration with positive staining for vimentin, a marker of dermal fibroblast, and differentiated epithelium that stained positively for cytokeratin, a marker of epidermis, three weeks after the implantation. Furthermore, Huang *et al.*[100] showed that bone marrow derived MSCs (BM-MSCs) delivered via an instructive (growth factor loaded) microsphere scaffold can have significant effects on enhancement of healing quality and sweat

gland repair during skin regeneration process. It was observed that after only three weeks, BM-MSC microsphere scaffold with encapsulated epidermal growth factor exhibited accelerated healing with increased re-epithelialization rates and less skin contraction. Additionally, histological and immunofluorescence staining analysis revealed appearance of sweat glands-like structures in regenerated tissue.

The use of microspheres to treat skin wounds is advantageous over currently available skin grafts because the microsphere method avoids the enzymatic steps to harvest grafts by culturing cells directly on the transplantation vehicles (microspheres) thereby, also reducing the fabrication time. Secondly, this method can reduce the inflammatory reactions caused after implantation using microspheres made from biocompatible and biodegradable materials. Lastly, the microspheres allow co-transplantation of multiple cell types that may enhance the skin regeneration.

HEART REGENERATION

Some of the challenges in cardiac tissue engineering include that engineered myocardium must contain a dense population of properly aligned and electrically connected cardiomyocytes. Moreover, these cells are highly metabolically active, form a well-coupled electromechanical syncytium therefore; they must be in intimate contact with the vascular system. Furthermore, the scaffold materials must be extremely resistant to foreign body reaction because fibrous encapsulation might electrically isolate the engineered tissue and cause arrhythmia. Lastly, most of the current methods for producing porous scaffolds utilize processing conditions that are not compatible with cell survival. To overcome these challenges, a different approach was recently developed with the formation of cell scaffolds by cross-linking hydrogel microparticles in the

presence of cardiomyocytes. Smith *et al.*[217] assembled poly(ethylene glycol) (PEG) microspheres around HL-1 cardiomyocytes to produce highly porous scaffolds. PEG microspheres were phase separated in dextran solutions causing them to rapidly de-swell and crosslink together, eliminating the need for serum protein-based crosslinking that could result in an antigenic response. This also led to a dramatic increase in the stiffness of the scaffolds and greatly improved the handling characteristics. HL-1 cardiomyocytes exhibited high cell viability following scaffold formation as evident from the 9-fold expansion in cell number over a two-week period. The cardiac functional markers, sarcomeric α-actinin and connexin 43, were expressed at 13 and 24 days after scaffold formation. HL-1 cells were spontaneously depolarizing 38 days after scaffold formation, which was visualized by confocal microscopy using a calcium-sensitive dye. Electrical stimulation resulted in synchronization of activation peaks throughout the scaffolds. These findings demonstrate that the fabricated PEG microsphere scaffolds can support the long-term three-dimensional culture of cells, suggesting applications in cardiovascular tissue engineering.

LIVER REGENERATION

The liver, the largest organ in the body, has a complex architecture and performs a myriad of functions. Even though the liver is highly regenerative, drugs and toxins or viral infections can cause extensive damage to hepatocytes, reducing function and regeneration. In the engineering of liver tissues, the creation of a proper biomimetic environment for hepatocytes growth and functionality is an important factor. The use of microspheres in liver tissue engineering is gaining attention because of the versatility that microspheres offer in guiding cell growth. This versatility includes not just the ease of scaffold assembly into various shapes suitable for

different tissue applications, but also offers easy and controllable surface modification for enhanced cell–material interaction. Zhu *et al.*[261] demonstrated this versatility by covalently conjugating PHBV microspheres with three proteins collagen I, laminin, and fibronectin using 1-ethyl-3-(3-dime- thylaminopropyl) carbodiimide and N-hydroxysuccinimide cross linkers. The results indicated that combination of the three ECM proteins on microsphere surfaces has a significant effect on the proliferation of Hep3B cells, thus better mimicking the *in vivo* environment for liver tissue engineering. The ability of PHBV microsphere scaffolds to encapsulate and then release hepatocyte growth factor (HGF) was also demonstrated. It was observed that the three-dimensional microsphere scaffolds with the direct delivery of HGF to the primary hepatocytes were proven to be able to better maintain their viability and phenotype than its delivery via the cell culture medium[263].

In liver tissue, hepatocytes not only interact with adjacent hepatocytes but also with non-parenchymal cells. Thus, cell–cell interactions and hormone stimulation play the central role in the regulation of cellular behaviors such as migration, differentiation, and proliferation. To maintain the hepatocytes function *in vitro*, open porous microspheres seem ideal, as they would enhance the transports of oxygen and nutrients, provide protection from exerted shear stress, provide heterotypic cell–cell contact within and between microspheres thereby building a functional tissue construct. Furthermore, these microspheres have the potentials for being injected *in vivo* into cavities, even of irregular shape and size, in a minimally invasive manner. Chou *et al.*[41] prepared porous PLGA microsphere scaffolds for constructing injectable three-dimensional hepatocyte spheroids. The porous sites of PLGA microspheres provided space for hepatocyte distribution within the microspheres. The feasibility of co-culturing these spheroids with other cell types was demonstrated by culturing them with human umbilical vein endothelial

cell, BMSCs, or NIH/3T3 cells. It was observed that hepatocellular-specific functions were sustained up to 2 weeks with co-culture demonstrating the potential of creating hepatic tissue using these microspheres.

NERVE REGENERATION

Nerve regeneration is a complex biological phenomenon. In the peripheral nervous system, nerves can regenerate on their own if injuries are small. Larger injuries must be surgically treated, typically with nerve grafts harvested from elsewhere in the body that further leads to donor site morbidity. Allografts provide an alternative option but with the increasing number of patients the availability of such grafts is limited. Moreover, there is also a risk of immune response associated with these grafts. Tissue-engineered strategies provide an attractive alternative but traditional scaffolds, which are tubular with and without inner lumen-like architecture, support regeneration along the walls of the scaffolds or the lumen only and do not possess enough surface area to house a large number of cells needed for complete and faster regeneration. Valmikinathan *et al.*[239] developed a novel spiral-shaped nanofibrous microsphere scaffold for peripheral nerve regeneration. These spiral scaffolds had optimal mechanical properties and also sufficient porosity to promote cellular ingrowth. They were also modified to present a nanofibrous surface to enhance cell attachment, migration and proliferation on the surface of the scaffolds. The *in vitro* tests conducted using Schwann cells showed that the nanofibrous spiral scaffolds promoted higher cell attachment and proliferation when compared to contemporary tubular scaffolds or nanofiber-based tubular scaffolds. Also, the nanofiber coating on the surfaces enhanced the surface area, mimicing the extracellular matrix and providing unidirectional alignment of cells along its direction.

CANCER/TUMOR MODELING

In vitro cancer models have been applied in pre-screening anticancer drugs where a two-dimensional (2-D) monolayer culture model serves as the standard to determine drug effects on growth inhibition and apoptosis. However, *in vivo* and clinical cancers are three-dimensional (3-D) and present differences from the 2-D model in terms of cell surface receptor expression, proliferation, extracellular matrix synthesis, cell density and metabolic function. These differences are one of the major reasons for poor co-relationship between *in vitro* and *in vivo* measurements[120].

One of the major thrusts in the field of cancer therapy is to develop better *in vitro* models that would mimic *in vivo* tumors, which will yield more practical assessment of drug efficacy prior to testing in animal models. For this reason, culture of cancer cells on a polymeric scaffold has become more attractive and is expected to provide improved *in vitro/in vivo* co-relationship for therapeutic evaluation. Because of their ability to provide large surface area for cell attachment and growth, porous microsphere scaffolds make 3-D suspension cultures feasible in a stirred suspension bioreactor. Moreover, microsphere scaffolds fabricated from biodegradable and non-cytotoxic materials, can also be used as a cancer cell transplantation vehicle for tumor construction in small animals, eliminating trypsinization step of cultured cells that causes perturbation of cell–cell interactions and serious damage on cell surface proteins[120]. Lastly, microsphere scaffolds can also serve the need to cryopreserve the tumor cells by shielding them from stresses associated with the freeze-thaw process.

Sahoo *et al.*[199] designed and evaluated biodegradable porous PLGA/PLA microparticles as a scaffold for growing breast cancer cells. PLA microparticles containing poly(vinyl alcohol)

(PVA) in the matrix structure (PLA-PVA) and treated with serum prior to cell seeding demonstrated better cell adhesion and cell growth than other formulations of microparticles. Cells were seen to grow into clumps, engulfing microparticles completely with time, and forming a 3-D tissue-like structure. The mechanism of better cell growth on PLA-PVA microparticles appears to be due to the PVA associated with the internal matrix structure of microparticles. To study the applicability of these porous microspheres in pre-screening anti-cancer drugs, Horning *et al.* evaluated the anti-proliferative activity of three anti-cancer drugs (doxorubicin, paclitaxel and tamoxifen), which are currently used in the treatment of breast cancer. The drug diffusion and cellular uptake studies revealed discrepancy in the drug efficacy in 2-D monolayer vs 3-D model. The overall results demonstrated significantly lower drug activities in 3-D model vs in 2-D monolayer[96]. Furthermore, Kang *et al.*[120] demonstrated that cell viability and metabolic activity of cancer cells did not significantly change during one freeze-thaw cycle when cultured on microsphere scaffolds.

Summary Of Microsphere Scaffolds In Other Tissue Engineering Applications

Microsphere based tissue engineering strategies to regenerate musculoskeletal tissue have primarily been focused on regenerating bone and cartilage however; lately they have been gaining attention to regenerate other tissue types as well. Due to their small size, microspheres allow the seeded cells to establish intimate contacts with their neighbors. These cell-cell contacts have great implication in regenerating tissues like heart, liver and peripheral nerves where cell-cell interaction plays an important role in carrying out the tissue function (electromechanical syncytium in cardiomyocytes), in regulating cellular behavior (hepatocyte migration and proliferation), and in guiding cell growth (to establish cell directionality in peripheral nerves).

Microspheres have also been applied to develop tissue models for studying tumors/cancers either *in vitro* or *in vivo* and screen anti-cancer agents as they allow the cells to be transferred easily without the need of trypsinization and also because of their stress-shielding abilities during cryopreservation. Thus, in this regard, more studies need to be conducted to realize the full potential of microsphere scaffolds in regenerating different tissues and developing cell and tissue models for studying diseases.

DISCUSSION

In the last decade, microsphere scaffolds have come into the spotlight because of their ability to combine controlled release functionalities for regulating tissue development and the skill to promote cell growth, so that unique superior structures could be fabricated for better tissue regeneration. The microspheres allow control over various aspects of scaffold parameters because of the versatility offered in terms of choice of material and methods for microsphere fabrication and sintering. In addition, microspheres can be used as carriers for a plethora of bioactive molecules thus holding potential for being used in gradient-based technologies to regenerate heterogeneous tissues and tissue interfaces. Lastly, due to their small size and injectability microspheres are being used to treat irregular shaped defects either alone or via shape-specific scaffolds fabricated through rapid prototyping technologies.

The synthetic biodegradable polyesters such as poly(lactide)s, poly(glycolide)s, and poly(lactide-*co*-glycolide)s have been widely used for fabricating microspheres (Tables 2.1 and 2.2) because of their biocompatibility, physical/mechanical properties, and controlled degradation profiles[4, 11, 19, 25, 26, 29, 30, 41, 42, 44, 46, 47, 51, 59, 60, 62, 64, 66, 73, 86, 90, 91, 99, 105-109, 112, 114-117, 121-125, 135, 137, 138, 140, 149-151, 160, 166-169, 171, 178, 183, 187, 190, 200, 208, 213, 215, 216, 228, 233, 239, 242, 246, 255, 257, 260].

While these polymers have yielded very positive results in tissue engineering application, there are some disadvantages associated with their use. First, these polyesters have the possibility of causing an aseptic inflammatory response due to their acidic byproducts. Moreover, these byproducts negatively affect the bioactivity of the encapsulated molecules. Lastly, the drop in pH, caused by the acidic byproducts, may further increase polymer degradation, leading to significant drop in the mechanical properties of the overall scaffold. Other synthetic biopolymers such as poly(propylene fumarate) (PPF) have the ability to be broken down into non-toxic waste products however, they lack the ability to induce cell differentiation. Often, these polymers have to be modified with natural macromolecules (peptides/proteins) to improve their bioactivity[67]. Natural polymers such as chitosan, gelatin, cellulose, etc. have also been investigated as microsphere fabrication materials (Table 2.2) because they are nontoxic, promote cell adhesion and migration, enhance wound healing, and are biodegradable at rates dependent on controllable factors such as molecular weight and crystallinity[14, 39, 69, 70, 73, 90, 100, 115-117, 140, 179, 230, 247, 261-263]. However, these polymers lack sufficient strength to be used in load bearing applications such as bone and cartilage. Thus, there is a need for a material that could combine the mechanical properties of the synthetic materials with cell affinity of the natural materials. For example, polyphosphazenes (Table 2.2) have recently been used for fabricating microsphere scaffolds for bone regeneration [29, 30, 184, 186]. Polyphosphazenes are a unique class of polymers that offer synthetic flexibility and a high degree of freedom in modulating their physical and chemical properties. They are organic-inorganic hybrid polymers with alternating phosphorus and nitrogen atoms in the backbone with every phosphorus atom bearing two organic side groups. These side groups can be substituted to form amino acid ester polyphosphazenes that have cell-affinity moieties. Moreover, the side group substitution also allows for tailoring the polymers' physico-

chemical properties such as glass transition temperature and degradation rate. Furthermore, these materials are capable of degrading into neutral and buffering degradation products. However, most of the currently used amino acid ester substituted polyphosphazenes are soft elastomeric polymers and may not be suitable for load bearing applications. Moreover, synthesis of polyphosphazenes is a complex and time intensive process that could further limit their use. Hence, search for an ideal material for microsphere fabrication is still on that would culminate in a material that combines the robustness of polyesters, functionality of natural polymers and flexibility of hybrid polyphosphazenes.

Not only there are a variety of matrix materials available for fabricating microspheres but there also exist numerous methods for their fabrication as well. These methods control their size and morphology and also influence the release behavior of the encapsulated molecule. Furthermore, sintering process parameters affect scaffold porosities and mechanical properties. For microspheres to provide clinically relevant tissue-engineered grafts for replacing current surgical standards, it is imperative that these fabrication and sintering technologies are easily scalable and able to generate reproducible microsphere scaffolds in substantial quantities.

A major advantage of microsphere scaffolds is that they possess inherent capabilities to provide controlled release of encapsulated molecules whereas in scaffolds fabricated via conventional methods the bioactive molecule is physically mixed into the scaffold matrix that leads to a burst release. Moreover, for providing controlled released traditional scaffolds themselves use microspheres with encapsulated factors. The versatility of microspheres to provide controlled release from tissue-engineered scaffolds has been exemplified in numerous studies[15, 20, 31, 33, 48, 52, 78, 95, 104, 109, 111, 119, 129-131, 133, 143-148, 153, 159, 165, 182, 194, 195, 197, 198, 219, 220, 236, 241, 243, 244, 248, 259, 264, 265]. However, during encapsulation a protein or growth factor is subjected to

harsh environments, which could result in either complete or partial loss of its bioactivity. To compensate for the loss of bioactivity, higher doses of protein are encapsulated that can further cause cytotoxicity in the regenerating tissue. Several stabilizing agents (like carbohydrates and carrier proteins) are used to prevent denaturation of the encapsulated protein however; success with these agents has been fairly limited. Recently, Mohan *et al.*[171] demonstrated that extracellular matrix (ECM) components (like chondroitin sulfate) could be encapsulated either singly or in conjunction with growth factor to direct cell differentiation in tissue-engineered constructs. These ECM materials are cheaper than growth factors and have the potential to act as (i) signaling molecules to elicit favorable cell response, and (ii) raw materials that can be bioresorbed, and thus integrated into the regenerating tissue. This alternative strategy to encapsulate ECM components can have profound implications in terms of lower cost and faster regulatory approval for more rapid translation of regenerative medicine products to the clinic.

Continuous gradient scaffolds have shown great promise in regenerating complex tissue and tissue interfaces because continuous gradient designs represent a seamless interfacial transition that better approximates the gradual, rather than sharp, interface between native tissues. Microsphere scaffolds can continuously provide both physical and chemical signal gradients simultaneously, thereby making them ideal candidates to engineer heterogeneous tissues and tissue interfaces. These scaffolds provide chemical and signal gradients through spatially and temporally controlled delivery of exogenous bioactive factors. The cells sense physical signal gradients in these scaffolds by detecting variations in microsphere size, pore size, material stiffness and surface physicochemical characteristics. These signal gradients in turn affect cell behaviors such as adhesion, spreading, motility, and survival, thereby causing them to differentiate into different cell types at different regions of the scaffold. These microsphere

scaffolds have been studied to regenerate osteochondral interface in the knee and the temporomandibular joints[59, 64, 169, 171, 213]. However, their potential in regenerating other biological primary (such as between soft tissue and bone, muscle, and tendon), or subsidiary interfaces (among articular cartilage layers, mineralized, and non-mineralized layers of fibrocartilage, tunicae of the vasculature, and dermal layering) is yet to be explored.

There is a growing impetus in the tissue engineering community to create injectable systems for in situ scaffold formation, thus avoiding complicated surgical procedures. Although injectable scaffolds have been around from mid 1990's, still they suffer from limitations like poor mechanical properties and inadequate porosities. Lately, microspheres have started to gain attention as injectable and/or moldable matrices that can be delivered via minimally invasive surgeries because of their spherical nature and ability to pass through small needles[42, 73, 91, 94, 99, 118, 121, 122, 124, 125, 149, 150, 166, 167, 187, 210, 257]. Moreover, they do not suffer from limitations, such as insufficient porosity and poor mechanical properties, associated with conventional injectable scaffolds. However, injectable microspheres made from synthetic polymers can leak from the defect site causing undesirable results in the surrounding tissue. This problem can be overcome by using natural polymers like gelatin that can be crosslinked via a chemical or UV light.

Since tissue-engineering aims to produce patient-specific biological substitutes to circumvent limitations of existing clinical treatments, it becomes necessary for the scaffolds not only to mimic the function of the native extracellular matrix but also its structure. The conventional scaffold fabrication techniques are highly process dependent rather than design dependent therefore, they are unable to fabricate scaffolds with complex geometries and architecture. On the other hand, rapid prototyping (RP) technologies offer complete user control in terms of structural features and are able to meet specific mechanical, mass-transport, and

external shape requirements for producing a scaffold. However, there are several challenges associated with the use of these RP technologies such as limited range of materials, bioactivity of the fabricated scaffold, as well as the issue of cell seeding. Recently, it was demonstrated that microspheres can be used as building blocks to fabricate scaffolds via SLS thereby opening a whole new area of materials that can be processed in RP technologies[69, 260]. Moreover, with the ability of microspheres to provide controlled release of bioactive factors and act as cell carriers the issues of bioactivity and cell seeding can be resolved as well.

In conclusion, the potential of microspheres as drug delivery vehicles has been explored for several decades, whereas their use as tissue engineering scaffolds has been only advocated over the last decade. The use of microsphere scaffolds has primarily been limited to bone and cartilage repair but their potential to regenerate other tissue types is yet to be realized. In this review, a variety of methods for microsphere fabrication and sintering were discussed and how these methods affect the microsphere and overall scaffold properties were also assessed. Hopefully, the assessment will help in designing microsphere scaffolds that will closely mimic the extracellular matrix of the target tissue. Furthermore, the versatility of the microsphere scaffolds was also discussed with respect to fabrication materials, encapsulated factors, and abilities to provide physicochemical gradients and shape-specific grafts. It is expected that the discussion of the versatility of microsphere scaffolds will stimulate the interest of researchers across the tissue-engineering field towards microsphere scaffolds thereby making them a front-runner among other scaffolding approaches in the race to create clinically relevant grafts for regenerative medicine.

CHAPTER 3: MICROSPHERE-BASED SCAFFOLDS CARRYING OPPOSING GRADIENTS OF CHONDROITIN SULFATE AND TRICALCIUM PHOSPHATE‡

ABSTRACT

Extracellular matrix (ECM) components such as chondroitin sulfate (CS) and tricalcium phosphate (TCP) serve as raw materials and thus spatial patterning of these raw materials may be leveraged to mimic the smooth transition of physical, chemical and mechanical properties at the bone-cartilage interface. We hypothesized that encapsulation of opposing gradients of these raw materials in high molecular weight poly(D,L-lactic-co-glycolic acid) (PLGA) microsphere-based scaffolds would enhance differentiation of rat bone marrow stromal cells (rBMSCs). The raw material encapsulation altered the microstructure of the microspheres and also influenced the cellular morphology that depended on the type of material encapsulated. Moreover, the mechanical properties of the raw material encapsulating microsphere-based scaffolds initially relied on the composition of the scaffolds and later on were primarily governed by the degradation of the polymer phase and newly synthesized extracellular matrix by the seeded cells. Furthermore, raw materials had a mitogenic effect on the seeded cells and led to increased glycosaminoglycan (GAG), collagen, and calcium content. Interestingly, the initial effects of raw material encapsulation on a per-cell basis might have been overshadowed by medium-regulated environment that appeared to favor osteogenesis. However, it is to be noted that *in vivo*, differentiation of the cells would be governed by the surrounding native environment. Thus, the results of this study demonstrated the potential of the raw materials in facilitating neo-tissue synthesis in microsphere-based scaffolds and perhaps in combination with bioactive signals,

‡Published as **Gupta V**, Mohan N, Berkland CJ, Detamore MS, Microsphere-Based Scaffolds Carrying Opposing Gradients Of Chondroitin Sulfate And Tricalcium Phosphate, *Frontiers in Bioengineering and Biotechnology*, 3: p. 1-15, 2015. (PMC4486839)

these raw materials may be able to achieve intricate cell differentiation profiles required for regenerating the osteochondral interface.

INTRODUCTION

A scaffold with opposing gradients of physical and chemical signals at the osteochondral interface may trigger simultaneous bone and cartilage regeneration by having a cooperative effect on tissue regeneration. Our previous studies have shown that 3D microsphere-based gradient scaffolds have the potential to guide the chondro- and osteogenic differentiation of cells in different regions of the scaffolds. Moreover, the gradients in signals have the ability to control patterning of cell phenotype and to secrete tissue-specific extracellular matrix (ECM) components to promote osteochondral interface regeneration[58, 63, 65, 169].

Chondroitin sulfate (CS), a glycosaminoglycan (GAG) and a key ECM component of cartilage, when incorporated into 3D scaffolds resulted in increased DNA, GAG and collagen accumulation by the cultured cells[134, 238]. Moreover, CS also enhanced their chondrogenic gene expression[34]. Likewise, bioactive ceramic beta-tricalcium phosphate (β-TCP) is widely used in bone tissue engineering because of its excellent oseteoconductivity, cellular adhesion, mechanical properties and faster degradation rate than other crystalline calcium phosphates. Scaffolds incorporating β-TCP have shown better potential for osteogenic differentiation than the scaffolds without it[152, 229, 234]. We have previously demonstrated that encapsulation of raw materials such as CS and bioactive glass (BG, possesses the capability to directly bind to bone) in low molecular weight (around 40-45 kDa) poly(D,L-lactic-co-glycolic acid) (PLGA) microsphere-based scaffolds created a favorable environment for cells to create a tissue-specific ECM. Additionally, evident regional variation in newly synthesized ECM indicated that the raw

materials could potentially be used to replace growth factors, thus holding tremendous clinical significance by providing a more streamlined path for regulatory approval and greater financial incentive for translation to the clinic[170].

The low molecular weight PLGA microsphere-based scaffolds are well suited for *in vitro* studies as signal release and cellular response to the encapsulated signals can be conveniently studied in these scaffolds because of rapid degradation of microspheres[2, 61, 63, 170, 215, 235]. Moreover, these low molecular weight scaffolds can also be used to study tissue regeneration in small animal model *in vivo* studies where skeletal changes occur at a faster rate compared to humans[65, 169, 188]. In order for a scaffold to be clinically effective and commercially successful, it is imperative that its biodegradation rate matches with the tissue regeneration rate in animal models that closely approximate the human regeneration rate. To begin exploring the clinical implications of our raw material microsphere gradient scaffolds, we need to translate our successes with scaffolds *in vitro* and *in vivo* with small animal models to scaffolds that can be employed in preclinical animal models. The foremost step in that direction will be to study cellular response toward encapsulated factors released from a scaffold system that can be employed in translational animal models (such as sheep, dogs, etc.). Therefore, the objective of this study was to investigate the *in vitro* response of raw material encapsulating microsphere-based scaffolds fabricated with high molecular weight PLGA as a first step to establish the clinical efficacy of these scaffolds. PLGA with an intrinsic viscosity (i.v.) of ~ 0.7 (M_W 106-112 kDa) was chosen for this study due to its relevance in large animal studies[77], and to correspond to an ongoing sheep study from our group. The polymer formulation used in the study represents a more translational product, inspired by a Coulter Foundation-funded project and input from Food and Drug Administration (FDA) regulatory consultant and business advisors. From this study,

we hope to gain an insight into parameters that can have profound implications during *in vivo* experiments.

In this study, we investigated whether the encapsulated raw materials (CS and TCP) in high molecular weight PLGA scaffolds can provide building blocks and facilitate differentiation of the seeded cells simultaneously in the direction of bone- and cartilage-like cells. 3D microsphere-based scaffolds were fabricated using high molecular weight PLGA microspheres encapsulating CS (for cartilage regeneration) and TCP (for bone regeneration) as raw materials. Additionally, scaffolds containing gradient of the raw materials were also fabricated via a gradient technology as previously reported[215]. The response of rat bone marrow-derived stromal cells (rBMSCs) to the raw materials was evaluated when cultured in a medium consisting of exogenous factors. We hypothesized that encapsulation of raw materials; CS and TCP, in high molecular weight PLGA microsphere-based scaffolds would enhance the differentiation of rBMSCs toward chondrogenic and osteogenic lineages, respectively. Moreover, we anticipate rBMSCs in gradient scaffolds to differentiate simultaneously along an osteochondral route as previously seen in low molecular weight scaffolds encapsulating CS and BG[170].

MATERIALS AND METHODS

MATERIALS

Poly(D,L-lactic-co-glycolic acid) (PLGA) (50:50, lauryl ester end group, M_W = 106 kDa) with an i.v. of 0.65 dL/g ("PLGA50:50"), and PLGA (75:25, lauryl ester end group, M_W = 112 kDa) with an i.v. of 0.69 dL/g ("PLGA75:25"), were obtained from Lakeshore Biomaterials (Birmingham, AL). Murine IGF-I was obtained from Peprotech, Inc. (Rocky Hill, NJ). Chondroitin-4-sulfate (lyophilized powder of CS A sodium salt from bovine trachea) and TCP

powder (< 200 nm particle) were obtained from Sigma (St. Louis, MO). All other reagents and organic solvents utilized were of cell culture or ACS grade.

FABRICATION OF MICROSPHERES

Three different types of microspheres were fabricated for the study: - (i) PLGA75:25 microspheres (PLGA), (ii) CS-$NaHCO_3$ encapsulated PLGA50:50 microspheres (CS), and (iii) TCP-encapsulated PLGA75:25 microspheres (TCP). The rationale for choosing PLGA with two different compositions was to correspond to an on going *in vivo* sheep study from our group. The relatively faster degrading polymer (PLGA50:50) was selected for its ability to release the raw materials quickly in the cartilage region to facilitate chondrogenesis whereas the slower degrading polymer (PLGA75:25) in the bone region was selected to lend more structural stability to the regenerating tissue. The CS-$NaHCO_3$ encapsulated microspheres were fabricated by adding 2% w/v CS and 2% w/v $NaHCO_3$ to 16% w/v PLGA50:50 dissolved in dichloromethane (DCM) and the TCP encapsulated microspheres were fabricated by adding 4% w/v TCP to 16% w/v PLGA75:25 dissolved in DCM. Using the PLGA-CS/TCP emulsions, microspheres were fabricated via our previously reported technology[18, 58, 61, 63, 65, 169, 170, 215]. Briefly, using acoustic excitation produced by an ultrasonic transducer (Branson Ultrasonics, Danbury, CT), regular jet instabilities were created in the polymer stream, thereby creating uniform polymer droplets. An annular carrier non-solvent stream of 0.5% w/v poly (vinyl alcohol) (PVA, 88% hydrolyzed, 25 kDa, Polysciences, Inc., Warrington, PA) in deionized water (DI H_2O) surrounding the polymer droplets was flowed using a coaxial nozzle that carried the emanated polymer droplets into a beaker containing the non-solvent solution at 0.5% w/v in DI H_2O to prevent aggregation of the droplets. The polymer droplets were stirred for 3-4 h to allow for solvent to evaporate and then

filtered and rinsed with DI H_2O to remove residual PVA and stored at -20°C. The particles were lyophilized for 48 h before further use.

SCAFFOLD FABRICATION

Gradient scaffolds ("GRADIENT" group) were prepared using our previously established technology[63, 169, 170, 215]. In brief, lyophilized microspheres (50–100 mg) of two different types, CS and TCP, were dispersed in DI H_2O and loaded into two separate syringes. The suspensions were then pumped at opposing flow rates using programmable syringe pumps (PHD 22/2000; Harvard Apparatus, Inc., Holliston, MA) into a cylindrical plastic mold (diameter ~ 4 mm) having a filter at the bottom until a height of about 6 mm was reached. The scaffolds were 3.8-4.0 mm in diameter and around 6 mm in height. The profile for these gradient constructs was linear, where the top one-fourth of the total height comprised of CS microspheres (1.5 mm), then the next one-fourth (1.5 mm) was a linear transition from CS to TCP microspheres, and the remaining half (3 mm) contained only TCP microspheres. The stacked microspheres were then sintered with ethanol-acetone (95:5 v/v) for 55 min. The scaffolds were further lyophilized for 48 h and sterilized with ethylene oxide for 12 h prior to cell seeding experiments. The control PLGA and other homogenous scaffolds, abbreviated as CS and TCP, were fabricated by packing the corresponding microspheres into the same molds, followed by sintering for 55 min, except for PLGA scaffolds (sintered for 45 min). The homogeneous scaffolds had dimensions similar to GRADIENT scaffolds (diameter 3.8-4.0 mm and height 6 mm). A total of four different groups were tested in the study and were named according to the composition of microspheres as: PLGA, CS, TCP, and GRADIENT.

CELL SEEDING OF SCAFFOLDS

rBMSCs were obtained from the femurs of 10 young male Sprague–Dawley rats (176–200 g, SASCO) following a University of Kansas approved IACUC protocol (175–08) and cultured in medium consisting of α–MEM supplemented with 10% FBS (MSC-Qualified, cat #10437-028) and 1% penicillin–streptomycin (P/S) (all from Invitrogen Life Technologies, Carlsbad, CA). When the cells were 80% to 90% confluent, they were trypsinized and re-plated at 7,000 cells/cm2. Seeding was performed when cells reached P4. Scaffolds were sterilized using ethylene oxide for 12 hours, allowed to ventilate overnight after sterilization, and placed in a 24-well plate. Cells (P4) were resuspended in culture medium at a concentration of approximately 10 million/mL. 80 μL of this cell suspension (~750K cells) was placed directly onto the top of the scaffold, which infiltrated the scaffold via capillary action[61]. Cells were allowed to attach for 1 h after which 2 mL of culture medium was added. After 24 h, the culture medium was replaced by 2 mL of differentiation medium consisting of α–MEM, 1% P/S, 10% FBS, 4 mM β-glycerophosphate (β-GP), 100 nM dexamethasone (DEX) (MP Biomedicals, Santa Ana, CA), 25 mM HEPES buffer (Fisher Scientific, Fairlawn, NJ), and 100 ng/mL murine IGF-I (Peprotech Inc., Rocky Hill, NJ). Every 48 h for 6 weeks, two-thirds of the differentiation medium was replaced with fresh medium.

SCANNING ELECTRON MICROSCOPY (SEM)

Scaffolds in culture were fixed in glutaraldehyde followed by dehydration in ethanol. Afterward, the scaffolds were lyophilized for 48 h prior to imaging. The PLGA, CS, TCP and GRADIENT acellular (week 0) and cellular (week 1.5) microsphere-based scaffolds were imaged using a LEO 1550 field emission scanning electron microscope at an accelerating voltage of 10kV.

MECHANICAL TESTING

Unconfined compression tests of the acellular (week 0) and cellular (week 6) microsphere-based scaffolds (n = 4-5) were conducted using a uniaxial testing apparatus (Instron Model 5848, Canton, MA) with a 50 N load cell. A custom-made stainless steel bath and compression-plate assembly were mounted in the apparatus[211]. Cylindrical scaffold samples were compressed to 80% strain at a strain rate of 1%/s under phosphate-buffered saline [PBS—0.138 M sodium chloride, 0.0027 M potassium chloride] at 37°C). Among all possible testing modalities, compression at a 1%/sec strain rate provides the most valuable information in terms of achieving high strain levels to view the entire stress-strain profile, which cyclic testing and stress relaxation/creep testing do not provide, and moreover a reproducible elastic modulus can be obtained without preconditioning as we have done in the past[55]. Compressive moduli of elasticity were calculated from the initial linear regions, ~5% strain, of the stress-strain curves as described previously[61, 63, 170, 215].

POROSITY MEASUREMENT

We have previously demonstrated a close match between theoretical porosities and porosities measured by porosimetry and microCT[114, 215]. Therefore, a fluid saturation method was used in this study to calculate the porosities of the scaffolds: -

$$V_B = 4m \div \pi d^2 h,$$

$$W_{Water} = W_W - W_D,$$

$$V_P = W_{Water} \div \rho_{Water},$$

$$\text{Porosity } (\varphi)(\%) = (V_P \div V_B) \times 100$$

where V_B, m, d, h, W_W, W_D, V_P are the bulk volume, mass, diameter, height, wet weight, dry weight, and pore volume of the scaffolds, respectively. W_{Water} and ρ_{Water} are the weight and density of water. Briefly, wet and dry weights of scaffolds were recorded after fabrication and porosities were determined by the above-described method.

BIOCHEMICAL ANALYSES

Engineered constructs (n = 5) were analyzed for matrix production at 0, 3, and 6 weeks. The samples were digested in two different types of digestion solution: - (i) Papain solution for DNA, GAG and hydroxyproline (HYP) content analyses, and (ii) Triton-X solution for calcium content and ALP activity analyses. The papain digestion solution consisted of 125 mg/mL papain (from papaya latex), 5 mM N-acetyl cysteine, 5 mM ethylenediaminetetraacetic acid, and 100 mM potassium phosphate buffer (20 mM monobasic potassium phosphate, 79 mM dibasic potassium phosphate) (all reagents from Sigma Aldrich) in DI H_2O. Engineered constructs were removed from culture in a sterile manner, placed in microcentrifuge tubes, homogenized with the papain solution (1 mL), and allowed to digest overnight in a 60°C water bath. The digested scaffolds were then centrifuged at 10,000 rpm for 5 minutes to pellet fragments of polymer and other impurities and stored at -20°C. Later, the supernatant was used to determine DNA, glycosaminoglycan (GAG), and hydroxyproline (HYP) contents using the Picogreen (Molecular Probes, Eugene, OR), dimethylmethylene blue (DMMB) (Biocolor, Newtownabbey, Northern Ireland), and HYP (cat #MAK008, Sigma Aldrich, St. Louis, MO) assays, respectively. For calcium and ALP analyses, constructs were digested in 0.05% Triton X-100 and the supernatants were placed in the -20°C before the analyses. Calcium content was assessed using a QuantiChromTM Calcium Assay Kit (DICA-500; QuantiChrom, Hayward, CA). Alkaline

phosphatase (ALP) activity was estimated by determining liberated p-nitrophenol (p-NITRO) rate (concentration/μg DNA per minute) as described elsewhere[28]. In the cases of GAG and calcium content, the values of acellular controls for CS and TCP groups (listed in Tables 3.1 and 3.2), respectively, were subtracted from the corresponding values of the cellular scaffolds at each time point in an effort to distinguish the bioactivity provided by the CS and TCP from the amounts retained in the scaffolds.

GENE EXPRESSION ANALYSES

Reverse transcriptase quantitative polymerase chain reaction (RT-qPCR) was performed for gene expression analyses in microsphere-based constructs (n = 3-5) at weeks 0, 1.5, 3, and 6. Certain groups at certain time points (indicated in results section) had insufficient sample size (n < 3) because some of the samples were lost during processing. In preparation for RT-qPCR, samples were first homogenized in 1 mL of Trizol reagent (Invitrogen), and the RNA was isolated according to the manufacturer's guidelines. Isolated RNA was cleaned using an RNeasy spin column method (Qiagen, Valencia, CA) and converted to complementary DNA using a TaqMan High Capacity kit (Applied Biosystems, Foster City, CA) in an Eppendorf Realplex Mastercycler. TaqMan Gene expression assays from Applied Biosystems for appropriate genes (Table 3.3) were run in the Eppendorf system. A $2^{-\Delta\Delta Ct}$ method was used to evaluate the relative level of expression for each target gene. For quantification, the PLGA constructs at week 0 were designated as the calibrator group and GAPDH expression as the endogenous control.

STATISTICAL ANALYSES

SPSS 21.0 (IBM, Armonk, NY) was used for constructing standard box plots for outlier elimination. For statistical inference in Sections Mechanical Testing and Porosity Measurements, a single factor analysis of variance (ANOVA) was performed with SPSS, followed by a Tukey's honestly significant difference post hoc test when significance was detected below the $p = 0.05$ value. In Sections Biochemical Analysis and Gene Expression Analysis, the statistical inference was performed using a two-factor ANOVA followed by a Tukey's honestly significant difference post hoc test when significance was detected below the $p = 0.05$ value. The model included the two factors (scaffold type and time) and the possible interactions between them. All quantitative results (numerical values and representative diagrams) are expressed as the average ± standard deviation.

RESULTS

SEM

Figures 3.1 and 3.2 represent the scanning electron micrographs of all four types of scaffolds. Figure 3.1 demonstrates that the fabricated microspheres were uniform in size (also refer Figure 3.10) and also illustrates the overall porous nature of microsphere-based scaffolds with interconnected pores. Additionally, it highlights the differences in microsphere morphology among the various scaffold groups. The microspheres in PLGA-only scaffolds (Figure 3.1A) were smooth with surface film layers being formed as a result of plasticization of PLGA with ethanol-acetone[215]. The microspheres in CS scaffolds (Figures 3.1B & 3.1D) had minute pores on their surface while the microspheres in TCP scaffolds had a rougher appearance (Figures 3.1C & 3.1E) than microspheres in the PLGA-only group. The GRADIENT scaffold image (Figure

3.1F) shows fusion between porous (CS) and rough (TCP) microspheres at the transition region of the scaffold. Apart from the differences in microsphere structure, variations were also observed in the cellular morphology of the cell-seeded constructs (Figure 3.2). At Day 10 (week 1.5), very few cells were observed in the PLGA-only scaffolds residing in pores between the adjacent microspheres, and these cells possessed a rounded morphology (Figure 3.2A). In contrast, a far greater number of cells could be seen in the other three groups with differences appearing in the cellular morphologies. Cells covered the surface of the microspheres almost completely in the CS scaffolds and appeared to be flat with cell-cell connections being evident at the sintering junctions between the adjacent microspheres (Figure 3.2B). Cells in the TCP scaffolds had a round appearance, and were clustered around the microsphere sintering junctions (Figure 3.2C). Both cell types with round (in clusters) and flat morphologies were present in the GRADIENT group (Figure 3.2D). However, no apparent morphological differences were observed in cells from distinct regions of the GRADIENT scaffold.

MECHANICAL TESTING

TCP acellular scaffolds had an average elastic modulus of 194 ± 16 kPa at week 0 that was 4- ($p < 0.05$), 4.8- ($p < 0.05$), and 2.8-fold ($p < 0.05$) higher than the moduli of PLGA, CS, and GRADIENT scaffolds, respectively (Figure 3.3A). Additionally, among the cell-seeded scaffolds, TCP constructs at week 6 had an average modulus of 0.84 ± 0.55 MPa that was 208.8-fold ($p < 0.05$) higher than the modulus of the CS group (Figure 3.3B). Surprisingly, it was observed that the PLGA constructs at week 6 had an average modulus of 11.4 ± 6.6 MPa (not shown in the figure) that was orders of magnitude higher than the moduli of the other three groups at that time.

No significant differences were observed between the elastic moduli of CS and GRADIENT groups at week 6.

POROSITY MEASUREMENT

The average porosity of CS group was 49.6 ± 4.4 % that was 2.4-fold ($p < 0.05$) higher than the porosity of the PLGA group (Table 3.4). Moreover, the porosities of the scaffolds in the CS group were also statistically significantly higher than the porosities of their counterparts in the TCP and GRADIENT groups. No significant differences in porosities were observed among any other groups.

BIOCHEMICAL ANALYSIS

DNA CONTENT

The DNA content results (Figure 3.4) revealed no significant differences in the amount of DNA present in the four distinct types of scaffolds at weeks 0 and 3. At week 6, the DNA content in CS scaffolds was 31.7- fold ($p < 0.05$) higher than the DNA content in the PLGA group. The TCP and GRADIENT groups also outperformed the PLGA control at week 6, with 15- ($p < 0.05$) and 18-fold ($p < 0.05$) higher DNA contents, respectively. Moreover, the DNA content in the CS group at week 6 was statistically significantly higher than the DNA contents in the TCP and GRADIENT groups at that time. Additionally, the CS, TCP and GRADIENT groups were observed to have statistically significantly higher DNA content at week 6 than their corresponding values at weeks 0 and 3 however, no significant differences in the DNA content over time were observed in the PLGA group.

GAG CONTENT

A trend similar to DNA content was observed in the GAG content (Figure 3.5A), where no significant differences appeared among groups at weeks 0 and 3. At week 6, the net GAG content of the CS scaffolds was 5.5-fold ($p < 0.05$) higher than the GAG content of the PLGA group. Moreover, the GAG content in the CS group at week 6 was also statistically significantly higher than the GAG contents in the TCP and GRADIENT groups. No significant differences in the GAG content were observed among the other three groups week 6, meaning that the CS group was the only group to statistically significantly outperform the PLGA control at that time. The GAG content in the CS scaffolds (22.2 ± 7.5 μg) at week 6 was found to be statistically significantly higher than its corresponding values at weeks 0 and 3. The TCP and the GRADIENT groups had significantly higher GAG content at week 6 than their respective values at week 0. Furthermore, the PLGA and TCP groups at week 3 had significantly higher GAG content when it was normalized to the DNA content than the normalized GAG content of the CS and GRADIENT groups at that time (Figure 3.5B). However, at week 6 only the TCP group statistically significantly differed from the PLGA group in the normalized GAG content. It must be noted that the values of GAG content obtained from the biochemical analysis represent both the GAGs present in the ECM secreted by the cells and the chondroitin sulfate released by the scaffold and then entrapped within the ECM. The values *do not* represent the CS left entrapped within the polymer matrix, as the GAG content of acellular controls was subtracted at each time point.

HYP CONTENT

At week 0, only the GRADIENT group outperformed the PLGA group in HYP content with 2.6-fold ($p < 0.05$) higher HYP content (Figure 3.6A). Moreover, the HYP content in the GRADIENT group at week 0 was statistically significantly higher than the HYP contents in the CS and TCP groups. Week 3 HYP content results showed that the CS and GRADIENT groups had 1.9- ($p < 0.05$) and 2.9-fold higher HYP content than the PLGA group, respectively. Also, the GRADIENT group at week 3 had statistically significantly higher HYP content than the CS and TCP groups. At week 6, both the CS and the GRADIENT groups outperformed the PLGA control, with HYP contents that were 2.2- ($p < 0.05$) and 2.1-fold ($p < 0.05$) higher, respectively. Additionally, the CS and GRADIENT groups had statistically significant higher HYP contents than the TCP group at week 6. The CS and GRADIENT groups were the only groups that showed statistically significant increases in HYP content over time. The HYP content in the CS group at week 6 was significantly higher than its corresponding values at weeks 0 and 3 whereas the HYP content in the GRADIENT group at week 3 was significantly higher than its HYP content at week 0. In the normalized HYP (per DNA) content, the PLGA, CS, and the GRADIENT groups were statistically significantly higher than the CS group at week 3 (Figure. 3.6B) with no significant differences occurring in the normalized HYP content among the PLGA, CS and GRADIENT groups. The PLGA and TCP groups at week 3 had statistically significantly higher normalized HYP content than their values at week 0 and 6, respectively. No significant differences were observed in the CS and GRADIENT groups over time in the normalized HYP content.

CALCIUM CONTENT

The calcium content analysis revealed no significant differences between the PLGA and CS groups at week 0 (Figure 3.7A). The calcium contents of TCP and GRADIENT scaffolds at week 0 are not reported because of insufficient sample size ($n < 3$), as some of the samples were lost during processing. At week 3, the calcium content in the PLGA group was statistically significantly greater than the calcium contents in the CS, TCP, and GRADIENT groups. Also, the calcium contents in the CS and TCP groups at week 3 were statistically significantly higher than the calcium content in the GRADIENT group. At week 6, the calcium contents in the CS and GRADIENT groups were 3.4- ($p < 0.05$) and 2.3-fold ($p < 0.05$) greater than the calcium content of the PLGA group. Moreover, the CS group calcium content at week 6 was observed to be statistically significantly higher than the calcium contents of the TCP and GRADIENT groups and the GRADIENT group was found to be significantly higher than the TCP group in calcium content at week 6. No significant differences were observed in the calcium contents of the PLGA and TCP groups at that time, meaning that only the CS and GRADIENT groups outperformed the PLGA control in calcium content at week 6. The calcium content of the PLGA group increased statistically significantly at week 3 from its week 0 value, followed by a decrease at week 6 that was not statistically significant. The CS group had significantly higher calcium content at week 6 than at weeks 0 and 3. In addition, the GRADIENT group had significantly more calcium at week 6 than at week 3. No significant differences in calcium content of the TCP group were observed over time. The normalized calcium content (Figure 3.7B) of PLGA scaffolds at week 3 was statistically significantly higher than the normalized calcium contents in the CS, TCP and GRADIENT groups. Additionally, the normalized calcium content in the TCP group at week 3 was statistically significantly higher than the normalized calcium contents of the

CS and GRADIENT groups. Furthermore, at week 6 the PLGA group's normalized calcium content was significantly higher than the normalized calcium content in the CS, TCP and GRADIENT groups. The normalized calcium contents in the PLGA group at weeks 3 and 6 were statistically significantly higher than its corresponding value at week 0. However; the normalized calcium contents in the PLGA and TCP groups at week 6 were statistically significantly lower than their corresponding values at week 3. Again, it is to be emphasized that the values of calcium content are intended to represent the calcium present in the ECM secreted by the cells, and the calcium released from the microspheres and retained by the construct, and not the calcium still entrapped within the polymeric matrix.

ALP ACTIVITY

At week 0, the ALP activities in the TCP and GRADIENT groups were 2.2- ($p < 0.05$) and 2.5-fold ($p < 0.05$) higher than the ALP activity in the PLGA group (Figure 3.8). Moreover, the ALP activities in the TCP and GRADIENT groups at week 0 were statistically significantly higher than the ALP activity in the CS group. No significant differences were observed in the ALP activities of PLGA and CS groups at week 0, meaning that only the TCP and GRADIENT groups outperformed the PLGA control in ALP activity at that time point. No significant differences in ALP activity were observed over time in the PLGA and CS groups. However, it was observed that the ALP activities of the TCP and GRADIENT groups at week 0 were statistically significantly higher than their corresponding values at weeks 3 and 6.

GENE EXPRESSION

SOX9 and COL2A1

Relative SOX9 expression (Figure 3.9A) showed no significant differences among groups at week 0 and also no significant differences among the CS, TCP and GRADIENT groups at week 1.5. The SOX9 expression for PLGA group is not reported at week 1.5 due to insufficient sample size ($n < 3$ as some of the samples were lost during processing). The SOX9 expression for the PLGA group at week 3 was statistically significantly higher than the SOX9 expression of the CS, TCP and GRADIENT groups. No significant differences among groups were observed in the SOX9 expression at week 6. The PLGA group was found to have statistically significantly higher SOX9 expression at week 3 than at weeks 0 and 6. No significant differences over time were observed in SOX9 expression within any of the other three groups.

The COL2A1 (collagen II) expression (Figure 3.9B) in the PLGA group followed a trend similar to SOX9 expression. No significant differences were observed in COL2A1 expression among the PLGA, CS, and GRADIENT groups at week 0 (the TCP group collagen II expression at week 0 is not reported due to insufficient sample size). The COL2A1 expression of the PLGA group at week 1.5 was statistically significantly higher than the COL2A1 expression of the CS and TCP groups. Additionally, the PLGA group had statistically significantly higher COL2A1 expression than the CS, TCP, and the GRADIENT groups at week 3. The CS group at week 3 had significantly higher COL2A1 expression than the TCP and GRADIENT groups. No significant differences in COL2A1 expression between the other two groups were observed at week 3. The CS group at week 6 outperformed the PLGA group in COL2A1 expression with 2.7-fold ($p < 0.05$) higher expression. Moreover, the CS group was statistically significantly higher in COL2A1 expression than the TCP and GRADIENT groups. No significant differences

were observed in COL2A1 expression among the other three groups at that time, meaning that only the CS group outperformed the PLGA control group in COL2A1 expression at week 6. The COL2A1 expression in the PLGA and CS groups peaked at week 3 with statistically significant higher expression at week 3 than their respective values at earlier time points of weeks 0 and 1.5 however, the expression values in these groups decreased significantly at week 6 compared to their week 3 COL2A1 expression values. No significant differences over time were observed within the other two groups.

ACAN AND COL1A1

No significant differences among groups were observed in the ACAN (aggrecan) expression at week 0 (Figure 3.9C). At week 1.5, the ACAN expression in the GRADIENT group was 11.8-fold ($p < 0.05$) higher than the PLGA group. Moreover, the ACAN expression in the GRADIENT group at week 1.5 was statistically significantly higher than the CS and TCP groups. No significant differences among other three groups were observed in the ACAN expression at that time, meaning that only the GRADIENT group outperformed the PLGA control group in ACAN expression at week 1.5. The ACAN expression of the CS group at week 3 was 10.5- fold ($p < 0.05$) higher than the PLGA group. In addition, the ACAN expression in the CS group at week 1.5 was significantly higher than the expression levels in the TCP and GRADIENT groups. Only the CS group outperformed the PLGA group in ACAN expression at week 3 as no significant differences were observed in ACAN expression among the other three groups. At week 6, the TCP group alone outperformed the PLGA group in ACAN expression with a 3.3-fold ($p < 0.05$) higher expression. Moreover, the TCP group also had statistically significantly higher expression than the CS and GRADIENT groups at week 6. No significant differences

were observed in ACAN expression over time in the PLGA group. The ACAN expression in the CS group at week 3 was statistically significantly higher than the ACAN expression at the other three time points in the group. The TCP group had statistically significantly higher ACAN expression at week 6 than at weeks 0, 1.5, and 3. Lastly, the GRADIENT group had statistically significantly higher ACAN expression at week 1.5 than ACAN expression at the other three weeks.

The COL1A1 (collagen I) expression (Figure 3.9D) of the GRADIENT at week 1.5 was 97-fold ($p < 0.05$) higher than the COL1A1 expression of the PLGA group, which was one of the only instances where a test group outperformed the PLGA control. In addition, the COL1A1 expression of the GRADIENT group was statistically significantly higher than the COL1A1 expression levels of the CS and TCP groups. No significant differences were observed in COL1A1 expression among groups at weeks 0, 3, and 6. Additionally, the week 1.5 COL1A1 expression of the GRADIENT group was statistically significantly higher than its COL1A1 expression at any other time point. No significant differences were observed over time in any other group in the COL1A1 expression.

RUNX2 AND BGLAP

RUNX2 expression (Figure 3.9E) showed no significant differences among groups at week 0. However, at week 1.5 the PLGA and GRADIENT groups had statistically significantly higher RUNX2 expression than the expression levels of the CS and TCP groups, but were not significantly different from each other. At week 3, the PLGA group had statistically significantly higher RUNX2 expression than the other three groups. Moreover, the CS group at week 3 had significantly higher RUNX2 expression than the TCP group. Week 6 expression levels indicated

that the TCP group had significantly higher RUNX2 expression than the CS and GRADIENT groups. The PLGA RUNX2 expression at week 3 was found to be statistically significantly higher than its corresponding values at week 0 and week 6, but was not significantly different from its week 1.5 value. The GRADIENT group RUNX2 expression at week 1.5 was statistically significantly higher than at its values at weeks 0 and 6, but did not differ significantly from its value at week 3. No significant differences over time were observed in the RUNX2 expression levels of the CS and TCP groups.

BGLAP expression (Figure 3.9F) showed no significant differences among groups at week 0 and no significant differences among the CS, TCP, and GRADIENT groups at week 1.5 (PLGA value at week 1.5 is not reported because of insufficient sample size. At week 3, the CS group had 10.4-fold ($p < 0.05$) higher BGLAP expression than the PLGA group. Moreover, the CS group had statistically significantly higher BGLAP expression than the TCP and GRADIENT groups. At week 6, the PLGA group had statistically significantly higher BGLAP expression than the GRADIENT group. In addition, the CS group expression level was significantly higher than the expression levels of the TCP and GRADIENT groups. The CS group BGLAP expression at week 3 was statistically significantly higher than its values at weeks 0, 1.5 and 6, respectively. In addition, the CS group BGLAP expression at week 6 was statistically significantly higher than its values at weeks 0 and 1.5, but was significantly lower than its week 3 value. No significant differences over time were observed in the BGLAP expression within any other group.

SPP1 AND IBSP

The SPP1 (osteopontin) expression (Figure 3.9G) showed no significant differences among groups at week 0. At week 1.5, the GRADIENT scaffolds had 248-fold ($p < 0.05$) higher SPP1 expression than the PLGA group, another example of gene expression in a test group outperforming the PLGA control. Moreover, the SPP1 expression in the GRADIENT group was statistically significantly higher than the CS and TCP groups. No significant differences among the CS, TCP and GRADIENT groups were observed in the SPP1 expression levels at week 3 (the PLGA group expression at week 3 is not reported due to insufficient sample size). Again, no significant differences among groups were observed at week 6. The CS group expression at week 3 was statistically significantly higher than at week 0. The GRADIENT group expression at week 1.5 was significantly higher than at weeks 0, 3, and 6. No significant differences over time were observed within any of the remaining two groups.

IBSP expression (Figure 3.9H) showed no significant differences among the CS, TCP and GRADIENT groups at week 1.5 (the values for CS, TCP, and GRADIENT groups at week 0; and the PLGA group at week 1.5 are not reported because of insufficient sample size). At week 3, the IBSP expression of the CS group was 1.8-fold ($p < 0.05$) higher than the PLGA group. In addition, the CS group IBSP expression at week 3 was statistically significantly higher than the TCP and GRADIENT groups. The PLGA group at week 3 also had significantly higher expression than the TCP and GRADIENT groups. No significant differences among groups were observed at week 6. The CS group IBSP expression at week 3 was statistically significantly higher than at weeks 1.5 and 6. No significant differences were observed over time within any of the other groups.

DISCUSSION

The current study for the first time demonstrated the feasibility of raw material encapsulation in high molecular weight PLGA microsphere-based scaffolds that could potentially be used in large animal models or human patients. This work builds on our previous efforts that spoke of the advantages of raw material encapsulation (in conjunction with growth factors) toward creating a new tissue-specific ECM in low molecular weight PLGA scaffolds[170]. Furthermore, employing opposing gradients of CS and TCP to provide bioactive cues and building blocks for simultaneous chondrogenic and osteogenic differentiation of cells is a promising approach for osteochondral interfacial tissue engineering. Additionally, to the best of our knowledge, we are the first group to encapsulate TCP in microsphere-based scaffolds for the bone part of our scaffolds. Most of the other groups utilizing microsphere-based scaffolds have relied on other calcium phosphates and minerals for engineering the bone tissue[46, 161, 228, 255].

The SEM images, depicting the overall porous nature of microsphere-based scaffolds with interconnections among the pores, were in agreement with our previous findings with these scaffolds fabricated with low molecular weight PLGA[215]. Moreover, raw material encapsulation did not affect the spherical nature of the microspheres; however, it was found to have altered the microstructure of the microspheres. Specifically, the CS microspheres had a porous surface that could be attributed to the solvent removal process during the microsphere fabrication step, as we have also observed previously[170]. The presence of sub-micron pores on the CS microspheres contributed toward higher average porosity in these scaffolds compared to the other three groups. The TCP encapsulating microspheres, on the other hand, did not possess pores on their surfaces, but had a rough surface instead. The surface roughness of these microspheres, specifically the presence of ridge-like features, may have resulted from the partitioning of TCP particles on the

surface of the microspheres. These surface characteristics of raw material encapsulating microspheres may have great implications in cell attachment or anchorage and also in diffusion of nutrients and wastes in and out of the scaffolds[189, 254]. Furthermore, raw material encapsulation impacted the cellular morphology of the seeded rBMSCs. Flat cells with significant cell spreading were observed in the CS and GRADIENT groups while cluster forming round cells could be seen in the TCP and GRAIDENT groups. Though the GRADIENT group contained both flat and round cells, no differences in cell morphologies were observed in cells from distinct regions of the scaffold. The different cell morphologies on microsphere-based scaffolds might suggest that cells responded favorably to the encapsulated raw materials, at least initially, which may have influenced their differentiation along discrete pathways. This initial cellular response to encapsulated raw materials could have pivotal significance in regenerating interfacial tissues that require differentiation of cells from a single source along multiple pathways.

Mechanical testing results demonstrated the compressive moduli of microsphere-based scaffolds to be in the range of articular cartilage (0.1-0.9 MPa) and within an order of magnitude of the moduli for cancellous bone (0.01-2 GPa)[128, 164, 251]. Moreover, the elastic modulus of TCP scaffolds at week 0 was found to be at least 3 times as large as any other group, thereby conforming to the observations of Lv *et al.,*[161] demonstrating that calcium phosphates enhance the mechanical properties of polymeric scaffolds. However, at week 6 the cell seeded TCP constructs had significantly higher modulus than the CS group alone. All the other groups, except for the CS group, had an increase in their elastic moduli from week 0. Differences among groups in degradation rates of the scaffolds, cell proliferation within the scaffolds, and ECM deposition could have all contributed to the increase in moduli. PLGA microspheres are known to degrade via bulk erosion where the rate-limiting step is the diffusion of water molecules into

the microsphere core. CS microspheres because of their porous nature may have allowed faster diffusion of the water molecules into their core, thereby initiating the polymer degradation more quickly than in the other three groups. Higher glycolic acid content in PLGA (PLGA50:50) of CS microspheres may have further accelerated polymer degradation in the CS group[2]. Additionally, swelling (Table 3.5) caused by penetration of water inside of the microspheres may have also played a part in the drop in elastic modulus of CS scaffolds[170]. On the other hand, swelling was absent (PLGA and TCP groups) or less pronounced (GRADIENT group) in the other three groups compared to the CS group, which may have prevented the drop in elastic moduli of scaffolds from the PLGA, TCP and GRADIENT groups at week 6. Moreover, polymer composition (PLGA75:25) and microsphere morphology (absence of minute pores on surface) may have allowed the PLGA, TCP and GRADIENT scaffolds to further retain their mechanical properties. Surprisingly, the PLGA scaffolds had a tremendous increase in modulus from week 0 to week 6, translating to an elastic modulus orders of magnitude higher than the moduli of the other three groups at week 6. We previously observed a similar trend in elastic moduli in raw material encapsulating low molecular weight PLGA scaffolds where deviations from the overall scaffold structure at week 6 led to a significant increase in elastic modulus[170]. Additionally, the elastic moduli of high molecular weight PLGA acellular scaffolds at week 6 (unpublished data) also hinted toward a similar phenomenon. Therefore, it is speculated that cellular contributions, in conjunction with polymer degradation led to microscopic changes in the scaffold morphology (closure of pores) that caused the elastic moduli of PLGA constructs to jump at week 6. However, further investigation is needed to better understand the degradation in these high molecular weight PLGA scaffolds and the mechanism of increase in their compressive moduli with time. Altogether, results from the mechanical testing provided information that

would be valuable in designing microsphere-based scaffolds for future *in vitro* and *in vivo* studies in rabbits, sheep, etc.

The biochemical content results were found to be consistent with the SEM observations. A small number of cells were observed on the PLGA scaffolds at Day 10, which agreed with the DNA content analysis that revealed low quantities of DNA on these scaffolds throughout the 6-week culture period. In contrast, the DNA contents of all the raw material encapsulating groups increased over time with significant differences appearing at week 6. Our DNA results on microsphere-based scaffolds suggest that raw material encapsulation encouraged rBMSC proliferation on these scaffolds, thus agreeing with the findings of some other groups showing that the raw materials such as CS and β-TCP could cast a positive influence on the proliferative capacity of rBMSCs[134, 229, 234, 238]. GAG data showed that the CS group had at least a three-fold higher GAG content than the rest of the groups at week 6. Since the GAG content of acellular constructs (Table 3.1) was subtracted at each time point, it is to be stressed that the data primarily represented GAG secreted by the cells and also released CS entrapped within the newly synthesized ECM. A trend similar to GAG content was seen in the HYP content of CS scaffolds suggesting that the encapsulated CS played a significant role in enhancing the cellular GAG and collagen secretion, thus having a modulatory effect on the seeded rBMSCs. However, observance of lower normalized GAG and HYP content in the CS group than the PLGA group suggest that the bioactive effects seen due to CS encapsulation may have been primarily due to the improvement in cellularity without sacrificing biosynthesis on a per cell basis. Calcium content analysis revealed some unanticipated results. The CS group had a significantly higher net calcium content than the other groups at week 6 and the PLGA group was higher in calcium per DNA content compared to rest of the groups at that time. The counter-intuitive phenomenon of

high calcium (or calcium per DNA) contents in the CS and PLGA groups could be attributed to culture medium components such as DEX, β-GP, and IGF-I. DEX is a glucocorticoid, which is used extensively *in vitro* as an osteogenic factor. β-GP is the common source for MSCs to form CaP deposits *in vitro*[76, 207]. IGF-I is an anabolic signal that does not necessarily influence the proliferation and differentiation of MSCs toward osteoblasts on its own, but it is an important molecule directing the differentiation of already osteogenically committed cells[93]. Thus, the presence of these components likely influenced the commitment of rBMSCs on the microsphere-based scaffolds toward osteogenesis. Furthermore, the ALP activities of the TCP and GRADIENT groups at week 0 were higher than their activities at week 6. The elevated ALP activities in these constructs at earlier time points may have been due to the medium components. However, failure to observe a similar effect in the other two groups hint that TCP encapsulation might have influenced their behavior initially as seen with the SEM micrographs as well. Lastly, higher normalized HYP and calcium contents in the TCP encapsulating scaffold groups than the CS group at later time points suggest that TCP encapsulation may have improved rBMSC performance by promoting their differentiation in addition to enhancing their proliferation (as seen with DNA content results).

Gene expression results were in agreement with the other results of the study. Relatively higher expressions of SOX9, COL2A1, and RUNX2 by the cells in the PLGA group at week 3 followed by higher mineral content at week 6 (as indicated by the biochemical data) suggest that the dexamethasone in culture the medium may have caused the rBMSCs in the PLGA scaffolds to go down the osteogenic pathway via a cartilage-like intermediate. Higher expression levels of chondrogenic markers (collagen II and aggrecan) in conjunction with up regulation of osteogenic markers (BGLAP and IBSP) by the cells in the CS group at week 3 than compared to the initial

time points suggest a similar phenomenon as observed in the PLGA group. Lower expression of BGLAP and IBSP in the TCP group than the CS group suggests that TCP presence inhibited expression of osteogenic markers by creating a substrate environment that was already high in mineral content, a phenomenon previously observed with hydroxyapatite encapsulating low molecular weight PLGA microsphere-based scaffolds[61]. The cells in the GRADIENT group showed relatively higher expression of ACAN and SPP1 (along with higher expression of RUNX2 by the cells in the group than at week 0) than the cells in the PLGA control group at week 1.5. The higher expression of some chondrogenic and osteogenic markers in the GRADIENT group at earlier time points may be due to faster maturation of rBMSCs toward cartilage- and bone-like cells in this group however, more evidence is needed to reinforce this speculation.

Overall, the results of the current study indicate that raw material encapsulation into microsphere-based scaffolds influenced the behavior of the seeded rBMSCs. Differences in the cell morphologies and greater cell numbers in the raw material groups leading to enhanced matrix synthesis in these groups demonstrates that the raw materials provide a head start in the (re)generation of tissues. It is of interest to infer the amount of matrix synthesized by cells in the scaffolds beyond the exogenously included amounts. Therefore, the biochemical content (CS and calcium) for the acellular constructs was subtracted from the content of the cell seeded constructs assuming that the acellular scaffolds degrade and release encapsulated molecules at the same rate as their cellular counterparts. However, we acknowledge that this assumption is weak as cells synthesizing new matrix, and perhaps altering the surrounding pH, etc., will influence the polymer degradation rate, but with the higher molecular weight PLGA, it should be a reasonable approximation that allows us to better evaluate differences among groups due to cellular

contribution. In addition, static seeding approach employed in this study has limitations associated with it due to the manual- and operator-dependent nature of the process. However, we followed a uniform manual seeding procedure and we think that the differences observed in the DNA content at week 0 (24 hours post seeding) among various scaffold type might have resulted more from the differences in cell attachment arising due to differences in scaffold composition than arising from variations in cell seeding. Moreover, we did not specifically explore the dosing effect of CS and TCP, but our group has demonstrated in the past that the concentration of the raw materials can have a significant effect on the differentiation of the cells[61]. Additionally, higher cell number, greater biochemical content and relatively higher expression of some osteogenic and chondrogenic markers in the GRADIENT group accentuated the advantages of using gradient-based strategies for engineering the osteochondral interface. However, we recognize that these scaffolds not being amenable to histology due to the stiffness of the polymer constructs, given the high molecular weight and slow degradation of the PLGA was a limitation of the study that would have further elaborated the differences among groups based on their regional material composition, but we have substantiated previously both *in vitro* and *in vivo* that regionalized tissue formation occurs in raw material gradient microsphere-based engineered constructs[169, 170]. Furthermore, the initial effects of raw material encapsulation on a per-cell basis might have been obscured by the culture medium components that appeared to favor osteogenesis. However, it is to be noted that *in vitro* advancements observed initially with raw material encapsulation could translate *in vivo* to a more favorable interaction with infiltrating MSCs, and perhaps facilitate differentiation in a native environment rather than in a medium-governed environment. Lastly, an important consideration in designing scaffolds for clinical use is determining the mechanical integrity. We have shown in our prior work that microsphere-

based scaffolds possess adequate mechanical properties for the regeneration of osteochondral tissues and the encapsulation of raw materials may impact those properties[61, 63, 170]. Our mechanical testing results in the current study also agreed with our previous findings; additionally, the results also suggested that the mechanical properties of microsphere-based scaffolds can be impacted by scaffold degradation and cellular matrix synthesized by the seeded cells. Additional cyclic testing in the future may yield interesting information about degree of hysteresis and narrower strain ranges about a fixed strain point (e.g., 5%) with a frequency sweep could yield interesting tan delta profiles as well, which we will consider for future studies.

Altogether, the overall findings emphasize the need to further refine the technology, perhaps by adjusting raw material concentration or by altering PLGA degradation rate. The degradation of the polymer will play a key role in tissue regeneration *in vivo*, where premature failure in scaffold mechanical properties can have a deleterious effect on the regenerating tissue and extended degradation in contrast could become an obstacle to tissue regeneration. Therefore, it is important to identify a polymer with a biodegradation rate comparable to the neo-tissue formation rate. Additionally, identifying raw material concentrations that are most efficacious in promoting osteogenesis and chondrogenesis would yield valuable information, which could then be leveraged for tailoring scaffold degradation in future sheep or any other large animal model studies. Nevertheless, the current study highlights several benefits of raw material microsphere gradient scaffold technology. The raw material encapsulating microsphere-based scaffolds attempt to regenerate both cartilage and bone simultaneously, thus stressing on the importance of growing cartilage and bone within the physical proximity of each other; many signaling pathways and endogenous proteins responsible for progenitor cell commitment to the osteoblast or chondrocyte lineages have a high degree of interrelatedness[88]. The raw materials apart from

being conductive to tissue (re)generation can also provide inductive signals to the surrounding cells guiding their differentiation. In addition, the raw materials provide clinical significance to microsphere gradient scaffolds, as these scaffolds may be tactically placed for swifter and less costly regulatory approval.

CONCLUSIONS

The present study assessed the *in vitro* response of microsphere-based scaffolds with clinical relevance fabricated using a raw material approach. Overall, the results demonstrated that the primary improvements observed with the raw materials−CS and TCP−were more due to greater initial interaction with cells and greater cellularity with comparable performance on a per-cell basis rather than on specifically driving differentiation. Moreover, the medium-governed environment that seemed to favor osteogenesis concealed the initial *in vitro* advancements observed with raw material encapsulation. Additionally, there was also evidence of faster maturation of rBMSCs in the raw material GRADIENT constructs that can be leveraged further to engineer the complex osteochondral interface. Therefore, a strategy combining the "building block" side of the raw material philosophy (as we have done here) with the "signaling" side, for example by including hydroxyapatite with the TCP, or maybe TGF-β with CS, or by altering the dose of CS (without TGF-β), in a scaffold with a biodegradation rate comparable to the neo-tissue formation rate, we may be able to achieve the differentiation profiles we seek *in vitro*.

CHAPTER 4: MICROSPHERE-BASED SCAFFOLDS ENCAPSULATING TRICALCIUM PHOSPHATE AND HYDROXYAPATITE§

ABSTRACT

Bioceramic mixtures of tricalcium phosphate (TCP) and hydroxyapatite (HAp) are widely used for bone regeneration because of their excellent cytocompatibility, osteoconduction, and osteoinduction. Therefore, we hypothesized that incorporation of a mixture of TCP and HAp in microsphere-based scaffolds would enhance osteogenesis of rat bone marrow stromal cells (rBMSCs) compared to a positive control of scaffolds with encapsulated bone-morphogenic protein-2 (BMP-2). Poly(D,L-lactic-co-glycolic acid) (PLGA) microsphere-based scaffolds encapsulating TCP and HAp mixtures in two different ratios (7:3 and 1:1) were fabricated with the same net ceramic content (30 wt%) to evaluate how incorporation of these ceramic mixtures would affect the osteogenesis in rBMSCs. Encapsulation of TCP/HAp mixtures impacted microsphere morphologies and the compressive moduli of the scaffolds. Additionally, TCP/HAp mixtures enhanced the end-point secretion of extracellular matrix (ECM) components relevant to bone tissue compared to the "blank" (PLGA-only) microsphere-based scaffolds as evidenced by the biochemical, gene expression, histology, and immunohistochemical characterization. Moreover, the TCP/HAp mixture groups even surpassed the BMP-2 positive control group in some instances in terms of matrix synthesis and gene expression. Lastly, gene expression data suggested that the rBMSCs responded differently to different TCP/HAp ratios presented to them. Altogether, it can be concluded that TCP/HAp mixtures stimulated the differentiation of rBMSCs toward an osteoblastic phenotype, and therefore may be beneficial in gradient microsphere-based scaffolds for osteochondral regeneration.

---

§To be submitted as **Gupta V**, Lyne D, Barragan M, Berkland C, Detamore M, Microsphere-Based Scaffolds Encapsulating Tricalcium Phosphate and Hydroxyapatite, *Biomaterials Science*, 2015.

INTRODUCTION

Several regenerative medicine strategies for osteochondral repair have relied on the use of bioceramics such as tricalcium phosphate (TCP) and hydroxyapatite (HAp) for regenerating the bone region of the tissue[56, 113, 155, 193, 205, 209]. TCP and HAp are both chemically similar to the inorganic component of bone and are osteoconductive because of their capability to bond with bone. TCP lacks osteoinductivity, while HAp is widely accepted to be osteoinductive[84, 157]. On the other hand, HAp degrades over the course of several years, whereas TCP may be resorbed into the new bone tissue[75, 223]. Numerous studies have shown that mixtures of TCP and HAp without the addition of any growth factors or cells can treat large bone defects, which supports their great clinical potential[22, 74, 258].

Microsphere-based scaffolds are promising substrates for musculoskeletal regeneration because of their structural attributes like rigidity in shape, ability to provide a porous network, and uniform mechanical properties[101]. Moreover, they offer a wide range of alternatives in terms of materials for microsphere matrices, and methods for microsphere fabrication and sintering[18, 21, 25, 29, 32, 184]. Our group has demonstrated that microsphere-based scaffolds can provide opposing signal gradients via spatio-temporal release of growth factors to facilitate regeneration of complex tissues such as the osteochondral interface[58, 63, 65, 169, 214, 215]. Furthermore, we have shown that opposing gradients of materials such as TCP and chondroitin sulfate can provide raw materials (i.e., bioactive signals and building blocks) to simultaneously guide the regional osteo- and chondrogenic differentiation of cells[89, 173]. Delivering raw materials in lieu of growth factors holds tremendous financial incentive for translation to the clinic by providing a more streamlined path for regulatory approval as well as saving on the cost of including the growth factor in the product. With regard to osteochondral regeneration, the ceramic mixtures can be combined with

chondrogenic raw materials in a gradient scaffold to regenerate the bone region of the tissue. To first evaluate the osteogenic response, the systematic approach is to assess the performance of homogenous microsphere-based scaffolds encapsulating bioceramic mixtures before employing them in a continuously graded design. Therefore, the objective of the current study was to investigate the *in vitro* response of homogenous microsphere-based scaffolds encapsulating TCP and HAp mixtures.

In the current study, we investigated whether encapsulation of a bioceramic mixture (TCP and HAp) in PLGA microsphere-based homogenous scaffolds would promote osteogenesis in rat bone marrow stromal cells (rBMSCs). Homogenous microsphere-based scaffolds were fabricated using PLGA microspheres encapsulating TCP and HAp mixtures in two of the most widely studied w/w ratios of 7:3 and 1:1 (TCP:HAp) with the same net ceramic content of 30 wt%[36, 71, 103]. The response of rBMSCs to the bioceramic mixtures was evaluated when cultured in a medium consisting of exogenous factors. Cell response to an osteogenic growth factor, bone morphogenetic protein (BMP)-2, encapsulated in microspheres has been studied in detail in our earlier work[63, 169]. Microsphere-based scaffolds with encapsulated BMP-2 served as the positive control, and "blank" microsphere-based scaffolds (i.e., no BMP-2, TCP or HAp) served as the negative control. We hypothesized that the bioceramic mixture encapsulating groups would outperform the BMP-2 group (positive control) in gene expression and extracellular matrix (ECM) synthesis relevant to bone tissue.

MATERIALS AND METHODS

MATERIALS

Poly(D,L-lactide-co-glycolide) (PLGA) (50:50 lactic acid:glycolic acid ratio, ester end group) with an intrinsic viscosity (i.v.) of 0.37 dL/g, was obtained from Evonik Industries (Essen, Germany). Human BMP-2 and Murine insulin-like growth factor (IGF)-I were obtained from PeproTech, Inc. (Rocky Hill, NJ). HAp and TCP powders (< 200 nm particle) were obtained from Sigma Aldrich (St. Louis, MO). All other reagents and organic solvents utilized were of cell culture or ACS grade.

PREPARATION OF MICROSPHERES

Four different types of microspheres were fabricated for the study: - (i) PLGA microspheres (BLANK), (ii) BMP-2 encapsulated PLGA microspheres (BMP), (iii) 7:3 w/w TCP:HAp-encapsulated in PLGA microspheres (abbreviated as TH73 or TCP/HAp 7:3), and (iv) 1:1 w/w TCP:HAp-encapsulated in PLGA microspheres (abbreviated TH11 or TCP/HAp 1:1). For fabricating BMP-2 encapsulated microspheres, BMP-2 was first reconstituted in 10 mg/ml bovine serum albumin (BSA) in phosphate buffered saline (PBS) (both from Sigma, St. Louis, MO). The reconstituted protein solution was mixed with 20% w/v PLGA dissolved in dichloromethane (DCM) at a loading of 60 ng BMP-2 per 1.0 mg of PLGA. The final mixture was then sonicated over ice (50% amplitude, 20 s). The TCP/HAp 7:3 and TCP/HAp 1:1 encapsulated microspheres were fabricated by adding 4.2% and 3% w/v TCP and 1.8% and 3% w/v HAp, respectively to 14% w/v PLGA dissolved in DCM. The net ceramic content encapsulated in TCP/HAp 7:3 and TCP/HAp 1:1 groups was 30 wt%. Using the PLGA-protein and PLGA-TCP/HAp emulsions, microspheres with mean diameters ranging from 172-186 μm

(Supplementary Figure 1), were fabricated via our previously reported technology[58, 61, 63, 65, 89, 114, 169, 172, 173, 214, 215, 224]. Briefly, using acoustic excitation produced by an ultrasonic transducer (Branson Ultrasonics, Danbury, CT), regular jet instabilities were created in the polymer stream, thereby creating uniform polymer droplets. An annular carrier non-solvent stream of 0.5% w/v poly (vinyl alcohol) (PVA, 88% hydrolyzed, 25 kDa, Polysciences, Inc., Warrington, PA) in deionized water (DI H_2O) carried the emanated polymer droplets (i.e., microspheres) into a beaker containing the non-solvent solution at 0.5% w/v in DI H_2O. The microspheres were stirred for 2-3 h to allow the solvent to evaporate, and then these microspheres were filtered, rinsed and stored at -20°C. The microspheres were then lyophilized for 48 h before further use.

SCAFFOLD FABRICATION

Scaffolds were prepared from the microspheres using our previously established technology[61, 63, 89, 172, 215, 224]. In brief, lyophilized microspheres (50-70 mg) were dispersed in DI H_2O and loaded into a syringe. The dispersion was then pumped using a programmable syringe pump (PHD 22/2000; Harvard Apparatus, Inc., Holliston, MA) into a cylindrical plastic mold (diameter ~ 4 mm) having a filter at the bottom until a height of about 2 mm was reached. The scaffolds were 3.8-4.0 mm in diameter and around 2 mm in height. The packed microspheres were then sintered with ethanol-acetone (95:5 v/v) for 55 min. The scaffolds were further lyophilized for 48 h and sterilized with ethylene oxide for 12 h prior to cell seeding experiments. A total of four different groups were tested in the study and were named according to the composition of microspheres as: BLANK, BMP, TH73 or TCP/HAp 7:3, and TH11 or TCP/HAp 1:1.

CELL SEEDING OF SCAFFOLDS

rBMSCs were obtained from the femurs of eight young male Sprague–Dawley rats (176–200 g, SASCO) following a University of Kansas approved IACUC protocol (175–08) and cultured in medium consisting of αMEM supplemented with 10% FBS (MSC-Qualified, cat #10437-028) and 1% penicillin–streptomycin (P/S) (both from Thermofisher Scientific, Waltham, MA). When the cells were 80% to 90% confluent, they were trypsinized and re-plated at 7,500 cells/cm^2. Seeding was performed when cells reached P4. Scaffolds were sterilized using ethylene oxide for 12 h, allowed to ventilate overnight after sterilization, and placed in a 48-well plate. Cells (P4) were resuspended in culture medium at a concentration of approximately 50 million/mL. 25 μL of this cell suspension (~1.25M cells) was placed directly onto the top of the scaffold, which infiltrated the scaffold via capillary action [61, 89]. Cells were allowed to attach for 1 h, after which 1 mL of culture medium was added. After 24 h, the culture medium was replaced by 1 mL of differentiation medium consisting of αMEM, 1% P/S, 10% FBS, 4 mM β-glycerophosphate (β-GP), 100 nM dexamethasone (DEX) (MP Biomedicals, Santa Ana, CA), 1% insulin-transferrin-selenium 100X (ITS) (Thermofisher Scientific, Waltham, MA), 1% non-essential amino acids (NEAA) (Thermofisher Scientific, Waltham, MA), 15 mM HEPES buffer (Thermofisher Scientific, Waltham, MA), and 100 ng/mL murine IGF-I. Every 48 h for 6 weeks, three-fourths of the differentiation medium was replaced with fresh medium.

SCANNING ELECTRON MICROSCOPY (SEM) AND ENERGY DISPERSION SPECTROSCOPY (EDS)

Microspheres and acellular scaffolds were imaged via a Versa 3D Dual Beam (FEI, Hillsboro, OR) scanning electron microscope (SEM) with a detector for energy dispersive spectroscopy

(EDS). The BMP and TH11 microspheres were cryo-fractured using a sharp blade and the dispersion of BMP-2, TCP and HAp within the microspheres was further analyzed using EDS at an accelerating voltage of 10 kV. Pixel maps for atomic calcium, nitrogen and phosphorus were generated using Aztec analysis software (Oxford Instruments, Abingdon, United Kingdom). The PLGA (BLANK) microspheres were also imaged as a negative control to confirm the absence of calcium, nitrogen and phosphorous in the EDS maps.

MECHANICAL TESTING

Unconfined compression tests of acellular (i.e., week 0) microsphere-based scaffolds (n = 6) were conducted using a uniaxial testing apparatus (Instron Model 5848, Canton, MA) with a 50 N load cell. A custom-made stainless steel bath and a compression-plate assembly were mounted in the apparatus[212]. Cylindrical scaffold samples were compressed to 40% strain at a strain rate of 10%/min under phosphate-buffered saline [PBS—0.138 M sodium chloride, 0.0027 M potassium chloride] at 37°C. Among all possible testing modalities, compression at a 10%/min strain rate provides the most valuable information in terms of achieving high strain levels to view the entire stress-strain profile, which cyclic testing and stress relaxation/creep testing do not provide, and moreover a reproducible elastic modulus can be obtained without preconditioning as we have done in the past[55]. Compressive moduli of elasticity were calculated from the initial linear regions, i.e., at ~5% strain, of the stress-strain curves as described previously[61, 63, 89, 172, 215].

POROSITY MEASUREMENT

We have previously demonstrated a close match between theoretical porosities and porosities measured by porosimetry and microCT[114, 215]. Therefore, a fluid saturation method as described previously[89] was used in this study to calculate the porosities of the scaffolds:

$$V_B = 4m \div \pi d^2 h,$$
$$W_{Water} = W_W - W_D,$$
$$V_P = W_{Water} \div \rho_{Water},$$
$$\text{Porosity } (\varphi)(\%) = (V_P \div V_B) \times 100\%$$

where V_B, m, d, h, W_W, W_D, V_P are the bulk volume, mass, diameter, height, wet weight, dry weight, and pore volume of the scaffolds, respectively. W_{Water} and ρ_{Water} are the weight and density of water. Briefly, wet and dry weights of scaffolds were recorded after fabrication and porosities were determined by the above-described method.

BIOCHEMICAL ANALYSES

Engineered constructs were analyzed for matrix production at 0 (i.e., 24 h post seeding), 3, and 6 weeks. The samples were digested in two different types of digestion solution (n = 6 for each): (i) Papain solution for DNA and hydroxyproline (HYP) content analyses, and (ii) Triton-X solution for calcium content and ALP activity analyses. The papain digestion solution consisted of 125 mg/mL papain (from papaya latex), 5 mM N-acetyl cysteine, 5 mM ethylenediaminetetraacetic acid, and 100 mM potassium phosphate buffer (20 mM monobasic potassium phosphate, 79 mM dibasic potassium phosphate) (all reagents from Sigma Aldrich) in DI H_2O. Engineered constructs were removed from culture in a sterile manner, placed in microcentrifuge tubes, homogenized with the papain solution (1 mL), and allowed to digest overnight in a 60°C water bath. The digested scaffolds were then centrifuged at 10,000 rpm for 5

minutes to pellet fragments of polymer and other impurities and stored at -20°C. Later, the supernatant was used to determine DNA and hydroxyproline (HYP) contents using the PicoGreen (Molecular Probes, Eugene, OR) and HYP (cat #MAK008, Sigma Aldrich, St. Louis, MO) assays, respectively. For calcium and ALP analyses, constructs were digested in 0.05% Triton X-100 (Sigma Aldrich, St. Louis, MO) and the supernatants were stored at -20°C before the analyses. Calcium content and alkaline phosphatase (ALP) activity were assessed using the QuantiChromTM Calcium Assay (DICA-500; QuantiChrom, Hayward, CA) and Alkaline Phosphatase Activity Colorimetric Assay (K412-500, Biovision, Milpitas, CA) kits, respectively. The calcium contents of the acellular controls for TCP/HAp 7:3 and TCP/HAp 1:1 groups were also measured at each time point in an effort to distinguish the bioactivity provided by TCP and HAp from the calcium amounts retained in the scaffolds. The calcium contents for the TCP/HAp 7:3 and TCP/HAp 1:1 groups (both cellular and acellular) at week 0 are not reported because of incomplete extraction of calcium from these scaffolds.

GENE EXPRESSION ANALYSES

Reverse transcriptase quantitative polymerase chain reaction (RT-qPCR) was performed for gene expression analyses in microsphere-based constructs (n = 6) at weeks 0, 1.5, 3, and 6. Certain groups at certain time points (indicated in Results section) had no Ct values, indicating that the fluorescence intensities in these samples did not cross the threshold fluorescence. These samples were marked as zero for RNA expression. RNA was isolated and purified using QIAshredders and an RNeasy Kit (Qiagen, Valencia, CA) according to the manufacturer's guidelines. Isolated RNA was converted to complementary DNA using a TaqMan High Capacity kit (Applied Biosystems, Foster City, CA) in an Eppendorf RealPlex Mastercycler. TaqMan Gene expression

assays from Applied Biosystems for appropriate genes (Table 4.1) were run in the Eppendorf system. A $2^{-\Delta\Delta Ct}$ method was used to evaluate the relative level of expression for each target gene. For quantification, the BLANK constructs at week 0 were designated as the calibrator group and GAPDH expression as the endogenous control.

HISTOLOGY AND IMMUNOHISTOCHEMISTRY (IHC)

At 6 weeks, microsphere-based constructs (n = 3) were soaked in 30% w/v sucrose (Thermofisher Scientific, Waltham, MA) solution in PBS for 24 h. Afterward, the constructs were equilibrated in optimal cutting temperature embedding medium (OCT, Tissue-Tek, Torrance, CA) overnight at 37°C and then frozen at -20°C. 10 μm thick sections were cut using a cryostat (Micron HM-550 OMP, Vista, CA) and stained using Hematoxylin (cell nuclei) and Eosin (cytoplasm); Masson's trichrome for collagen, cell nuclei, and cytoplasm; Alizarin red for calcium phosphates; von Kossa for mineralization; and Sudan Black for residual polymer. Acellular constructs (n = 2) at week 6 from the TCP/HAp 7:3 and TCP/HAp 1:1 groups were also stained using Alizarin red and von Kossa. The sections from cellular constructs were stained for the presence of collagen type I using immunohistochemistry (IHC). Mouse monoclonal anti-collagen type I (1:200 dilution; Thermofisher Scientific, Waltham, MA) primary antibody was used for the immunostaining. Following the primary antibody, biotinylated secondary antibody was used followed with the ABC complex (Vector Laboratories, Burlingame, CA). The antibodies were visualized with the diaminobenzidine (DAB) substrate per the manufacturer's (Vector Laboratories, Burlingame, CA) protocol. Negative controls were also run with the primary antibody omitted.

STATISTICAL ANALYSES

GraphPad Prism 6 statistical software (GraphPad Software, Inc., La Jolla, CA) was used to compare experimental groups using a one-factor ANOVA (sections 2.6 and 2.7) or a two-factor ANOVA (sections 2.8 and 2.9) followed by a *Tukey's post hoc* test, where $p < 0.05$ was considered significant. Additionally, standard box plots were constructed to eliminate outliers. All quantitative results are reported as average ± standard deviation within text or as average + standard deviation within figures.

RESULTS

SEM AND EDS

Figure 4.2 represents the scanning electron micrographs of all four types of microspheres. The microspheres in the BLANK (i.e., PLGA only) group had a smooth surface, while the microspheres in the BMP, TH73 (TCP/HAp 7:3), and TH11 (TCP/HAp 1:1) groups had minute pores on their surfaces. The BLANK and the BMP microspheres had a spherical morphology, whereas the TH73 and TH11 microspheres had a deflated soccer ball-like appearance with obvious indentations on the surfaces of the microspheres. Figure 4.3 depicts the distribution of atomic calcium (Ca), nitrogen (N) and phosphorous (P) in the interior of BLANK, BMP, and TH11 microspheres. As expected, the three elements were essentially absent from the BLANK microspheres. Nitrogen was uniformly distributed inside the BMP microspheres as demonstrated by the spectral maps. The EDS maps also depicted the presence of phosphorus and calcium in the BMP microspheres. Calcium and phosphorous were uniformly distributed inside the TH11 microspheres, while nitrogen was absent from the TCP/HAp 1:1 group. Figure 4.4 represents the

SEM images of all of the scaffold groups used for the study. All scaffolds were porous in nature with interconnected pores.

MECHANICAL TESTING

BLANK scaffolds had an average compressive modulus of 330 ± 120 kPa that was 80% ($p < 0.05$) and 40-fold ($p < 0.05$) higher than the moduli of TCP/HAp 7:3 and TCP/HAp 1:1 scaffolds, respectively (Figure 4.5). The average moduli of the BMP and TCP/HAp 7:3 groups were 35-fold ($p < 0.05$) and 22-fold ($p < 0.05$) higher than the modulus of the TCP/HAp 1:1 group, respectively. No significant differences in compressive modulus were observed between the BMP and TCP/HAp 7:3 groups, or between the BMP and BLANK groups.

POROSITY MEASUREMENT

The average porosity of the TCP/HAp 1:1 group was 47.7 ± 5.0%, which was 1.9-fold ($p < 0.05$), 1.5-fold ($p < 0.05$), and 1.3-fold ($p < 0.05$) higher than the porosities of the BLANK, BMP, and TCP/HAp 7:3 groups, respectively (Figure 4.6). The porosity of the TCP/HAp 7:3 group was 1.5-fold ($p < 0.05$) higher than the porosity of the BLANK group. No significant differences in porosities were observed between the BLANK and BMP groups.

BIOCHEMICAL ANALYSIS

DNA CONTENT

At week 0, the BLANK group had 8.3-fold ($p < 0.05$) and 3.1-fold ($p < 0.05$) higher DNA content than the TCP/HAp 7:3 and TCP/HAp 1:1 groups, respectively (Figure 4.7). The DNA content of the BMP group at week 0 was 7.2-fold ($p < 0.05$) and 2.7-fold ($p < 0.05$) higher than

the DNA contents of the TCP/HAp 7:3 and TCP/HAp 1:1 groups, respectively. No significant differences in DNA content were observed between the TCP/HAp 7:3 and TCP/HAp 1:1 groups at week 0. Additionally, no significant differences were observed in DNA content among the groups at weeks 3 or 6. The DNA contents in the BLANK and BMP groups at week 0 were statistically significantly higher than their corresponding values at later time points, while no significant changes in DNA content were observed in the TCP/HAp 7:3 and TCP/HAp 1:1 groups over time. The BLANK group at week 0 had 22-fold ($p < 0.05$) and 8.6-fold ($p < 0.05$) higher amounts of DNA than its values at weeks 3 and 6, respectively. The BMP group at week 0 had 29-fold ($p < 0.05$) and 6-fold ($p < 0.05$) higher DNA content than its corresponding values at weeks 3 and 6, respectively.

HYDROXYPROLINE (HYP) CONTENT

At week 0, the BLANK group had 11-fold ($p < 0.05$) higher net HYP content than the BMP group (Figure 4.8A). No significant differences in net HYP content were observed among any other groups at week 0. Additionally, no significant differences in net HYP content were observed among the groups at week 3. Week 6 net HYP content results showed that only the TCP/HAp 7:3 group outperformed the BLANK control, with HYP content that was 2.7-fold ($p < 0.05$) higher. No significant differences in net HYP content were observed among any other groups at week 6. Only the BMP and TCP/HAp 7:3 groups showed significant changes in net HYP content over time. The BMP group at week 6 had 13-fold ($p < 0.05$) higher net HYP than its corresponding value at week 0. The net HYP contents of the TCP/HAp 7:3 group at weeks 3 and 6 were 9.6-fold ($p < 0.05$) and 15-fold ($p < 0.05$) higher than its HYP content at week 0, respectively. In the normalized HYP (per DNA) content, no significant differences were

observed among the groups at weeks 0 and 3 (Figure 4.8B). At week 6, both the TCP/HAp 7:3 and TCP/HAp 1:1 groups outperformed the BLANK control in normalized HYP content with values that were 14-fold ($p < 0.05$) and 6.9-fold ($p < 0.05$) higher, respectively. Moreover, the normalized HYP contents in the TCP/HAp 7:3 and TCP/HAp 1:1 groups at week 6 were 15-fold ($p < 0.05$) and 7.9-fold ($p < 0.05$) higher than the HYP content in the BMP group, respectively. Additionally, the normalized HYP content in the TCP/HAp 7:3 group at week 6 was 2-fold ($p < 0.05$) higher than the HYP content in the TCP/HAp 1:1 group. Only the TCP/HAp 7:3 and TCP/HAp 1:1 groups showed significant changes in normalized HYP content over time. The TCP/HAp 7:3 group at week 6 had 35-fold ($p < 0.05$) and 3.4-fold ($p < 0.05$) higher normalized HYP content than its matching values at weeks 0 and 3, respectively. The TCP/HAp 1:1 group at week 6 had 6.7-fold ($p < 0.05$) higher normalized HYP content than its value at week 0.

ALP ACTIVITY

No significant differences were observed in the ALP activities among the groups at weeks 0 and 3 (Figure 4.9). However, at week 6, the TCP/HAp 7:3 and TCP/HAp 1:1 groups outperformed the BLANK control in ALP activity, with activities that were 40-fold ($p < 0.05$) and 20-fold ($p < 0.05$) higher, respectively. Additionally, the TCP/HAp 7:3 and TCP/HAp 1:1 groups at week 6 surpassed the BMP group in ALP activity, with activities that were 40-fold ($p < 0.05$) and 20-fold ($p < 0.05$) higher, respectively. Also, the ALP activity of the TCP/HAp 7:3 group at week 6 was 2-fold ($p < 0.05$) higher than the ALP activity of the TCP/HAp 1:1 group. Only the TCP/HAp 7:3 showed significant changes in ALP activity over time, with its week 6 activity being 1.8-fold ($p < 0.05$) and 3.3-fold ($p < 0.05$) higher than its activities at weeks 0 and 3, respectively.

CALCIUM CONTENT

The calcium contents for the cellular BLANK and BMP constructs at week 0 were 32.7 ± 5.3 μg and 54 ± 19 μg, respectively. The calcium contents for the TCP/HAp 7:3 and TCP/HAp 1:1 groups (both cellular and acellular) at week 0 are not reported because of inadequate extraction of calcium from these scaffolds at that time point. Week 3 calcium content results showed no significant differences among groups at that time point (Figure 4.10). At week 6, the calcium content of the BMP group was 1.7-fold ($p < 0.05$) higher than the calcium content of the TCP/HAp 1:1 group. The calcium content of the TCP/HAp 7:3 group at week 6 was 3.3-fold ($p < 0.05$) higher than the calcium content of the TCP/HAp 7:3 [Acellular] group. No significant differences were observed in calcium content among the other groups at week 6. The BLANK group at week 3 had 21-fold ($p < 0.05$) and 1.7-fold ($p < 0.05$) higher calcium content than its corresponding values at weeks 0 and 6, respectively. Additionally, the calcium content of the BLANK group at week 6 was 12-fold ($p < 0.05$) higher than its calcium content at week 0. The BMP group at weeks 3 and 6 had 12-fold ($p < 0.05$) and 10-fold ($p < 0.05$) higher calcium contents than its matching value at week 0, respectively. The calcium content of the TCP/HAp 1:1 group at week 3 was 1.7-fold ($p < 0.05$) higher than its corresponding value at week 6. The TCP/HAp 7:3 [Acellular] and TCP/HAp 1:1 [Acellular] groups at week 3 had 3.9-fold ($p < 0.05$) and 3.2-fold ($p < 0.05$) higher amounts of calcium than their matching values at week 6, respectively. No other group showed statistically significant changes in calcium content over time.

GENE EXPRESSION

RUNX2 AND COL1A1

Both the BLANK and the BMP groups at week 0 had 3-fold ($p < 0.05$) higher relative RUNX2 expression than the expression of the TCP/HAp 7:3 group (Figure 4.11A). No significant differences were observed in the RUNX2 expression at week 0 among the BLANK, BMP and TCP/HAp 1:1 groups. At week 1.5, the RUNX2 expression for the TCP/HAP 7:3 group was 2.1-fold ($p < 0.05$) and 3.8-fold ($p < 0.05$) higher than the expression values for the BMP and TCP/HAp 1:1 groups, respectively. No significant differences in RUNX2 expression were observed among the groups at weeks 3 and 6. The TCP/HAp 7:3 and TCP/HAp 1:1 groups were the only groups that showed statistically significant changes in RUNX2 expression over time. The TCP/HAp 7:3 group at week 0 had 7.3-fold ($p < 0.05$) higher expression than at week 6. At week 1.5, the TCP/HAp 7:3 group had 4.2-fold ($p < 0.05$) and 31-fold ($p < 0.05$) higher RUNX2 expression than its matching values at weeks 0 and 6, respectively. Moreover, the TCP/HAp 7:3 group at week 3 had 18-fold ($p < 0.05$) higher RUNX2 expression than its expression at week 6. The TCP/HAP 1:1 group at week 3 had 3.7-fold ($p < 0.05$), 4.3-fold ($p < 0.05$), and 2.8-fold ($p < 0.05$) higher RUNX 2 expression than its expression values at weeks 0, 1.5, and 6, respectively.

The COL1A1 (collagen I) expression values (Figure 4.11B) of the BLANK, BMP, and TCP/HAp 1:1 groups at week 0 were 2-fold ($p < 0.05$), 2-fold ($p < 0.05$), and 1.7-fold ($p < 0.05$) higher than the expression value of the TCP/HAp 7:3 group, respectively. No significant differences were observed in COL1A1 expression among the BLANK, BMP, and TCP/HAp 1:1 groups at week 0. Additionally, no significant differences were observed in COL1A1 expression among the groups at weeks 1.5 and 3. At week 6, the TCP/HAP 1:1 group outperformed the BLANK and BMP controls in COL1A1 expression with 7.5-fold ($p < 0.05$) and 15-fold ($p <$

0.05) higher expression, respectively. In addition, the TCP/HAp 1:1 group at week 6 had 60-fold ($p < 0.05$) higher COL1A1 expression than the TCP/HAp 7:3 group at that time point. All of the groups showed statistically significant changes in COL1A1 expression over time. The BLANK group at week 0 had 5.4-fold ($p < 0.05$), 9.8-fold ($p < 0.05$), and 12-fold ($p < 0.05$) higher COL1A1 expression than its corresponding values at weeks 1.5, 3, and 6, respectively. The BMP group at week 0 had 7.4-fold ($p < 0.05$), 11-fold ($p < 0.05$), and 24-fold ($p < 0.05$) higher COL1A1 expression than its matching values at weeks 1.5, 3, and 6, respectively. The COL1A1 expression values of the TCP/HAp 7:3 group at weeks 0 and 1.5 were 48-fold ($p < 0.05$) and 34-fold ($p < 0.05$) higher than its week 6 value, respectively. The TCP/HAp 1:1 group at week 0 had 3.8-fold ($p < 0.05$) and 2.1-fold ($p < 0.05$) higher COL1A1 expression than its corresponding expression at weeks 1.5 and 3, respectively. Additionally, the TCP/HAp 1:1 group at week 6 had 2.7-fold ($p < 0.05$) higher COL1A1 expression than its matching value at week 1.5.

BGLAP AND IBSP

The BGLAP expression values for the BLANK group at weeks 1.5, 3, and 6; BMP group at weeks 1.5 and 3; TCP/HAp 7:3 group at week 3; and TCP/HAp 1:1 group at weeks 1.5 and 3, were marked as zero because the fluorescence intensities in these samples did not cross the threshold fluorescence. BGLAP expression (Figure 4.11C) showed no significant differences among groups at week 0. At week 1.5, the relative BGLAP expression of the TCP/HAp 7:3 group was statistically significantly ($p < 0.05$) higher than the expression of the BLANK, BMP, and TCP/HAp 1:1 groups. No significant differences were observed in BGLAP expression among the groups at week 3. Week 6 BGLAP expression showed that the BMP group expression was statistically significantly ($p < 0.05$) higher than the expression of the BLANK group. In

addition, the BMP group BGLAP expression at week 6 was 74-fold ($p < 0.05$) higher than the expression of the TCP/HAp 7:3 group. No significant differences in BGLAP expression were observed at week 6 between the BMP and TCP/HAp 1:1 groups. Only the BMP and TCP/HAp 7:3 groups showed statistically significant changes in BGLAP expression over time. The BMP group at week 6 had statistically significantly ($p < 0.05$) higher BGLAP expression than its expression values at weeks 1.5 and 3. The TCP/HAp 7:3 group at week 1.5 had 14-fold ($p < 0.05$) and 113-fold ($p < 0.05$) higher BGLAP expression than its corresponding values at weeks 0 and 6. Moreover, the TCP/HAp 7:3 group at weeks 1.5 and 6 had statistically significantly ($p < 0.05$) higher BGLAP expression than its value at week 3.

The IBSP expression values for the BLANK group at weeks 1.5 and 3; BMP group at weeks 3 and 6; TCP/HAp 7:3 group at weeks 1.5, 3, and 6; and TCP/HAp 1:1 group at weeks 1.5 and 3, were marked as zero because the fluorescence intensities in these samples did not cross the threshold fluorescence. No significant differences were observed in IBSP expression among the groups at weeks 0, 1.5 and 3 (Figure 4.11D). The TCP/HAp 1:1 group at week 6 outperformed the BLANK control with 98-fold ($p < 0.05$) higher IBSP expression. Moreover, the IBSP expression for the TCP/HAp 1:1 group at week 6 was statistically significantly ($p < 0.05$) higher than the expression of the BMP and TCP/HAp 7:3 groups. Only the TCP/HAp 1:1 group showed statistical significant changes in IBSP expression over time. The TCP/HAp 1:1 group at week 6 had 193-fold ($p < 0.05$) higher IBSP expression than its corresponding expression at week 0. Additionally, the TCP/HAp 1:1 group at week 6 had statistically significantly ($p < 0.05$) higher expression than its matching values at weeks 1.5 and 3.

HISTOLOGY AND IMMUNOHISTOCHEMISTRY

Figure 4.12 represents the histological staining for the BLANK, BMP, TH73 (TCP/HAp 7:3), and TH11 (TCP/HAp 1:1) groups at week 6. From H&E staining, it was clear that the BLANK and BMP groups were primarily tissue without any evidence of spherical microsphere shapes as observed in the TH73 and TH11 groups. Additionally, H&E images indicated toward higher cell numbers in the BLANK and BMP groups compared to the TCP/HAp groups. Masson's trichrome staining images showed no apparent differences in staining intensities between the BLANK and BMP groups or between the TCP/HAp 7:3 and TCP/HAp 1:1 groups. The TCP/HAp groups had higher numbers of blue stained specks for collagen (indicated by arrows in than those observed in the BLANK and BMP groups. Alizarin red and von Kossa staining for calcium and calcium deposits was observed in all of the groups. The TCP/HAp 7:3 group stained more intensely for calcium and calcium deposits than the TCP/HAp 1:1 group, while no differences in staining intensities were observed between the BLANK and BMP groups. Additionally, the TCP/HAp groups had higher staining intensities for both the Alizarin Red and von Kossa than the staining intensities in the BLANK and BMP groups. The higher staining intensities for Alizarin red and von Kossa in the TCP/HAp scaffolds could be attributed to inherent calcium present in these scaffolds, which was confirmed by the histological images of the acellular TCP/HAp scaffolds (Figure 4.13). All of the groups stained positively for Sudan Black, and microsphere architecture was evident in the TCP/HAp groups, whereas no discernable microsphere shapes were noted in the BLANK and BMP groups. The observance of intact microsphere structure with Sudan Black staining suggest that TCP and HAp encapsulation might have altered polymer degradation, which was also indicated by the macroscopic observations where the culture medium in the acellular BLANK and BMP scaffolds became

acidic more rapidly than the medium in their TCP/HAp counterparts (Figure 4.14). Immunohistochemical (IHC) staining of week 6 microsphere-based scaffolds was positive for collagen I (Figure 4.15). Collagen I staining was more intense in the TCP/HAp 1:1 group than the staining in the BLANK and TCP/HAp 7:3 groups. Moreover, the BMP group had more intense staining for collagen I than the staining in the BLANK group.

DISCUSSION

The current study was the first to examine the effects of encapsulating TCP and HAp mixtures for stimulating osteogenesis in microsphere-based scaffolds. This work builds on our previous efforts establishing that incorporation of inorganic materials such as TCP, HAp, and bioactive glass (BG) alone in microsphere-based scaffolds provides both bioactive cues and building blocks for osteogenic differentiation of cells[61, 89, 169, 172, 173]. Additionally, it has been shown by others that combining TCP and HAp for bone regeneration is a promising strategy given that a combination of these materials provides both osteoinductive and osteoconductive cues to the surrounding cells[71, 85, 98, 103, 132, 141, 201, 203]. Furthermore, we have previously demonstrated that higher concentrations (10 and 20 wt%) of TCP and HAp in microsphere-based scaffolds were more favorable for synthesis of ECM components relevant to bone tissue, thus providing the motivation for encapsulating even higher concentrations of TCP and HAp than our previous reported studies[61, 89]. Hence, the present study investigated the response of rBMSCs to TCP/HAp mixtures, encapsulated at a concentration of 30 wt%, during osteogenic differentiation on microsphere-based scaffolds.

The SEM images depicted that all four types of microspheres were uniform in size, with average microsphere diameter ranging between 172-186 μm (Figure 4.1). The BMP, TH73

(TCP/HAP 7:3), and TH11 (TCP/HAp 1:1) microspheres possessed micron and sub-micron pores on their surface, which could be attributed to the solvent removal process during microsphere fabrication[214]. Additionally, it was observed that the TH73 and TH11 microspheres had a deflated soccer ball-like shape. The deflated shape and the presence of pores on the surface of the microspheres may have contributed toward higher average porosities in the TCP/HAp 7:3 and TCP/HAp 1:1 scaffolds compared to the BLANK group. The deflated shapes might have resulted from the incongruent solvent exchange across the microsphere surface as a direct consequence of changes in emulsion viscosity due to addition of TCP/HAp mixtures into the polymer phase. We observed a similar phenomenon with PLGA microspheres containing bioactive glass (BG), where these microspheres were spherical in shape at the time of fabrication but lost their shape during the droplet hardening step[172]. Similar to our observations, Bao *et al*.[12] noted that the encapsulation of biphasic calcium phosphates (BCP) at a concentration of 30% or higher in poly(ε-caprolactone) microspheres fabricated using the emulsion solvent-evaporation method, also resulted in irregularly-shaped microspheres. It was suggested that the viscosity of the dispersion mixture of polymer and BCP increased with BCP concentrations higher than 30%, thereby affecting the dispersibility of the microemulsion in the continuous phase and also the efflux velocity of solvent during the solvent exchange that further led to non-uniform shaped microspheres with sunken structures. Although we noticed differences in microsphere morphologies among the groups, the scaffolds in all the groups were found to be porous in nature with interconnections among the pores, which agreed with our previous findings[89, 215]. Furthermore, the elemental distribution of calcium and phosphorus as observed via EDS confirmed the uniform distribution of calcium phosphates inside the TCP/HAp microspheres with no evidence of agglomeration at any site. The BMP microspheres depicted the presence of

phosphorus that could be attributed to the PBS buffer used for reconstitution of the protein. The presence of calcium in BMP microspheres could be regarded as artifacts of the automatic peak identification software used for the EDS analysis[177].

Uniaxial compression testing results showed that the compressive moduli of microsphere-based scaffolds were within an order of magnitude of the moduli for cancellous bone[128, 250]. The compressive modulus of BLANK scaffolds was found to be at least 2 times as large as the moduli of the TCP/HAP 7:3 and TCP/HAp 1:1 groups, while the porosities of the TCP/HAp groups were at least 1.5 times larger than the porosity of the BLANK scaffolds. The compressive modulus results agreed with our previous findings that the presence and subsequent modification of microspheres by calcium phosphates led to lower moduli of TCP/HAp scaffolds compared to the BLANK controls[61, 214]. Additionally, the modulus of TCP/HAp 1:1 scaffolds was significantly lower than the moduli of the BMP and TCP/HAp 7:3 groups. The lower modulus in the TCP/HAp 1:1 group may be attributed to its higher porosity as it has been shown that the compressive modulus is inversely related to the porosity of scaffolds[175, 222].

The biochemical content results revealed some interesting trends. It was observed that the TCP/HAp scaffolds at week 0 (24 h post seeding) had significantly lower DNA contents than the BLANK and BMP controls. Kucharska *et al.*[139] observed a similar trend in initial cell numbers when they cultured MG-63 osteoblast-like cells on chitosan-TCP microsphere based scaffolds. The cell numbers on the chitosan-TCP scaffolds were significantly lower than the controls 48 h post seeding; however, the elevated ALP activity of the cells at that time point suggested that the cells on the chitosan-TCP were being directed toward osteogenic differentiation as early as 2 days after seeding. Our ALP data at week 0 hint toward a similar phenomenon where rBMSCs were being directed toward osteogenic differentiation; however, no significant differences were

observed in the ALP activities among groups at week 0. Although the DNA content was lower in the TCP/HAp groups initially, no significant differences were observed in DNA content among the study groups at later time points. The HYP and ALP results suggest that the incorporation of TCP and HAp in microsphere-based scaffolds enhanced synthesis of bone-relevant ECM components over time. The TCP/HAp groups at 6 weeks had roughly 8 times the amount of collagen per cell (HYP/DNA) as the BLANK and BMP controls, a trend we previously observed with HAp-only microsphere-based scaffolds with comparable HYP amounts compared to the HAp-only scaffolds[61]. In addition, the ALP activities in the TCP/HAp groups at week 6 were approximately 20 times higher than the activities in the BLANK and BMP groups at that time point. The total calcium content analysis suggests that the calcium detected in the TCP/HAp groups predominantly represented the inherent calcium remaining in these scaffolds. However, it was observed that the calcium content in the TCP/HAp 7:3 group at week 6 was about 1.4 times higher than the calcium content of its acellular equivalent. Additionally, the TCP/HAp 7:3 calcium content at week 6 was comparable to its week 3 value, indicating that the cells might have retarded microsphere degradation, perhaps by covering the microspheres with collagen, etc. Higher secretion of calcium by the cells or incorporation of inherent calcium into the newly synthesized might have also contributed to the observed differences in calcium content between the acellular and cellular scaffolds in the TCP/HAp 7:3 group.

Gene expression data highlighted some key differences in the differentiation of rBMSCs on TCP/HAp scaffolds compared to those on the BLANK and BMP scaffolds. The TCP/HAp groups compared to the BLANK and BMP controls had lower expression values for RUNX2, COL1A1, and IBSP expression early on and had higher expression values at later time points. These differences in the expression of TCP/HAP groups and controls indicated that the presence

of TCP/HAp may have inhibited expression of osteogenic markers initially[61, 89]. On the other hand, elevated expression of osteogenic genes in the TCP/HAp groups at later time points signifies that the incorporation of ceramic mixture propelled the differentiation of the seeded cells toward osteogenic lineage. Furthermore, differences in gene expression were observed between the TCP/HAp encapsulating groups with both the groups showing fluctuating expressions for RUNX2, COL1A1, and BGLAP over time. These oscillating expression patterns in the TCP/HAp groups may suggest that the rBMSCs responded differently to different TCP/HAp ratios in microsphere-based scaffolds[6, 71, 85, 103, 141].

Histological images of the engineered constructs at week 6 suggested higher cell numbers in the BLANK and BMP groups compared to the TCP/HAp groups. However, failure to observe any statistically significant differences in DNA content at week 6 among groups suggest that observed differences in cell number (if any) might have been due to differences in initial cell attachment. Masson's trichrome images pointed toward higher collagen synthesis in the TCP/HAp groups, thus agreeing with the biochemical results of the study that demonstrated higher collagen synthesis (on per cell basis) in TCP/HAp constructs at 6 weeks. Additionally, collagen I IHC images depicted that the TCP/HAp 1:1 scaffolds at week 6 stained more intensely for collagen I than the TCP/HAp 7:3 scaffolds, further concurring with the gene expression data where COL1A1 expression in TCP/HAp 1:1 scaffolds at week 6 was significantly higher than the TCP/HAp 1:1 group at that time point. Alizarin red and von Kossa stains demonstrated that all scaffold groups possessed a mineral matrix of calcium and calcium phosphates at week 6, with the TCP/HAp encapsulating groups exhibiting the most-intense staining. Additionally, the staining intensities for Alizarin red and von Kossa stains were higher in the TCP/HAp 7:3 group at week 6 than the intensities in the TCP/HAp 1:1 group at that time point. Furthermore, it was

observed that the mineral staining intensities in the TCP/HAp 7:3 group at week 6 were higher than their acellular counterparts (Figure 4.13). The TCP/HAp constructs are expected to stain positive for mineralization because of inherent mineral present in these scaffolds. The higher mineral staining intensities in the TCP/HAp 7:3 at week 6 suggest that the cells in the TCP/HAp 7:3 group either made more calcium or utilized inherent calcium as a raw material in the ECM, thereby agreeing with the calcium content results. Sudan Black staining indicated presence of residual polymer in all of the groups after 6 weeks of culture, although residual spherical shapes of the microspheres were evident only in the TCP/HAp groups. Additionally, the TCP/HAp scaffolds had a lower degree of swelling throughout the 6-week culture period than the BLANK and BMP scaffolds. The observance of intact microsphere structure with Sudan Black staining and less severity of the macroscopic changes in the TCP/HAp groups suggest that TCP and HAp encapsulation might have retarded polymer degradation due to their intrinsic buffering capacity[1].

Overall, the results of the current study demonstrated that TCP/HAp encapsulation into microsphere-based scaffolds altered microsphere morphology, impacted the mechanical properties of the scaffolds (i.e., reduced moduli) and influenced the differentiation of the seeded rBMSCs toward an osteogenic lineage. Higher end point ECM synthesis and enhanced expression of osteogenic markers in TCP/HAp groups relative to the BMP-2 group suggest that the TCP/HAp encapsulation fast-tracked the osteogenic commitment of cells on these scaffolds. Additionally, biochemical and gene expression evidence was presented for the TCP/HAp groups outperforming the BLANK and BMP controls. Furthermore, differences in gene expression profiles between the TCP/HAp groups hint that the cells responded differently to two different ratios of TCP and HAp presented to them. Lastly, we did not specifically explore degradation of the TCP/HAp scaffolds; however, our histological and macroscopic findings indicate that the

presence of TCP/HAp altered polymer degradation in microsphere-based scaffolds[181, 256]. Altogether, it can be concluded that TCP/HAp mixtures when incorporated into microsphere-based gradient scaffolds may be able to enhance the performance of the bone-like region of the engineered construct by providing raw materials for the regenerating tissue.

CHAPTER 5: MICROSPHERE-BASED SCAFFOLDS ENCAPSULATING CHONDROITIN SULFATE OR DECELLULARIZED CARTILAGE**

ABSTRACT

Extracellular matrix (ECM) materials such as decellularized cartilage (DCC) and chondroitin sulfate (CS) may be attractive chondrogenic materials for cartilage regeneration. The goal of the current study was to investigate the effects of encapsulation of DCC and CS in homogeneous microsphere-based scaffolds, and to test the hypothesis that encapsulation of these ECM materials would induce chondrogenesis of rat bone marrow stromal cells (rBMSCs). Four different types of homogeneous scaffolds were fabricated from microspheres of poly(D,L-lactic-co-glycolic acid) (PLGA): Blank (PLGA only; negative control), transforming growth factor (TGF)-β_3 encapsulated (positive control), DCC encapsulated, and CS encapsulated. These scaffolds were then seeded with rBMSCs and cultured for 6 weeks. The DCC and CS encapsulation altered the morphological features of the microspheres, resulting in higher porosities in these groups. Moreover, the mechanical properties of the scaffolds were impacted due to differences in the degree of sintering, with the CS group exhibiting the highest compressive modulus. Biochemical evidence suggested a mitogenic effect of DCC and CS encapsulation on rBMSCs with the matrix synthesis boosted primarily by the inherently present ECM components. An important finding was that the cell seeded CS and DCC groups at week 6 had up to an order of magnitude higher GAG contents than their acellular counterparts. Gene expression results indicated a suppressive effect of DCC and CS encapsulation on rBMSC chondrogenesis with differences in gene expression patterns existing between the DCC and CS groups. Overall, DCC and CS were easily included in microsphere-based scaffolds; however,

To be submitted as **Gupta V, Tenny K, Barragan M, Berkland C, Detamore M, Microsphere-Based Scaffolds Encapsulating Chondroitin Sulfate and Decellularized Cartilage, *Journal of Biomedical Materials Research Part A*, 2015.

there is a requirement to further refine their concentrations to achieve the differentiation profiles we seek *in vitro*.

INTRODUCTION

Scaffold-based regenerative strategies for osteochondral tissue that take into consideration physiological and hierarchical variations in properties of native bone and cartilage have been increasingly gaining attention[56, 155, 205, 209]. Several of these strategies employ extracellular matrix (ECM)-based materials because of their ability to regulate behavior such as migration, proliferation and differentiation of resident or transplanted cells[17, 37]. For cartilage regeneration, cartilage matrix has been used as a chondroinductive material because of its potential to retain bioactive molecules to which the regenerating tissue is naturally predisposed to respond[17, 38, 83, 227]. Moreover, materials like chondroitin sulfate (CS), the major sulfated glycosaminoglycan (GAG) found in the ECM of native cartilage, are used for cartilage regeneration because of their ability to create a favorable microenvironment for cells[102, 163, 202].

Microsphere-based scaffolds possess an immense potential for musculoskeletal regeneration because of their characteristics like rigidity in shape, ability to provide a porous network, and uniform mechanical properties[101]. Additionally, they offer a variety of alternatives in terms of materials for microsphere matrices, and methods for microsphere fabrication and sintering[18, 21, 25, 29, 32, 184]. We have previously demonstrated that three-dimensional (3D) microsphere-based gradient scaffolds containing gradients of growth factors are capable of directing cell phenotype by influencing them to secrete tissue-specific ECM components to promote osteochondral regeneration[58, 63, 65, 169]. In addition, we have shown that microsphere-based scaffolds containing gradients of CS and tricalcium phosphate can provide "raw materials"

for synthesis of new ECM components, and in combination with growth factors (or alone) can furnish the surrounding progenitor cells with bioactive signals for their differentiation along the chondro- and osteogenic lineages in different regions of the scaffolds[89, 172, 173]. Furthermore, we recently evaluated the response of decellularized cartilage (DCC) encapsulation in homogeneous microsphere-based scaffolds. The DCC encapsulation at a concentration of 10 wt% evoked a biosynthetic response from the seeded rat bone marrow stromal cells (rBMSCs) with comparable gene expression to cells seeded on transforming growth factor-β_3 (TGF-β_3) encapsulated scaffolds[227]. To establish the benefits of our raw material gradient microsphere-based scaffolds, it is imperative to identify raw materials that are most efficacious in promoting osteogenesis and chondrogenesis. For determining the leading chondrogenic materials, the most rational step would be to evaluate the performance of homogeneous microsphere-based scaffolds incorporating chondrogenic materials in propelling chondrogenesis. Therefore, the objective of this study was to investigate the effects of encapsulating a higher concentration of ECM materials (DCC and CS), compared to what we have previously used, on influencing rBMSC chondrogenesis in homogeneous microsphere-based scaffolds. The results would have implications for identifying raw material concentrations that can then be combined with osteogenic raw materials for use in microsphere-based gradient scaffolds toward osteochondral repair.

In the present study, we investigated whether encapsulated raw materials (DCC and CS) at a higher concentration in poly(D,L-lactic-co-glycolic acid) (PLGA) microsphere-based scaffolds would provide building blocks and drive the differentiation of the seeded cells toward a chondrogenic lineage. Homogeneous microsphere-based scaffolds were fabricated encapsulating DCC and CS (at a concentration of 30 wt%) as chondrogenic raw materials. The response of

seeded rBMSCs to the raw materials was evaluated when cultured for 6 weeks in a medium consisting of dissolved factors. We hypothesized that encapsulation of raw materials, DCC or CS, in homogeneous microsphere-based scaffolds would induce chondrogenesis in rBMSCs.

MATERIALS AND METHODS

MATERIALS

All reagents for the decellularization process were purchased from Sigma–Aldrich (St. Louis, MO) unless otherwise noted. Poly(D,L-lactic-co-glycolic acid) (PLGA) (50:50 lactic acid: glycolic acid ratio, ester end group) with an intrinsic viscosity (i.v.) of 0.37 dl/g, was obtained from Evonik Industries (Essen, Germany). Human TGF-β_3 and Murine insulin-like growth factor (IGF)-I were obtained from PeproTech, Inc. (Rocky Hill, NJ). Chondroitin sulfate A sodium salt (from bovine trachea) was obtained from Sigma (St. Louis, MO). All other reagents and organic solvents utilized were of cell culture or ACS grade. Two porcine knees obtained from a Berkshire hog (castrated male that was approximately 7-8 months old and weighed 120 kg) were purchased from a local abattoir (Bichelmeyer Meats, Kansas City, KS).

TISSUE RETRIEVAL AND DECELLULARIZATION

Articular cartilage was harvested from hip and knee joint surfaces using scalpels and immediately rinsed in phosphate buffered saline (PBS). PBS was then drained from the cartilage and the tissue was stored at -20 °C. After freezing overnight, the cartilage was thawed and coarsely cryoground with dry ice pellets using a cryogenic tissue grinder (BioSpec Products, Bartlesville, OK). The dry ice was allowed to sublime overnight in the freezer. Decellularization of the cartilage was performed using our previously described protocol[225, 227]. Coarse-ground

cartilage particles were packed into dialysis tubing (3500 MWCO) and stored in hypertonic salt solution (HSS) overnight at room temperature with gentle agitation (70 rpm). The packets were then subjected to 220 rpm agitation with two reciprocating washes, encompassing triton X-100 (0.01% v/v) followed with HSS, to permeabilize intact cellular membranes. The tissue was then treated overnight with benzonase (0.0625 KU ml^{-1}) at 37 ºC and later treated with sodium-lauroylsarcosine (NLS, 1% v/v) overnight to further lyse cells and denature cellular proteins. After NLS exposure, the tissue was washed with ethanol (40% v/v) at 50 rpm and subjected to organic exchange resins to extract the organic solvents at 65 rpm. Afterward, the tissue was washed in saline-mannitol solution at 50 rpm followed by two hours of rinsing with DI water at 220 rpm. The tissue was then removed from the packets and was frozen and lyophilized. The decellularized cartilage (DCC) particles were further cryoground into a fine powder with a freezer-mill (SPEX SamplePrep, Metuchen, NJ) and then lyophilized. The DCC powder was filtered using a 45 μm mesh (ThermoFisher Scientific, Waltham, MA) to remove large particles and then frozen until use.

PREPARATION OF MICROSPHERES

Four different types of microspheres were fabricated for the study: (i) PLGA microspheres (BLANK), (ii) TGF-β_3 encapsulated in PLGA microspheres (TGF), (iii) DCC encapsulated in PLGA microspheres (DCC), and (iv) Chondroitin sulfate encapsulated in PLGA microspheres (CS). For fabricating TGF-β_3 encapsulated microspheres, TGF-β_3 was first reconstituted in 10 mM citric acid. The reconstituted protein solution was mixed with 20% w/v PLGA dissolved in dichloromethane (DCM) at a loading of 30 ng TGF-β_3 per 1.0 mg of PLGA. The final mixture was then sonicated over ice (50% amplitude, 20 s). The DCC and CS encapsulated microspheres

were fabricated by adding 6% w/v DCC or 6% w/v CS to 14% w/v PLGA dissolved in DCM, respectively. Using the PLGA-protein and PLGA-DCC/CS emulsions, microspheres were fabricated via our previously reported technology[58, 61, 63, 65, 89, 114, 169, 172, 173, 214, 215, 227]. In brief, using acoustic excitation produced by an ultrasonic transducer (Branson Ultrasonics, Danbury, CT), regular jet instabilities were created in the polymer stream, thereby creating uniform polymer droplets. An annular carrier non-solvent stream of 0.5% w/v poly (vinyl alcohol) (PVA, 88% hydrolyzed, 25 kDa, Polysciences, Inc., Warrington, PA) in deionized water (DI H_2O) carried the droplets (i.e., nicrospheres) into a beaker containing the non-solvent solution at 0.5% w/v in DI H_2O (cold PVA solution in case of DCC microspheres). The microspheres were stirred for 1 h to allow for solvent to evaporate and then filtered, rinsed and stored at -20°C. The microspheres were then lyophilized for 48 h before further use.

SCAFFOLD FABRICATION

Scaffolds were prepared using our previously established technology[58, 61, 63, 65, 89, 169, 172, 173, 214, 215, 227]. Briefly, lyophilized microspheres (30-50 mg) were dispersed in DI H_2O and loaded into a syringe. The dispersion was then pumped using a programmable syringe pump (PHD 22/2000; Harvard Apparatus, Inc., Holliston, MA) into a cylindrical plastic mold (diameter ~ 4 mm) having a filter at the bottom until a height of about 2 mm was reached. The scaffolds were 3.8-4.0 mm in diameter and around 2 mm in height. The packed microspheres were then sintered with ethanol-acetone (95:5 v/v) for 55 min. The scaffolds were lyophilized for 48 h and sterilized with ethylene oxide for 12 h prior to cell seeding experiments. A total of four different groups were tested in the study and were named according to the composition of microspheres as: BLANK, TGF, DCC, and CS.

CELL SEEDING OF SCAFFOLDS

rBMSCs were obtained from the femurs of eight young male Sprague–Dawley rats (176–200 g, SASCO) following a University of Kansas approved IACUC protocol (175–08) and cultured in medium consisting of αMEM supplemented with 10% FBS (MSC-Qualified, cat #10437-028) and 1% penicillin–streptomycin (P/S) (all from Thermofisher Scientific, Waltham, MA). When the cells were 80% to 90% confluent, they were trypsinized and re-plated at 7,500 cells/cm^2. Seeding was performed when cells reached P4. Scaffolds were sterilized using ethylene oxide for 12 h, allowed to ventilate overnight after sterilization, and placed in a 48-well plate. Cells (P4) were resuspended in culture medium at a concentration of approximately 50 million/mL. 25 μL of this cell suspension (~1.25M cells) was placed directly onto the top of the scaffold, which infiltrated the scaffold via capillary action.[61, 89] Cells were allowed to attach for 1 h, after which 1 mL of culture medium was added. After 24 h, the culture medium was replaced by 1 mL of differentiation medium consisting of αMEM, 1% P/S, 10% FBS, 50 μg/mL ascorbic acid (Sigma, St. Louis, MO), 40 μg/mL L-proline (Sigma, St. Louis, MO), 100 μM sodium pyruvate (Thermofisher Scientific, Waltham, MA), 100 nM dexamethasone (DEX) (MP Biomedicals, Santa Ana, CA), 1% insulin-transferrin-selenium 100X (ITS) (Thermofisher Scientific, Waltham, MA), 1% non-essential amino acids (NEAA) (Thermofisher Scientific, Waltham, MA), 15 mM HEPES buffer (Thermofisher Scientific, Waltham, MA), and 100 ng/mL murine IGF-I. Every 48 h for 6 weeks, three-fourths of the differentiation medium was replaced with fresh medium.

SCANNING ELECTRON MICROSCOPY (SEM) AND ENERGY DISPERSION SPECTROSCOPY (EDS)

Microspheres and acellular scaffolds were imaged via a Versa 3D Dual Beam (FEI, Hillsboro, OR) scanning electron microscope (SEM) with a detector for energy dispersive spectroscopy (EDS). The microspheres were cryo-fractured using a sharp blade, and the dispersion of TGF-β_3, DCC and CS within the microspheres was further analyzed using EDS at an accelerating voltage of 10 kV. Pixel maps for atomic nitrogen and sulfur were generated using Aztec analysis software (Oxford Instruments, Abingdon, United Kingdom). The PLGA (BLANK) microspheres were also imaged to confirm the absence of nitrogen and sulfur in the EDS maps (Figure 5.1).

MECHANICAL TESTING

Unconfined compression tests of acellular (i.e., week 0) microsphere-based scaffolds (n = 6) were conducted using a uniaxial testing apparatus (Instron Model 5848, Canton, MA) with a 50 N load cell. A custom-made stainless steel bath and a compression-plate assembly were mounted in the apparatus[212]. Cylindrical scaffold samples were compressed to 40% strain at a strain rate of 10%/min in phosphate-buffered saline [PBS—0.138 M sodium chloride, 0.0027 M potassium chloride] at 37°C. Compressive moduli of elasticity were calculated from the initial linear regions of the stress-strain curves (i.e., at ~5% strain) as described previously[61, 89, 172, 214, 215, 227].

POROSITY MEASUREMENT

A fluid saturation method as described previously[89] was used in this study to calculate the porosities of the scaffolds:

$$V_B = 4m \div \pi d^2 h,$$
$$W_{Water} = W_W - W_D,$$

$$V_P = W_{Water} \div \rho_{Water},$$
$$\text{Porosity } (\varphi)(\%) = (V_P \div V_B) \times 100\%$$

where V_B, m, d, h, W_W, W_D, V_P are the bulk volume, mass, diameter, height, wet weight, dry weight, and pore volume of the scaffolds, respectively. W_{Water} and ρ_{Water} are the weight and density of water. Briefly, wet and dry weights of scaffolds were recorded after fabrication and porosities were determined by the above-described equations.

BIOCHEMICAL ANALYSES

Engineered constructs (n = 6) were analyzed for matrix production at 0 (i.e., 24 h post seeding), 3, and 6 weeks. The samples were digested in papain solution consisting of 125 mg/mL papain (from papaya latex), 5 mM N-acetyl cysteine, 5 mM ethylenediaminetetraacetic acid, and 100 mM potassium phosphate buffer (20 mM monobasic potassium phosphate, 79 mM dibasic potassium phosphate) (all reagents from Sigma Aldrich) in DI H_2O. Engineered constructs were removed from culture in a sterile manner, placed in microcentrifuge tubes, homogenized with the papain solution (1 mL), and allowed to digest overnight in a 60°C water bath. The digested scaffolds were then centrifuged at 10,000 rpm for 5 minutes to pellet fragments of polymer and other impurities and stored at -20°C. Later, the supernatant was used to determine DNA, GAG, and hydroxyproline (HYP) contents using the PicoGreen (Molecular Probes, Eugene, OR), dimethylmethylene blue (DMMB) (Biocolor, Newtownabbey, Northern Ireland), and HYP (cat #MAK008, Sigma Aldrich, St. Louis, MO) assays, respectively. The acellular controls from the DCC group were also analyzed for their inherent DNA, HYP and GAG content while the CS group acellular scaffolds were evaluated for their GAG content only at weeks 0, 3, and 6. The DNA content values of the acellular DCC scaffolds were subtracted from the corresponding

values of their cellular counterparts at each time point in an effort to distinguish cell proliferation on the cellular DCC scaffolds from the residual DNA present in these scaffolds.

GENE EXPRESSION ANALYSES

Reverse transcriptase quantitative polymerase chain reaction (RT-qPCR) was performed for gene expression analyses in microsphere-based constructs (n = 6) at weeks 0, 1.5, 3, and 6. Certain groups at certain time points (indicated in Results section) had no Ct values, indicating that the fluorescence intensities in these samples did not cross the threshold fluorescence. These samples were marked as zero for RNA expression. RNA was isolated and purified using QIAshredders and an RNeasy Kit (Qiagen, Valencia, CA) according to the manufacturer's guidelines. Isolated RNA was converted to complementary DNA using a TaqMan High Capacity kit (Applied Biosystems, Foster City, CA) in an Eppendorf RealPlex Mastercycler. TaqMan Gene expression assays from Applied Biosystems for appropriate genes (Table 5.1) were run in the Eppendorf system. A $2^{-\Delta\Delta Ct}$ method was used to evaluate the relative level of expression for each target gene. For quantification, the BLANK constructs at week 0 were designated as the calibrator group and GAPDH expression as the endogenous control.

HISTOLOGY AND IMMUNOHISTOCHEMISTRY (IHC)

At 6 weeks, microsphere-based constructs (n = 3) were soaked in 30% w/v sucrose (Thermofisher Scientific, Waltham, MA) solution in PBS for 24 h. Afterward, the constructs were equilibrated in optimal cutting temperature embedding medium (OCT, Tissue-Tek, Torrance, CA) overnight at 37°C and then frozen at -20°C. 10 μm thick sections were cut using a cryostat (Micron HM-550 OMP, Vista, CA) and stained using Hematoxylin (cell nuclei) and

Eosin (cytoplasm); Masson's trichrome for collagen, cell nuclei, and cytoplasm; Safranin O for GAGs; and Sudan Black for residual polymer. Acellular constructs (n = 2) at week 6 from the DCC and CS groups were also stained using Safranin O. The sections from cellular constructs were stained for the presence of collagen type I, collagen type II and aggrecan using immunohistochemistry (IHC). Mouse monoclonal primary antibodies (all from Thermofisher Scientific, Waltham, MA) against collagen type I (1:200 dilution), collagen type II (1:200 dilution), and aggrecan (1:50 dilution) were used for the immunostaining. Following the primary antibody, biotinylated secondary antibody was used followed with the ABC complex (Vector Laboratories, Burlingame, CA). The antibodies were visualized with the diaminobenzidine (DAB) substrate per the manufacturer's (Vector Laboratories) protocol. Negative controls were also run with the primary antibody omitted. Histological and IHC staining images from the CS constructs could not be obtained as the sections washed off the slides during the procedures of staining, washing, dehydration, and clearing.

STATISTICAL ANALYSES

GraphPad Prism 6 statistical software (GraphPad Software, Inc., La Jolla, CA) was used to compare experimental groups using a one-factor ANOVA (sections 2.7 and 2.8) or a two-factor ANOVA (sections 2.9 and 2.10) followed by a *Tukey's post hoc* test, where $p < 0.05$ was considered significant. Additionally, standard box plots were constructed to eliminate outliers. All quantitative results are reported as average ± standard deviation.

RESULTS

TISSUE DECELLULARIZATION

Following decellularization and cryo-grinding, the DNA, GAG, and HYP contents were reduced by 44% ($p < 0.05$), 23% ($p < 0.05$), and 23% ($p < 0.05$), respectively.

SEM AND EDS

Figure 5.2 represents the scanning electron micrographs of microspheres and scaffolds from the four different groups. All four types of microspheres had a spherical morphology with the BLANK, TGF, and CS microspheres depicting a smooth surface while the DCC microspheres possessed a rough surface. The microspheres in the TGF, DCC, and CS groups had micron and sub-micron sized pores present throughout the surface while no pores were observed on the surface of the BLANK microspheres. The images of the scaffolds demonstrated the overall porous nature of microsphere-based scaffolds with similar degrees of microsphere sintering (extent of interconnections) among the BLANK, TGF and DCC groups; however, the microspheres in the CS scaffolds appeared to be fused more with each other than what was observed in the other three groups. Figure 5.3 illustrates the distribution of atomic nitrogen (N) and sulfur (S) in the interior of TGF, DCC and CS microspheres. Nitrogen was distributed uniformly within the TGF, DCC, and CS microspheres. Sulfur was observed to be present inside the TGF, DCC and CS microspheres. The spectral maps for the BLANK microspheres showed that the nitrogen and sulfur were essentially absent from these microspheres (Supplementary Figure 5.1).

MECHANICAL TESTING

The average compressive moduli for BLANK, TGF, DCC, and CS scaffolds were 102 ± 56 kPa, 38 ± 20 kPa, 16.5 ± 3.7 kPa, and 166 ± 71 kPa, respectively (Figure 5.4). The compressive modulus for the CS group was 4.4-fold ($p < 0.05$) and 10-fold ($p < 0.05$) higher than the moduli of the TGF and DCC groups, respectively. No significant differences were observed in compressive modulus among the BLANK, TGF and DCC groups.

POROSITY MEASUREMENT

The average porosity of the CS group was 1.7-fold ($p < 0.05$), 1.8-fold ($p < 0.05$), and 1.1-fold ($p < 0.05$) higher than the average porosities of the BLANK, TGF, and DCC groups, respectively (Figure 5.5). The porosity of the DCC group was 1.5-fold ($p < 0.05$) and 1.6-fold ($p < 0.05$) higher than the porosities of the BLANK and TGF groups, respectively. No significant differences in porosities were observed between the BLANK and TGF groups.

BIOCHEMICAL ANALYSIS

DNA CONTENT

At week 0, the DCC and CS groups outperformed the BLANK group in DNA content with 2.7-fold ($p < 0.05$) and 5.3-fold ($p < 0.05$) higher DNA contents, respectively (Figure 5.6). Additionally, the DCC and CS groups at week 0 had 1.8-fold ($p < 0.05$) and 3.6-fold ($p < 0.05$) higher DNA contents than the DNA content in the TGF group, respectively. Moreover, the CS group at week 0 had 2-fold ($p < 0.05$) higher DNA content than the DCC group. No significant differences in DNA content were observed between the BLANK and TGF groups at week 0. At week 3, the CS group had 88-fold ($p < 0.05$), 82-fold ($p < 0.05$), and 15-fold ($p < 0.05$) more

DNA than the BLANK, TGF, and DCC groups, respectively. Similarly, the CS group at week 6 had 3.6-fold ($p < 0.05$), 3.3-fold ($p < 0.05$), and 2.6-fold ($p < 0.05$) more DNA than the BLANK, TGF, and DCC groups, respectively. No significant differences in DNA content were observed among the BLANK, TGF, and DCC groups at weeks 3 or 6. All of the groups showed statistically significant decreases in DNA contents with time. The BLANK group at week 0 had 35-fold ($p < 0.05$) more DNA than its matching value at week 3. The TGF group at week 0 had 48-fold ($p < 0.05$) and 2.5-fold ($p < 0.05$) more DNA than its corresponding values at weeks 3 and 6, respectively. The DCC group at week 0 had 15-fold ($p < 0.05$) and 3.5-fold ($p < 0.05$) higher DNA content than at weeks 3 and 6, respectively. Week 0 DNA content in the CS group was 2.1-fold ($p < 0.05$) and 2.7-fold ($p < 0.05$) higher than its matching values at weeks 3 and 6, respectively. It must be noted that the values of DNA content obtained in the DCC group represent the amount of DNA present as a result of cell proliferation in these scaffolds. The values *do not* represent the residual amount of DNA present in these scaffolds, as the leftover DNA from the acellular DCC controls was subtracted at each time point.

GAG CONTENT

The GAG content in the CS group at week 0 was 81-fold ($p < 0.05$), 60-fold ($p < 0.05$) and 6.2-fold ($p < 0.05$) higher than the GAG contents in the BLANK, TGF, and DCC groups, respectively (Figure 5.7A). Similarly, the GAG content in the CS group at week 3 was 80-fold ($p < 0.05$), 60-fold ($p < 0.05$) and 19-fold ($p < 0.05$) higher than the GAG contents in the BLANK, TGF, and DCC groups, respectively. No significant differences in GAG content were observed among the BLANK, TGF, and DCC groups at weeks 0 and 3. At week 6, the GAG content in the

CS group was 4.2-fold ($p < 0.05$) and 2.6-fold ($p < 0.05$) higher than the GAG contents in the BLANK and TGF groups, respectively.

Most notably, the CS and DCC groups at week 6 had up to an order of magnitude higher GAG contents than their acellular counterparts. Specifically, the CS group GAG content at week 6 was 7.5-fold ($p < 0.05$) higher than the GAG content of the CS [Acellular] group. Likewise, the DCC group at week 6 had 10-fold ($p < 0.05$) higher GAG content than the DCC [Acellular] group. No significant differences in GAG content were observed between the BLANK and TGF groups at week 6. Only the CS and DCC groups showed statistically significant changes in GAG content over time. The GAG contents in the CS and CS [Acellular] groups at week 0 were 2.3-fold ($p < 0.05$) and 15-fold ($p < 0.05$) higher than their corresponding values at weeks 6, respectively. Additionally, week 3 GAG amounts in the CS and CS [Acellular] groups were 2.2-fold ($p < 0.05$) and 12-fold ($p < 0.05$) higher than their matching values at week 6, respectively. On the other hand, the DCC group had 6.9-fold ($p < 0.05$) more GAG at week 6 than at week 3. No significant differences in GAG content were observed in the BLANK, TGF, and DCC [Acellular] groups over time.

HYDROXYPROLINE (HYP) CONTENT

The HYP content results revealed that the DCC group at week 0 had 185-fold ($p < 0.05$), 244-fold ($p < 0.05$), and 71-fold ($p < 0.05$) higher HYP content than the BLANK, TGF, and CS groups, respectively (Figure 5.7B). In addition, the DCC group at week 0 outperformed the DCC [Acellular] with a HYP content that was 1.2-fold ($p < 0.05$) higher. Week 3 HYP content results showed that the HYP content in the DCC group was 189-fold ($p < 0.05$), 458-fold ($p < 0.05$), and 52-fold ($p < 0.05$) higher than in the BLANK, TGF, and CS groups, respectively. Likewise, the

HYP content in the DCC group at week 6 was 83-fold ($p < 0.05$), 99-fold ($p < 0.05$), and 62-fold ($p < 0.05$) higher than in the BLANK, TGF, and CS groups, respectively. No significant differences in HYP content were observed among the BLANK, TGF, and CS groups at weeks 0, 3, or 6. Only the DCC and DCC [Acellular] groups showed statistically significant differences in HYP over time. The DCC group at week 0 had 1.6-fold ($p < 0.05$) 1.7-fold ($p < 0.05$) higher HYP content than at weeks 3 and 6, respectively. The HYP content in the DCC [Acellular] group at week 0 was 1.4-fold ($p < 0.05$) and 1.7-fold ($p < 0.05$) higher than its matching values at weeks 3 and 6, respectively.

GENE EXPRESSION

SOX9 AND COL2A1

The BLANK group at week 0 had 31-fold ($p < 0.05$) and 1.1-fold ($p < 0.05$) higher SOX9 expression than the DCC and CS groups, respectively (Figure 5.8A). The TGF group SOX9 expression at week 0 was 1.4-fold ($p < 0.05$), 44-fold ($p < 0.05$), and 1.6-fold ($p < 0.05$) higher than the SOX9 expression of the BLANK, DCC, and CS groups, respectively. The CS group at week 0 also had 27-fold ($p < 0.05$) higher SOX9 expression than the DCC group. No significant differences in SOX9 expression were observed among the groups at weeks 1.5, 3, or 6. The SOX9 expression for all of the groups at week 1.5 and beyond was essentially negligible, with the BLANK, TGF, and CS groups showing statistically significant decrease in expression from their corresponding week 0 values.

The COL2A1 expression values for the BLANK group at weeks 1.5, 3, and 6; TGF group at weeks 3 and 6; DCC group at weeks 1.5, 3, and 6; and CS group at weeks 1.5, 3, and 6, were marked as zero because the fluorescence intensities in these samples did not cross the threshold

fluorescence. The TGF group at week 0 had 11-fold ($p < 0.05$) and 2.4-fold ($p < 0.05$) higher COL2A1 expression than the DCC and CS groups, respectively (Figure 5.8B). The BLANK and the CS groups at week 0 had 10-fold ($p < 0.05$) and 4.9-fold ($p < 0.05$) higher COL2A1 expression than the DCC group, respectively. No significant differences in COL2A1 expression were observed among the groups at weeks 1.5, 3, or 6. The BLANK, TGF, and CS groups showed statistically significant changes in COL2A1 expression values over time while no significant differences in COL2A1 expression were observed in the DCC group over time. The week 0 COL2A1 expression values for the BLANK, TGF, and CS groups were statistically significantly higher than their corresponding values at weeks 1.5, 3, and 6.

ACAN AND COL1A1

The TGF group at week 0 had 1.5-fold ($p < 0.05$), 20-fold ($p < 0.05$), and 1.5-fold ($p < 0.05$) higher ACAN expression than the expression levels of the BLANK, DCC, and CS groups, respectively (Figure 5.8C). Both the BLANK and the CS group at week 0 had 13-fold ($p < 0.05$) higher ACAN expression than the DCC group at that time point. No significant differences in ACAN expression were observed among the groups at weeks 1.5, 3 or 6. All the groups at week 1.5 and beyond had negligible ACAN expression, with the BLANK, TGF, and CS groups exhibiting statistically significant decrease in expression from their corresponding week 0 values.

The BLANK, TGF, and CS groups at week 0 had 4.6-fold ($p < 0.05$), 7.7-fold ($p < 0.05$), and 3.5-fold ($p < 0.05$) higher COL1A1 expression than the DCC group, respectively (Figure 5.8D). The TGF group at week 0 had 1.7-fold ($p < 0.05$) and 2.2-fold ($p < 0.05$) higher COL1A1 expression than the BLANK and CS groups, respectively. At week 1.5, the DCC group outperformed the BLANK, TGF, and CS groups in COL1A1 expression with expression value

that was 8.6-fold ($p < 0.05$), 3.6-fold ($p < 0.05$), and 4.3-fold ($p < 0.05$) higher, respectively. No significant differences in COL1A1 expression were observed among the groups at weeks 3 or 6. All of the groups showed statistically significant changes in COL1A1 expression over time. The BLANK group at week 0 had 12-fold ($p < 0.05$), 300-fold ($p < 0.05$), and 60-fold ($p < 0.05$) higher COL1A1 expression than its expression at weeks 1.5, 3, and 6, respectively. The TGF and the CS groups showed a similar pattern to the BLANK group in COL1A1 expression. The TGF group COL1A1 expression at week 0 was 8.3-fold ($p < 0.05$), 333-fold ($p < 0.05$), and 100-fold ($p < 0.05$) higher than at weeks 1.5, 3, and 6, respectively. The CS group at week 0 had 4.5-fold ($p < 0.05$), 5-fold ($p < 0.05$), 7.5-fold ($p < 0.05$) higher COL1A1 expression than at weeks 1.5, 3, and 6, respectively. The COL1A1 expression in the DCC group peaked at week 1.5 with an expression value that was 3.3-fold ($p < 0.05$) and 5.4-fold ($p < 0.05$) higher than at weeks 0 and 6, respectively.

RUNX2, COL10A1, AND IBSP

The BLANK, TGF, and CS groups at week 0 had 13-fold ($p < 0.05$), 15-fold ($p < 0.05$), and 13-fold ($p < 0.05$) higher RUNX2 expression than the DCC group, respectively (Figure 5.8E). No significant differences were observed in RUNX2 expression among the BLANK, TGF, and CS groups at week 0. Additionally, no significant differences were observed in RUNX2 expression among all the groups at weeks 1.5, 3, or 6. The RUNX2 expression for all of the groups at week 1.5 and beyond was negligible, with the BLANK, TGF, and CS groups showing statistically significant decrease in expression from their corresponding week 0 values.

The COL10A1 expression values for the BLANK group at weeks 1.5, 3, and 6; TGF group at weeks 3 and 6; DCC group at weeks 1.5, 3, and 6; and CS group at weeks 1.5, 3, and 6,

were marked as zero because the fluorescence intensities in these samples did not cross the threshold fluorescence. No significant differences were observed in COL10A1 expression among the groups at any time point (Figure 5.8F). All of the groups had negligible COL10A1expression at week 1.5 and beyond with statistically significant decrease in expression from their corresponding week 0 values.

The IBSP expression values for the BLANK group at weeks 3 and 6, and the CS group at week 6, were marked as zero because the fluorescence intensities in these samples did not cross the threshold fluorescence. The BLANK group at week 0 had 2.1-fold ($p < 0.05$), 10-fold ($p < 0.05$), and 1.9-fold ($p < 0.05$) higher IBSP expression than the expression values of the TGF, DCC, and CS groups, respectively (Figure 5.8G). The IBSP expression values of the TGF and CS group at week 0 were 4.9-fold ($p < 0.05$) and 5.3-fold ($p < 0.05$) higher than the IBSP expression of the DCC group, respectively. No significant differences were observed in IBSP expression among the groups at weeks 1.5, 3, or 6. The BLANK, TGF, and CS groups had negligible IBSP expression at week 1.5 and beyond with statistically significant decrease in expression from their corresponding week 0 values. On the other hand, the DCC group had negligible IBSP expression at week 3 and 6 with no statistically significant differences in its expression values over time.

HISTOLOGY AND IMMUNOHISTOCHEMISTRY (IHC)

Figure 5.9 represents the histological images from the BLANK, TGF, and DCC groups at week 6. The sections from the CS scaffolds washed off during the staining process after multiple careful attempts, therefore no histological and IHC images are available from the CS scaffolds. H&E images showed that the cells in the BLANK and TGF groups were present primarily around the

periphery of the microspheres, whereas cells in the DCC group were also found to have infiltrated the microspheres. No differences were observed in Safranin O (stains GAGs orange) staining intensities among the groups at week 6. Masson's trichrome, which stains collagen dark blue, depicted the staining intensities to be greater in the TGF and DCC groups than in the BLANK group. All of the groups stained for Sudan Black, with higher staining intensities in the BLANK and TGF groups than in the DCC group. In addition, the spherical shape of the microspheres was still evident only in the DCC group. Figure 5.10 depicts the IHC images obtained from the BLANK, TGF, and DCC groups at week 6. All three of the groups stained positively for collagen I, with staining intensities in the BLANK and TGF groups being higher than the intensity in the DCC group. No differences in collagen II staining intensities were observed among the BLANK, TGF, and DCC groups. Aggrecan staining was more intense in the BLANK and TGF groups than in the DCC group. The aggrecan staining in the DCC group appeared to be distributed in clusters within the microspheres themselves, perhaps indicative of the encapsulated DCC itself.

DISCUSSION

The current study for the first time compared the effects of encapsulating DCC versus CS in promoting the chondrogenic differentiation of mesenchymal stem cells. DCC or CS could potentially supply the neighboring cells with raw materials (i.e., bioactive signals and building blocks) for differentiation along the chondrogenic lineage[17, 37, 193, 226]. Our previous studies have shown that the incorporation of DCC or CS, at concentrations of 10 or 20 wt%, in microsphere-based scaffolds rendered the scaffolds bioactive, which further led to greater cell numbers compared to the "blank" (PLGA-only) controls and also enhanced matrix synthesis by the seeded

rBMSCs[89, 172, 227]. In the present study, DCC or CS were incorporated at higher concentrations (30 wt%) in microsphere-based scaffolds than our previous iterations of these scaffolds and the potential of encapsulated DCC or CS were evaluated side-by-side to influence the chondrogenic differentiation of rBMSCs.

The SEM images depicted that all four types of microspheres were uniform in size, with average microsphere diameter ranging between 160-180 μm (Figure 5.11). The TGF, DCC, and CS microspheres possessed minute pores on their surface formed perhaps as a result of particulate leaching during solvent evaporation[89, 172, 214, 227]. The DCC encapsulation imparted the PLGA microspheres a rough appearance, differing from our prior work where PLGA microspheres encapsulating DCC at a concentration of 10 wt% had a smooth surface[227]. The higher concentrations of DCC encapsulated in the current study might have resulted in an uneven surface of the DCC microspheres. The microsphere-based scaffolds from all of the four groups were observed to be porous in nature with interconnected pores, as we have consistently observed in previous work[89, 215]. Additionally, it was noted that microspheres in the CS scaffolds had a relatively higher degree of sintering than the degree of sintering observed in the other three groups. Failure to observe a similar effect in the DCC group may have indicated differences in partitioning of CS and DCC in the polymeric microspheres that might have contributed to the higher extent of sintering in the CS group. The EDS maps for atomic nitrogen and sulfur demonstrate that TGF, DCC, and CS were uniformly distributed throughout the interior of the microspheres in the corresponding groups with no evidence of agglomeration at any site. The presence of sulfur in the TGF microspheres could be attributed to the Cysteine (C) and Methionine (M) amino acid residues present in TGF-β_3.

In contrast to our previous findings[172, 227], it was observed that the compressive modulus of CS group was significantly higher than the moduli of the TGF and DCC groups. The higher compressive modulus of CS scaffolds may be attributed to a higher degree of microsphere sintering observed in the CS group. The DCC and CS groups also had significantly higher porosities than the control groups. The higher porosities in the DCC and CS groups is likely associated with the presence of minute pores on the surface of the microspheres that imparted them an additional level of microporosity in addition to the macroporosity obtained from the microsphere sintering[89].

With regard to biochemical content, the CS groups at all time points had significantly higher cell numbers (i.e., DNA content) than the other three groups. Additionally, it was observed that the DCC group at week 0 had significantly higher cell numbers than controls at that time point. The higher cell numbers in the CS scaffolds is indicative of higher cell proliferation in these scaffolds, as CS is known to have a mitogenic effect on the proliferation of MSCs[72, 89, 202, 237]. The higher cell numbers in the DCC scaffolds at week 0 maybe attributed to the rough surface of microspheres that might have promoted initial cell attachment[27, 126]. We observed a similar phenomenon previously in DCC-coated microspheres where the DCC coated scaffold groups had higher cell numbers at week 0[227]. Higher concentrations of DCC used in the current study led to higher amounts of DCC being present on the surface of the microsphere thus, aiding in initial cell attachment by providing additional cell adhesion sites. The CS and DCC groups outperformed the other three groups in GAG and HYP contents at all time points, respectively. Higher amounts of GAG and HYP in the CS and DCC groups is likely ascribed to the inherent GAGs and collagen present in these scaffolds that decreased over time as the scaffolds degraded. It was noted that at week 0, the cell seeded DCC group had a significantly

higher HYP content than its acellular counterpart, highlighting the contribution of cell proliferation to matrix synthesis in the DCC scaffolds. A major finding of the study was that the cellular DCC and CS groups at week 6 had significantly higher GAG contents than their acellular equivalents, suggestive of enhanced matrix production and/or rentention/incorporation by the seeded cells in the DCC and CS groups. Together, these findings suggest that CS and DCC encapsulation in microsphere-based scaffolds promote new cartilage-related matrix synthesis, and supports our previous findings of a modulatory effect of CS and DCC on rBMSCs[89, 227].

It is to be noted that the expression of the osteogenic markers, RUNX2 and IBSP, remained low in all of the groups throughout the 6-week culture period indicating that the rBMSCs did not appreciably differentiate toward the osteogenic lineage in any of the scaffold groups, which might be a limitation with using mesenchymal stem cells that themselves have a tendency for exhibiting a hypertrophic phenotype[218]. The gene expression results for SOX9, COL2A1, and ACAN showed that the expression of these genes was largely suppressed in the DCC and CS groups at week 0 compared to the control groups at that time point, with the CS group outperforming the DCC group at week 0, although reassuringly the positive control TGF group outperformed the BLANK group in SOX9 and ACAN expression. The lower expression of chondrogenic markers in the DCC and CS groups early on indicated that the DCC and CS inhibited the expression of chondrogenic markers by creating an environment that is already high in cartilage-like ECM components. We observed a similar phenomenon in hydroxyapatite (HAp) and tricalcium phosphate (TCP) encapsulated microsphere-based scaffolds where the expression of osteogenic markers in MSCs was largely suppressed due to the presence of inherent minerals in the scaffolds[61, 89]. Additionally, the chondrogenic gene expression in the DCC group did not

increase over time, which was in contrast to the findings of some other groups utilizing cartilage matrix, where chondrogenic gene expression in the cartilage matrix scaffolds either was maintained or increased over time[83, 174]. Failure to observe up-regulation of the chondrogenic genes at later time points in the DCC group hint that the decellularization process might have impaired some critical cartilage matrix components required for cells to guide them toward a chondrogenic lineage[127]. Since decellularization can result in changes in cartilage matrix, we believe that the encapsulation of other forms of cartilage matrix (e.g. devitalized cartilage, DVC) might enhance the chondro-inductivity of microsphere-based scaffolds, which is a matter of further investigation. In our prior work, we have demonstrated the raw materials like CS in combination with growth factors like TGF-β_3 can enhance the secretion of cartilage specific matrix components. Moreover, Almeida *et al.*[3] noticed that a combination of cartilage-ECM-derived scaffold and stimulation with TGF-β_3 can induce chondrogenesis in human fat-pad-derived stem cells, so perhaps encapsulating CS, DCC or DVC in combination with the growth factor may provide a synergistic effect, thus boosting the chondrogenic potential of microsphere-based scaffolds.

The histological images at week 6 pointed toward higher cell numbers in the BLANK and TGF groups than in the DCC group; however, no significant differences were observed in the DNA content among the three groups at week 6. The cells in the BLANK and TGF groups were found to be predominantly present around the periphery of the microspheres, while cells in the DCC group were also observed within the microsphere matrix, suggesting that the porous nature of DCC microspheres allowed for cell infiltration to occur within the microsphere matrix or perhaps there was residual DNA from the DCC itself. The Safranin-O staining intensities were not different among the BLANK, TGF, and DCC groups, which was consistent with no observed

differences in the GAG content among the three groups at that time point. The Masson's trichrome images were in agreement with our HYP content results, both showing that the DCC group had higher collagen content than the BLANK and TGF groups at week 6. The higher net collagen content in the DCC group was due to the inherent collagen present in the DCC scaffolds as confirmed by the Masson's trichrome staining images of the acellular DCC scaffolds (Figure 5.12). Sudan Black staining hinted that encapsulation of DCC altered polymer degradation (perhaps accelerating it). The staining intensities for residual polymer were significantly higher in the BLANK and TGF groups than the intensity in the DCC group. PLGA microspheres degrade via bulk erosion where the rate-limiting step is the diffusion of water molecules into the microsphere core. DCC microspheres because of their porous nature might have allowed faster diffusion of water molecules into their core, thereby initiating polymer degradation more quickly than in the BLANK and TGF groups. The IHC images illustrated that the BLANK and TGF groups stained more intensely for collagen I and aggrecan. The gene expression results showed higher expression of collagen I and aggrecan in the BLANK and TGF groups than the DCC group at week 0; however, no significant differences in the expression of these two genes were observed among the groups at later time points.

In conclusion, the results of the current study demonstrated that encapsulation of DCC and CS altered the morphological and structural properties of both the microspheres and the scaffolds. Moreover, the encapsulation of DCC and CS led to enhanced cell attachment and proliferation on microsphere-based scaffolds thereby, corroborating with our earlier studies suggesting that both DCC and CS are bioactive when incorporated into microsphere-based scaffolds[89, 227]. By providing an environment rich in GAGs and collagen, the DCC and CS scaffolds initially impeded the chondrogenic gene expression in rBMSCs however; biochemical

evidence suggested of a modulatory effect of DCC and CS on matrix synthesis by rBMSCs. Additionally, the differences highlighted between the DCC and CS groups by the biochemical content analysis and the gene expression patterns hint that rBMSCs responded differently to both DCC and CS encapsulated into the microsphere-based scaffolds. Although the cellular response did not provide compelling evidence of DCC and CS enhancing chondrogenesis in microsphere-based scaffolds, the increased GAG content in these groups relative to acellular controls after 6 weeks was encouraging. There is a need to further refine the technology by using even higher concentrations of CS and DCC, or perhaps different forms of cartilage matrix (e.g. devitalized cartilage), or combinations of these raw materials with TGF-β.

CHAPTER 6: MICROSPHERE-BASED SCAFFOLDS CARRYING OPPOSING GRADIENTS OF DECELLULARIZED CARTILAGE AND DEMINERALIZED BONE MATRIX FOR IN VIVO OSTEOCHONDRAL REGENERATION††

ABSTRACT

Extracellular matrix (ECM) 'raw materials' such as demineralized bone matrix (DBM) and cartilage matrix have emerged as leading scaffolding materials for osteochondral regeneration due to their ability to facilitate progenitor/resident cell recruitment, infiltration, and differentiation without adding growth factors. Scaffolds comprised of synthetic polymers are robust but generally lack signals for guiding cell differentiation. We hypothesized that opposing gradients of decellularized cartilage (DCC) and DBM in polymeric microsphere-based scaffolds would provide superior osteochondral regeneration compared to polymer-only scaffolds *in vivo*. Poly(D,L-lactic-co-glycolic acid) (PLGA) microsphere-based scaffolds were fabricated, either with opposing gradients of DCC and DBM encapsulated (GRADIENT) or without DCC and DBM (BLANK control), and implanted into rabbit osteochondral defects in medial femoral condyles. After 12 weeks, gross morphological evaluation showed that the repair tissue in about 30% of the implants was either slightly or significantly depressed, hinting toward rapid polymer degradation in scaffolds from both of the groups. Additionally, no differences were observed in gross morphology of the repair tissue between the PLGA and GRADIENT groups. Mechanical testing revealed no significant differences in model parameter values between the two groups. Histological observations demonstrated that the repair tissue in both of the groups was fibrous in nature with the cells demonstrating notable proliferation and matrix deposition activity. No adverse inflammatory response was observed in any of the implants from the two groups.

---

††To be submitted as **Gupta V**, Lyne D, Laflin A, Zabel T, Barragan M, Bunch J, Pacicca D, Detamore M, Microsphere-Based Scaffolds Carrying Opposing Gradients Of Decellularized Cartilage And Demineralized Bone Matrix For *In Vivo* Osteochondral Regeneration, *Regenerative Engineering and Translational Medicine*, 2015.

Overall, the results emphasize the need to improve the technology in terms of altering the DBM and DCC concentrations, and tailoring the polymer degradation to these concentrations.

INTRODUCTION

Cartilage injuries are difficult to treat because of the limited capacity of cartilage to heal. Even though the osteochondral tissue consists of dissimilar tissues, cartilage and bone, it is known that repair of cartilage is associated with the repair of subchondral bone[156]. Additionally, there are several benefits of growing cartilage and bone within physical proximity to one another. Many biochemical and biomechanical cues responsible for progenitor cell commitment to the osteoblast or chondrocyte lineages have a high degree of interrelatedness[50, 87, 191]. Therefore, several regenerative medicine strategies for osteochondral repair are focused on regenerating both bone and cartilage simultaneously in a plethora of designs in which stratified and continuously graded designs have emerged as the frontrunners[57, 155, 209]. Our research group has shown that three-dimensional (3D) microsphere-based scaffolds with opposing gradients of bioactive signals can direct the differentiation of surrounding progenitor cells simultaneously and regionally toward osteogenesis and chondrogenesis[63, 215]. Moreover, we have demonstrated that these microsphere-based gradient scaffolds can lead to promising osteochondral repair when implanted *in vivo* in rabbits[58, 65].

In the last few years, there has been an increased interest in fabricating scaffolds from extracellular matrices (ECM) for regenerative medicine[23, 97]. For osteochondral regeneration, cartilage matrix and demineralized bone matrix (DBM) have widely gained attention because of their ability to influence resident cell behavior, such as migration, proliferation and differentiation.[37] Both cartilage matrix and DBM allow for constructive remodeling by providing

tissue-specific raw materials (i.e., bioactive signals and building blocks).[17] DBM is commonly used as a bone graft material and presently there are about 25 different DBM products commercially available in the market[68]. Cartilage matrix, on the other hand, has started to gain considerable attention in the last few years for cartilage regeneration[3, 16, 83, 174, 204], with an emphasis on native tissue-derived, decellularized cartilage (DCC)[226]. Scaffolds derived from DBM and DCC have shown great promise within the field of osteochondral regeneration in part because of their ability to guide cell differentiation and provide raw materials for neo-tissue formation. However, various processing reagents used to obtain DBM or DCC often compromise their mechanical performance[17, 37].

The goal of the current study was to fabricate a scaffold that possesses instructive properties of ECM-based materials to guide cell differentiation and mechanical integrity of strong synthetic materials to support joint function during tissue regeneration. Furthermore, we have previously demonstrated that gradient microsphere-based scaffolds have the ability to control patterning of cell phenotype and secrete tissue-specific ECM components for promoting osteochondral repair[58, 63, 65, 89, 169, 172, 173]. Our hypothesis was that microsphere-based scaffolds containing gradients of DBM and DCC would lead to regionalized tissue formation when implanted *in vivo* into rabbit osteochondral defects and outperform the "blank" (no DBM or DCC) microsphere-based scaffolds. To test our hypothesis, we fabricated poly(D,L-lactic acid-co-glycolic acid) (PLGA) microsphere-based scaffolds with encapsulated DCC and DBM in opposing gradients, and implanted them into induced femoral condyle osteochondral defects in rabbit knees for 12 weeks. Additionally, PLGA-only microsphere-based scaffolds were also implanted into the contralateral knees of each rabbits as a control.

MATERIALS AND METHODS

MATERIALS

All reagents for the decellularization process were purchased from Sigma–Aldrich (St. Louis, MO) unless otherwise noted. All other reagents and organic solvents utilized were of USP or ACS grade. PLGA (50:50 lactic acid:glycolic acid ratio, acid end group) with an intrinsic viscosity (i.v.) of 0.37 dL/g, was obtained from Evonik Industries (Essen, Germany). Human demineralized bone matrix (DBM) pellets were received from Biomet, Inc (Warsaw, IN). Two porcine knees from one Berkshire hog (castrated male, approximately 7-8 months old, and weighing 120 kg) were purchased from a local abattoir (Bichelmeyer Meats, Kansas City, KS). Ten New Zealand White rabbits were obtained from Harlan Laboratories (Indianapolis, IN) in accordance with the University of Kansas IUCAC procedures (Protocol #175-21).

CARTILAGE HARVEST AND DECELLULARIZATION

Articular cartilage was harvested from hip and knee joint surfaces and stored at -20°C. After freezing overnight, the cartilage was thawed and coarsely cryoground with dry ice pellets using a cryogenic tissue grinder (BioSpec Products, Bartlesville, OK). The dry ice was allowed to sublime overnight in the freezer. Decellularization of the cartilage was performed using our previously described method[45, 225, 227]. Coarse ground decellularized particles were packed into dialysis tubing (3500 MWCO) and stored in hypertonic salt solution (HSS) overnight at room temperature with gentle agitation (70 rpm). The packets were then subjected to 220 rpm agitation with two reciprocating washes of triton X-100 (0.01% v/v) followed by HSS to permeabilize cell membranes. The tissue was then treated overnight with benzonase (0.0625 KU ml^{-1}) at 37ºC and overnight with sodium-lauroylsarcosine (NLS, 1% v/v) to further lyse cells and denature cellular

proteins. The tissue was then washed with ethanol (40% v/v) at 50 rpm and subjected to organic exchange resins to extract the organic solvents at 65 rpm. Afterward, the tissue was washed in saline-mannitol solution at 50 rpm followed by two hours of rinsing with DI water at 220 rpm. The tissue was removed from the packets and frozen and lyophilized. The decellularized cartilage (DCC) particles were further cryoground into a fine powder with a freezer-mill (SPEX SamplePrep, Metuchen, NJ) and then lyophilized. The DCC powder was filtered using a 45 μm mesh (ThermoFisher Scientific, Waltham, MA) to remove large particles and then frozen until use.

MICROSPHERE FABRICATION

Three different types of microspheres were fabricated for the study: (i) PLGA-only microspheres (BLANK), (ii) DBM encapsulated PLGA microspheres (DBM), and (iii) DCC encapsulated PLGA microspheres (DCC). Prior to microsphere fabrication, DBM pellets were first cryoground into a fine powder using the freezer-mill and then lyophilized. The DBM powder was filtered using a 45 μm mesh (ThermoFisher Scientific, Waltham, MA) to remove large particles. The DBM and DCC encapsulated microspheres were fabricated by adding 2% w/v DBM or 2% w/v DCC to 18% w/v PLGA dissolved in DCM, respectively. Using the PLGA-DBM and PLGA-DCC emulsions, microspheres with mean diameters ranging from 240-270 μm were fabricated via our previously reported technology[58, 61, 63, 65, 89, 169, 172, 173, 214, 215, 227]. In brief, acoustic excitation produced by an ultrasonic transducer (Branson Ultrasonics, Danbury, CT), created regular jet instabilities in the polymer stream, thereby resulting in uniform polymer droplets (Figure 6.1). An annular carrier non-solvent stream of 0.5% w/v poly (vinyl alcohol) (PVA, 88% hydrolyzed, 25 kDa, Polysciences, Inc., Warrington, PA) in deionized water (DI

H_2O) carried the emanated polymer droplets (i.e., microspheres) into a beaker containing the non-solvent solution. The microspheres were stirred for 1 h to allow the solvent to evaporate, and then these microspheres were filtered, rinsed and stored at -20°C. The microspheres were lyophilized for 48 h before further use.

SCAFFOLD FABRICATION

Gradient scaffolds ("GRADIENT" group) were fabricated using our previously established technology.[58, 63, 65, 89, 169, 172, 173, 214, 215] Briefly, lyophilized DBM and DCC microspheres (50-100 mg) were dispersed in DI H_2O and loaded into two separate syringes. The suspensions were then pumped at opposing flow rates using programmable syringe pumps (PHD 22/2000; Harvard Apparatus, Inc., Holliston, MA) into a cylindrical plastic mold (diameter ~ 3.6 mm) having a filter at the bottom until a height of about 2 mm was reached. The scaffolds were 3.5-3.6 mm in diameter and 2 mm in height. The profile for these gradient scaffolds was linear, where the top one-fourth of the total height comprised of DCC microspheres (0.5 mm), then the next one-fourth (0.5 mm) was a linear transition from DCC to DBM microspheres, and the remaining half (1 mm) contained only DBM microspheres (Figure 6.2). The stacked microspheres were then sintered with ethanol-acetone (95:5 v/v) for 55 min. The scaffolds were further lyophilized for 48 h and sterilized with ethylene oxide for 12 h prior to animal implantation experiments. The control BLANK scaffolds were fabricated by packing the "blank" (PLGA-only) microspheres into the same molds, followed by sintering for 55 min. The BLANK scaffolds had dimensions similar to GRADIENT scaffolds (diameter 3.5-3.6 mm and height 2 mm). A total of two scaffold groups were tested in the study and were named according to the composition of microspheres as: BLANK and GRADIENT.

SURGICAL PROCEDURE

Surgical procedures were conducted under an approved IACUC protocol at the University of Kansas (protocol #175-21), with a total of 10 rabbits. Following analgesic delivery, stable general anesthesia, and antibiotic administration, hair was shaved from area around each knee. Before the procedure, rabbits were provided with a lactated ringer injection or saline bolus (150-200 cc) subcutaneously at multiple injection sites around the neck and shoulders to ensure proper hydration and to maintain blood pressure. The surgical area was disinfected with alternate scrubs of Betadine and 70% ethanol, and then draped. Only strict aseptic techniques and sterile instruments were used, and the surgeons wore sterile gown, masks and head covers. All surgical tools, including drill, were sterilized before surgery. A medial parapatellar incision was made, sufficient to allow exposure of the medial condyle. The tibia was lightly pushed to displace it laterally to allow exposure of the medial femoral condyle. A pilot hole was drilled through the cartilage and the subchondral bone in the central load-bearing region of the medial condyle using a 1.5 mm drill. The defect was then enlarged to 3.5 mm diameter and to the depth of 2 mm using a 3.5 mm drill with depth gauge. The defect was then filled by press fitting one of the two engineered plugs, either BLANK or GRADIENT, into it (Figure 6.3). Due to differences in relative diameters of scaffolds and drill bits, there were some scaffolds that required excessive force to press-fit them into the defect, resulting in some degree of implant crumbling. We observed an estimate of 5% implant crumbling in the following animals: Rabbit 1 right knee and Rabbit 6 right knee, and 10–15% implant crumbling in Rabbit 6 left knee. After press-fitting the implant, the joint was then washed of debris with sterile saline, the patella and femur were relocated, and the articular capsule and bursae were closed with an absorbable suture, and then the skin was closed with a non-absorbable closure. The same procedure was performed on the

contralateral knee but with the alternative plug construct implanted (Table 6.1). After both procedures were finished, rabbits were returned to their cages. Analgesics were administered as needed based on pain assessment. The knee joints were allowed unconstrained movement postoperatively.

GROSS MORPHOLOGICAL ASSESSMENT

After 12 weeks, all implants were scored blindly by three independent co-authors based on the presence of repair tissue or implant at the defect site, the edge integration at the boundaries of newly regenerated tissue and the native cartilage, the smoothness of the repair tissue, the surface degree of filling at the defect site, the color of the regenerated cartilage, and the amount of repair tissue present relative to the total defect area. The scoring criteria are listed in Table 6.2. Thereafter, the joints were photographed and processed for mechanical testing or histology.

MECHANICAL TESTING

After retrieval, eight femurs (Table 6.1) were wrapped in gauze, soaked in a protease inhibitor solution (0.15 M NaCl; EDTA, 2 mM; benzamidine HCl, 5 mM; N-ethyl malemide, 10 mM; and PMSF, 1 mM) and stored at -20°C until the day of testing[9]. Each frozen femur was thawed at room temperature for 1 h in the protease inhibitor solution. Afterward, medial femoral condyles (MFCs) were carefully separated from the rest of the tissue with a handheld hacksaw. Each MFC was affixed to a stainless steel platform using cyanoacrylate adhesive, placed in a custom made bath and submerged in the protease inhibitor solution[173]. The temperature of the bath was maintained at 37 °C at all times during the testing. A uniaxial testing apparatus (Instron 5848 Microtester, Canton, MA) was used for both cartilage thickness measurement and unconfined

indentation stress relaxation tests. A total of three sites were tested to determine the thickness, whereas indentation was performed only at the central region of the implant site. Thickness was measured via a thin needle that was inserted into the implant site perpendicularly to the specimen surface at a constant rate of 0.5 mm/min. The force and displacement were measured, and needle movement was terminated when the force reached 2 N. Specimen thickness was determined using a force displacement curve. A change in slope indicated the point where the needle contacted the subchondral bone[196]. For indentation stress relaxation testing, the tare-loaded (0.01 N) implant site was subjected to 10% strain (at a ramp rate of 0.01%/s) using a solid spherical tip stainless steel indenter (1.5 mm diameter), and then allowed to relax for a period of 1000 s[173].

FINITE ELEMENT ANALYSIS

The unconfined compression stress relaxation response of the test specimens was curve fitted using a finite element analyses in which cartilage was modeled as a biphasic material[176]. The porous extracellular matrix was described by a solid mixture of a neo-Hookean ground matrix reinforced by a continuous, random distribution of fibril bundles sustaining tension only; the hydraulic permeability was assumed constant[7, 8, 24]. The model had a total of five material constants: Elastic modulus (E) and Poisson's ratio (ν) for the neo-Hookean solid, the fibril modulus (k_{si}) and the power-law exponent (β) for the spherical fiber distribution, and the constant hydraulic permeability (k). It was assumed *a priori* that $\beta = 2$ (to produce a linear tensile response in the range of small strains, consistent with the known behavior of cartilage) so that the parameter optimization was only performed on E, ν, k_{si} and k[7]. The finite element analyses for curve-fitting the experimental data and modeling the contact between indenter and the specimen, were performed with the open-source program FEBio available in the public

domain[162]. Curve fitting was performed using FEBio's built-in least-squares parameter optimization routine, based on the Levenberg-Marquardt algorithm. The contact was modeled using an impermeable spherical indenter with a diameter of 1.5 mm and a cylindrical disk (representing the tissue) of diameter of 6 mm, and 1 mm height. The model tissue diameter was chosen to be 4 times the indenter diameter to simulate the indentation experiment where the cartilage radius is much larger than the indenter radius. Due to symmetry, only a wedge of the geometry was modeled. The indenter produced a compressive deformation of 10% of the thickness. The contact interface between the indenter and the construct was assumed to be frictionless. In the model, the bottom of the construct was fixed to a rigid impermeable substrate. Fluid was assumed to escape from the free boundaries not in direct contact with the indenter[173]. The model consisted of 321 hexahedral 8-node elements and 546 nodes. The mesh was biased along the thickness to produce thinner elements near the top and bottom surfaces; a coarser mesh was also employed at the far ends along the length. FEM results were visualized using the FEBio Postview environment.

HISTOLOGICAL AND IMMUNOHISTOCHEMICAL (IHC) ANALYSES

Eight femurs (Table 6.1) were decalcified in 0.5N HCl with 0.1% gluteraldehyde for 9 days at 4°C. The decalcification solution was changed every 48 h. The femurs were then washed and defatted in 70% and 100% ethanol for 24 h, respectively. Thereafter, the femurs were cryoprotected by immersion in 5% sucrose and then 10% sucrose in PBS for 2 h each, followed by 20% sucrose in PBS for 16 h at room temperature[40]. The femurs were then equilibrated in optimal cutting temperature embedding medium (OCT, Tissue-Tek, Torrance, CA) overnight at 37°C and then frozen at -20°C. 10 μm thick sections were cut using a cryostat (Micron HM-550

OMP, Vista, CA) and stained using hematoxylin (cell nuclei) and eosin (cytoplasm); safranin-O/fast green (glycosaminoglycans); and Sudan black for residual polymer. A modified O'Driscoll scoring system (Table 6.3) was used for the analysis[80, 173, 185]. Histological scoring was performed by three independent co-authors and the average scores were calculated. The sections from all of the implants were stained for the presence of collagen types I & II via immunohistochemistry (IHC). IHC for one implant in the GRADIENT group was not performed, as an adequate number of sections could not be obtained. Mouse monoclonal primary antibodies (Thermofisher Scientific, Waltham, MA) against collagen type I (1:200 dilution) and collagen type II (1:250 dilution) were used for IHC. Following the primary antibody, biotinylated secondary antibody was used followed with the ABC complex (Vector Laboratories, Burlingame, CA). The antibodies were visualized with the diaminobenzidine (DAB) substrate per the manufacturer's protocol (Vector Laboratories). Negative controls were also run with the primary antibody omitted.

STATISTICAL ANALYSES

GraphPad Prism 6 statistical software (GraphPad Software, Inc., La Jolla, CA) was used to compare experimental groups using an unpaired t-test, where $p < 0.05$ was considered significant. All quantitative results are reported as average ± standard deviation.

RESULTS

TISSUE DECELLULARIZATION

Following decellularization and cryo-grinding processes, the DNA content of the native cartilage was reduced by 44% ($p < 0.05$). The GAG and hydroxyproline contents were both reduced by 23% ($p < 0.05$).

POSTSURGICAL COURSE

At 2 weeks, one rabbit (with the BLANK implant in the right knee and the GRADIENT implant in the left knee) was euthanized prematurely due to luxation at L6-L7 caused by sudden jumping in the cage. At 7 weeks, another rabbit (with the BLANK implant in the left knee and the GRADIENT implant in the right knee) was euthanized prematurely because of chronic lameness. The premature euthanasia of two rabbits brought the sample number down to $n = 8$ for gross morphological analysis, $n = 4$ for mechanical testing, and $n = 4$ for histology and IHC in both the BLANK and GRADIENT groups. All of the other animals continued to exhibit normal movement during the 12-week period.

GROSS MORPHOLOGICAL ASSESSMENT

Gross signs of inflammation (swelling or reddening of the joint) or infection were not observed in any of the rabbits upon visual inspection of the joint surface at the time of tissue retrieval. The synovial fluid had a normal color. Additionally, no signs of degeneration were noted on the opposing joint surfaces. Figure 6.4 represents the morphological scores and the amount of repair tissue present at the defect site in both the BLANK and the GRADIENT groups. Figure 6.5

shows the representative gross morphological images of the implants receiving highest, mean**,** and lowest morphological scores in both the BLANK and the GRADIENT groups.

The average morphological score in the BLANK group was 6.0 ± 0.5 out of a maximum possible score of 10 with a highest score of 8.0 while the only BLANK implant that crumbled during implantation received a score of 3.3. All of the rabbits that received the BLANK implants had more than 80% of the defect area filled with repair tissue, except for two that had 63% and 55% of the defect area filled with the repair tissue. All of the animals receiving the BLANK implants (except for one) had intermediate smoothness of the repair tissue, with half of them showing complete edge integration with the native tissue. Six of the implants in the BLANK group had slightly depressed repair tissue, with one implant having completely flush and one having significantly depressed surface degree of filling. 75% of the animals in the BLANK group had translucent regenerated tissue, while the remaining 25% had an opaque appearance of the repair tissue.

The GRADIENT group average morphological score was 5.2 ± 0.8 out of 10, with the highest score being 8.7 in the group. The GRADIENT implants that crumbled during implantation received average scores of 3.3 and 1.3. The percentage of repair tissue present at the defect site in the GRADIENT group ranged from 7-100% with an average of 61 ± 11%. No statistically significant differences were observed in either the average morphological scores or the amount of repair tissue present at the defect site between the BLANK and the GRADIENT groups. Almost all of the animals in the GRADIENT group showed complete integration of the repair tissue with the native tissue, with two animals showing partial integration and one showing no integration at all. 63% of the rabbits receiving the GRADIENT implant had high or intermediate smoothness of the repair tissue, while the remaining 37% had a rough appearance of

the regenerated tissue. Half of the animals in the GRADIENT group had either completely flush or slightly depressed regenerated tissue whereas the other half had significantly depressed repair tissue. All the animals in the GRADIENT group had either translucent or opaque appearance of the repair tissue.

MECHANICAL TESTING AND FINITE ELEMENT ANALYSIS

The elastic modulus, fiber modulus, permeability and Poisson's ration are represented graphically in Figure 6.6. The average elastic moduli, obtained from curve fitting the indentation stress relaxation data, for the PLGA and GRADIENT groups were 250 ± 160 and kPa and 150 ± 94 kPa, respectively. The fiber moduli for the BLANK and the GRADIENT groups were found to be 79 ± 21 kPa and 110 ± 27 kPa, respectively. No statistically significant differences were observed in the elastic and fiber moduli between the BLANK and GRADIENT groups. The BLANK group had an average hydraulic permeability of $1.71 \pm 0.54 \times 10^{-6}$ $mm^4/mN.s$ and the GRADIENT group had a permeability of $1.74 \pm 0.79 \times 10^{-6}$ $mm^4/mN.s$. The Poisson's ratios for the BLANK and GRADIENT groups were 0.18 ± 0.075 and 0.050 ± 0.028, respectively. No statistically significant differences were observed in the hydraulic permeabilities and Poisson's ratios between the BLANK and GRADIENT groups.

HISTOLOGY AND IMMUNOHISTOCHEMISTRY

Both the BLANK and GRADIENT groups had an average histological score close to 10 (out of a maximum possible 28) with the BLANK group having a mean score of 7.6 ± 0.9 and the GRADIENT group having a mean score of 7.4 ± 0.6 (difference not statistically significant).

The histological and IHC images from all of the implants in the BLANK group are depicted in Figure 6.7. The first column shows the images of the implant that received the highest histological score (10.2). No depression was observed in the regenerated tissue. The repair tissue possessed high cellularity with robust proliferative activity. Most of the cells in the defect area resembled fibrous chondrocytes. A few regions near the edges of the defect site had chondrocytes with lacunae; however, no columnar arrangement was observed in these chondrocytes. The regenerated cartilage had a thickness greater than the surrounding cartilage with partial bonding to the native tissue observed at both the edges of the defect site. The repair tissue stained slightly for Safranin-O in the areas near the edges of the defect site toward subchondral bone. The defect area toward the subchondral bone consisted largely of flat cells surrounded by loose stromal tissue and numerous blood vessels. The appearance of premature trabecular bone presented some evidence of subchondral bone regeneration. No adverse inflammatory response was observed within the defect area, although a few macrophages were observed in the area. The IHC images showed that the loose connective tissue present in the defect area stained heavily for collagen I while some collagen II staining was also observed at the defect edges adjacent to subchondral bone. The implant receiving the second highest histological score of 7.3 in the BLANK group showed significantly depressed repair tissue at the defect site. The regenerated tissue largely resembled fibrous tissue with most of the cells having a flat appearance. A few cells at the surface of the defect site appeared to have chondroblast-like morphology. The regenerated tissue showed severe disruptions; however, no cysts were noted in the repair tissue. The defect site did not stain for Safranin-O while the surrounding native tissue showed slight Safranin-O staining. Toward the subchondral bone region, the defect area showed signs of osteoblastic activity with minimal bone regeneration. No adverse inflammatory response

was observed in the defect area. The repair tissue stained positively for collagen I, whereas collagen II staining was predominantly absent from the repair tissue. The third column illustrates the histological and IHC images from the implant that received a histological score of 6.7 in the BLANK group. Although the repair tissue filled the defect space almost completely, the regenerated tissue appeared crumbly. Severe disruptions were noticed in the regenerated tissue. Most of the cells in the defect area had a flat morphology that resembled fibroblasts. Some chondrocyte-like cells with a few cell clusters were observed in the areas near the edges of the defect. In addition, light Safranin-O staining was observed near the edges of the defect site. The adjacent native cartilage showed some signs of degenerative changes with moderate hypocellularity and slight staining. No subchondral bone regeneration was observed in the defect area, although some blood vessels were noticed in region. The repair tissue stained positively for collagen I and also stained slightly for collagen II. The histological images for the implant that received the lowest score of 6.0 in the BLANK group showed a large chunk of native osteochondral tissue present at the defect site, which might have been a result of tissue processing during sectioning and staining. The regenerated tissue in the implant was significantly depressed compared to the native tissue. The cartilage at the surface of the defect area resembled fibrocartilage while the deeper regions showed the presence of loose connective tissue. Both the repair and native tissues did not stain for Safranin-O. No subchondral bone regeneration was observed and the defect area presented signs of mild inflammatory response with the appearance of some macrophages and multi-nucleated giant cells. The repair tissue stained positively for collagen I, while it did not stain for collagen II.

Figure 6.8 illustrates the histological and IHC images from all the implants in the GRADIENT group. The defect area in the implant that received the highest histological score of

8.7 in the GRADIENT area was almost completely full. The repair tissue was slightly depressed compared to the native tissue. The regenerated tissue at the surface had lacunated chondrocytes with some cell clusters; however, no columnar arrangement of cells was observed. The regenerated cartilage was thinner than the surrounding native cartilage and no bonding was observed between the regenerated and native tissues. The repair tissue stained slightly for Safranin-O at one edge of the defect. The adjacent cartilage showed minimal signs of degeneration with mild hypocellularity. Although, some small blood vessels were observed in the bone region of the defect, no subchondral bone regeneration was observed. Additionally, a void area was noticed in the subchondral bone region. Minimal signs of inflammation were observed in the defect region as noticed by with the appearance of a few macrophages. The repair tissue stained positively for collagen I while only moderate collagen II staining was observed in the defect area. The implant receiving the second highest score, 8.0, in the GRADIENT group also showed depressed tissue relative to the native tissue. Most of the regenerated cartilage resembled fibrocartilage with the cells showing a significant amount of proliferative activity. Some cells at the edges had chondrocyte-like morphology and were arranged in isogenic groups. The regenerated cartilage had lower thickness compared to the native tissue and stained slightly for Safranin-O near the defect edges. In the subchondral region, small trabeculae were observed that suggested toward bone remodeling. No adverse inflammatory response was observed in the defect area. The IHC images showed that the regenerated tissue stained positively for collagen I, whereas no collagen II staining was observed in the defect area. The implant receiving a score of 6.7 in the GRADIENT group also possessed repair tissue that was significantly depressed compared to the native tissue. The repair tissue in the cartilage part of the defect area resembled fibrocartilage with the cells demonstrating good

proliferative activity. The regenerated cartilage was partially bonded with the native tissue on one side of the defect. The adjacent native cartilage showed some signs of degenerative changes as indicated by moderate hypocellularity in the surrounding native cartilage. The defect area showed no to minimal signs of subchondral bone reconstruction with mild inflammatory response as observed by the presence of a few giant multinucleated cells. The tissue in the defect area stained positively for collagen I. Slight collagen II staining was also observed in the areas adjacent to the defect edges. The lowest scoring implant in the GRADIENT group received a histological score of 6.0. The histological images showed that the repair tissue was significantly depressed compared to the native tissue, with the repair tissue predominantly resembling loose connective tissue. The subchondral bone region consisted of vascular connective tissue. Safranin-O staining was absent from the defect as well as the native tissue area. Due to inadequate number of sections obtained from the implant, IHC images are not reported for the implant.

Figure 6.9 shows the Sudan Black staining images for the implants that received the highest and lowest histological scores in both the BLANK and GRADIENT groups. Only a few areas of intense staining (depicted by red arrows) were observed in all of the implants with most of the defect site showing none to mild staining.

DISCUSSION

The present study for the first time evaluated the *in vivo* response of microencapsulating demineralized bone matrix (DBM) and cartilage matrix in polymeric microsphere-based scaffolds toward osteochondral repair. Moreover, to the best of our knowledge, we are the first group to encapsulate DBM in microsphere-based scaffolds for the bone region of the scaffold.

The other groups employing microsphere-based scaffolds have banked on other calcium phosphates and minerals for engineering the bone tissue[46, 161, 228, 255].

From the gross morphological evaluation, it was observed that in 50% of the total implants (both of the groups combined) about one-fourth of the defect area was empty. Additionally, 5 out of the total 16 implants had either slightly or significantly depressed repair tissue. No statistically significant differences were observed in the BLANK and GRADIENT groups in the amount of defect area fill; however, the average fill area in the GRADIENT group was lower than the average fill area in the BLANK group. Moreover, 50% of the implants in the GRADIENT group had significantly depressed regenerated tissue whereas the corresponding number in the BLANK group was 13%. The presence of empty area and the observance of depressed tissue might have resulted from the rapid degradation of polymer, with even faster degradation occurring in the GRADIENT group. Our prior work involving gradient microsphere-based scaffolds for osteochondral regeneration with a comparable polymer (i.v. 0.34-0.36 dL/g) as we have used in the current study, showed a defect fill of more than 95% in all of the implants at 12 weeks[169]. The amount of repair tissue present in defect site in the current study was about 80% and 60% for the BLANK and GRADIENT groups, respectively. Lower amounts of repair tissue in the current study most likely resulted from the rapid scaffold degradation, which is a direct consequence of polymer degradation. It is believed that DBM and DCC encapsulation might have affected microsphere morphology, which might have resulted in faster degradation of the polymer; however, no analysis was done to assess polymer degradation, which can be a subject matter for subsequent studies. We have previously observed that encapsulation of raw materials such as chondroitin sulfate and DCC result in minute pores on the surface of PLGA microspheres that can accelerate polymer degradation[2, 89, 172, 227]. Increasing concentrations of

raw materials on one hand might accelerate but on the other might provide momentum to tissue regeneration for impeding the deleterious effects caused by rapid polymer degradation. Furthermore, it was observed that some of the implants crumbled during implantation that might have further accelerated scaffold degradation. The implants that crumbled in both of the groups received the lowest morphological scores, further suggesting that implant crumbling might have also affected scaffold degradation. The implant crumbling might have resulted due to slight mismatch between scaffold and defect diameters. The scaffold diameter was intentionally kept slightly larger than the defect diameter to allow for press-fitting of the implant[169]. In addition, variations in force applied due to the manual press-fitting approach might have caused some implants to crumble, which can be avoided by using an automated approach (maybe a delivery device) for implanting the scaffold. The average morphological scores in the BLANK and GRADIENT groups were similar to each other, although there were some differences observed in the macroscopic properties of the repair tissue between the two groups. The repair tissue in the GRADIENT group had better edge integration with the peripheral native tissue than the edge integration observed in the BLANK group. On the other hand, the repair tissue smoothness in the BLANK group surpassed the smoothness of the repair tissue in the GRADIENT group.

The elastic moduli, fiber moduli, permeability, and Poison's ratio values of the repair tissue in the BLANK and GRADIENT groups fell within the previously reported values of these parameters[9, 35]. No statistically significant differences were observed in any of the four model parameters for mechanical testing between the BLANK and GRADIENT groups. It was reported that the Poisson's ratio of cartilage can be as low as 0.02 in unconfined compression, but never more than 0.5[8, 240]. The Poisson's ratio values appeared to be lower in the GRADIENT group than those observed in the BLANK group, indicating higher apparent compressibility of the

tissue and a propensity for more fluid transport in the GRADIENT group[9]. However, no statistically significant differences were observed in the Poisson's ratios between the BLANK and GRADIENT groups to support that claim.

The histological findings revealed that there were no significant differences in the average histological scores between the BLANK and GRADIENT groups. It should be noted that the histological and IHC images depict a general trend of regeneration within each group; however, the trend was not uniform in all of the sections, as these are representative sections taken from the entire defect area of the regenerated tissue. The cellular morphology observed in the repair tissues in both of the groups resembled those of fibroblasts with the cells demonstrating significant proliferative activity. The defect site in both of the groups was largely filled with a vascularized loose connective tissue; however, some implants showed a presence of a fibrocartilage layer on the top. Although the thickness of the regenerated cartilage was less than the thickness of the adjacent native cartilage, it was observed that the regenerated tissue was partially bonded with the native tissue at both sides of the defect. Some collagen II staining was also observed in both of the groups especially around the edges of the defect area; however, the regenerated tissue predominantly stained for collagen I, indicating that the regenerated cartilage was fibrous in nature. Additionally, both of the groups showed a mild inflammatory response in the subchondral bone region. The inflammatory response may have been a manifestation of tissue remodeling response that can have profound implications in clinical success of microsphere-based scaffolds[154]. The presence of premature bone trabeculae in some of the implants in both the groups also hint toward the regeneration or remodeling response in the defect site. However, both the BLANK and GRADIENT groups showed void areas in the subchondral bone region, which indicate toward rapid polymer degradation that further may have

led to depressed repair tissue overall in both the groups. Sudan black staining images revealed that the defect sites in both the groups were predominantly absent of residual polymer except for a few small dark-staining spots that indicated minimal leftover polymer or polymer degradation products. The absence of residual polymer in both the BLANK and GRADIENT groups further hint toward rapid polymer degradation in microsphere-based scaffolds that most likely adversely affected the regeneration of the tissue in the defect site.

Overall, the results of the current study demonstrated that structural integrity of microsphere-based scaffolds is an important parameter than can have significant impact on the tissue regeneration. The degradation of the polymer in the scaffolds will play a key role in tissue regeneration *in vivo*, where extended degradation could become an obstacle to tissue regeneration and in contrast rapid degradation could have a deleterious effect on the regenerating tissue, supposedly the cause of below par regeneration observed in the current study. Thus, we acknowledge that there should be a more detailed look at polymer degradation as a function of encapsulated raw materials for subsequent *in vitro* and *in vivo* studies to identify formulations that more closely approximates the tissue regeneration rate in animals and humans. Additionally, emphasis is laid on the need to better match scaffold dimensions with defect dimensions or perhaps employ a scaffold delivery device that can further minimize surgeon-to-surgeon variations during scaffold implantation. Nevertheless, the current study hints that employing gradients of DBM and DCC might be beneficial for osteochondral regeneration as indicated by better integration of the regenerated tissue with the peripheral native tissue, thus providing a motivation for further refining the technology by altering the concentrations of DBM and DCC, and attuning polymer degradation to these concentrations.

CHAPTER 7: CONCLUSION

Predecessors to this work developed microsphere-based scaffolds containing opposing gradients of proteins and established the feasibility of the concept for driving *in vitro* chondro- and osteogenesis, and stimulating *in vivo* osteochondral regeneration in rabbit osteochondral defects[58, 63, 65, 215]. Moreover, it was illustrated that a gradient in both material composition and encapsulated proteins can enhance secretion of tissue specific matrix proteins[169, 172]. Within this thesis, microsphere-based scaffolds encapsulating only ECM materials were developed, with the goal of providing the surrounding cells with raw materials (bioactive signals and building blocks) to facilitate their differentiation along bone and cartilage lineages. The studies within this thesis progressed to demonstrating the *in vitro* efficacy of raw material encapsulation in clinically relevant scaffold system, to refining composition of raw materials in homogenous microsphere-based scaffolds for enhancing *in vitro* osteogenesis and chondrogenesis, and then finally to evaluating the *in vivo* response of raw material encapsulation in gradient microsphere-based scaffolds.

In vitro assessment of clinically relevant microsphere-based scaffolds fabricated using the raw material approach depicted that the encapsulated raw materials, CS and TCP, altered the microstructure of the microspheres and also influenced cellular morphologies. The mechanical properties of the raw material encapsulating microsphere-based scaffolds initially relied on the composition of the scaffolds and later on were governed by polymer degradation and newly synthesized ECM by the seeded cells. Additionally, raw materials had a mitogenic effect on the seeded rBMSCs and led to increased glycosaminoglycan (GAG), collagen, and calcium content. However, it was noted that the initial effects of raw material encapsulation on a per-cell basis might have been overshadowed by medium-regulated environment that appeared to favor

osteogenesis. Most importantly, the results of the study demonstrated the potential of the raw materials in facilitating neo-tissue synthesis in microsphere-based scaffolds and also presented evidence for faster maturation of rBMSCs in gradient scaffolds.

Incorporation of TCP and HAp mixtures for enhancing osteogenesis affected the morphological and mechanical properties of the microsphere-based scaffolds. The microspheres encapsulating TCP and HAp exhibited a porous surface and possessed a deflated soccer ball-like shape, which further elevated the overall porosities and lowered the compressive moduli of scaffolds. The explicit reasons for lower compressive moduli in TCP and HAp encapsulating groups are currently unclear, but may relate to poor polymer healing at microsphere sintering junctions caused by irregularities in microsphere shape. Using a polymer with high molecular weight might prevent the drop in compressive moduli caused by TCP and HAp encapsulation, as suggested by the results of the previous study where TCP encapsulation in high molecular weight PLGA led to higher compressive modulus compared to PLGA-only scaffolds. Interestingly, it was observed that the TCP and HAp encapsulation fast-tracked the osteogenic commitment of cells on these scaffolds as indicated by the higher end point ECM synthesis and enhanced expression of osteogenic genes compared to the control formulations. Thus, future investigations should focus on leveraging these TCP and HAp mixtures for *in vivo* osteochondral regeneration by incorporating them into gradient scaffolds fabricated with a polymer having a degradation rate that closely approximates the tissue regeneration rate.

CS and DCC encapsulation revealed that incorporation of these materials affect the morphological characteristics of microsphere-based scaffolds without compromising their mechanical integrity. The DNA content results suggested that CS and DCC encapsulation encouraged initial cell attachment and proliferation on these scaffolds with some biochemical

evidence indicating toward modulatory effect of CS and DCC on matrix synthesis by the seeded cells. Expression of chondrogenic genes was suppressed in the CS and DCC group at initial time points indicating that the cells sensed their surrounding environment, which was high in GAGs and collagens. To achieve the desired chondrogenic differentiation profile, subsequent studies should consider altering the dose of CS and DCC in microsphere-based scaffolds that could then be employed *in vivo* in a continuously graded design for osteochondral regeneration.

The results of the *in vivo* study stressed the need to utilize a polymer with a biodegradation rate comparable to the neo-tissue formation rate. 50% of the implants had an average defect fill that was less than 75%, indicating that the PLGA used in the study might have degraded too quickly, limiting the amount of tissue regeneration in the defect area. Moreover, implant crumbling during implantation might have contributed to the degradation of the scaffold, thus suggesting the importance of better matching scaffold and defect dimensions. However, some benefits of the 'raw material' approach were noted in the microsphere-based scaffolds comprised of opposing gradients of DBM and DCC. The regenerated tissue in the gradient scaffolds integrated better with the peripheral native tissue than the repair tissue in the PLGA-only control group. The regenerated tissue in both of the groups showed an inflammatory response that might suggest an immune response or of a remodeling response, which requires further investigation. Future studies should concentrate on investigating polymer degradation rate and its effect on tissue regeneration. Moreover, adjusting DBM and DCC concentrations or perhaps using allogeneic raw materials could achieve effective osteochondral repair.

The evidence presented with this thesis readily demonstrates that using a raw material encapsulating microsphere-based scaffold approach for facilitating osteochondral regeneration is feasible and in many instances efficacious. In addition, emphasis is being laid on examining the

interplay between scaffold degradation and neo-tissue formation, where premature failure in scaffold mechanical properties can have a deleterious effect on the regenerating tissue and extended degradation in contrast could become an obstacle to tissue regeneration. Fine-tuning the dose of raw materials could further supplement the regenerative capacity of these raw material encapsulating microsphere-based scaffolds. Although higher concentrations (than the previous iterations) of raw materials were evaluated in this thesis, increasing concentrations of the raw materials with ultimately fabricating raw material-only microsphere-based scaffolds would bridge the gap between the 'scaffolds' and 'signals' side of the traditional tissue engineering triad (i.e., cells, signals, and scaffolds). As highlighted in Chapter 2, the use of microsphere-based scaffolds has been predominantly focused in musculoskeletal tissue regeneration; however, the future of microsphere-based scaffolds combined with raw material approach may lie in regenerating other complex types of tissue. Eventually, the idea of employing raw material encapsulating microsphere-based scaffolds for tissue regeneration has been taken from concept to design, produced encouraging results for osteochondral regeneration, and has opened up new avenues of research to consider and challenges to overcome.

REFERENCES

1. Agrawal C. M. and K. A. Athanasiou. Technique to control pH in vicinity of biodegrading PLA-PGA implants. *Journal of biomedical materials research* 38: 105-114, 1997.

2. Alexis F. Factors affecting the degradation and drug-release mechanism of poly(lactic acid) and poly[(lactic acid)-co-(glycolic acid)]. *Polymer International* 54: 36-46, 2004.

3. Almeida H. V., Y. Liu, G. M. Cunniffe, K. J. Mulhall, A. Matsiko, C. T. Buckley, F. J. O'Brien and D. J. Kelly. Controlled release of transforming growth factor-β3 from cartilage-extra-cellular-matrix-derived scaffolds to promote chondrogenesis of human-joint-tissue-derived stem cells. *Acta biomaterialia* 10: 4400-4409, 2014.

4. Amini A. R., D. J. Adams, C. T. Laurencin and S. P. Nukavarapu. Optimally porous and biomechanically compatible scaffolds for large-area bone regeneration. *Tissue engineering. Part A* 18: 1376-1388, 2012.

5. Ando S., D. Putnam, D. W. Pack and R. Langer. PLGA microspheres containing plasmid DNA: Preservation of supercoiled DNA via cryopreparation and carbohydrate stabilization. *Journal of pharmaceutical sciences* 88: 126-130, 1999.

6. Arinzeh T. L., T. Tran, J. Mcalary and G. Daculsi. A comparative study of biphasic calcium phosphate ceramics for human mesenchymal stem-cell-induced bone formation. *Biomaterials* 26: 3631-3638, 2005.

7. Ateshian G. A. and R. L. Mauck. Sliding contact loading enhances the tensile properties of mesenchymal stem cell-seeded hydrogels. *European ...* 2012.

8. Ateshian G. A., V. Rajan, N. O. Chahine, C. E. Canal and C. T. Hung. Modeling the Matrix of Articular Cartilage Using a Continuous Fiber Angular Distribution Predicts Many Observed Phenomena. *Journal of biomechanical engineering* 131: 061003, 2009.

9. Athanasiou K. A., M. P. Rosenwasser, J. A. Buckwalter, T. I. Malinin and V. C. Mow. Interspecies comparisons of in situ intrinsic mechanical properties of distal femoral cartilage. *Journal of orthopaedic research : official publication of the Orthopaedic Research Society* 9: 330-340, 2005.

10. Bach A. D., J. P. Beier, J. Stern-Staeter and R. E. Horch. Skeletal muscle tissue engineering. *Journal of cellular and molecular medicine* 8: 413-422, 2004.

11. Bao M., Q. Zhou, W. Dong, X. Lou and Y. Zhang. Ultrasound-modulated shape memory and payload release effects in a biodegradable cylindrical rod made of chitosan-functionalized PLGA microspheres. *Biomacromolecules* 14: 1971-1979, 2013.

12. Bao T.-Q., R.-A. Franco and B.-T. Lee. Preparation and characterization of novel poly(ε-caprolactone)/biphasic calcium phosphate hybrid composite microspheres. *Journal of biomedical materials research* 98B: 272-279, 2011.

13. Barbe M. F., S. Gallagher, V. S. Massicotte, M. Tytell, S. N. Popoff and A. E. Barr-Gillespie. The interaction of force and repetition on musculoskeletal and neural tissue responses and sensorimotor behavior in a rat model of work-related musculoskeletal disorders. *BMC musculoskeletal disorders* 14: 303, 2013.

14. Barrias C. C., C. C. Ribeiro, M. Lamghari, C. S. Miranda and M. A. Barbosa. Proliferation, activity, and osteogenic differentiation of bone marrow stromal cells cultured on calcium titanium phosphate microspheres. *Journal of Biomedical Materials Research Part A* 72: 57-66, 2005.

15. Basmanav F. B., G. T. Kose and V. Hasirci. Sequential growth factor delivery from complexed microspheres for bone tissue engineering. *Biomaterials* 29: 4195-4204, 2008.

16. Beck E. C., M. Barragan, M. H. Tadros, E. A. Kiyotake, F. M. Acosta, S. L. Kieweg and M. S. Detamore. Chondroinductive Hydrogel Pastes Composed of Naturally Derived Devitalized Cartilage. *Annals of biomedical engineering* 1-18, 2016.

17. Benders K. E. M., P. R. van Weeren, S. F. Badylak, D. B. F. Saris, W. J. A. Dhert and J. Malda. Extracellular matrix scaffolds for cartilage and bone regeneration. *TRENDS in Biotechnology* 31: 171-178, 2013.

18. Berkland C., K. Kim and D. W. Pack. Fabrication of PLG microspheres with precisely controlled and monodisperse size distributions. *Journal of controlled release : official journal of the Controlled Release Society* 73: 59-74, 2001.

19. Bhamidipati M., B. Sridharan, A. M. Scurto and M. S. Detamore. Subcritical CO2 sintering of microspheres of different polymeric materials to fabricate scaffolds for tissue engineering. *Materials Science and Engineering: C* 33: 4892-4899, 2013.

20. Biondi M., L. Indolfi, F. Ungaro, F. Quaglia, M. I. La Rotonda and P. A. Netti. Bioactivated collagen-based scaffolds embedding protein-releasing biodegradable microspheres: tuning of protein release kinetics. *Journal of Materials Science: Materials in Medicine* 20: 2117-2128, 2009.

21. Blaker J. J., J. C. Knowles and R. M. Day. Novel fabrication techniques to produce microspheres by thermally induced phase separation for tissue engineering and drug delivery. *Acta biomaterialia* 4: 264-272, 2008.

22. Bloemers F. W., T. J. Blokhuis, P. Patka, F. C. Bakker, B. W. Wippermann and H. J. T. M. Haarman. Autologous bone versus calcium‐phosphate ceramics in treatment of experimental bone defects. *Journal of Biomedical Materials Research Part B: Applied Biomaterials* 66: 526-531, 2003.

23. Boccafoschi F., M. Botta, L. Fusaro, F. Copes, M. Ramella and M. Cannas. Decellularized biological matrices: an interesting approach for cardiovascular tissue repair and regeneration. *Journal of Tissue Engineering and Regenerative Medicine* 2015.

24. Bonet J. *Nonlinear continuum mechanics for finite element analysis*. 1997.

25. Borden M., M. Attawia and C. T. Laurencin. The sintered microsphere matrix for bone tissue engineering: in vitro osteoconductivity studies. *Journal of biomedical materials research* 61: 421-429, 2002.

26. Borden M., S. F. El-Amin, M. Attawia and C. T. Laurencin. Structural and human cellular assessment of a novel microsphere-based tissue engineered scaffold for bone repair. *Biomaterials* 24: 597-609, 2003.

27. Boyan B. D., T. W. Hummert, D. D. Dean and Z. Schwartz. Role of material surfaces in regulating bone and cartilage cell response. *Biomaterials* 17: 137-146, 1996.

28. Boyan B. D., Z. Schwartz, L. Bonewald and L. Swain. Localization of 1, 25-(OH) 2D3-responsive alkaline phosphatase in osteoblast-like cells (ROS 17/2.8, MG 63, and MC 3T3) and growth cartilage cells in culture. *Journal of Biological Chemistry* 264: 11879-11886, 1989.

29. Brown J. L., L. S. Nair and C. T. Laurencin. Solvent/non-solvent sintering: a novel route to create porous microsphere scaffolds for tissue regeneration. *Journal of biomedical materials research. Part B, Applied biomaterials* 86: 396-406, 2008.

30. Brown J. L., M. S. Peach, L. S. Nair, S. G. Kumbar and C. T. Laurencin. Composite scaffolds: bridging nanofiber and microsphere architectures to improve bioactivity of mechanically competent constructs. *Journal of Biomedical Materials Research Part A* 95: 1150-1158, 2010.

31. Brown K. V., B. Li, T. Guda, D. S. Perrien, S. A. Guelcher and J. C. Wenke. Improving bone formation in a rat femur segmental defect by controlling bone morphogenetic protein-2 release. *Tissue engineering. Part A* 17: 1735-1746, 2011.

32. Brown L. R., W. R. Gombotz and M. S. Healy. Very low temperature casting of controlled release microspheres. US Patent Office, 1991.

33. Chen F.-M., Y.-M. Zhao, H.-H. Sun, T. Jin, Q.-T. Wang, W. Zhou, Z.-F. Wu and Y. Jin. Novel glycidyl methacrylated dextran (Dex-GMA)/gelatin hydrogel scaffolds containing microspheres loaded with bone morphogenetic proteins: formulation and characteristics. *Journal of controlled release : official journal of the Controlled Release Society* 118: 65-77, 2007.

34. Chen W.-C., Y.-H. Wei, I. M. Chu and C.-L. Yao. Effect of chondroitin sulphate C on the in vitro and in vivo chondrogenesis of mesenchymal stem cells in crosslinked type II collagen scaffolds. *Journal of Tissue Engineering and Regenerative Medicine* 7: 665-672, 2013.

35. Chen X., Y. Zhou, L. Wang, M. H. Santare, L. Q. Wan and X. L. Lu. Determining Tension–Compression Nonlinear Mechanical Properties of Articular Cartilage from Indentation Testing. *Annals of biomedical engineering* 1-11, 2015.

36. Chen Y., J. Wang, X. Zhu, Z. Tang, X. Yang, Y. Tan, Y. Fan and X. Zhang. Enhanced effect of β-tricalcium phosphate phase on neovascularization of porous calcium phosphate ceramics: In vitro and in vivo evidence. *Acta biomaterialia* 11: 435-448, 2015.

37. Cheng C. W., L. D. Solorio and E. Alsberg. Decellularized tissue and cell-derived extracellular matrices as scaffolds for orthopaedic tissue engineering. *Biotechnology advances* 32: 462-484, 2014.

38. Cheng N.-C., B. T. Estes, T.-H. Young and F. Guilak. Engineered cartilage using primary chondrocytes cultured in a porous cartilage-derived matrix. *Regenerative Medicine* 6: 81-93, 2011.

39. Chesnutt B. M., A. M. Viano, Y. Yuan, Y. Yang, T. Guda, M. R. Appleford, J. L. Ong, W. O. Haggard and J. D. Bumgardner. Design and characterization of a novel chitosan/nanocrystalline calcium phosphate composite scaffold for bone regeneration. *Journal of Biomedical Materials Research Part A* 88: 491-502, 2009.

40. Chevrier A., E. Rossomacha, M. D. Buschmann and C. D. Hoemann. Optimization of histoprocessing methods to detect glycosaminoglycan, collagen type II, and collagen type I in decalcified rabbit osteochondral sections. *Journal of Histotechnology* 28: 165-175, 2005.

41. Chou M.-J., C.-H. Hsieh, P.-L. Yeh, P.-C. Chen, C.-H. Wang and Y.-Y. Huang. Application of open porous poly(D,L-lactide-co-glycolide) microspheres and the strategy of hydrophobic seeding in hepatic tissue cultivation. *Journal of Biomedical Materials Research Part A* 101: 2862-2869, 2013.

42. Chung H. J., I. K. Kim, T. G. Kim and T. G. Park. Highly open porous biodegradable microcarriers: in vitro cultivation of chondrocytes for injectable delivery. *Tissue engineering. Part A* 14: 607-615, 2008.

43. Chung H. J. and T. G. Park. Surface engineered and drug releasing pre-fabricated scaffolds for tissue engineering. *Advanced Drug Delivery Reviews* 59: 249-262, 2007.

44. Clark A., T. A. Milbrandt, J. Z. Hilt and D. A. Puleo. Tailoring properties of microsphere-based poly(lactic-co-glycolic acid) scaffolds. *Journal of Biomedical Materials Research Part A* 2013.

45. Converse G. L., M. Armstrong, R. W. Quinn, E. E. Buse, M. L. Cromwell, S. J. Moriarty, G. K. Lofland, S. L. Hilbert and R. A. Hopkins. Effects of cryopreservation, decellularization and novel extracellular matrix conditioning on the quasi-static and time-dependent properties of the pulmonary valve leaflet. *Acta biomaterialia* 8: 2722-2729, 2012.

46. Cushnie E. K., Y. M. Khan and C. T. Laurencin. Amorphous hydroxyapatite-sintered polymeric scaffolds for bone tissue regeneration: physical characterization studies. *Journal of Biomedical Materials Research Part A* 84: 54-62, 2008.

47. Das A., S. Tanner, D. A. Barker, D. Green and E. A. Botchwey. Delivery of S1P receptor-targeted drugs via biodegradable polymer scaffolds enhances bone regeneration in a critical size cranial defect. *Journal of Biomedical Materials Research Part A* 2013.

48. de Boer R., A. Borntraeger, A. M. Knight, M.-N. Hébert-Blouin, R. J. Spinner, M. J. A. Malessy, M. J. Yaszemski and A. J. Windebank. Short- and long-term peripheral nerve regeneration using a poly-lactic-co-glycolic-acid scaffold containing nerve growth factor and glial cell line-derived neurotrophic factor releasing microspheres. *Journal of Biomedical Materials Research Part A* 100: 2139-2146, 2012.

49. De Nardo L., S. Bertoldi, A. Cigada, M. C. Tanzi, H. J. Haugen and S. Farè. Preparation and characterization of shape memory polymer scaffolds via solvent casting/particulate leaching. *Journal of applied biomaterials & functional materials* 10: 119-126, 2012.

50. de Vries–van Melle M. L., R. Narcisi, N. Kops, W. J. Koevoet, P. K. Bos, J. M. Murphy, J. A. Verhaar, P. M. van der Kraan and G. J. van Osch. Chondrogenesis of mesenchymal stem cells in an osteochondral environment is mediated by the subchondral bone. *Tissue Engineering Part A* 20: 23-33, 2013.

51. Decaris M. L., B. Y. Binder, M. A. Soicher, A. Bhat and J. K. Leach. Cell-Derived Matrix Coatings for Polymeric Scaffolds. *Tissue engineering. Part A* 18: 2148-2157, 2012.

52. DeFail A. J., C. R. Chu, N. Izzo and K. G. Marra. Controlled release of bioactive TGF-beta 1 from microspheres embedded within biodegradable hydrogels. *Biomaterials* 27: 1579-1585, 2006.

53. Dellinger J. G., J. Cesarano and R. D. Jamison. Robotic deposition of model hydroxyapatite scaffolds with multiple architectures and multiscale porosity for bone tissue engineering. *Journal of Biomedical Materials Research Part A* 82: 383-394, 2007.

54. Dellinger J. G., A. M. Wojtowicz and R. D. Jamison. Effects of degradation and porosity on the load bearing properties of model hydroxyapatite bone scaffolds. *Journal of Biomedical Materials Research Part A* 77: 563-571, 2006.

55. Detamore M. S. and K. A. Athanasiou. Tensile Properties of the Porcine Temporomandibular Joint Disc. *Journal of biomechanical engineering* 125: 558-558, 2003.

56. Di Luca A., C. Van Blitterswijk and L. Moroni. The osteochondral interface as a gradient tissue: From development to the fabrication of gradient scaffolds for regenerative medicine. *Birth Defects Research Part C: Embryo Today: Reviews* 105: 34-52, 2015.

57. Dormer N. H., C. J. Berkland and M. S. Detamore. Emerging Techniques in Stratified Designs and Continuous Gradients for Tissue Engineering of Interfaces. *Annals of biomedical engineering* 38: 2121-2141, 2010.

58. Dormer N. H., K. Busaidy, C. J. Berkland and M. S. Detamore. Osteochondral interface regeneration of rabbit mandibular condyle with bioactive signal gradients. In: *Journal of oral and maxillofacial surgery : official journal of the American Association of Oral and Maxillofacial Surgeons*2011, p. e50-57.

59. Dormer N. H., K. Busaidy, C. J. Berkland and M. S. Detamore. Osteochondral interface regeneration of rabbit mandibular condyle with bioactive signal gradients. *Journal of oral and maxillofacial surgery : official journal of the American Association of Oral and Maxillofacial Surgeons* 69: e50-57, 2011.

60. Dormer N. H., V. Gupta, A. M. Scurto, C. J. Berkland and M. S. Detamore. Effect of different sintering methods on bioactivity and release of proteins from PLGA microspheres. *Materials Science and Engineering: C* 33: 4343-4351, 2013.

61. Dormer N. H., Y. Qiu, A. M. Lydick, N. D. Allen, N. Mohan, C. J. Berkland and M. S. Detamore. Osteogenic Differentiation of Human Bone Marrow Stromal Cells in Hydroxyapatite-Loaded Microsphere-Based Scaffolds. In: *Tissue Engineering Part A* Mary Ann Liebert, Inc. 140 Huguenot Street, 3rd Floor New Rochelle, NY 10801 USA 2012, p. 757-767.

62. Dormer N. H., Y. Qiu, A. M. Lydick, N. D. Allen, N. Mohan, C. J. Berkland and M. S. Detamore. Osteogenic differentiation of human bone marrow stromal cells in hydroxyapatite-loaded microsphere-based scaffolds. *Tissue engineering. Part A* 18: 757-767, 2012.

63. Dormer N. H., M. Singh, L. Wang, C. J. Berkland and M. S. Detamore. Osteochondral interface tissue engineering using macroscopic gradients of bioactive signals. In: *Ann Biomed Eng*2010, p. 2167-2182.

64. Dormer N. H., M. Singh, L. Wang, C. J. Berkland and M. S. Detamore. Osteochondral interface tissue engineering using macroscopic gradients of bioactive signals. *Annals of biomedical engineering* 38: 2167-2182, 2010.

65. Dormer N. H., M. Singh, L. Zhao, N. Mohan, C. J. Berkland and M. S. Detamore. Osteochondral interface regeneration of the rabbit knee with macroscopic gradients of bioactive signals. In: *Journal of Biomedical Materials Research Part A*2012, p. 162-170.

66. Dormer N. H., M. Singh, L. Zhao, N. Mohan, C. J. Berkland and M. S. Detamore. Osteochondral interface regeneration of the rabbit knee with macroscopic gradients of bioactive signals. *Journal of Biomedical Materials Research Part A* 100: 162-170, 2012.

67. Dreifke M. B., N. A. Ebraheim and A. C. Jayasuriya. Investigation of potential injectable polymeric biomaterials for bone regeneration. *Journal of Biomedical Materials Research Part A* 101: 2436-2447, 2013.

68. Drosos G. I., K. I. Kazakos, P. Kouzoumpasis and D.-A. Verettas. Safety and efficacy of commercially available demineralised bone matrix preparations: a critical review of clinical studies. *Injury* 38: S13-S21, 2007.

69. Duan B., W. L. Cheung and M. Wang. Optimized fabrication of Ca-P/PHBV nanocomposite scaffolds via selective laser sintering for bone tissue engineering. *Biofabrication* 3: 2011.

70. Duan B., M. Wang, W. Y. Zhou and W. L. Cheung. Synthesis of Ca–P nanoparticles and fabrication of Ca–P/PHBV nanocomposite microspheres for bone tissue engineering applications. *Applied Surface Science* 255: 529-533, 2008.

71. Ebrahimi M., P. Pripatnanont, S. Suttapreyasri and N. Monmaturapoj. In vitrobiocompatibility analysis of novel nano-biphasic calcium phosphate scaffolds in different composition ratios. *Journal of biomedical materials research* 102: 52-61, 2013.

72. Fan H., Y. Hu, C. Zhang, X. Li, R. Lv, L. Qin and R. Zhu. Cartilage regeneration using mesenchymal stem cells and a PLGA–gelatin/chondroitin/hyaluronate hybrid scaffold. *Biomaterials* 27: 4573-4580, 2006.

73. Fang J., Y. Zhang, S. Yan, Z. Liu, S. He, L. Cui and J. Yin. Poly(l-glutamic acid)/chitosan polyelectrolyte complex porous microspheres as cell microcarriers for cartilage regeneration. *Acta biomaterialia* 10: 276-288, 2014.

74. Fellah B. H., O. Gauthier, P. Weiss, D. Chappard and P. Layrolle. Osteogenicity of biphasic calcium phosphate ceramics and bone autograft in a goat model. *Biomaterials* 29: 1177-1188, 2008.

75. Fielding G. and S. Bose. SiO 2 and ZnO dopants in three-dimensionally printed tricalcium phosphate bone tissue engineering scaffolds enhance osteogenesis and angiogenesis in vivo. *Acta biomaterialia* 9: 9137-9148, 2013.

76. Fiorentini E., D. Granchi, E. Leonardi, N. Baldini and G. Ciapetti. Effects of osteogenic differentiation inducers on in vitro expanded adult mesenchymal stromal cells. *The International Journal of Artificial Organs* 34: 998-1011, 2011.

77. Fonseca C., M. Caminal, D. Peris, J. Barrachina, P. J. Fabregas, F. Garcia, J. J. Cairo, F. Godia, A. Pla and J. Vives. An arthroscopic approach for the treatment of osteochondral focal defects with cell-free and cell-loaded PLGA scaffolds in sheep. *Cytotechnology* 66: 345-354, 2014.

78. Francis L., D. Meng, J. C. Knowles, I. Roy and A. R. Boccaccini. Multi-functional P(3HB) microsphere/45S5 Bioglass-based composite scaffolds for bone tissue engineering. *Acta biomaterialia* 6: 2773-2786, 2010.

79. Freitas S., H. P. Merkle and B. Gander. Microencapsulation by solvent extraction/evaporation: reviewing the state of the art of microsphere preparation process technology. *Journal of Controlled Release* 102: 313-332, 2005.

80. Frisbie D., S. Bowman, H. Colhoun, E. DiCarlo, C. Kawcak and C. McIlwraith. Evaluation of autologous chondrocyte transplantation via a collagen membrane in equine articular defects–results at 12 and 18 months. *Osteoarthritis and Cartilage* 16: 667-679, 2008.

81. Gallagher S. and J. R. Heberger. Examining the interaction of force and repetition on musculoskeletal disorder risk: a systematic literature review. *Human Factors: The Journal of the Human Factors and Ergonomics Society* 55: 108-124, 2013.

82. Garkhal K., S. Verma, K. Tikoo and N. Kumar. Surface modified poly(L-lactide-co-ε-caprolactone) microspheres as scaffold for tissue engineering. *Journal of biomedical materials research* 82A: 747-756, 2007.

83. Garrigues N. W., D. Little, J. Sanchez‐Adams, D. S. Ruch and F. Guilak. Electrospun cartilage‐derived matrix scaffolds for cartilage tissue engineering. *Journal of Biomedical Materials Research Part A* 102: 3998-4008, 2014.

84. GĂśtz W., S. Lenz, C. Reichert, K. Henkel, L. Pernicka, K. Gundlach, T. Gredes, T. Gerber, T. Gedrange and F. Heinemann. A preliminary study in osteoinduction by a nano-crystalline hydroxyapatite in the mini pig. *Folia histochemica et cytobiologica* 48: 589-588, 2011.

85. Ghanaati S., M. Barbeck, R. Detsch, U. Deisinger, U. Hilbig, V. Rausch, R. Sader, R. E. Unger, G. Ziegler and C. J. Kirkpatrick. The chemical composition of synthetic bone substitutes influences tissue reactions in vivo: histological and histomorphometrical analysis of the cellular inflammatory response to hydroxyapatite, beta-tricalcium phosphate and biphasic calcium phosphate ceramics. *Biomedical materials (Bristol, England)* 7: 2012.

86. Ghanbar H., C. J. Luo, P. Bakhshi, R. Day and M. Edirisinghe. Preparation of porous microsphere-scaffolds by electrohydrodynamic forming and thermally induced phase separation. *Materials science & engineering. C, Materials for biological applications* 33: 2488-2498, 2013.

87. Gordeladze J. O., F. Djouad, J.-M. Brondello, D. Noël, I. Duroux-Richard, F. Apparailly and C. Jorgensen. Concerted stimuli regulating osteo-chondral differentiation from stem cells: phenotype acquisition regulated by microRNAs. *Acta Pharmacologica Sinica* 30: 1369-1384, 2009.

88. Gordeladze J. O., F. Djouad and J. M. Brondello. Concerted stimuli regulating osteo-chondral differentiation from stem cells: phenotype acquisition regulated by microRNAs. *Acta Pharmacologica ...* 2009.

89. Gupta V., N. Mohan, C. Berkland and M. S. Detamore. Microsphere-Based Scaffolds Carrying Opposing Gradients of Chondroitin Sulfate and Tricalcium Phosphate. *Frontiers in Bioengineering and Biotechnology* 3: 2015.

90. Habraken W. J. E. M., H. B. Liao, Z. Zhang, J. G. C. Wolke, D. W. Grijpma, A. G. Mikos, J. Feijen and J. A. Jansen. In vivo degradation of calcium phosphate cement incorporated into biodegradable microspheres. *Acta biomaterialia* 6: 2200-2211, 2010.

91. Habraken W. J. E. M., J. G. C. Wolke, A. G. Mikos and J. A. Jansen. Injectable PLGA microsphere/calcium phosphate cements: physical properties and degradation characteristics. *Journal of biomaterials science. Polymer edition* 17: 1057-1074, 2006.

92. Habraken W. J. E. M., J. G. C. Wolke, A. G. Mikos and J. A. Jansen. Porcine gelatin microsphere/calcium phosphate cement composites: an in vitro degradation study. *Journal of biomedical materials research. Part B, Applied biomaterials* 91: 555-561, 2009.

93. Hayrapetyan A., J. A. Jansen and J. J. J. P. van den Beucken. Signaling Pathways Involved in Osteogenesis and Their Application for Bone Regenerative Medicine. In: *Tissue Engineering Part B: Reviews*2014, p. 140819120840001.

94. Hong S.-J., H.-S. Yu and H.-W. Kim. Tissue Engineering Polymeric Microcarriers with Macroporous Morphology and Bone-Bioactive Surface. *Macromolecular bioscience* 9: 639-645, 2009.

95. Hori Y., A. M. Winans and D. J. Irvine. Modular injectable matrices based on alginate solution/microsphere mixtures that gel in situ and co-deliver immunomodulatory factors. *Acta biomaterialia* 5: 969-982, 2009.

96. Horning J. L., S. K. Sahoo, S. Vijayaraghavalu, S. Dimitrijevic, J. K. Vasir, T. K. Jain, A. K. Panda and V. Labhasetwar. 3-D Tumor Model for In VitroEvaluation of Anticancer Drugs. *Molecular Pharmaceutics* 5: 849-862, 2008.

97. Hoshiba T., H. Lu, N. Kawazoe and G. Chen. Decellularized matrices for tissue engineering. *Expert opinion on biological therapy* 10: 1717-1728, 2010.

98. Hu J., Y. Zhou, L. Huang, J. Liu and H. Lu. Effect of nano-hydroxyapatite coating on the osteoinductivity of porous biphasic calcium phosphate ceramics. *BMC musculoskeletal disorders* 15: 114, 2014.

99. Hu X., H. Shen, F. Yang, X. Liang, S. Wang and D. Wu. Modified composite microspheres of hydroxyapatite and poly(lactide-co-glycolide) as an injectable scaffold. *Applied Surface Science* 292: 764-772, 2014.

100. Huang S., G. Lu, Y. Wu, E. Jirigala, Y. Xu, K. Ma and X. Fu. Mesenchymal stem cells delivered in a microsphere-based engineered skin contribute to cutaneous wound healing and sweat gland repair. *Journal of dermatological science* 66: 29-36, 2012.

101. Huang W., X. Li, X. Shi and C. Lai. Microsphere based scaffolds for bone regenerative applications. *Biomaterials Science* 2014.

102. Huang Z., P. Nooeaid, B. Kohl, J. A. Roether, D. W. Schubert, C. Meier, A. R. Boccaccini, O. Godkin, W. Ertel and S. Arens. Chondrogenesis of human bone marrow mesenchymal stromal cells in highly porous alginate-foams supplemented with chondroitin sulfate. *Materials Science and Engineering: C* 50: 160-172, 2015.

103. Imranul Alam M., I. Asahina, K. Ohmamiuda, K. Takahashi, S. Yokota and S. Enomoto. Evaluation of ceramics composed of different hydroxyapatite to tricalcium phosphate ratios as carriers for rhBMP-2. *Biomaterials* 22: 1643-1651, 2001.

104. Ionescu L. C., G. C. Lee, B. J. Sennett, J. A. Burdick and R. L. Mauck. An anisotropic nanofiber/microsphere composite with controlled release of biomolecules for fibrous tissue engineering. *Biomaterials* 31: 4113-4120, 2010.

105. Jabbarzadeh E., M. Deng, Q. Lv, T. Jiang, Y. M. Khan, L. S. Nair and C. T. Laurencin. VEGF-incorporated biomimetic poly(lactide-co-glycolide) sintered microsphere scaffolds for bone tissue engineering. *Journal of biomedical materials research. Part B, Applied biomaterials* 100: 2187-2196, 2012.

106. Jabbarzadeh E., T. Jiang, M. Deng, L. S. Nair, Y. M. Khan and C. T. Laurencin. Human endothelial cell growth and phenotypic expression on three dimensional poly(lactide-co-glycolide) sintered microsphere scaffolds for bone tissue engineering. *Biotechnology and bioengineering* 98: 1094-1102, 2007.

107. Jabbarzadeh E., L. S. Nair, Y. M. Khan, M. Deng and C. T. Laurencin. Apatite nano-crystalline surface modification of poly(lactide-co-glycolide) sintered microsphere scaffolds for bone tissue engineering: implications for protein adsorption. *Journal of biomaterials science. Polymer edition* 18: 1141-1152, 2007.

108. Jabbarzadeh E., T. Starnes, Y. M. Khan, T. Jiang, A. J. Wirtel, M. Deng, Q. Lv, L. S. Nair, S. B. Doty and C. T. Laurencin. Induction of angiogenesis in tissue-engineered scaffolds designed for bone repair: a combined gene therapy-cell transplantation approach. *Proceedings of the National Academy of Sciences* 105: 11099-11104, 2008.

109. Jaklenec A., A. Hinckfuss, B. Bilgen, D. M. Ciombor, R. Aaron and E. Mathiowitz. Sequential release of bioactive IGF-I and TGF-beta 1 from PLGA microsphere-based scaffolds. *Biomaterials* 29: 1518-1525, 2008.

110. Jaklenec A., E. Wan, M. E. Murray and E. Mathiowitz. Novel scaffolds fabricated from protein-loaded microspheres for tissue engineering. *Biomaterials* 29: 185-192, 2008.

111. Jaklenec A., E. Wan, M. E. Murray and E. Mathiowitz. Novel scaffolds fabricated from protein-loaded microspheres for tissue engineering. *Biomaterials* 29: 185-192, 2008.

112. Jang J.-H. and L. D. Shea. Controllable delivery of non-viral DNA from porous scaffolds. *Journal of controlled release : official journal of the Controlled Release Society* 86: 157-168, 2003.

113. Jeon J. E., C. Vaquette, T. J. Klein and D. W. Hutmacher. Perspectives in Multiphasic Osteochondral Tissue Engineering. *The Anatomical Record* 297: 26-35, 2013.

114. Jeon J. H., M. Bhamidipati, B. Sridharan, A. M. Scurto, C. J. Berkland and M. S. Detamore. Tailoring of processing parameters for sintering microsphere-based scaffolds with dense-phase carbon dioxide. *Journal of biomedical materials research. Part B, Applied biomaterials* 101: 330-337, 2013.

115. Jiang T., W. I. Abdel-Fattah and C. T. Laurencin. In vitro evaluation of chitosan/poly(lactic acid-glycolic acid) sintered microsphere scaffolds for bone tissue engineering. *Biomaterials* 27: 4894-4903, 2006.

116. Jiang T., Y. Khan, L. S. Nair, W. I. Abdel-Fattah and C. T. Laurencin. Functionalization of chitosan/poly(lactic acid-glycolic acid) sintered microsphere scaffolds via surface heparinization for bone tissue engineering. *Journal of Biomedical Materials Research Part A* 93: 1193-1208, 2010.

117. Jiang T., S. P. Nukavarapu, M. Deng, E. Jabbarzadeh, M. D. Kofron, S. B. Doty, W. I. Abdel-Fattah and C. T. Laurencin. Chitosan-poly(lactide-co-glycolide) microsphere-based scaffolds for bone tissue engineering: in vitro degradation and in vivo bone regeneration studies. *Acta biomaterialia* 6: 3457-3470, 2010.

118. Jin G.-Z., J.-H. Park, S.-J. Seo and H.-W. Kim. Dynamic cell culture on porous biopolymer microcarriers in a spinner flask for bone tissue engineering: a feasibility study. *Biotechnology Letters* 36: 1539-1548, 2014.

119. Ju Y. M., B. Yu, L. West, Y. Moussy and F. Moussy. A dexamethasone-loaded PLGA microspheres/collagen scaffold composite for implantable glucose sensors. *Journal of Biomedical Materials Research Part A* 93: 200-210, 2010.

120. Kang S.-W. and Y. H. Bae. Cryopreservable and tumorigenic three-dimensional tumor culture in porous poly(lactic-co-glycolic acid) microsphere. *Biomaterials* 30: 4227-4232, 2009.

121. Kang S.-W., O. Jeon and B.-S. Kim. Poly(lactic-co-glycolic acid) microspheres as an injectable scaffold for cartilage tissue engineering. *Tissue engineering* 11: 438-447, 2005.

122. Kang S.-W., W.-G. La and B.-S. Kim. Open Macroporous Poly(lactic-co-glycolic Acid) Microspheres as an Injectable Scaffold for Cartilage Tissue Engineering. *Journal of biomaterials science. Polymer edition* 20: 399-409, 2009.

123. Kang S.-W., S.-W. Seo, C. Y. Choi and B.-S. Kim. Porous Poly(Lactic-Co-Glycolic Acid) Microsphere as Cell Culture Substrate and Cell Transplantation Vehicle for Adipose Tissue Engineering. *Tissue Engineering Part C-Methods* 14: 25-34, 2008.

124. Kang S.-W., H. S. Yang, S.-W. Seo, D. K. Han and B.-S. Kim. Apatite-coated poly(lactic-co-glycolic acid) microspheres as an injectable scaffold for bone tissue engineering. *Journal of biomedical materials research* 85A: 747-756, 2008.

125. Kang S.-W., J.-R. Yoon, J.-S. Lee, H. J. Kim, H.-W. Lim, H. C. Lim, J.-H. Park and B.-S. Kim. The use of poly(lactic-co-glycolic acid) microspheres as injectable cell carriers for cartilage regeneration in rabbit knees. *Journal of biomaterials science. Polymer edition* 17: 925-939, 2006.

126. Kay S., A. Thapa, K. M. Haberstroh and T. J. Webster. Nanostructured polymer/nanophase ceramic composites enhance osteoblast and chondrocyte adhesion. *Tissue engineering* 8: 753-761, 2002.

127. Keane T. J., I. T. Swinehart and S. F. Badylak. Methods of tissue decellularization used for preparation of biologic scaffolds and in vivo relevance. *Methods* 84: 25-34, 2015.

128. Keaveny T. M. and W. C. Hayes. Mechanical properties of cortical and trabecular bone. *Bone. A treatise* 7: 285-344, 1993.

129. Kempen D. H. R., M. C. Kruyt, L. Lu, C. E. Wilson, A. V. Florschutz, L. B. Creemers, M. J. Yaszemski and W. J. A. Dhert. Effect of autologous bone marrow stromal cell seeding and bone morphogenetic protein-2 delivery on ectopic bone formation in a microsphere/poly(propylene fumarate) composite. *Tissue engineering. Part A* 15: 587-594, 2009.

130. Kempen D. H. R., L. Lu, T. E. Hefferan, L. B. Creemers, A. Maran, K. L. Classic, W. J. A. Dhert and M. J. Yaszemski. Retention of in vitro and in vivo BMP-2 bioactivities in sustained delivery vehicles for bone tissue engineering. *Biomaterials* 29: 3245-3252, 2008.

131. Kempen D. H. R., L. Lu, C. Kim, X. Zhu, W. J. A. Dhert, B. L. Currier and M. J. Yaszemski. Controlled drug release from a novel injectable biodegradable microsphere/scaffold composite based on poly(propylene fumarate). *Journal of Biomedical Materials Research Part A* 77: 103-111, 2006.

132. Khan A. Comparison of TCP and TCP/HA Hybrid Scaffolds for Osteoconductive Activity. 2010, p. 1-7.

133. Kim H., T. Zahir, C. H. Tator and M. S. Shoichet. Effects of dibutyryl cyclic-AMP on survival and neuronal differentiation of neural stem/progenitor cells transplanted into spinal cord injured rats. *PLoS ONE* 6: e21744, 2011.

134. Kim H. D., J. Heo, Y. Hwang, S.-Y. Kwak, O. K. Park, H. Kim, S. Varghese and N. S. Hwang. Extracellular-Matrix-Based and Arg-Gly-Asp-Modified Photopolymerizing Hydrogels for Cartilage Tissue Engineering. *Tissue engineering. Part A* 141114124207000, 2014.

135. Kim S.-S., S.-J. Gwak, C. Y. Choi and B.-S. Kim. Skin regeneration using keratinocytes and dermal fibroblasts cultured on biodegradable microspherical polymer scaffolds. *Journal of biomedical materials research. Part B, Applied biomaterials* 75: 369-377, 2005.

136. KIM T., J. YOON, D. Lee and T. PARK. Gas foamed open porous biodegradable polymeric microspheres. *Biomaterials* 27: 152-159, 2006.

137. Kofron M. D., J. A. Cooper, S. G. Kumbar and C. T. Laurencin. Novel tubular composite matrix for bone repair. *Journal of Biomedical Materials Research Part A* 82: 415-425, 2007.

138. Kofron M. D., N. C. Opsitnick, M. A. Attawia and C. T. Laurencin. Cryopreservation of tissue engineered constructs for bone. *Journal of orthopaedic research : official publication of the Orthopaedic Research Society* 21: 1005-1010, 2003.

139. Kucharska M., K. Walenko, M. Lewandowska-Szumieł, T. Brynk, J. Jaroszewicz and T. Ciach. Chitosan and composite microsphere-based scaffold for bone tissue engineering:

evaluation of tricalcium phosphate content influence on physical and biological properties. *Journal of Materials Science: Materials in Medicine* 26: 143-112, 2015.

140. Kumbar S. G., U. S. Toti, M. Deng, R. James, C. T. Laurencin, A. Aravamudhan, M. Harmon and D. M. Ramos. Novel mechanically competent polysaccharide scaffolds for bone tissue engineering. *Biomedical materials (Bristol, England)* 6: 065005, 2011.

141. Kurashina K., H. Kurita, Q. Wu, A. Ohtsuka and H. Kobayashi. Ectopic osteogenesis with biphasic ceramics of hydroxyapatite and tricalcium phosphate in rabbits. *Biomaterials* 23: 407-412, 2002.

142. Lakhkar N. J., J.-H. Park, N. J. Mordan, V. Salih, I. B. Wall, H.-W. Kim, S. P. King, J. V. Hanna, R. A. Martin, O. Addison, J. F. W. Mosselmans and J. C. Knowles. Titanium phosphate glass microspheres for bone tissue engineering. *Acta biomaterialia* 8: 4181-4190, 2012.

143. Lee J. E., K. E. Kim, I. C. Kwon, H. J. Ahn, S.-H. Lee, H. Cho, H. J. Kim, S. C. Seong and M. C. Lee. Effects of the controlled-released TGF-beta 1 from chitosan microspheres on chondrocytes cultured in a collagen/chitosan/glycosaminoglycan scaffold. *Biomaterials* 25: 4163-4173, 2004.

144. Lee J. E., S. E. Kim, I. C. Kwon, H. J. Ahn, H. Cho, S.-H. Lee, H. J. Kim, S. C. Seong and M. C. Lee. Effects of a chitosan scaffold containing TGF-beta1 encapsulated chitosan microspheres on in vitro chondrocyte culture. *Artificial Organs* 28: 829-839, 2004.

145. Lee J. W., K. S. Kang, S. H. Lee, J.-Y. Kim, B.-K. Lee and D.-W. Cho. Bone regeneration using a microstereolithography-produced customized poly(propylene fumarate)/diethyl fumarate photopolymer 3D scaffold incorporating BMP-2 loaded PLGA microspheres. *Biomaterials* 32: 744-752, 2011.

146. Lee J. W., K.-J. Kim, K. S. Kang, S. Chen, J. W. Rhie and D.-W. Cho. Development of a bone reconstruction technique using a solid free-form fabrication (SFF)-based drug releasing scaffold and adipose-derived stem cells. *Journal of Biomedical Materials Research Part A* 101: 1865-1875, 2013.

147. Lee M., B. M. Wu, M. Stelzner, H. M. Reichardt and J. C. Y. Dunn. Intestinal smooth muscle cell maintenance by basic fibroblast growth factor. *Tissue engineering. Part A* 14: 1395-1402, 2008.

148. Li B., T. Yoshii, A. E. Hafeman, J. S. Nyman, J. C. Wenke and S. A. Guelcher. The effects of rhBMP-2 released from biodegradable polyurethane/microsphere composite scaffolds on new bone formation in rat femora. *Biomaterials* 30: 6768-6779, 2009.

149. Liang C., H. Li, C. Li, Z. Yang, X. Zhou, Y. Tao, Y. Xiao, F. Li and Q. Chen. Fabrication of a Layered Microstructured Polymeric Microspheres as a Cell Carrier for Nucleus Pulposus Regeneration. *Journal of biomaterials science. Polymer edition* ahead-of-print: 1-16, 2012.

150. Liang C. Z., H. Li, Y. Q. Tao, X. P. Zhou, Z. R. Yang, Y. X. Xiao, F. C. Li, B. Han and Q. X. Chen. Dual delivery for stem cell differentiation using dexamethasone and bFGF in/on

polymeric microspheres as a cell carrier for nucleus pulposus regeneration. *Journal of Materials Science: Materials in Medicine* 23: 1097-1107, 2012.

151. Liang H., K. Wang, A. L. Shimer, X. Li, G. Balian and F. H. Shen. Use of a bioactive scaffold for the repair of bone defects in a novel reproducible vertebral body defect model. *Bone* 47: 197-204, 2010.

152. Liao H.-T., M.-Y. Lee, W.-W. Tsai, H.-C. Wang and W.-C. Lu. Osteogenesis of adipose-derived stem cells on polycaprolactone–β-tricalcium phosphate scaffold fabricated via selective laser sintering and surface coating with collagen type I. *Journal of Tissue Engineering and Regenerative Medicine* n/a-n/a, 2013.

153. Liu H., L. Zhang, P. Shi, Q. Zou, Y. Zuo and Y. Li. Hydroxyapatite/polyurethane scaffold incorporated with drug-loaded ethyl cellulose microspheres for bone regeneration. *Journal of biomedical materials research. Part B, Applied biomaterials* 95: 36-46, 2010.

154. Londono R. and S. F. Badylak. Biologic Scaffolds for Regenerative Medicine: Mechanisms of In vivo Remodeling. *Annals of biomedical engineering* 43: 577-592, 2015.

155. Lopa S. and H. Madry. Bioinspired Scaffolds for Osteochondral Regeneration. *Tissue engineering. Part A* 20: 2052-2076, 2014.

156. Lu S., J. Lam, J. E. Trachtenberg, E. J. Lee, H. Seyednejad, J. J. J. P. van den Beucken, Y. Tabata, F. K. Kasper, D. W. Scott, M. E. Wong, J. A. Jansen and A. G. Mikos. Technical Report: Correlation Between the Repair of Cartilage and Subchondral Bone in an Osteochondral Defect Using Bilayered, Biodegradable Hydrogel Composites. *Tissue Engineering Part C-Methods* 21: 1216-1225, 2015.

157. Lü X., J. Wang, B. Li, Z. Zhang and L. Zhao. Gene expression profile study on osteoinductive effect of natural hydroxyapatite. *Journal of Biomedical Materials Research Part A* 102: 2833-2841, 2014.

158. Luciani A., V. Coccoli, S. Orsi, L. Ambrosio and P. A. Netti. PCL microspheres based functional scaffolds by bottom-up approach with predefined microstructural properties and release profiles. *Biomaterials* 29: 4800-4807, 2008.

159. Lupu-Haber Y., O. Pinkas, S. Boehm, T. Scheper, C. Kasper and M. Machluf. Functionalized PLGA-doped zirconium oxide ceramics for bone tissue regeneration. *Biomedical microdevices* 2013.

160. Lv Q., L. Nair and C. T. Laurencin. Fabrication, characterization, and in vitro evaluation of poly(lactic acid glycolic acid)/nano-hydroxyapatite composite microsphere-based scaffolds for bone tissue engineering in rotating bioreactors. *Journal of Biomedical Materials Research Part A* 91: 679-691, 2009.

161. Lv Q., L. Nair and C. T. Laurencin. Fabrication, characterization, and in vitro evaluation of poly(lactic acid glycolic acid)/nano-hydroxyapatite composite microsphere-based scaffolds for

bone tissue engineering in rotating bioreactors. In: *Journal of Biomedical Materials Research Part A*2009, p. 679-691.

162. Maas S. A., B. J. Ellis, G. A. Ateshian and J. A. Weiss. FEBio: finite elements for biomechanics. *Journal of biomechanical engineering* 134: 011005, 2012.

163. Madeira C., A. Santhagunam, J. B. Salgueiro and J. M. Cabral. Advanced cell therapies for articular cartilage regeneration. *TRENDS in Biotechnology* 33: 35-42, 2015.

164. Mansour J. M. Biomechanics of cartilage. *... : the mechanics and pathomechanics of human ...* 2003.

165. Meng D., L. Francis, I. D. Thompson, C. Mierke, H. Huebner, A. Amtmann, I. Roy and A. R. Boccaccini. Tetracycline-encapsulated P(3HB) microsphere-coated 45S5 Bioglass(®)-based scaffolds for bone tissue engineering. *Journal of Materials Science: Materials in Medicine* 2013.

166. Mercier N. R., H. R. Costantino, M. A. Tracy and L. J. Bonassar. A novel injectable approach for cartilage formation in vivo using PLG microspheres. *Annals of biomedical engineering* 32: 418-429, 2004.

167. Mercier N. R., H. R. Costantino, M. A. Tracy and L. J. Bonassar. Poly(lactide-co-glycolide) microspheres as a moldable scaffold for cartilage tissue engineering. *Biomaterials* 26: 1945-1952, 2005.

168. Mittal A., P. Negi, K. Garkhal, S. Verma and N. Kumar. Integration of porosity and bio-functionalization to form a 3D scaffold: cell culture studies and in vitro degradation. *Biomedical materials (Bristol, England)* 5: 045001, 2010.

169. Mohan N., N. H. Dormer, K. L. Caldwell, V. H. Key, C. J. Berkland and M. S. Detamore. Continuous gradients of material composition and growth factors for effective regeneration of the osteochondral interface. *Tissue engineering. Part A* 17: 2845-2855, 2011.

170. Mohan N., V. Gupta, B. Sridharan, A. Sutherland and M. S. Detamore. The potential of encapsulating “raw materials” in 3D osteochondral gradient scaffolds. In: *Biotechnol. Bioeng.*2013, p. 829-841.

171. Mohan N., V. Gupta, B. Sridharan, A. Sutherland and M. S. Detamore. The potential of encapsulating “raw materials” in 3D osteochondral gradient scaffolds. *Biotechnology and bioengineering* n/a-n/a, 2013.

172. Mohan N., V. Gupta, B. Sridharan, A. Sutherland and M. S. Detamore. The potential of encapsulating “raw materials” in 3D osteochondral gradient scaffolds. *Biotechnology and bioengineering* 111: 829-841, 2014.

173. Mohan N., V. Gupta, B. P. Sridharan, A. J. Mellott, J. T. Easley, R. H. Palmer, R. A. Galbraith, V. H. Key, C. J. Berkland and M. S. Detamore. Microsphere-based gradient implants for osteochondral regeneration: a long-term study in sheep. *Regenerative Medicine* 2015.

174. Moradi A., F. Ataollahi, K. Sayar, S. Pramanik, P.-P. Chong, A. A. Khalil, T. Kamarul and B. Pingguan-Murphy. Chondrogenic potential of physically treated bovine cartilage matrix derived porous scaffolds on human dermal fibroblast cells. *Journal of Biomedical Materials Research Part A* 104: 245-256, 2016.

175. Moroni L., J. R. de Wijn and C. A. van Blitterswijk. 3D fiber-deposited scaffolds for tissue engineering: Influence of pores geometry and architecture on dynamic mechanical properties. *Biomaterials* 27: 974-985, 2006.

176. Mow V. C., M. C. Gibbs, W. M. Lai, W. B. Zhu and K. A. Athanasiou. Biphasic indentation of articular cartilage--II. A numerical algorithm and an experimental study. *Journal of biomechanics* 22: 853-861, 1989.

177. Newbury D. E. Mistakes encountered during automatic peak identification of minor and trace constituents in electron-excited energy dispersive X-ray microanalysisThis article …. *Scanning* 2009.

178. Newman K. D. and M. W. McBurney. Poly(d,l lactic-co-glycolic acid) microspheres as biodegradable microcarriers for pluripotent stem cells. *Biomaterials* 25: 5763-5771, 2004.

179. Nguyen D. T., J. D. McCanless, M. M. Mecwan, A. P. Noblett, W. O. Haggard, R. A. Smith and J. D. Bumgardner. Balancing mechanical strength with bioactivity in chitosan-calcium phosphate 3D microsphere scaffolds for bone tissue engineering: air- vs. freeze-drying processes. *Journal of biomaterials science. Polymer edition* 24: 1071-1083, 2013.

180. Nguyen P. K., C. G. Snyder, J. D. Shields, A. W. Smith and D. L. Elbert. Clickable Poly(ethylene glycol)-Microsphere-Based Cell Scaffolds. *Macromolecular chemistry and physics* 214: 948-956, 2013.

181. Niemelä T. Effect of β-tricalcium phosphate addition on the in vitro degradation of self-reinforced poly-l,d-lactide. *Polymer Degradation and Stability* 89: 492-500, 2005.

182. Niu X., Y. Fan, X. Liu, X. Li, P. Li, J. Wang, Z. Sha and Q. Feng. Repair of bone defect in femoral condyle using microencapsulated chitosan, nanohydroxyapatite/collagen and poly(L-lactide)-based microsphere-scaffold delivery system. *Artificial Organs* 35: E119-128, 2011.

183. Nojehdehian H., F. Moztarzadeh, H. Baharvand, H. Nazarian and M. Tahriri. Preparation and surface characterization of poly-L-lysine-coated PLGA microsphere scaffolds containing retinoic acid for nerve tissue engineering: in vitro study. *Colloids and surfaces. B, Biointerfaces* 73: 23-29, 2009.

184. Nukavarapu S. P., S. G. Kumbar, J. L. Brown, N. R. Krogman, A. L. Weikel, M. D. Hindenlang, L. S. Nair, H. R. Allcock and C. T. Laurencin. Polyphosphazene/nano-hydroxyapatite composite microsphere scaffolds for bone tissue engineering. *Biomacromolecules* 9: 1818-1825, 2008.

185. O'Driscoll S. W., F. W. Keeley and R. B. Salter. Durability of regenerated articular cartilage produced by free autogenous periosteal grafts in major full-thickness defects in joint

surfaces under the influence of continuous passive motion. A follow-up report at one year. *The Journal of Bone & Joint Surgery* 70: 595-606, 1988.

186. Oredein-McCoy O., N. R. Krogman, A. L. Weikel, M. D. Hindenlang, H. R. Allcock and C. T. Laurencin. Novel factor-loaded polyphosphazene matrices: potential for driving angiogenesis. *Journal of Microencapsulation* 26: 544-555, 2009.

187. Park J. S., K. Park, D. G. Woo, H. N. Yang, H.-M. Chung and K.-H. Park. PLGA microsphere construct coated with TGF-beta 3 loaded nanoparticles for neocartilage formation. *Biomacromolecules* 9: 2162-2169, 2008.

188. Pearce A. I., R. G. Richards, S. Milz, E. Schneider and S. G. Pearce. Animal models for implant biomaterial research in bone: A review. *European Cells & Materials* 13: 1-10, 2007.

189. Persson M., G. S. Lorite, H. E. Kokkonen, S.-W. Cho, P. P. Lehenkari, M. Skrifvars and J. Tuukkanen. Effect of bioactive extruded PLA/HA composite films on focal adhesion formation of preosteoblastic cells. *Colloids and surfaces. B, Biointerfaces* 121: 409-416, 2014.

190. Petrie Aronin C. E., K. W. Sadik, A. L. Lay, D. B. Rion, S. S. Tholpady, R. C. Ogle and E. A. Botchwey. Comparative effects of scaffold pore size, pore volume, and total void volume on cranial bone healing patterns using microsphere-based scaffolds. *Journal of Biomedical Materials Research Part A* 89: 632-641, 2009.

191. RADIN E. L., M. G. EHRLICH, R. Chernack, P. Abernethy, I. L. PAUL and R. M. ROSE. Effect of repetitive impulsive loading on the knee joints of rabbits. *Clinical Orthopaedics and Related Research* 131: 288-293, 1978.

192. Ravichandran R., S. Sundarrajan, J. R. Venugopal, S. Mukherjee and S. Ramakrishna. Advances in polymeric systems for tissue engineering and biomedical applications. *Macromolecular bioscience* 12: 286-311, 2012.

193. Renth A. N. and M. S. Detamore. Leveraging "raw materials" as building blocks and bioactive signals in regenerative medicine. *Tissue Engineering Part B: Reviews* 18: 341-362, 2012.

194. Reyes R., B. De la Riva, A. Delgado, A. Hernández, E. Sánchez and C. Évora. Effect of triple growth factor controlled delivery by a brushite-PLGA system on a bone defect. *Injury* 43: 334-342, 2012.

195. Roam J. L., P. K. Nguyen and D. L. Elbert. Controlled release and gradient formation of human glial-cell derived neurotrophic factor from heparinated poly (ethylene glycol) microsphere-based scaffolds. *Biomaterials* 35: 6473-6481, 2014.

196. Roemhildt M. L., K. M. Coughlin, G. D. Peura, B. C. Fleming and B. D. Beynnon. Material properties of articular cartilage in the rabbit tibial plateau. *Journal of biomechanics* 39: 2331-2337, 2006.

197. Rooney G. E., A. M. Knight, N. N. Madigan, L. Gross, B. Chen, C. V. Giraldo, S. Seo, J. J. Nesbitt, M. Dadsetan, M. J. Yaszemski and A. J. Windebank. Sustained delivery of dibutyryl cyclic adenosine monophosphate to the transected spinal cord via oligo [(polyethylene glycol) fumarate] hydrogels. *Tissue engineering. Part A* 17: 1287-1302, 2011.

198. Royce S. M., M. Askari and K. G. Marra. Incorporation of polymer microspheres within fibrin scaffolds for the controlled delivery of FGF-1. *Journal of biomaterials science. Polymer edition* 15: 1327-1336, 2004.

199. Sahoo S. K., A. K. Panda and V. Labhasetwar. Characterization of Porous PLGA/PLA Microparticles as a Scaffold for Three Dimensional Growth of Breast Cancer Cells. *Biomacromolecules* 6: 1132-1139, 2005.

200. Salerno A., R. Levato, M. A. Mateos-Timoneda, E. Engel, P. A. Netti and J. A. Planell. Modular polylactic acid microparticle-based scaffolds prepared via microfluidic emulsion/solvent displacement process: Fabrication, characterization, and in vitromesenchymal stem cells interaction study. *Journal of biomedical materials research* 101A: 720-732, 2012.

201. Sanda M., M. Shiota, M. Fujii, K. Kon, T. Fujimori and S. Kasugai. Capability of new bone formation with a mixture of hydroxyapatite and beta-tricalcium phosphate granules. *Clinical Oral Implants Research* 26: 1369-1374, 2014.

202. Sawatjui N., T. Damrongrungruang, W. Leeanansaksiri, P. Jearanaikoon, S. Hongeng and T. Limpaiboon. Silk fibroin/gelatin–chondroitin sulfate–hyaluronic acid effectively enhances in vitro chondrogenesis of bone marrow mesenchymal stem cells. *Materials Science and Engineering: C* 52: 90-96, 2015.

203. Schopper C., F. Ziya-Ghazvini, W. Goriwoda, D. Moser, F. Wanschitz, E. Spassova, G. Lagogiannis, A. Auterith and R. Ewers. HA/TCP compounding of a porous CaP biomaterial improves bone formation and scaffold degradation--a long-term histological study. *Journal of biomedical materials research. Part B, Applied biomaterials* 74: 458-467, 2005.

204. Schwarz S., L. Koerber, A. F. Elsaesser, E. Goldberg-Bockhorn, A. M. Seitz, L. Dürselen, A. Ignatius, P. Walther, R. Breiter and N. Rotter. Decellularized cartilage matrix as a novel biomatrix for cartilage tissue-engineering applications. *Tissue Engineering Part A* 18: 2195-2209, 2012.

205. Seo S. J., C. Mahapatra, R. K. Singh, J. C. Knowles and H. W. Kim. Strategies for osteochondral repair: Focus on scaffolds. *Journal of Tissue Engineering* 5: 1-14, 2014.

206. Shi X., K. Su, R. R. Varshney, Y. Wang and D.-A. Wang. Sintered microsphere scaffolds for controlled release and tissue engineering. *Pharmaceutical research* 28: 1224-1228, 2011.

207. Shi X., Y. Wang, R. R. Varshney, L. Ren, Y. Gong and D.-A. Wang. Microsphere-based drug releasing scaffolds for inducing osteogenesis of human mesenchymal stem cells in vitro. *European Journal of Pharmaceutical Sciences* 39: 59-67, 2010.

208. Shi X., Y. Wang, R. R. Varshney, L. Ren, Y. Gong and D.-A. Wang. Microsphere-based drug releasing scaffolds for inducing osteogenesis of human mesenchymal stem cells in vitro. *European journal of pharmaceutical sciences : official journal of the European Federation for Pharmaceutical Sciences* 39: 59-67, 2010.

209. Shimomura K., Y. Moriguchi, C. D. Murawski, H. Yoshikawa and N. Nakamura. Osteochondral Tissue Engineering with Biphasic Scaffold: Current Strategies and Techniques. *Tissue Engineering Part B: Reviews* 140226120351005, 2014.

210. Shin U. S., J.-H. Park, S.-J. Hong, J.-E. Won, H.-S. Yu and H.-W. Kim. Porous biomedical composite microspheres developed for cell delivering scaffold in bone regeneration. *Materials Letters* 64: 2261-2264, 2010.

211. Singh M. Tensile Properties of the Mandibular Condylar Cartilage. *Journal of biomechanical engineering* 130: 011009, 2008.

212. Singh M. and M. S. Detamore. Stress Relaxation Behavior of Mandibular Condylar Cartilage Under High-Strain Compression. *Journal of biomechanical engineering* 131: 061008-061008, 2009.

213. Singh M., N. Dormer, J. R. Salash, J. M. Christian, D. S. Moore, C. Berkland and M. S. Detamore. Three-dimensional macroscopic scaffolds with a gradient in stiffness for functional regeneration of interfacial tissues. *Journal of Biomedical Materials Research Part A* 94: 870-876, 2010.

214. Singh M., N. Dormer, J. R. Salash, J. M. Christian, D. S. Moore, C. Berkland and M. S. Detamore. Three‐dimensional macroscopic scaffolds with a gradient in stiffness for functional regeneration of interfacial tissues. *Journal of Biomedical Materials Research Part A* 94: 870-876, 2010.

215. Singh M., C. P. Morris, R. J. Ellis, M. S. Detamore and C. Berkland. Microsphere-based seamless scaffolds containing macroscopic gradients of encapsulated factors for tissue engineering. *Tissue Engineering Part C-Methods* 14: 299-309, 2008.

216. Singh M., B. Sandhu, A. Scurto, C. Berkland and M. S. Detamore. Microsphere-based scaffolds for cartilage tissue engineering: using subcritical CO(2) as a sintering agent. *Acta biomaterialia* 6: 137-143, 2010.

217. Smith A. W., C. E. Segar, P. K. Nguyen, M. R. MacEwan, I. R. Efimov and D. L. Elbert. Long-term culture of HL-1 cardiomyocytes in modular poly(ethylene glycol) microsphere-based scaffolds crosslinked in the phase-separated state. *Acta biomaterialia* 8: 31-40, 2012.

218. Somoza R. A., J. F. Welter, D. Correa and A. I. Caplan. Chondrogenic differentiation of mesenchymal stem cells: challenges and unfulfilled expectations. *Tissue Engineering Part B: Reviews* 20: 596-608, 2014.

219. Son J. S., M. Appleford, J. L. Ong, J. C. Wenke, J. M. Kim, S. H. Choi and D. S. Oh. Porous hydroxyapatite scaffold with three-dimensional localized drug delivery system using

biodegradable microspheres. *Journal of controlled release : official journal of the Controlled Release Society* 153: 133-140, 2011.

220. Soran Z., R. S. T. Aydın and M. Gümüşderelioğlu. Chitosan scaffolds with BMP-6 loaded alginate microspheres for periodontal tissue engineering. *Journal of Microencapsulation* 29: 770-780, 2012.

221. Subia B., J. Kundu and S. C. Kundu. Biomaterial scaffold fabrication techniques for potential tissue engineering applications. *Tissue engineering* 2010.

222. Sudarmadji N., J. Y. Tan, K. F. Leong, C. K. Chua and Y. T. Loh. Investigation of the mechanical properties and porosity relationships in selective laser-sintered polyhedral for functionally graded scaffolds. *Acta biomaterialia* 7: 530-537, 2011.

223. Sungjin C. Implantation of tetrapod-shaped granular artificial bones or β-tricalcium phosphate granules in a canine large bone-defect model. *The Journal of Veterinary Medical Science* 76: 229, 2014.

224. Sutherland A. J. Bioactive Microsphere-Based Scaffolds Containing Decellularized Cartilage Bioactive Microsphere-Based Scaffolds. *Macromolecular bioscience* 15: 979-989.

225. Sutherland A. J., E. C. Beck, S. C. Dennis, G. L. Converse, R. A. Hopkins, C. J. Berkland and M. S. Detamore. Decellularized Cartilage May Be a Chondroinductive Material for Osteochondral Tissue Engineering. *PLoS ONE* 10: e0121966-0121913, 2015.

226. Sutherland A. J., G. L. Converse, R. A. Hopkins and M. S. Detamore. The Bioactivity of Cartilage Extracellular Matrix in Articular Cartilage Regeneration. *Advanced healthcare materials* 4: 29-39, 2014.

227. Sutherland A. J. and M. S. Detamore. Bioactive Microsphere-Based Scaffolds Containing Decellularized Cartilage. *Macromolecular bioscience* 15: 979-989, 2015.

228. Tahriri M. and F. Moztarzadeh. Preparation, Characterization, and In Vitro Biological Evaluation of PLGA/Nano-Fluorohydroxyapatite (FHA) Microsphere-Sintered Scaffolds for Biomedical Applications. *Applied Biochemistry and Biotechnology* 172: 2465-2479, 2014.

229. Takahashi Y., M. Yamamoto and Y. Tabata. Osteogenic differentiation of mesenchymal stem cells in biodegradable sponges composed of gelatin and β-tricalcium phosphate. In: *Biomaterials*2005, p. 3587-3596.

230. Tallawi M. Proteinoid/hydroxyapatite hybrid microsphere composites. *Journal of biomedical materials research. Part B, Applied biomaterials* 96: 261-266, 2011.

231. Tan J. Y., C. K. Chua and K. F. Leong. Fabrication of channeled scaffolds with ordered array of micro-pores through microsphere leaching and indirect Rapid Prototyping technique. *Biomedical microdevices* 15: 83-96, 2013.

232. Tang G., H. Zhang, Y. Zhao, Y. Zhang, X. Li and X. Yuan. Preparation of PLGA Scaffolds with Graded Pores by Using a Gelatin-Microsphere Template as Porogen. *Journal of biomaterials science. Polymer edition* 2011.

233. Thorrez L., J. Shansky, L. Wang, L. Fast, T. VandenDriessche, M. Chuah, D. Mooney and H. Vandenburgh. Growth, differentiation, transplantation and survival of human skeletal myofibers on biodegradable scaffolds. *Biomaterials* 29: 75-84, 2008.

234. Todo M. and T. Arahira. In vitro bone formation by mesenchymal stem cells with 3D collagen/β-TCP composite scaffold. *Conference proceedings : ... Annual International Conference of the IEEE Engineering in Medicine and Biology Society. IEEE Engineering in Medicine and Biology Society. Annual Conference* 2013: 409-412, 2013.

235. Tracy M. Factors affecting the degradation rate of poly(lactide-co-glycolide) microspheres in vivo and in vitro. *Biomaterials* 20: 1057-1062, 1999.

236. Ungaro F., M. Biondi, I. d'Angelo, L. Indolfi, F. Quaglia, P. A. Netti and M. I. La Rotonda. Microsphere-integrated collagen scaffolds for tissue engineering: effect of microsphere formulation and scaffold properties on protein release kinetics. *Journal of controlled release : official journal of the Controlled Release Society* 113: 128-136, 2006.

237. Uygun B. E., S. E. Stojsih and H. W. Matthew. Effects of immobilized glycosaminoglycans on the proliferation and differentiation of mesenchymal stem cells. *Tissue Engineering Part A* 15: 3499-3512, 2009.

238. Uygun B. E., S. E. Stojsih and H. W. T. Matthew. Effects of immobilized glycosaminoglycans on the proliferation and differentiation of mesenchymal stem cells. *Tissue engineering. Part A* 15: 3499-3512, 2009.

239. Valmikinathan C. M., J. Tian, J. Wang and X. Yu. Novel nanofibrous spiral scaffolds for neural tissue engineering. *Journal of neural engineering* 5: 422-432, 2008.

240. Wang C. C., J.-M. Deng, G. A. Ateshian and C. T. Hung. An automated approach for direct measurement of two-dimensional strain distributions within articular cartilage under unconfined compression. *Journal of biomechanical engineering* 124: 557-567, 2002.

241. Wang H., O. C. Boerman, K. Sariibrahimoglu, Y. Li, J. A. Jansen and S. C. G. Leeuwenburgh. Comparison of micro- vs. nanostructured colloidal gelatin gels for sustained delivery of osteogenic proteins: Bone morphogenetic protein-2 and alkaline phosphatase. *Biomaterials* 33: 8695-8703, 2012.

242. Wang J. and X. Yu. Preparation, characterization and in vitro analysis of novel structured nanofibrous scaffolds for bone tissue engineering. *Acta biomaterialia* 6: 3004-3012, 2010.

243. Wang L., C. Li, Y. Chen, S. Dong, X. Chen and Y. Zhou. Poly(lactic-co-glycolic) acid/nanohydroxyapatite scaffold containing chitosan microspheres with adrenomedullin delivery for modulation activity of osteoblasts and vascular endothelial cells. *BioMed research international* 2013: 530712, 2013.

244. Wang X., E. Wenk, X. Zhang, L. Meinel, G. Vunjak-Novakovic and D. L. Kaplan. Growth factor gradients via microsphere delivery in biopolymer scaffolds for osteochondral tissue engineering. *Journal of controlled release : official journal of the Controlled Release Society* 134: 81-90, 2009.

245. Wang Y., U.-J. Kim, D. J. Blasioli, H.-J. Kim and D. L. Kaplan. In vitro cartilage tissue engineering with 3D porous aqueous-derived silk scaffolds and mesenchymal stem cells. *Biomaterials* 26: 7082-7094, 2005.

246. Wang Y., X. Shi, L. Ren, Y. Yao, F. Zhang and D.-A. Wang. Poly(lactide-co-glycolide)/titania composite microsphere-sintered scaffolds for bone tissue engineering applications. *Journal of biomedical materials research. Part B, Applied biomaterials* 93: 84-92, 2010.

247. Watanabe M., H. Li, J. Roybal, M. Santore, A. Radu, J.-I. Jo, M. Kaneko, Y. Tabata and A. Flake. A tissue engineering approach for prenatal closure of myelomeningocele: comparison of gelatin sponge and microsphere scaffolds and bioactive protein coatings. *Tissue engineering. Part A* 17: 1099-1110, 2011.

248. Wei G., Q. Jin, W. V. Giannobile and P. X. Ma. Nano-fibrous scaffold for controlled delivery of recombinant human PDGF-BB. *Journal of controlled release : official journal of the Controlled Release Society* 112: 103-110, 2006.

249. Weiss A. J. and A. Elixhauser. *Trends in Operating Room Procedures in U.S. Hospitals, 2001–2011: Statistical Brief #171*. Rockville (MD): Agency for Health Care Policy and Research (US), 2006.

250. Williams S. K., D. Amiel, S. T. Ball, R. T. Allen, V. W. Wong, A. C. Chen, R. L. Sah and W. D. Bugbee. Prolonged storage effects on the articular cartilage of fresh human osteochondral allografts. *The Journal of Bone & Joint Surgery* 85: 2111-2120, 2003.

251. Williams S. K., D. Amiel, S. T. Ball, R. T. Allen, V. W. Wong, A. C. Chen, R. L. Sah and W. D. Bugbee. Prolonged storage effects on the articular cartilage of fresh human osteochondral allografts. *The Journal of Bone and Joint Surgery (American)* 85-A: 2111-2120, 2003.

252. Wong D. J. and H. Y. Chang. *Skin tissue engineering*. Cambridge (MA): Harvard Stem Cell Institute, 2008.

253. Wright L. D., R. T. Young, T. Andric and J. W. Freeman. Fabrication and mechanical characterization of 3D electrospun scaffolds for tissue engineering. *Biomedical materials (Bristol, England)* 5: 055006, 2010.

254. Wu S. D., H. Zhang, X. D. Dong, C. Y. Ning and A. Fok. Physicochemical properties and< i> in vitro</i> cytocompatibility of modified titanium surfaces prepared via micro-arc oxidation with different calcium concentrations. *Applied Surface ...* 329: 347-355, 2014.

255. Xu W., L. Wang, Y. Ling, K. Wei and S. Zhong. Enhancement of compressive strength and cytocompatibility using apatite coated hexagonal mesoporous silica/poly(lactic acid-glycolic acid) microsphere scaffolds for bone tissue engineering. *RSC Advances* 4: 13495, 2014.

256. Yang F., W. Cui, Z. Xiong, L. Liu, J. Bei and S. Wang. Poly(l,l-lactide-co-glycolide)/tricalcium phosphate composite scaffold and its various changes during degradation in vitro. *Polymer Degradation and Stability* 91: 3065-3073, 2006.

257. Yu Z., T. Zhu, C. Li, X. Shi, X. Liu, X. Yang and H. Sun. Improvement of intertrochanteric bone quality in osteoporotic female rats after injection of polylactic acid-polyglycolic acid copolymer/collagen type I microspheres combined with bone mesenchymal stem cells. *International orthopaedics* 36: 2163-2171, 2012.

258. Yuan H., H. Fernandes, P. Habibovic, J. de Boer, A. M. Barradas, A. de Ruiter, W. R. Walsh, C. A. van Blitterswijk and J. D. de Bruijn. Osteoinductive ceramics as a synthetic alternative to autologous bone grafting. *Proceedings of the National Academy of Sciences* 107: 13614-13619, 2010.

259. Zhai P., X. B. Chen and D. J. Schreyer. Preparation and characterization of alginate microspheres for sustained protein delivery within tissue scaffolds. *Biofabrication* 5: 015009, 2013.

260. Zhou W. Y., S. H. Lee, M. Wang, W. L. Cheung and W. Y. Ip. Selective laser sintering of porous tissue engineering scaffolds from poly(L: -lactide)/carbonated hydroxyapatite nanocomposite microspheres. *Journal of Materials Science: Materials in Medicine* 19: 2535-2540, 2008.

261. Zhu X. H., S. K. Gan, C.-H. Wang and Y. W. Tong. Proteins combination on PHBV microsphere scaffold to regulate Hep3B cells activity and functionality: A model of liver tissue engineering system. *Journal of biomedical materials research* 83A: 606-616, 2007.

262. Zhu X. H., Y. Tabata, C.-H. Wang and Y. W. Tong. Delivery of basic fibroblast growth factor from gelatin microsphere scaffold for the growth of human umbilical vein endothelial cells. *Tissue engineering. Part A* 14: 1939-1947, 2008.

263. Zhu X. H., C.-H. Wang and Y. W. Tong. In vitro characterization of hepatocyte growth factor release from PHBV/PLGA microsphere scaffold. *Journal of Biomedical Materials Research Part A* 89: 411-423, 2009.

264. Zilberman M. and O. Grinberg. HRP-loaded bioresorbable microspheres: effect of copolymer composition and molecular weight on microstructure and release profile. *Journal of biomaterials applications* 22: 391-407, 2008.

265. Zilberman M. and I. Shraga. Microsphere-based bioresorbable structures loaded with proteins for tissue regeneration applications. *Journal of Biomedical Materials Research Part A* 79: 370-379, 2006.

APPENDIX A: Figures

CHAPTER 1: No Figures

CHAPTER 2: Figures 2.1-2.12

CHAPTER 3: Figures 3.1-3.10

CHAPTER 4: Figures 4.1-4.15

CHAPTER 5: Figures 5.1-5.12

CHAPTER 6: Figures 6.1-6.9

CHAPTER 7: No Figures

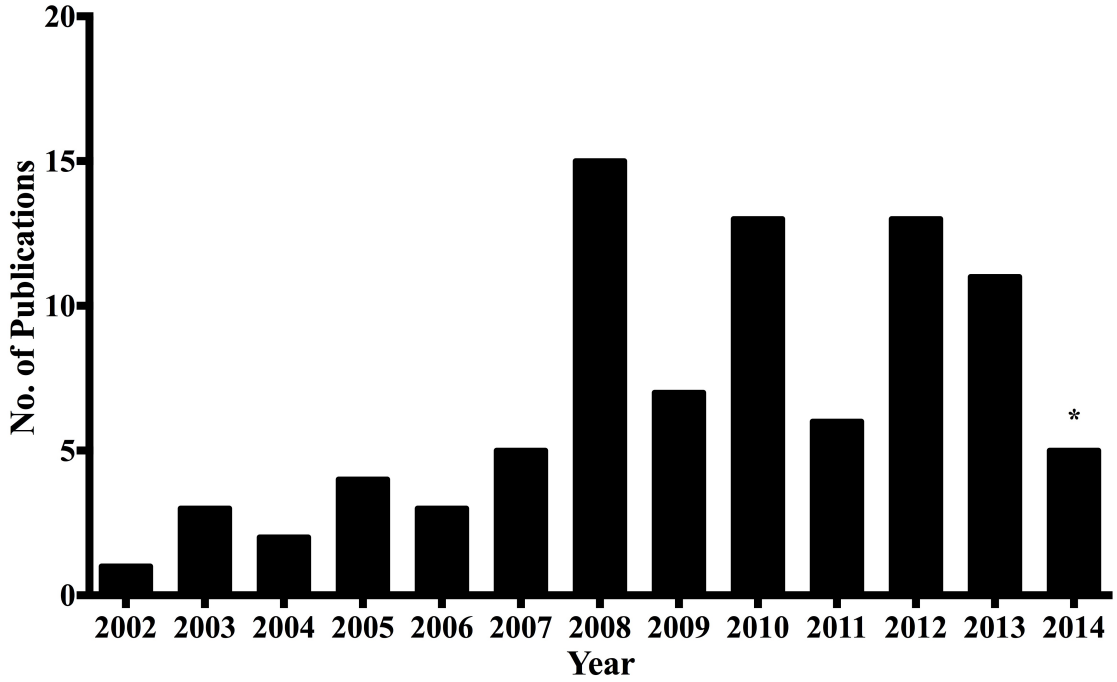

Figure 2.1: Number of publications based on 'Microsphere Scaffolds' in tissue engineering and regenerative medicine

Number of published articles on microsphere scaffolds in the field of tissue engineering and regenerative medicine since the first reported use of such scaffolds in 2002. Data represent search results in *Web of Science* database. * Results up to July 2014.

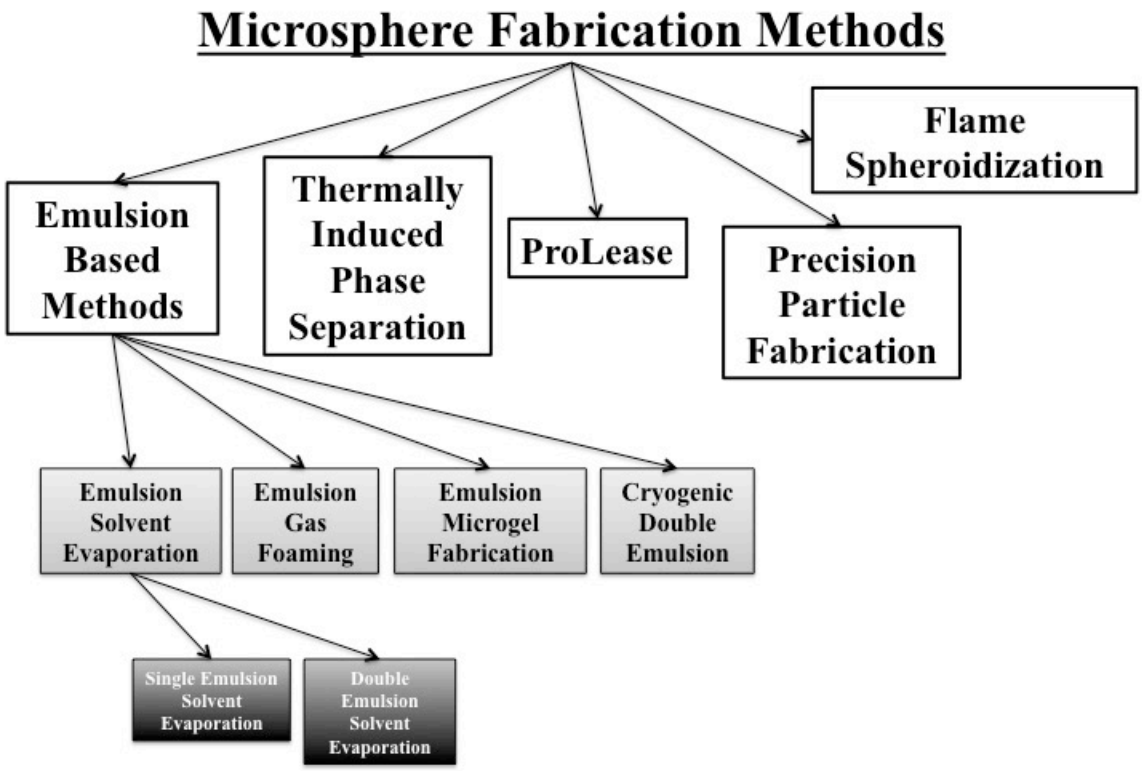

Figure 2.2: Microsphere fabrication methods

Numerous methods are available for fabricating microspheres; however, emulsion-based methods are most widely used for microsphere fabrication in the tissue engineering field.

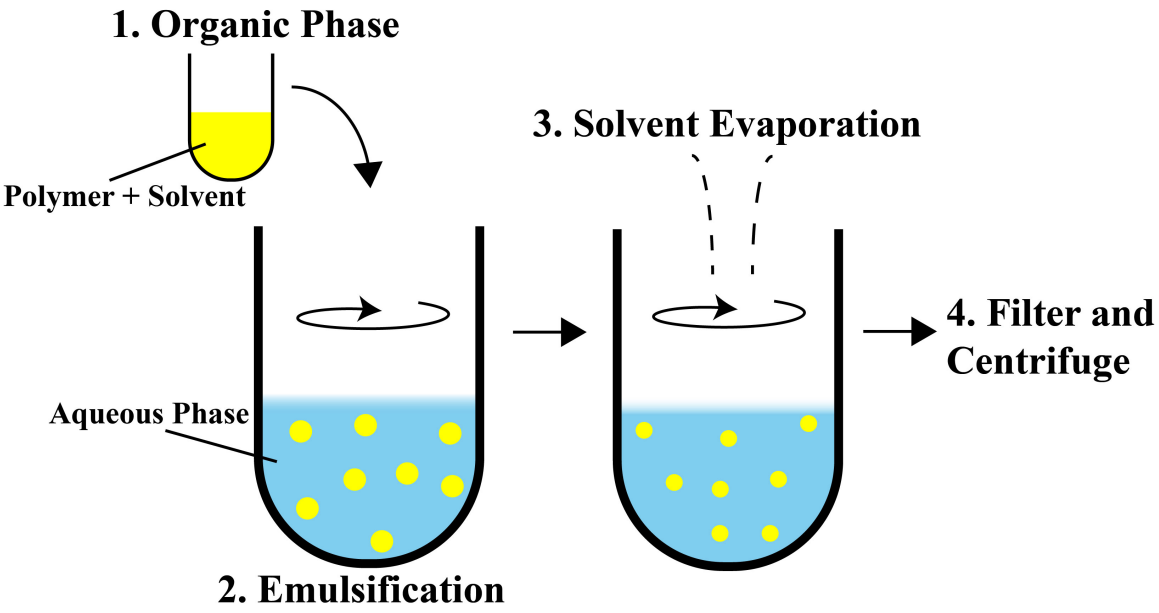

Figure 2.3: Single emulsion solvent evaporation (SESE) method for microsphere fabrication

In the SESE method, the microsphere matrix (containing either dissolved or dispersed bioactive molecule) is emulsified into the aqueous phase followed by microsphere hardening through solvent evaporation and polymer precipitation.

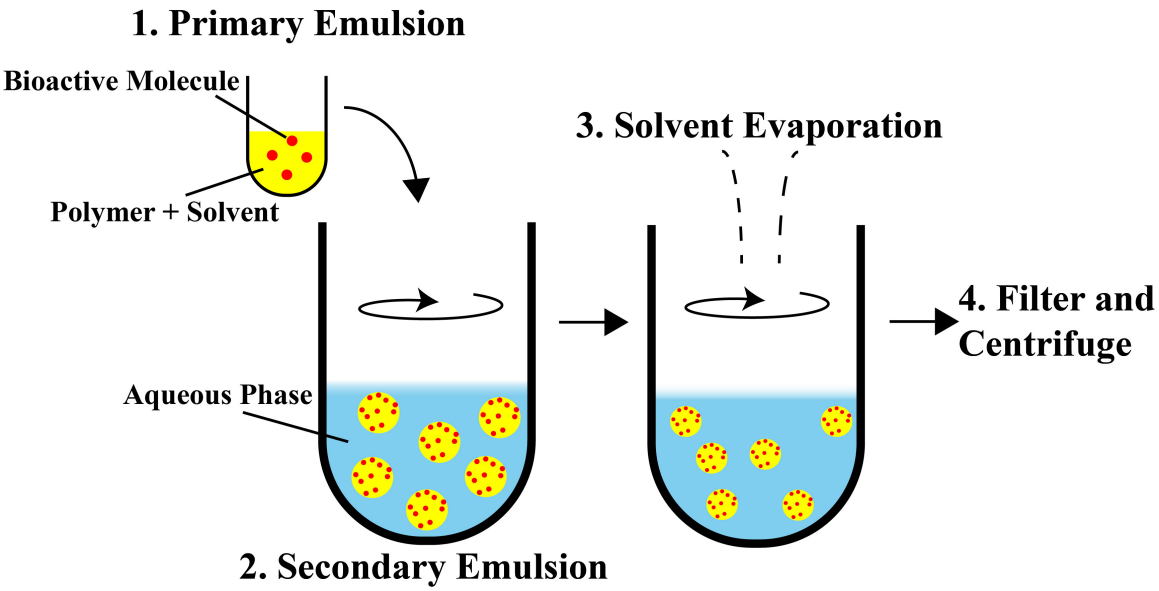

Figure 2.4: Double emulsion solvent evaporation (DESE) method for microsphere fabrication

In DESE method, an aqueous solution of the bioactive compound is first dispersed in the matrix solution forming primary emulsion, which is then further emulsified to form secondary emulsion followed by microsphere hardening.

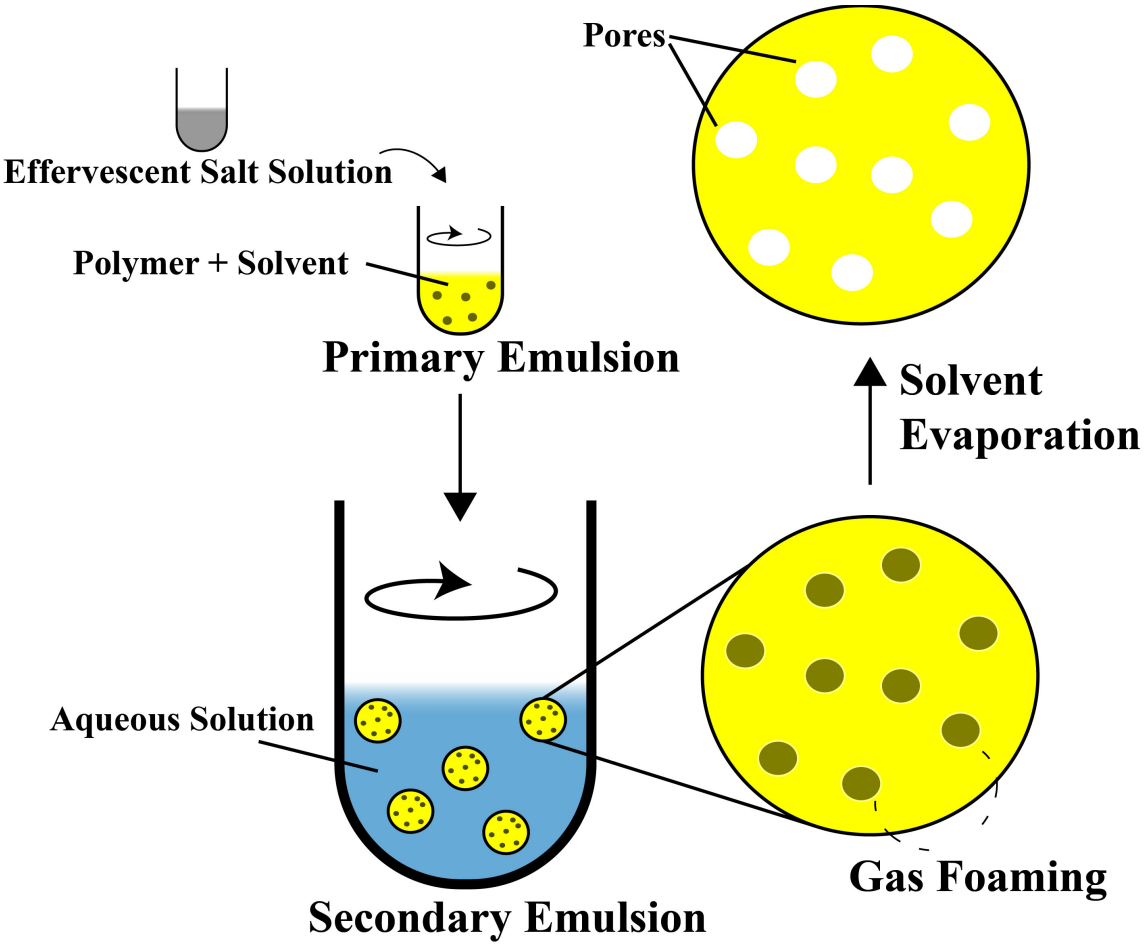

Figure 2.5: Emulsion gas foaming method for microsphere fabrication

In the emulsion gas foaming method, an effervescent salt is dissolved in the organic phase that acts as a gas foaming agent, generating gas bubbles when the primary emulsion contacts the secondary aqueous phase.

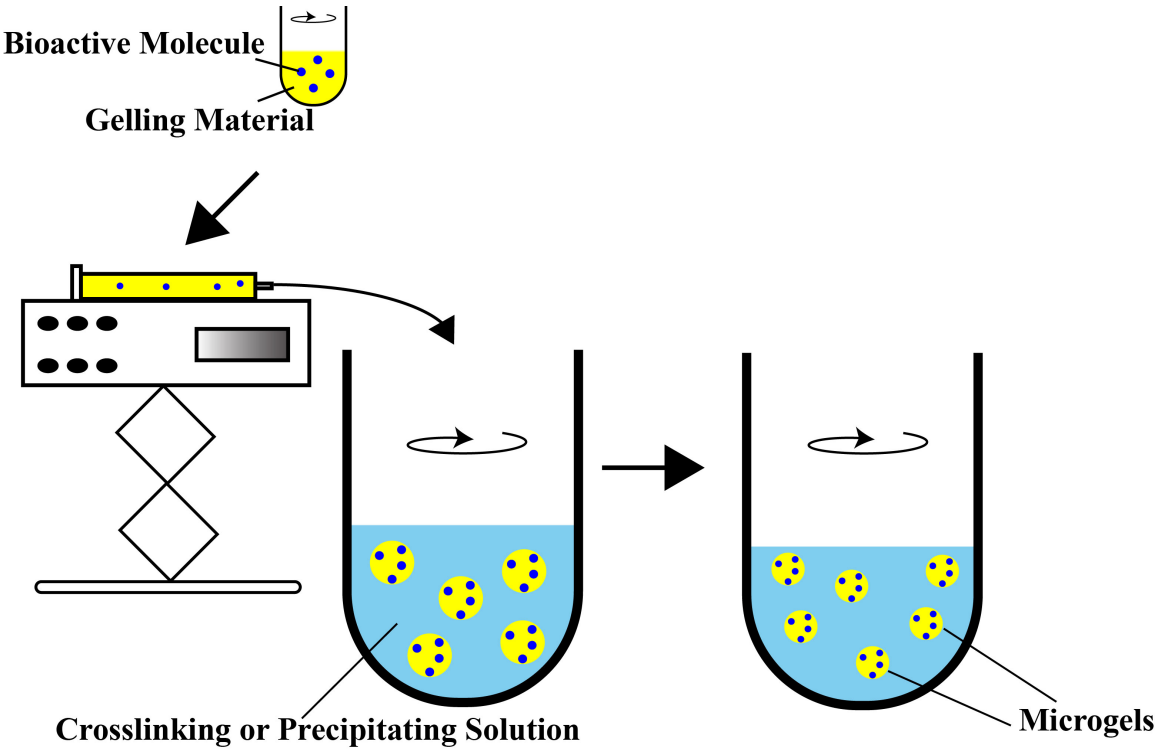

Figure 2.6: Emulsion microgel microsphere fabrication method

Emulsion microgel fabrication involves production of micron or sub-micron sized gel spheres (microgels) using hydrophilic materials via ionic crosslinking, chemical crosslinking and co-precipitation in an emulsion.

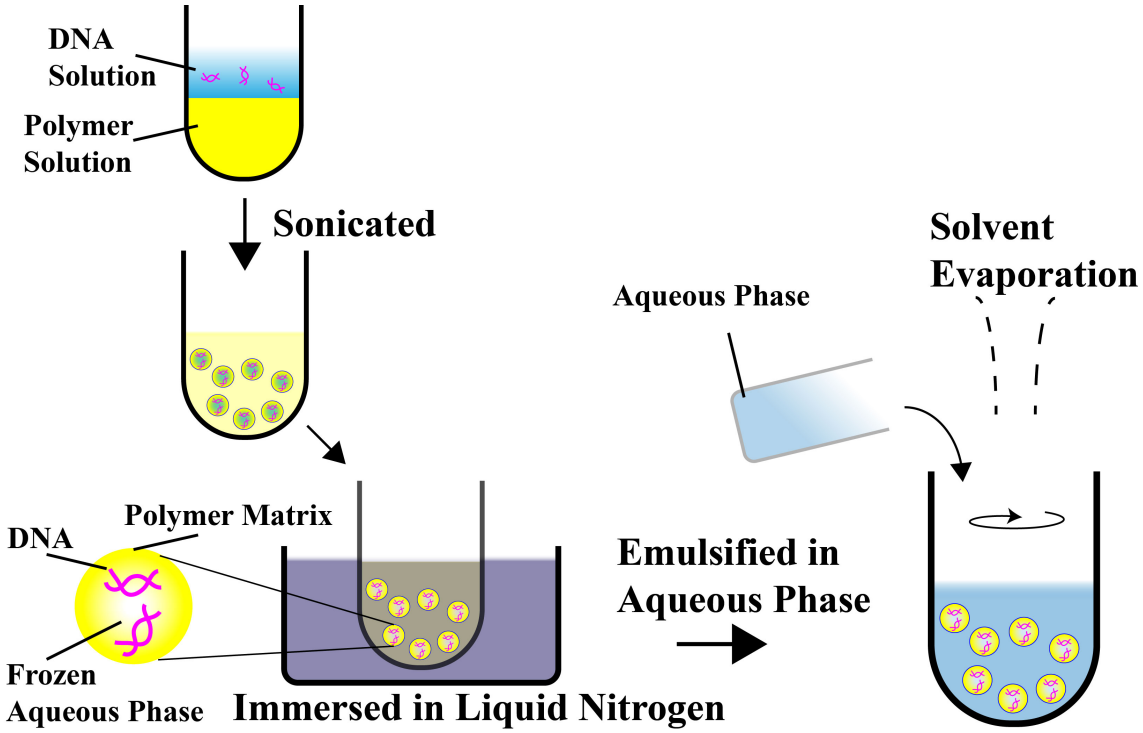

Figure 2.7: Cryopreparation method for microsphere fabrication

Cryopreparation involves lowering the temperature of the DNA-containing primary emulsion below the freezing point of the aqueous inner phase resulting in a solid particulate suspension prior to homogenization to form the secondary emulsion.

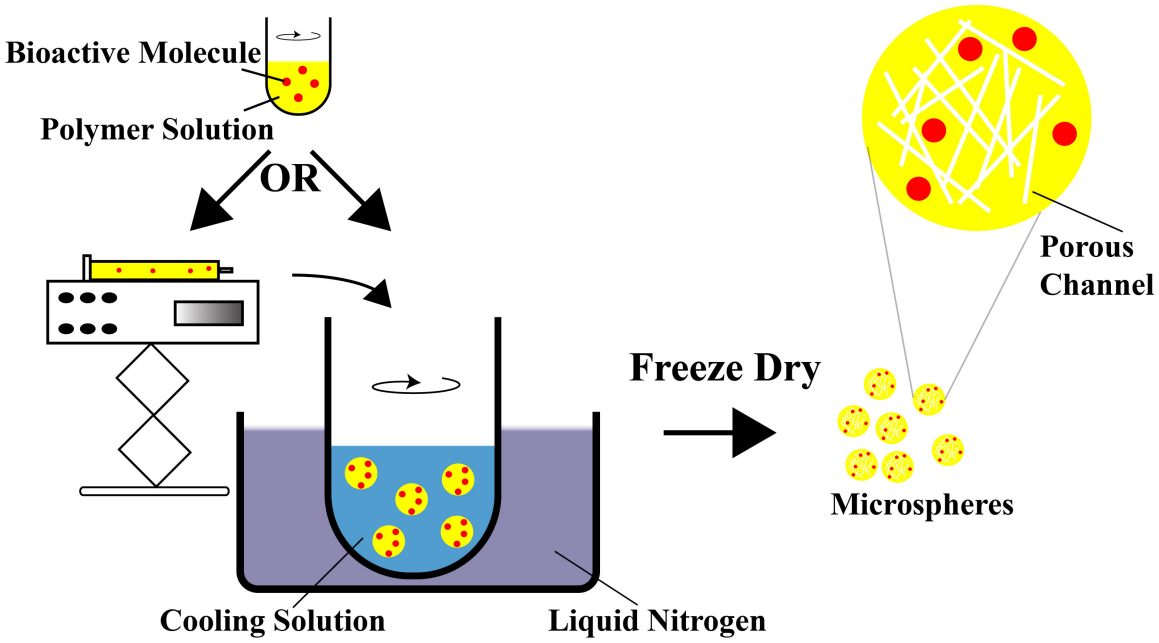

Figure 2.8: Thermally induced phase separation (TIPS) for microsphere fabrication

In thermally induced phase separation method, a solvent with a low boiling point that easily sublimes is used. Solvent dissolved matrix material (usually a polymer) droplets are either preformed via an emulsion or directly dropped (via a syringe or sprayed through a nozzle) into the cooling solution to generate porous microspheres.

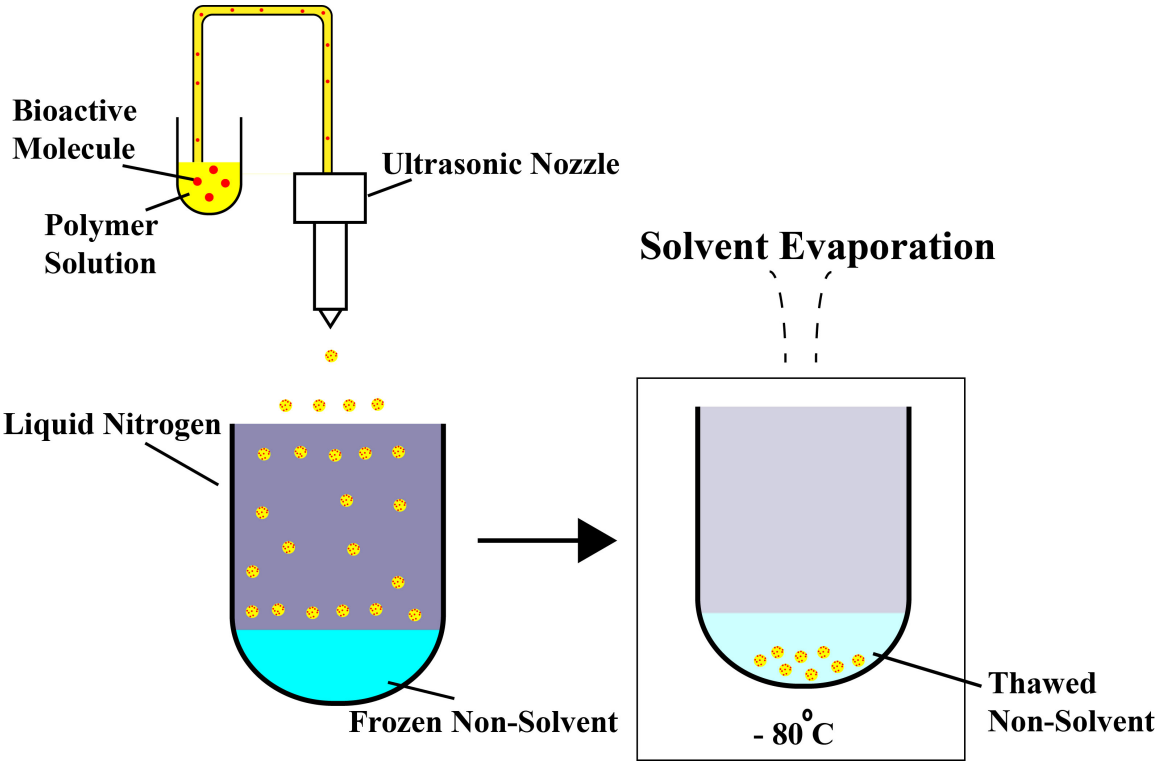

Figure 2.9: ProLease process for microsphere fabrication

In the ProLease process, the polymer/active agent mixture is atomized into a vessel containing a liquid non-solvent, alone or frozen and overlaid with a liquefied gas, at a temperature below the freezing point of the polymer/active agent solution. The atomized droplets freeze into microspheres upon contacting the cold liquefied gas, then sink onto the frozen non-solvent layer. The frozen non-solvent is then thawed. As the non-solvent thaws, the microspheres that are still frozen sink into the liquid non-solvent. The solvent in the microspheres then thaws and is slowly extracted into the non-solvent, resulting in hardened microspheres containing active agent.

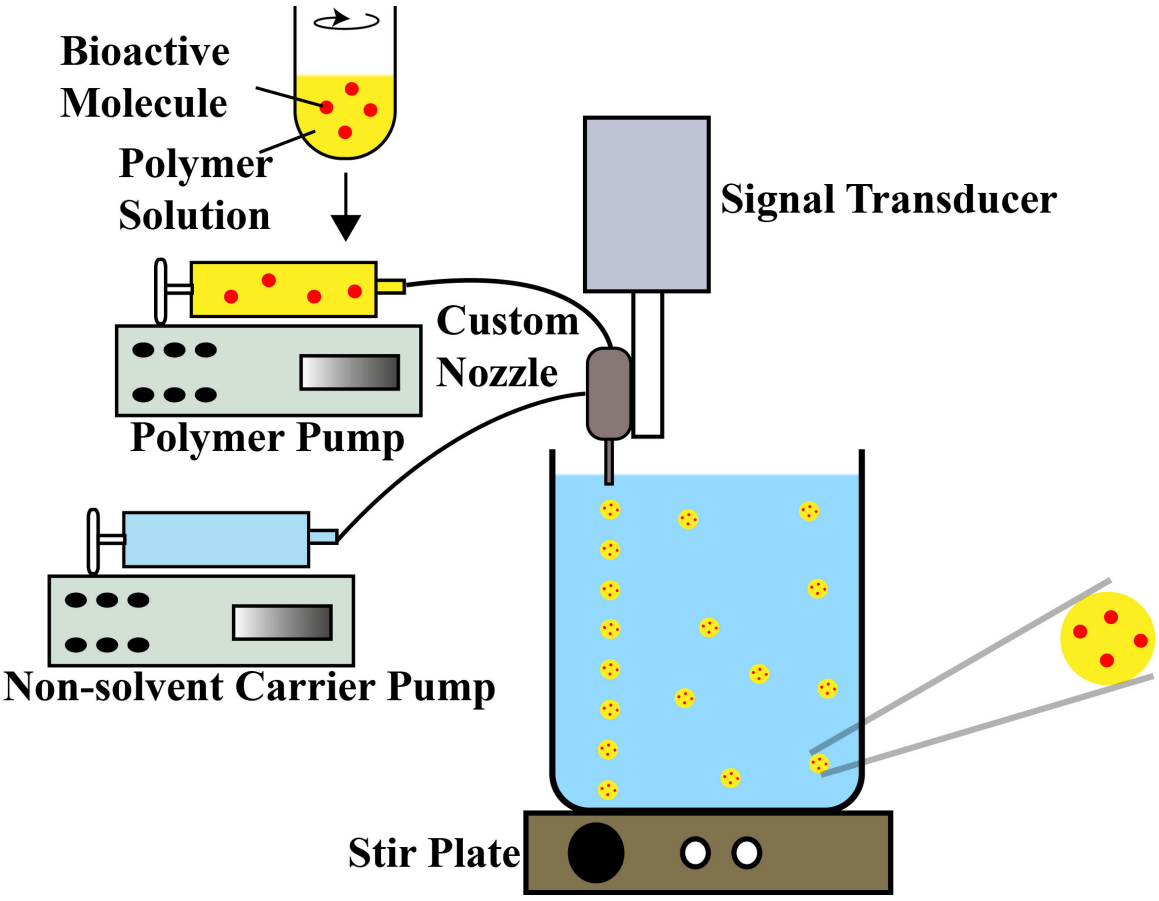

Figure 2.10: Precision particle fabrication (PPF) method for microsphere fabrication

In PPF, a solution containing the microsphere matrixis passed through a small nozzle to form a smooth cylindrical jet. A piezoelectric transducer driven by a wave generator at a frequency tuned to match the flow rate and the desired drop size vibrates the nozzle. The mechanical excitation launches a wave of acoustic energy along the liquid jet generating periodic instabilities that, in turn, breaks the liquid jet into a train of uniform droplets. An annular flow of a non-solvent phase around the matrix jet is employed that is pumped at a linear velocity greater than that of the matrix stream. The frictional contact between the two streams generates an additional downward force that effectively pulls the microsphere solution away from the orifice of the nozzle. The microsphere matrix stream is accelerated by this force and, therefore, thinned to a degree depending on the difference in linear velocities of the two streams.

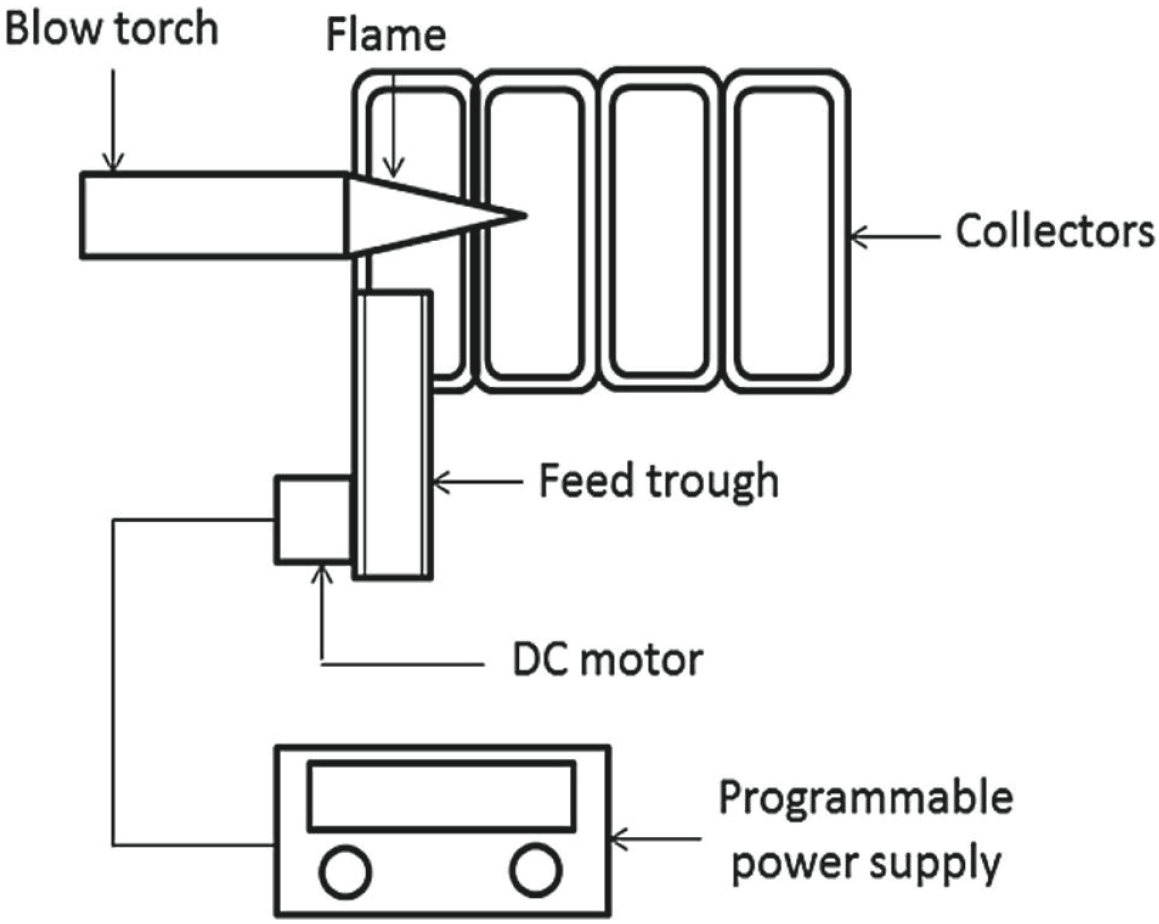

Figure 2.11: Schematic for flame spheroidization apparatus[142]

In flame spheroidization, the particles pass into the flame and travel along the flame axis. The particles undergo spheroidization due to surface tension forces and are then collected in the glass boxes placed one after the other below the flame.

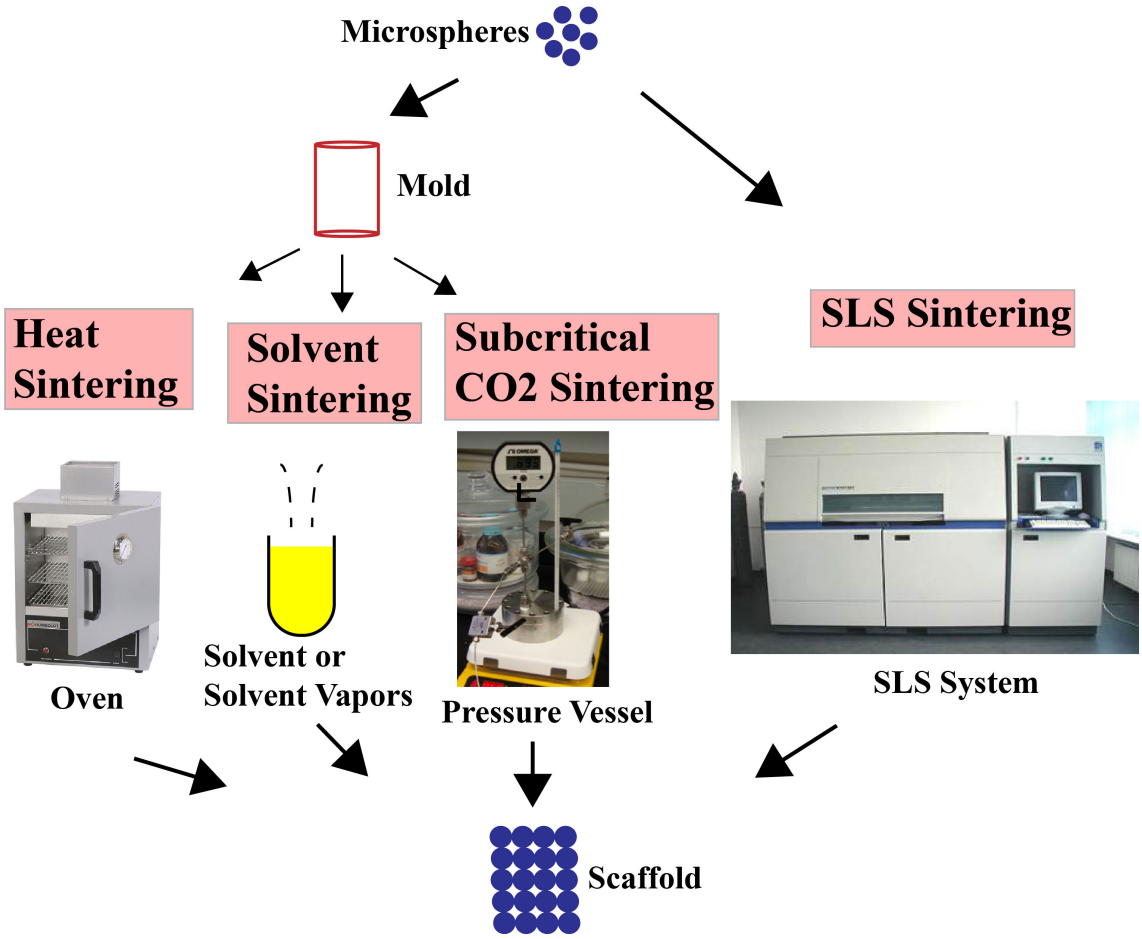

Figure 2.12: Microsphere sintering methods

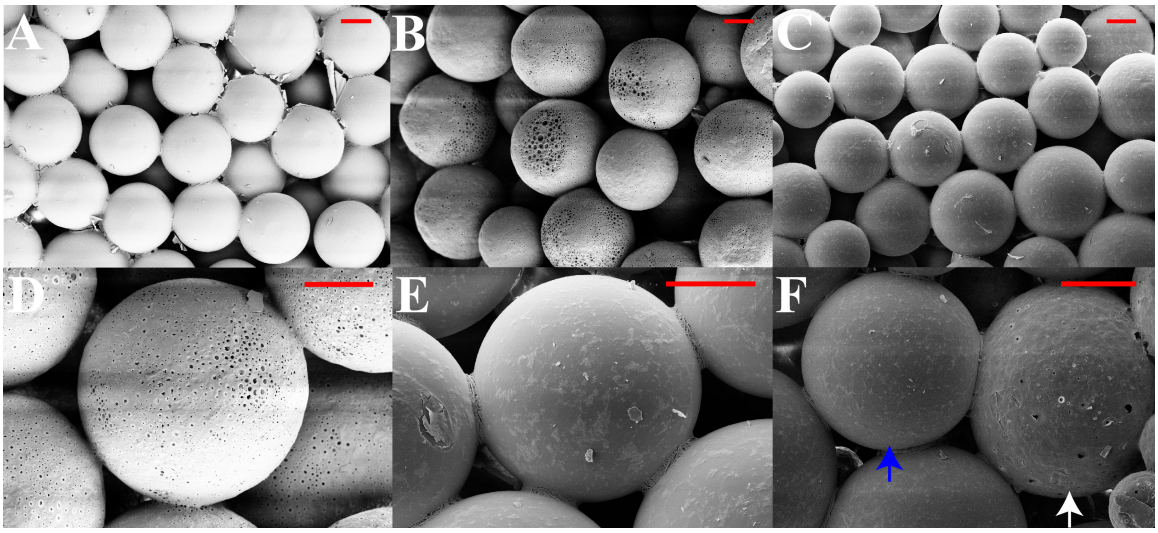

Figure 3.1: Scanning electron micrographs of acellular microsphere-based scaffolds

(A) PLGA, (B & D) CS, (C & E) TCP, and (F) GRADIENT at the CS (white arrow)-TCP (blue arrow) transition region. The images reveal the distinct morphological features of the microspheres in different scaffold groups. Note the porous nature of CS microspheres and rough surface of TCP microspheres. Scale bars: 100 μm.

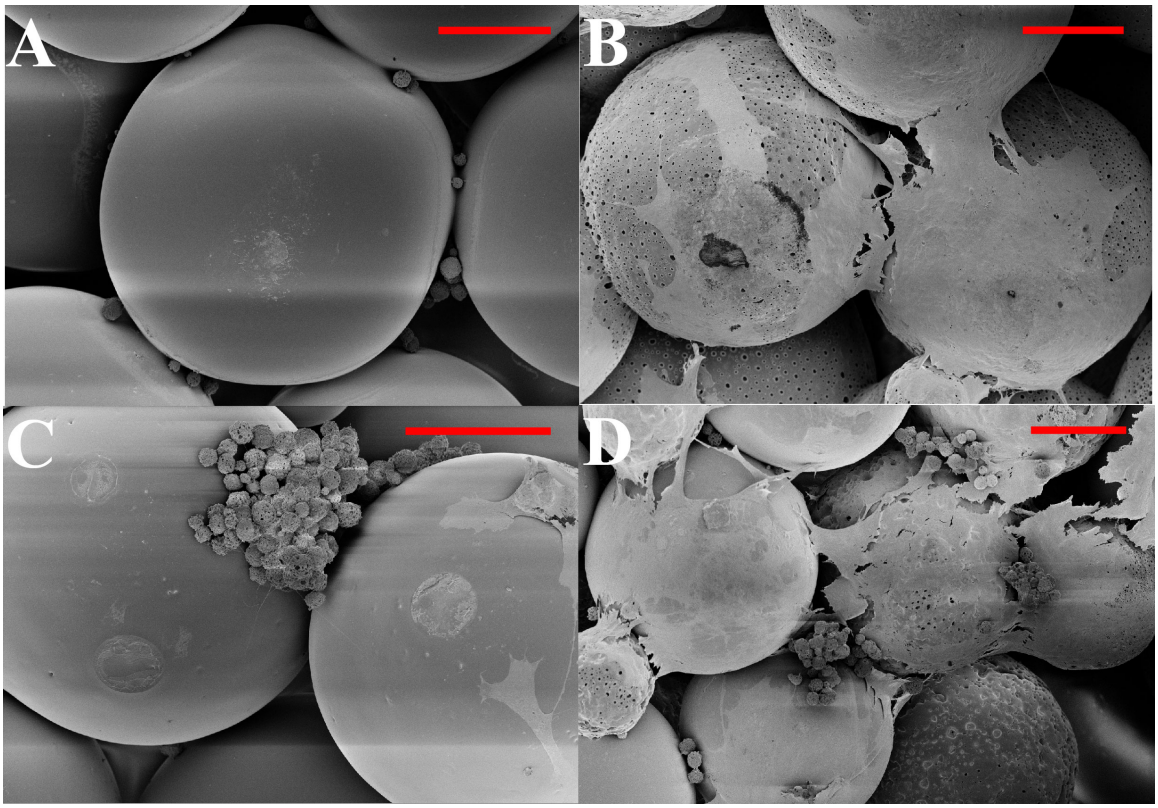

Figure 3.2: Cellular morphology of rBMSCs seeded on microsphere-based scaffolds

(A) PLGA, (B) CS, (C) TCP, and (D) GRADIENT groups. Note the differences in cellular morphology in different scaffold groups at day 10 (week 1.5). Flat cells were observed in the CS group whereas cluster forming cells were observed in the TCP group. The GRADIENT group contained both flat and cluster forming cells. Scale bars: 100 μm.

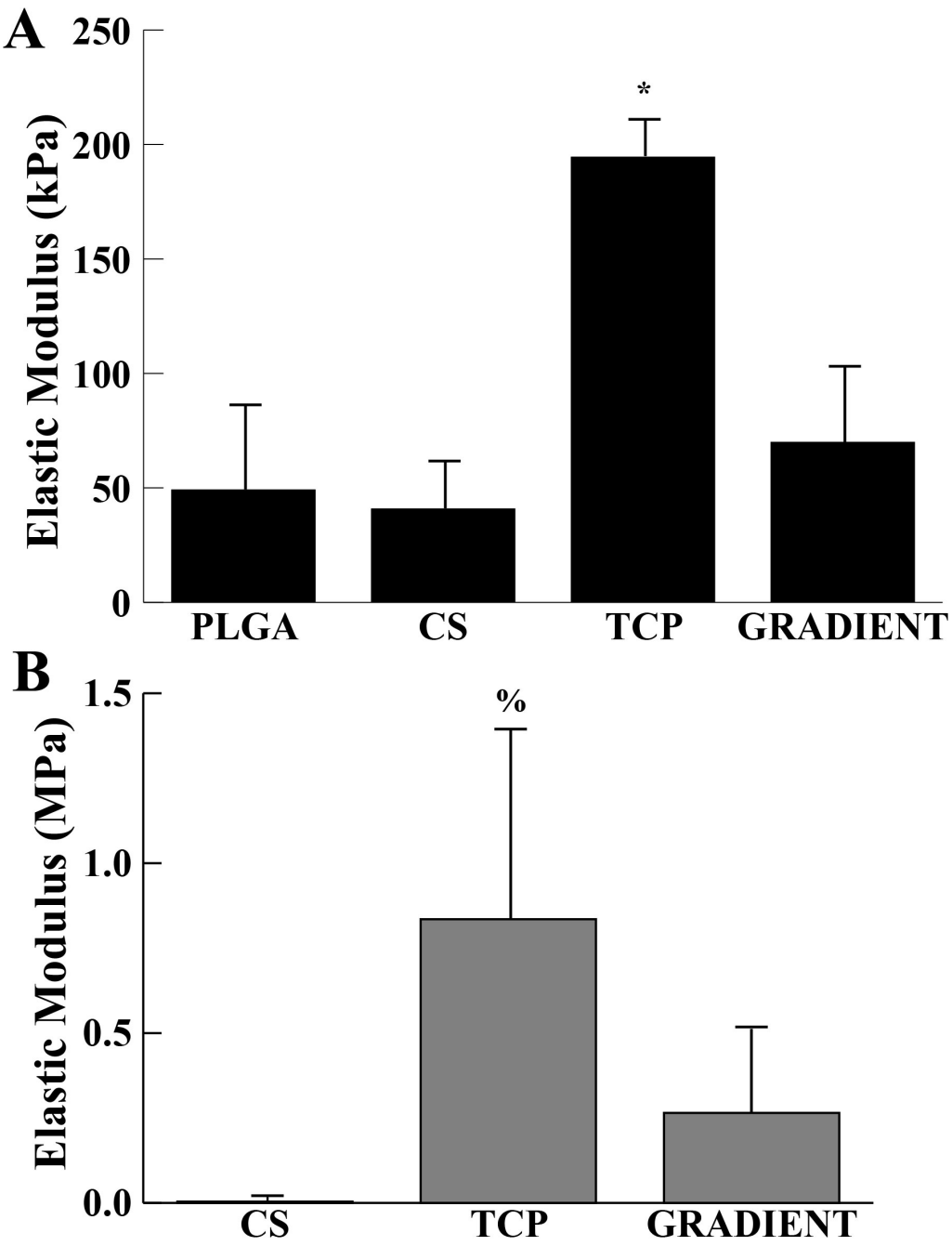

Figure 3.3: Compressive elastic modulus

(A) Acellular constructs at week 0. (B) Cellular constructs at week 6. Both the acellular and cell seeded TCP scaffolds had significantly higher modulus. All values are expressed as the average + standard deviation (n = 3-5). The TCP group (both acellular and cellular) had significantly higher modulus than the other groups. *significant change over the other three groups, %significant change over the CS group ($p < 0.05$). PLGA constructs at week 6 are not shown in the figure.

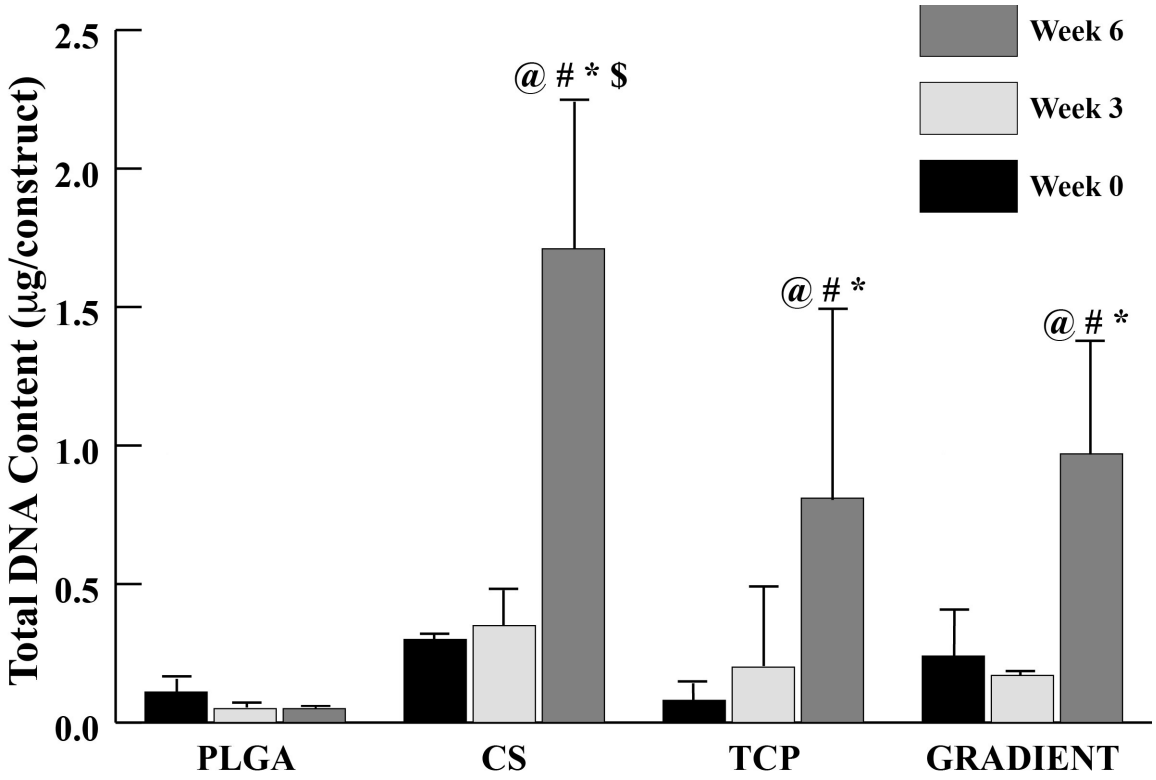

Figure 3.4: Total DNA content as measured in the microsphere-based scaffolds

The CS, TCP and GRADIENT groups had significantly higher DNA content than the PLGA group at week 6. All values are expressed as the average + standard deviation (n = 3-5). The CS group at week 6 had significantly higher cell numbers compared to the other groups. @significant change over week 0 value, #significant change over its value at previous time point, *significant change over the PLGA group at same time point and $significant change over the TCP and GRADIENT groups at same time point ($p < 0.05$).

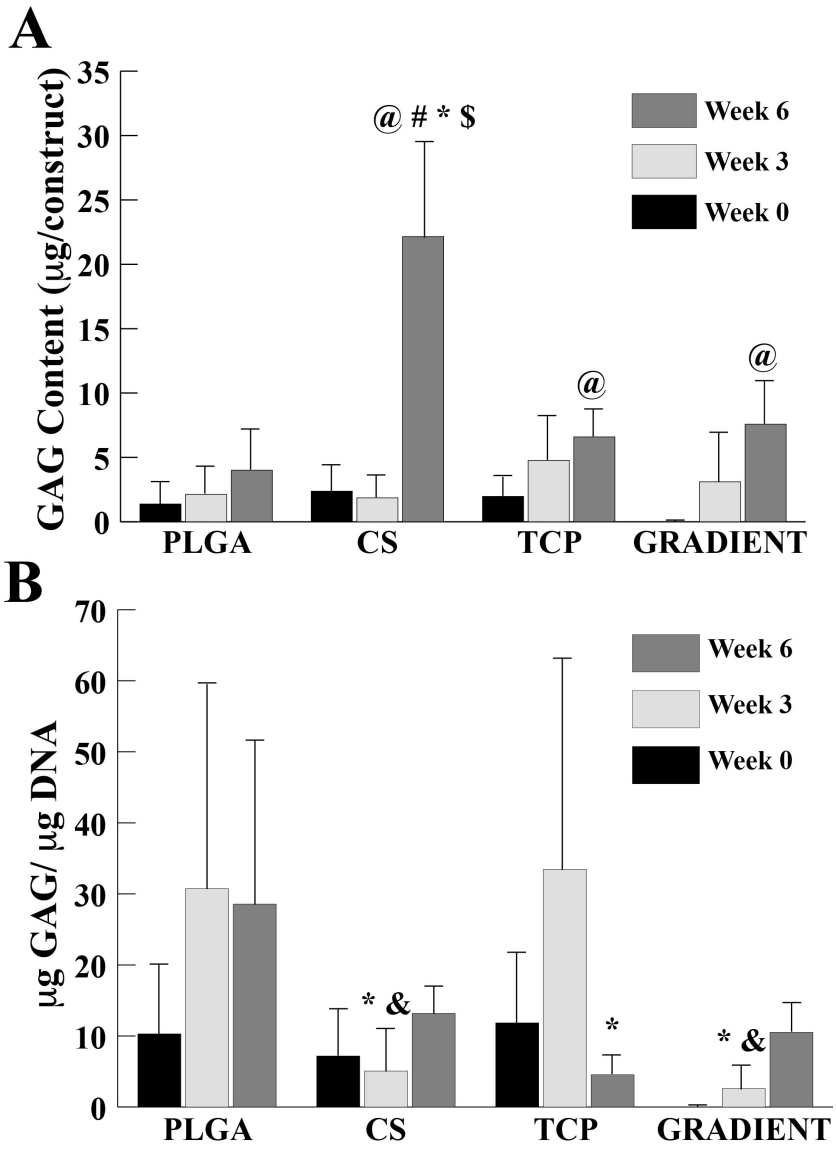

Figure 3.5: GAG content as measured in the microsphere-based scaffolds

(A) Total GAG content in micrograms per construct. (B) Normalized GAG content in micrograms per micrograms DNA. The CS group had significantly higher net GAG content than the other three groups at week 6. All values are expressed as the average + standard deviation (n = 3-5). The CS group at week 6 surpassed the other three groups in net GAG content. @significant change over week 0 value, #significant change over its value at previous time point, *significant change over the PLGA group at same time point, $significant change over the TCP and GRADIENT groups at same time point, and &significant change over the TCP group at same time point ($p < 0.05$).

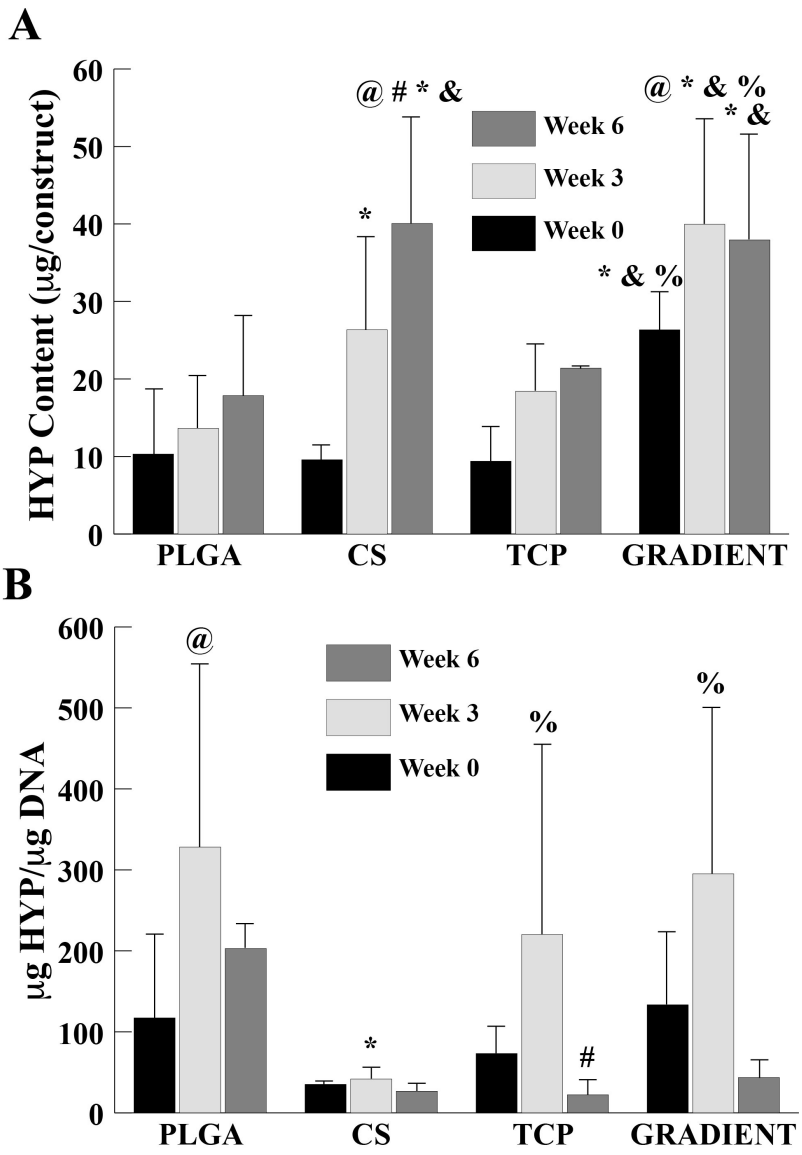

Figure 3.6: HYP content as measured in the microsphere-based scaffolds

(A) Total HYP content in micrograms per construct. (B) Normalized HYP content in micrograms per micrograms DNA. The CS and GRADIENT groups had significantly higher net HYP content than the PLGA group at weeks 3 and 6. All values are expressed as the average + standard deviation (n = 3-5). The CS and GRADIENT groups at week 6 had significantly higher net HYP content than the other two groups. @significant change over week 0 value, #significant change over its value at previous time point, *significant change over the PLGA group at same time point, &significant change over the TCP group at same time point, and %significant change over the CS group at same time point ($p < 0.05$).

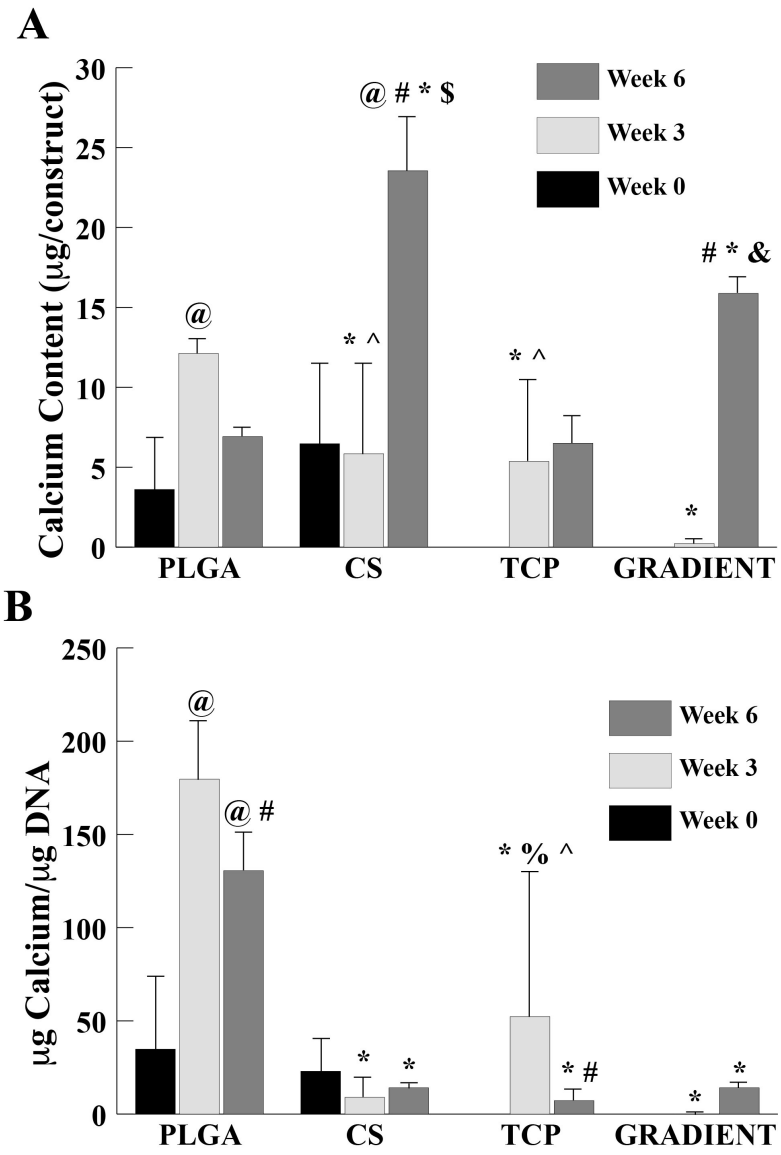

Figure 3.7: Calcium content as measured in the microsphere-based scaffolds

(A) Total calcium content in micrograms per construct. (B) Normalized calcium content in micrograms per micrograms DNA. The PLGA group had significantly higher normalized calcium content than the other three groups at weeks 3 and 6. All values are expressed as the average + standard deviation (n = 3-5). The CS and GRAIDENT groups at week 6 had significantly higher net calcium content than the other two groups. @significant change over week 0 value, #significant change over its value at previous time point, *significant change over the PLGA group at same time point, $significant change over the TCP and GRADIENT groups at same time point, &significant change over the TCP group at same time point, ^significant change over the GRADIENT group at same time point, and %significant change over the CS group at same time point ($p < 0.05$).

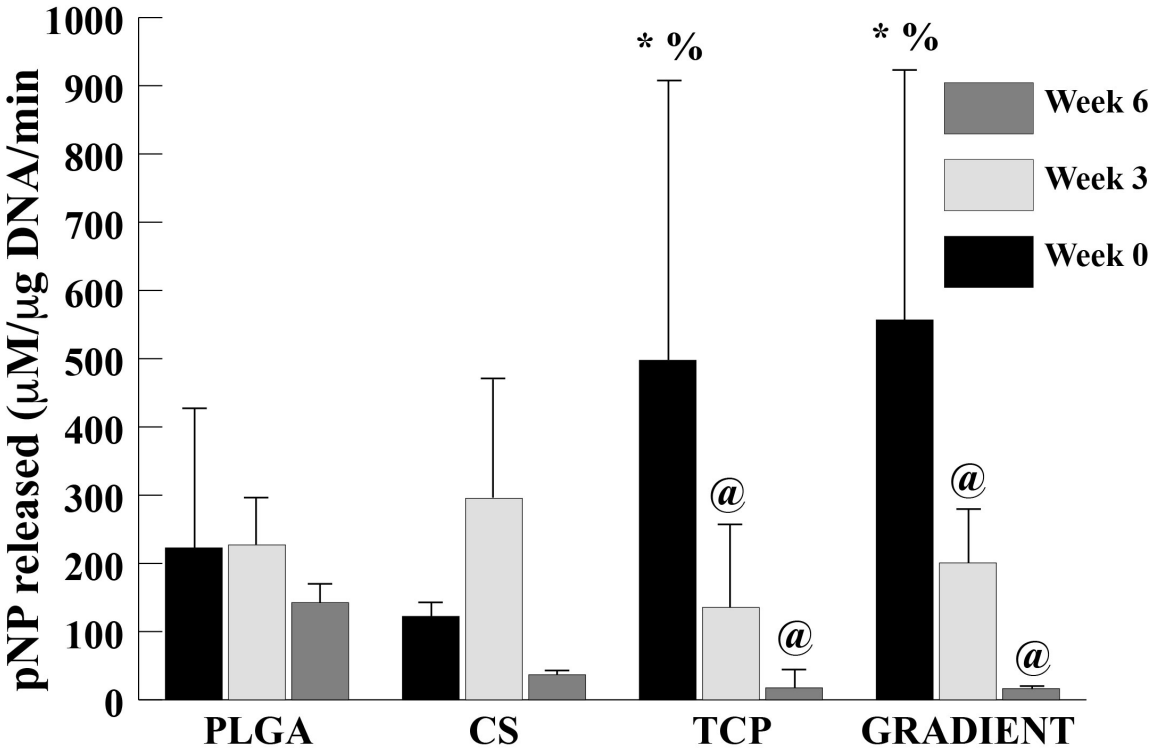

Figure 3.8: ALP activity in micromolar pNP released per micrograms DNA per minute

The TCP and GRADIENT groups had significantly higher ALP activities than the PLGA group at week 0. All values are expressed as the average + standard deviation (n = 3-5). The TCP and GRADIENT groups at week 0 had significantly higher ALP activities than the activities in the other two groups. @significant change over week 0 value, *significant change over the PLGA group at same time point, and %significant change over the CS group at same time point ($p < 0.05$).

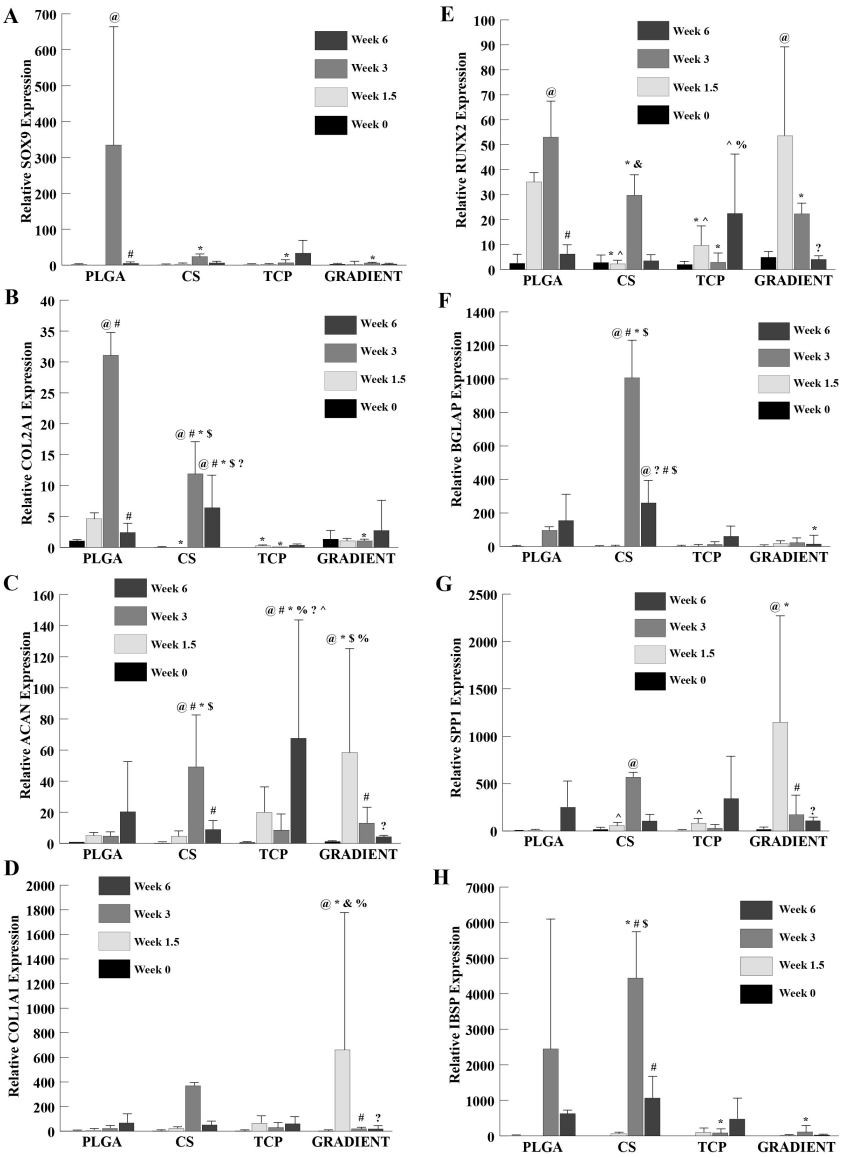

Figure 3.9. Relative gene expression

All values are expressed as the average + standard deviation (n = 3-5). The GRADIENT group had significantly higher expression of ACAN and SPP1 than the PLGA group at week 1.5. (A) SOX9 expression, (B) COL2A1 expression, (C) ACAN expression, (D) COL1A1 expression, (E) RUNX2 expression, (F) BGLAP expression, (G) SPP1 expression, and (H) IBSP expression. The GRADIENT group at week 1.5 outperformed the other three groups in ACAN and COL1A1 expression. @significant change over week 0 value, #significant change over its value at previous time point, *significant change over the PLGA group at same time point, $significant change over the TCP and GRADIENT groups at same time point, ?significant change over week 1.5 value, %significant change over the CS group at same time point, &significant change over the TCP group at same time point, and ^significant change over the GRADIENT group at same time point ($p < 0.05$).

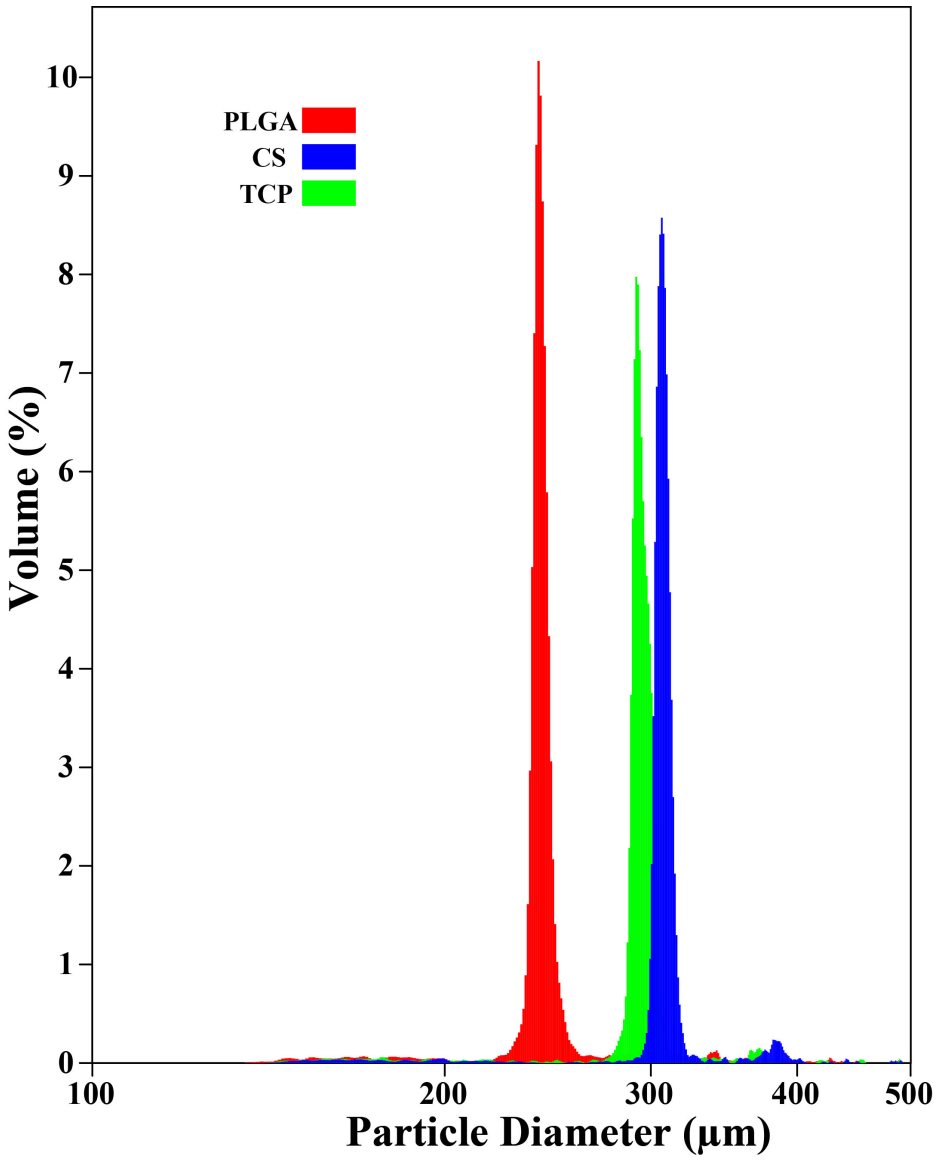

Figure 3.10: Microsphere size distribution graph

Mean particle size for PLGA, CS, and TCP groups were 238 µm, 296 µm, and 283 µm, respectively.

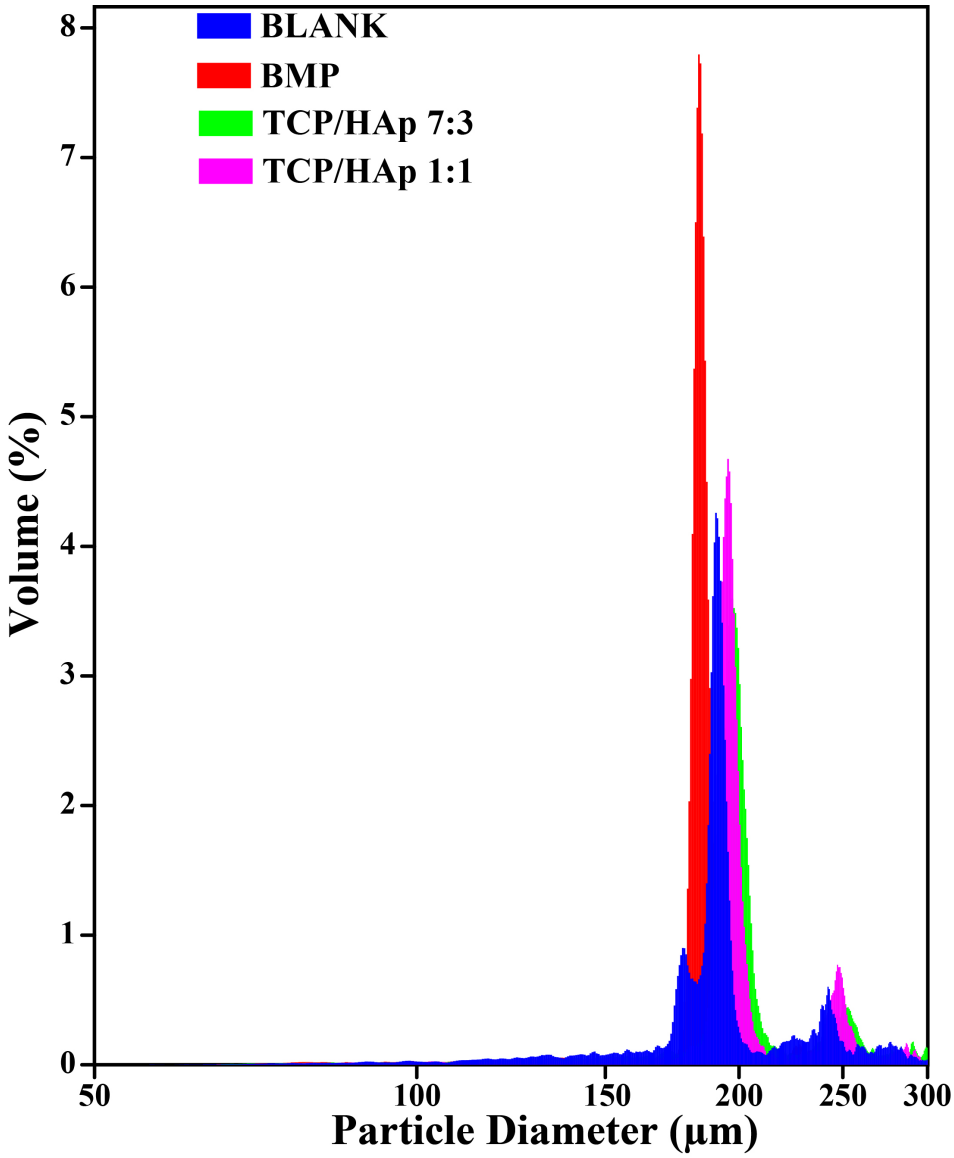

Figure 4.1: Size distribution graph for all four types of microspheres used in the study

All of the microspheres were uniform in size with average microsphere diameter ranging between 172-186 µm.

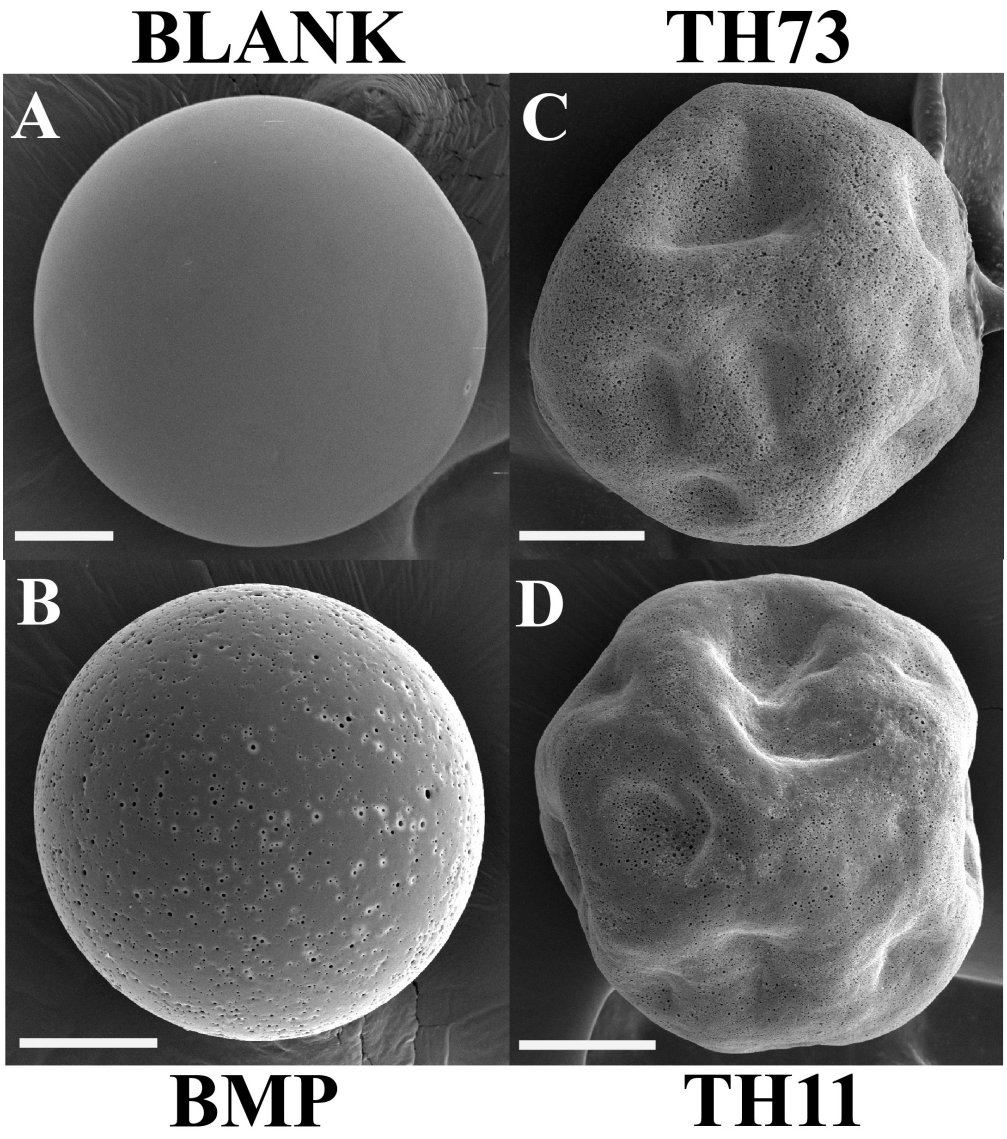

Figure 4.2: Scanning electron micrographs of microspheres

BLANK (PLGA-only), BMP (PLGA with BMP-2 encapsulated), TH73 (PLGA with 30 wt% TCP/HAp 7:3), and TH11 (PLGA with 30 wt% TCP/HAp 1:1) microspheres. The images reveal the distinct morphological features of the microspheres used in different scaffold groups; note the porous nature of the surface of the BMP microspheres, and the deviation from the perfect spherical form for the TH73 and TH11 microspheres. Scale bars: 50 μm.

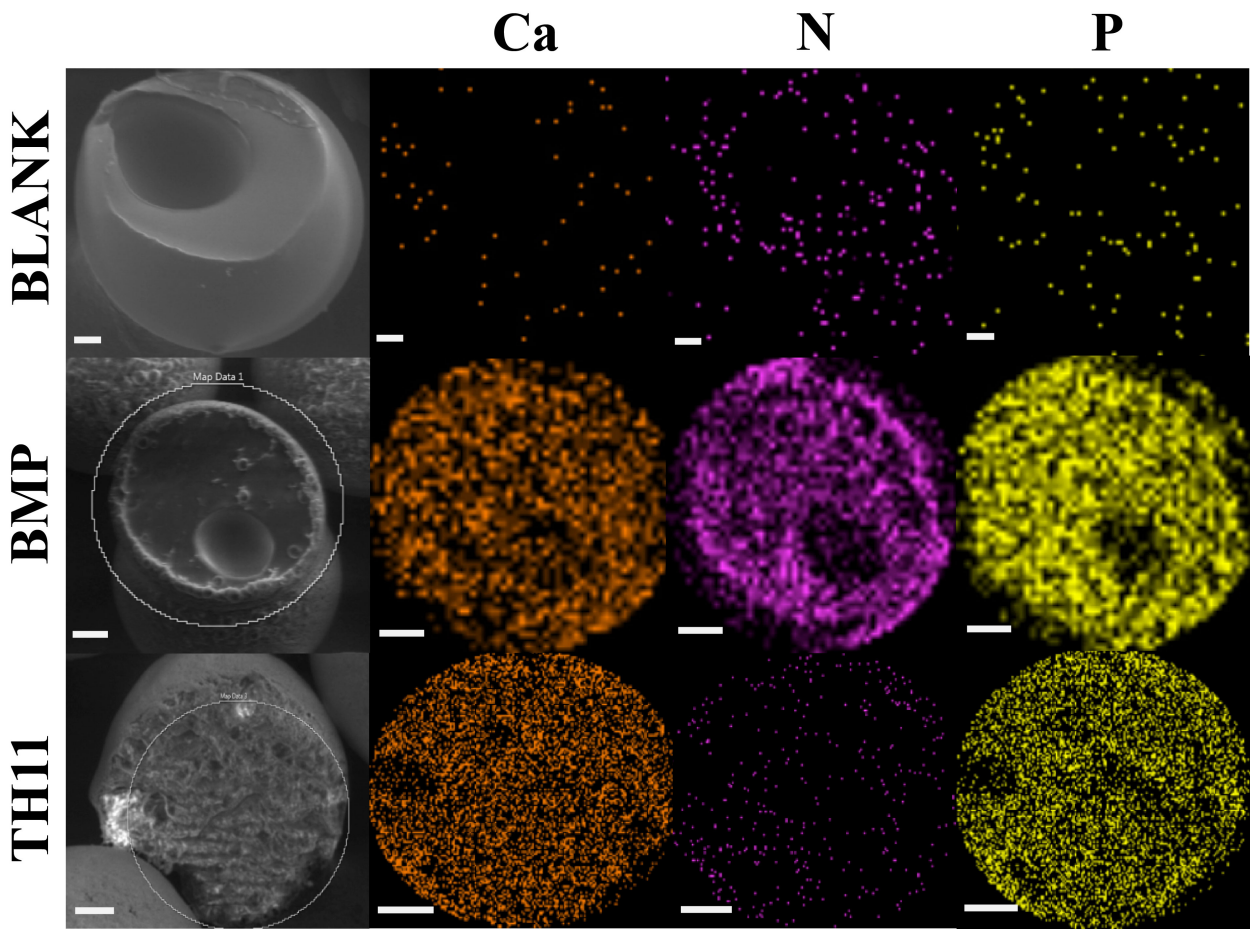

Figure 4.3: Scanning electron micrographs (left column) and energy dispersive spectral maps of cryo-fractured microspheres for atomic calcium (Ca), nitrogen (N), and phosphorous (P)

BLANK (PLGA-only), BMP (PLGA with BMP-2 encapsulated), and TH11 (PLGA with 30 wt% TCP/HAp 1:1). Note the uniform distribution of nitrogen in BMP microspheres and of calcium and phosphorus in the TH11 microspheres. Scale bars: 25 μm.

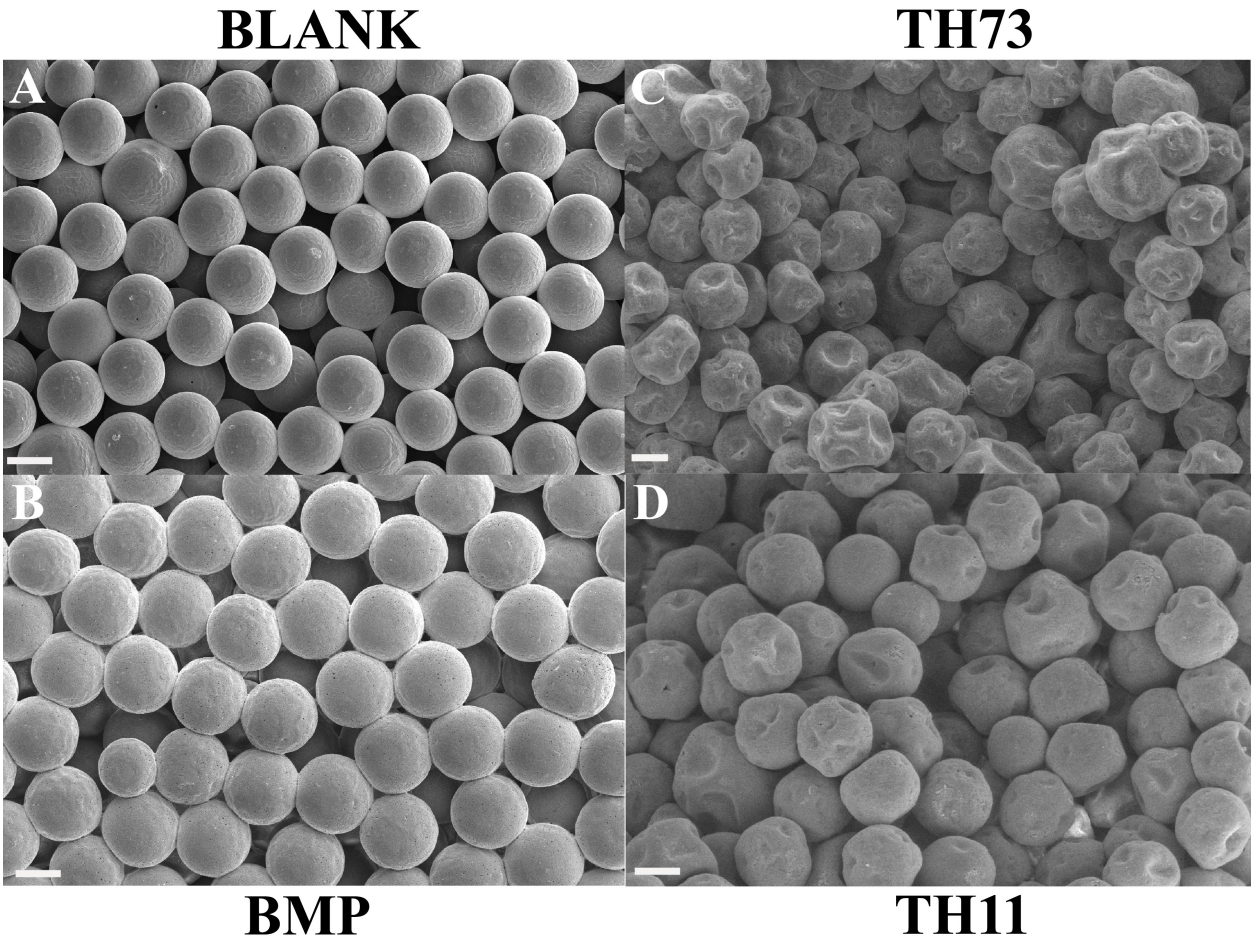

Figure 4.4: Scanning electron micrographs of acellular microsphere-based scaffolds

BLANK (PLGA-only), BMP (PLGA with BMP-2 encapsulated), TH73 (PLGA with 30 wt% TCP/HAp 7:3), and TH11 (PLGA with 30 wt% TCP/HAp 1:1) scaffolds. All of the scaffolds were porous in nature with interconnected pores. Scale bars: 100 μm.

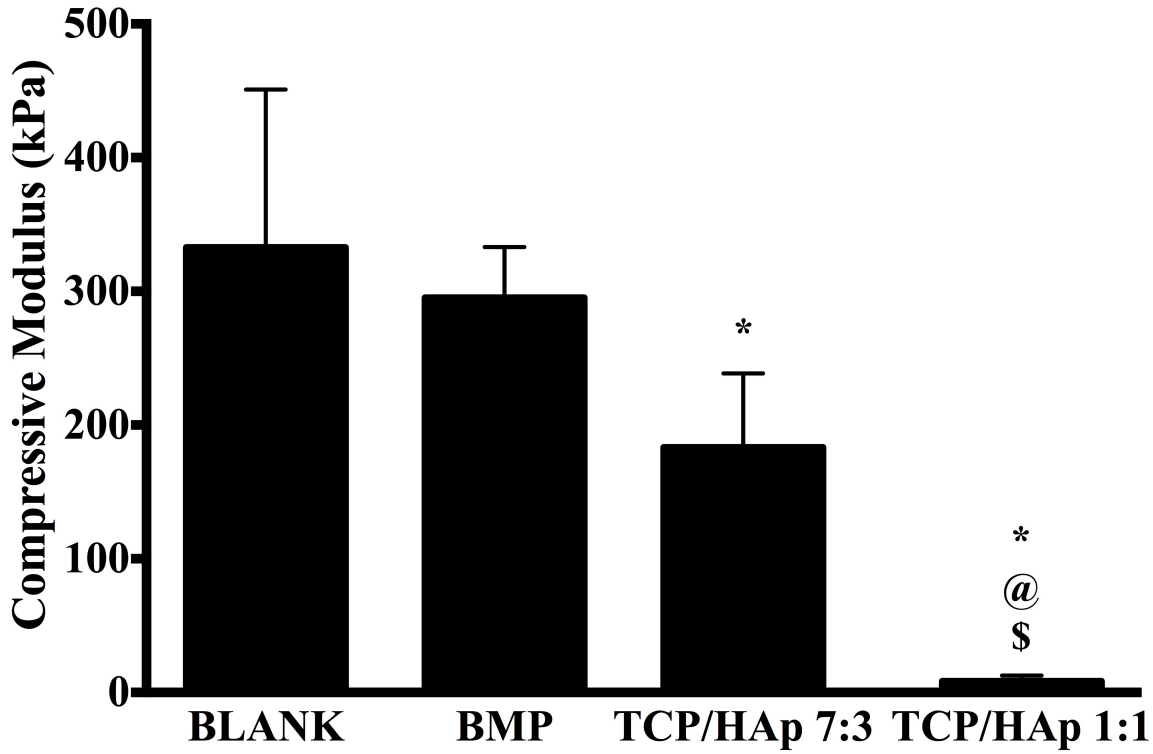

Figure 4.5: Average compressive moduli of elasticity of acellular microsphere-based scaffolds at week 0

All values are expressed as the average + standard deviation (n = 6). The TCP/HAp groups had significantly lower moduli than the BLANK and BMP controls. *significant difference from the BLANK negative control group, @significant difference from the BMP positive control group, and $significant difference from the TCP/HAp 7:3 group ($p < 0.05$).

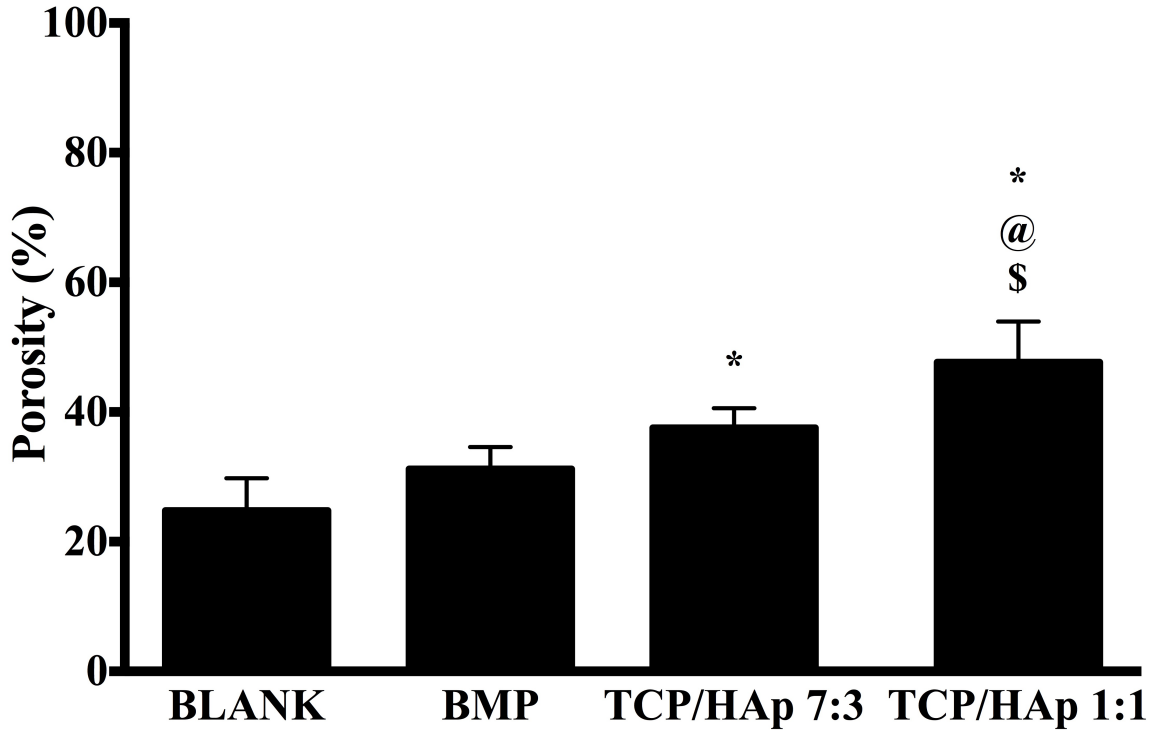

Figure 4.6. Average porosities of different scaffold groups

All values are expressed as the average + standard deviation (n = 6). The TCP/HAp groups had significantly higher porosities than the BLANK and BMP controls. *significant difference from the BLANK negative control group, @significant difference from the BMP positive control group, and $significant difference from the TCP/HAp 7:3 group ($p < 0.05$).

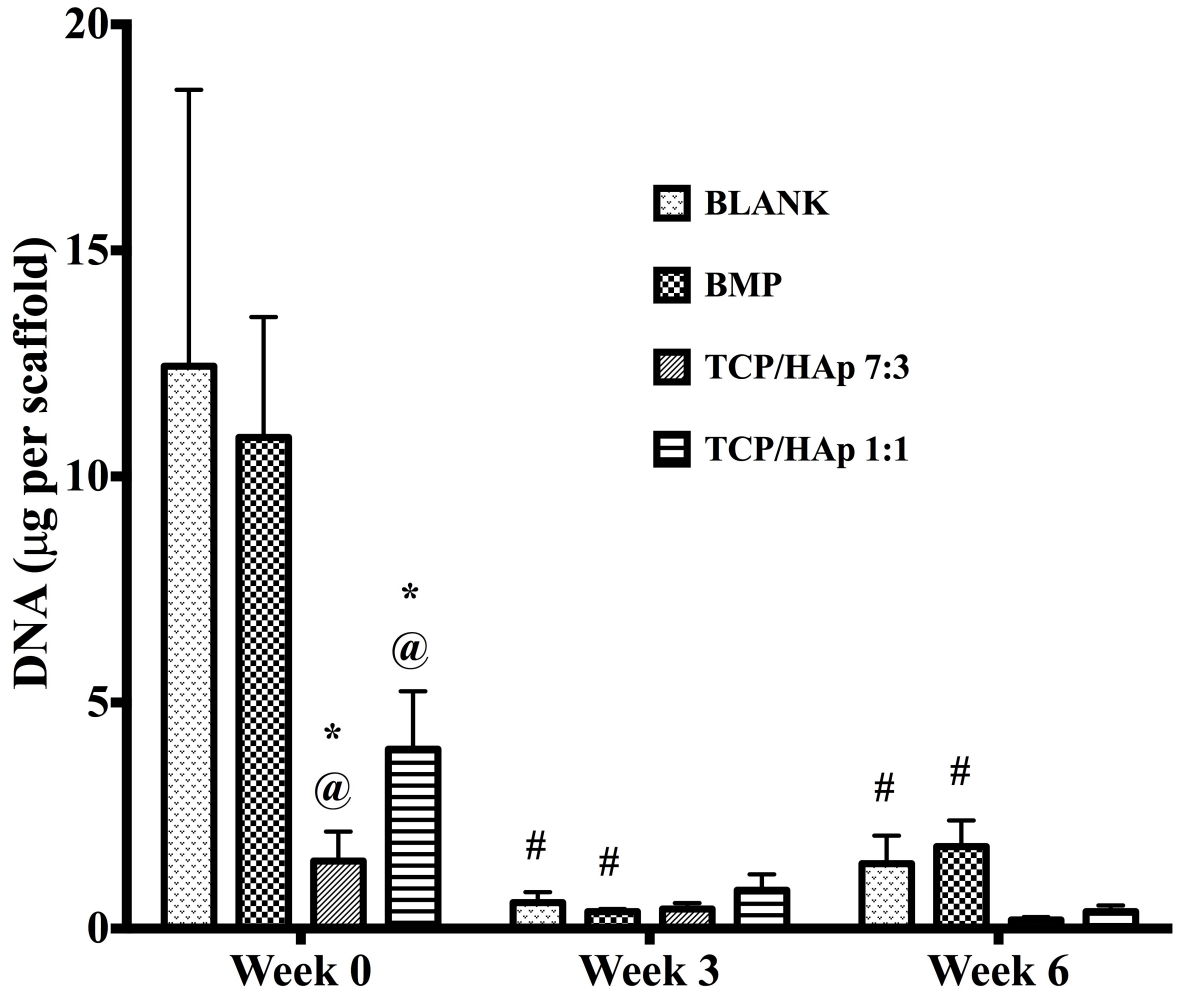

Figure 4.7: Total DNA content as measured in the microsphere-based scaffolds

All values are expressed as the average + standard deviation (n = 6). The TCP/HAp groups had significantly lower DNA content than the BLANK and BMP controls at week 0, while no significant differences were observed among the groups at later time points. *significant difference from the BLANK negative control group at same time point, @significant difference from the BMP positive control group at same time point, and #significant change from its value at week 0 ($p < 0.05$).

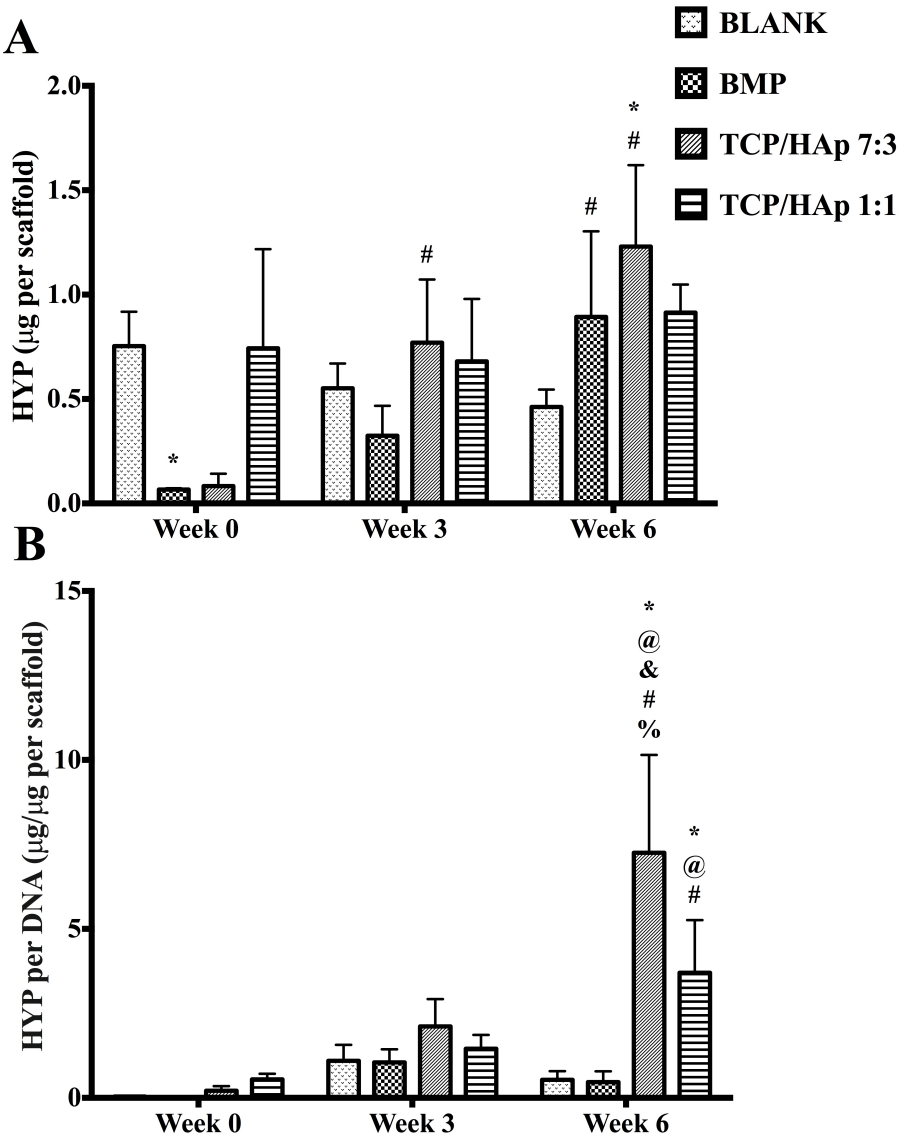

Figure 4.8: HYP content as measured in the microsphere-based scaffolds

(A) Total HYP content in micrograms per construct. (B) Normalized HYP content in micrograms per microgram of DNA. All values are expressed as the average + standard deviation (n = 6). The TCP/HAp groups had significantly higher normalized HYP content than the BLANK and BMP controls at week 6. *significant difference from the BLANK negative control group at same time point, @significant difference from the BMP positive control group at same time point, &significant difference from the TCP/HAp 1:1 group at same time point, #significant change from its value at week 0, and %significant change from its value at week 3 ($p < 0.05$).

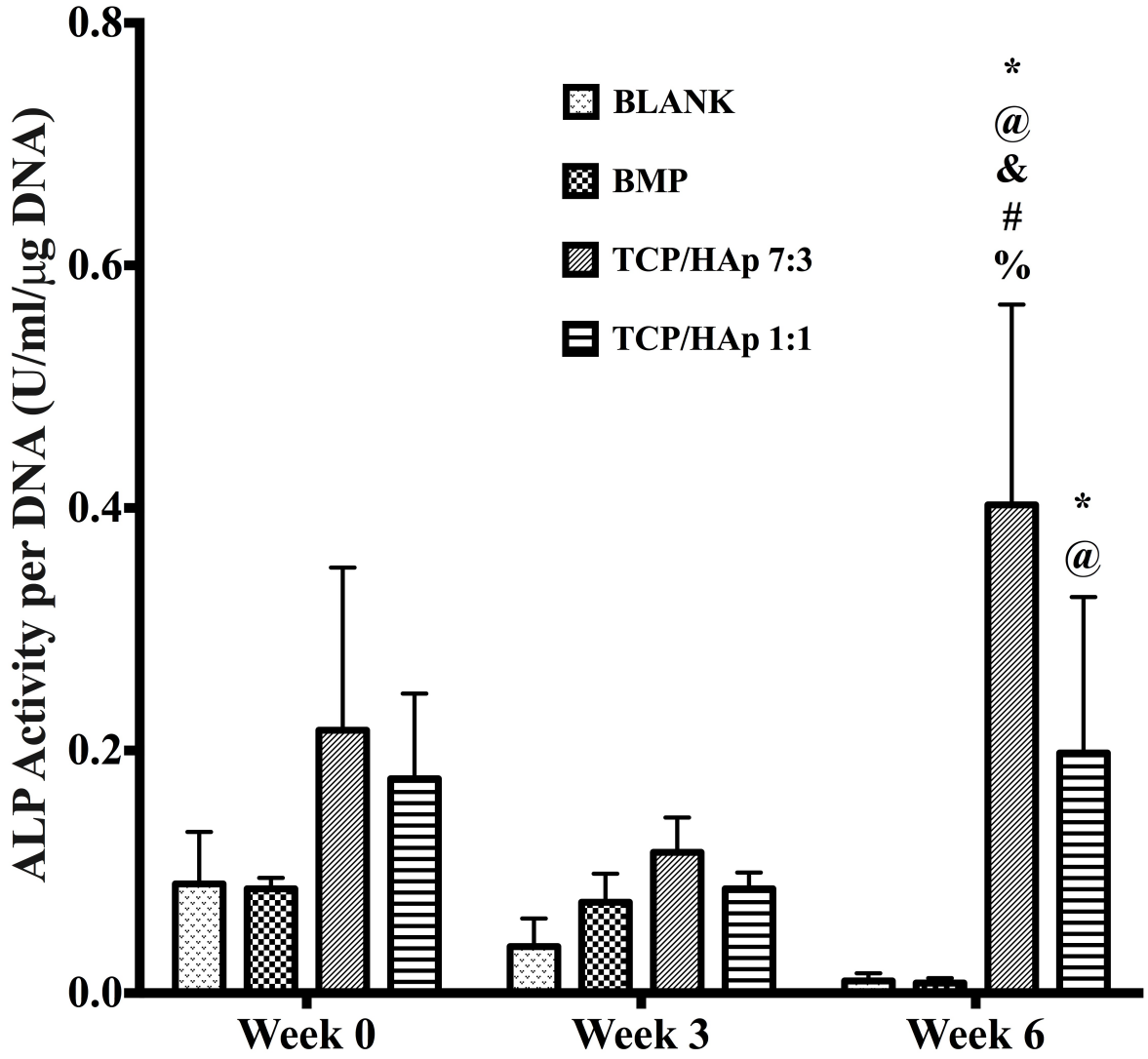

Figure 4.9: ALP activity in 'Glycine Units' per micrograms DNA

Glycine Unit refers to the amount of enzyme causing the hydrolysis of one micromole of pNPP per minute at pH 9.6 and 25°C (glycine buffer). All values are expressed as the average + standard deviation (n = 6). The TCP/HAp groups outperformed the BLANK and BMP controls in ALP activity at week 6. *significant difference from the BLANK negative control group at same time point, @significant difference from the BMP positive control group at same time point, &significant difference from the TCP/HAp 1:1 group at same time point, #significant change from its value at week 0, and %significant change from its value at week 3 ($p < 0.05$).

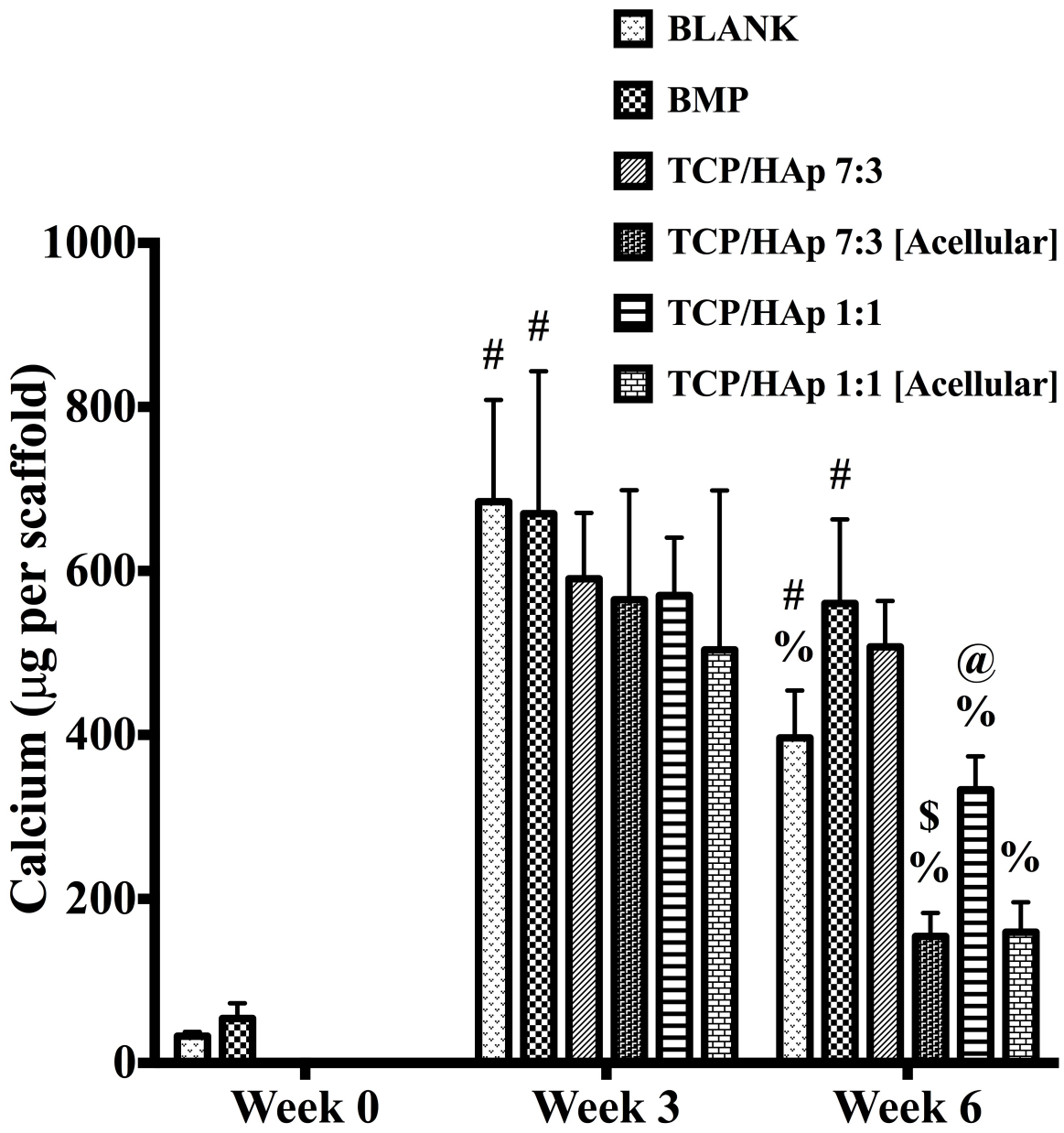

Figure 4.10: Total calcium content as measured in the microsphere-based scaffolds

The calcium contents of the TCP/HAp 7:3 and TCP/HAp 1:1 constructs (both cellular and acellular) at week 0 are not reported because of inadequate extraction of calcium from these scaffolds. All values are expressed as the average + standard deviation (n = 6). The TCP/HAp 7:3 group had significantly higher calcium than the TCP/HAp 7:3 [Acellular] group at week 6. @significant difference from the BMP positive control group at same time point, $significant difference from the TCP/HAp 7:3 group at same time point, #significant change from its value at week 0, and %significant change from its value at week 3 ($p < 0.05$).

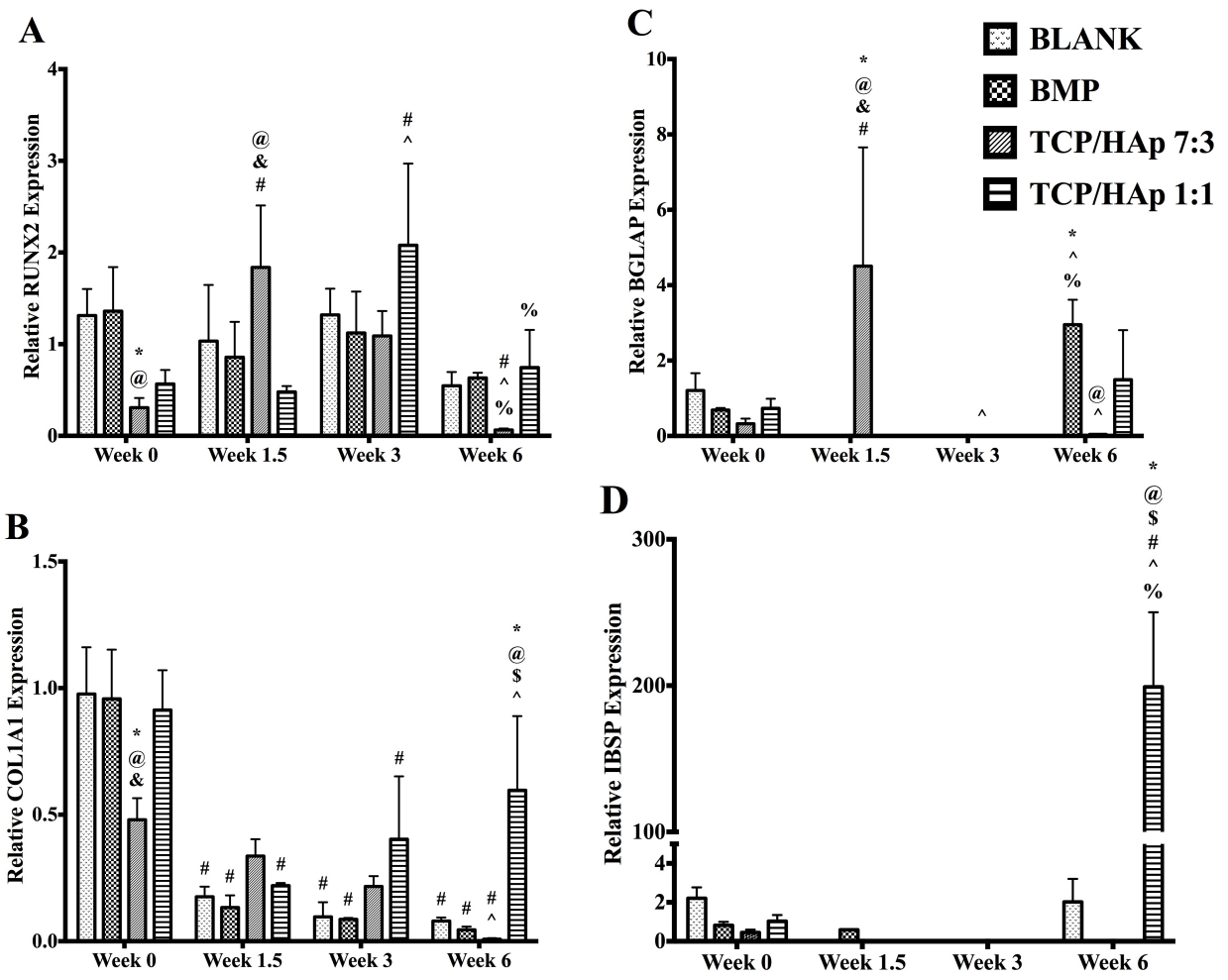

Figure 4.11: Relative gene expression

All values are expressed as the average + standard deviation (n = 6). The gene expression of the TCP/HAp groups was lower compared to that of the BLANK and BMP controls initially; however, it was higher at later time points. *significant difference from the BLANK negative control group at same time point, @significant difference from the BMP positive control group at same time point, $significant difference from the TCP/HAp 7:3 group at same time point, & significant difference from the TCP/HAp 1:1 group at same time point, # significant change from its value at week 0, ^ significant change from its value at week 1.5, and % significant change from its value at week 3 ($p < 0.05$).

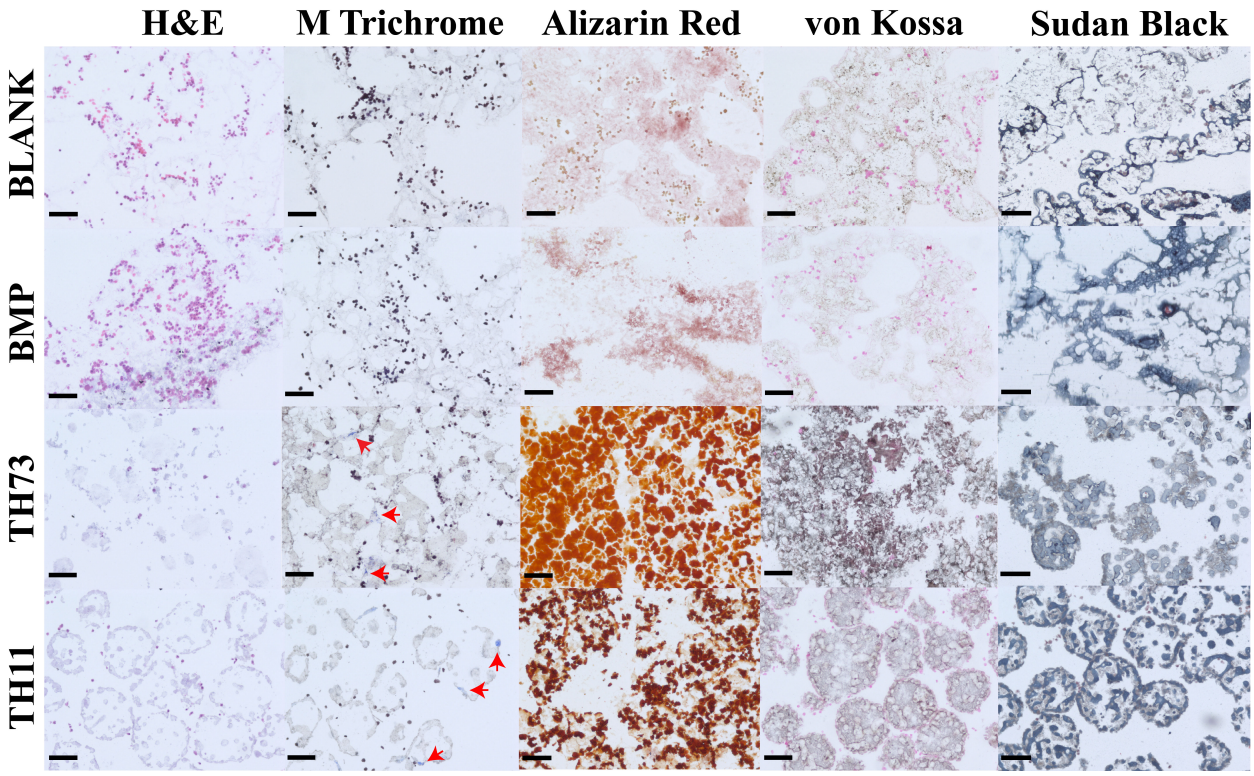

Figure 4.12. Histological staining of cell-seeded microsphere-based constructs at week 6

BLANK, BMP, TH73 (TCP/HAp 7:3), and TH11 (TCP/HAp 1:1) scaffolds were stained for H&E (A-D), Masson's trichrome (E-H), Alizarin red (I-L), von Kossa (M-P), and Sudan black (Q-T). The TCP/HAp groups showed deposits of collagen (indicated by arrows), while no such deposits were observed in the BLANK and BMP controls. Scale bars: 100 μm.

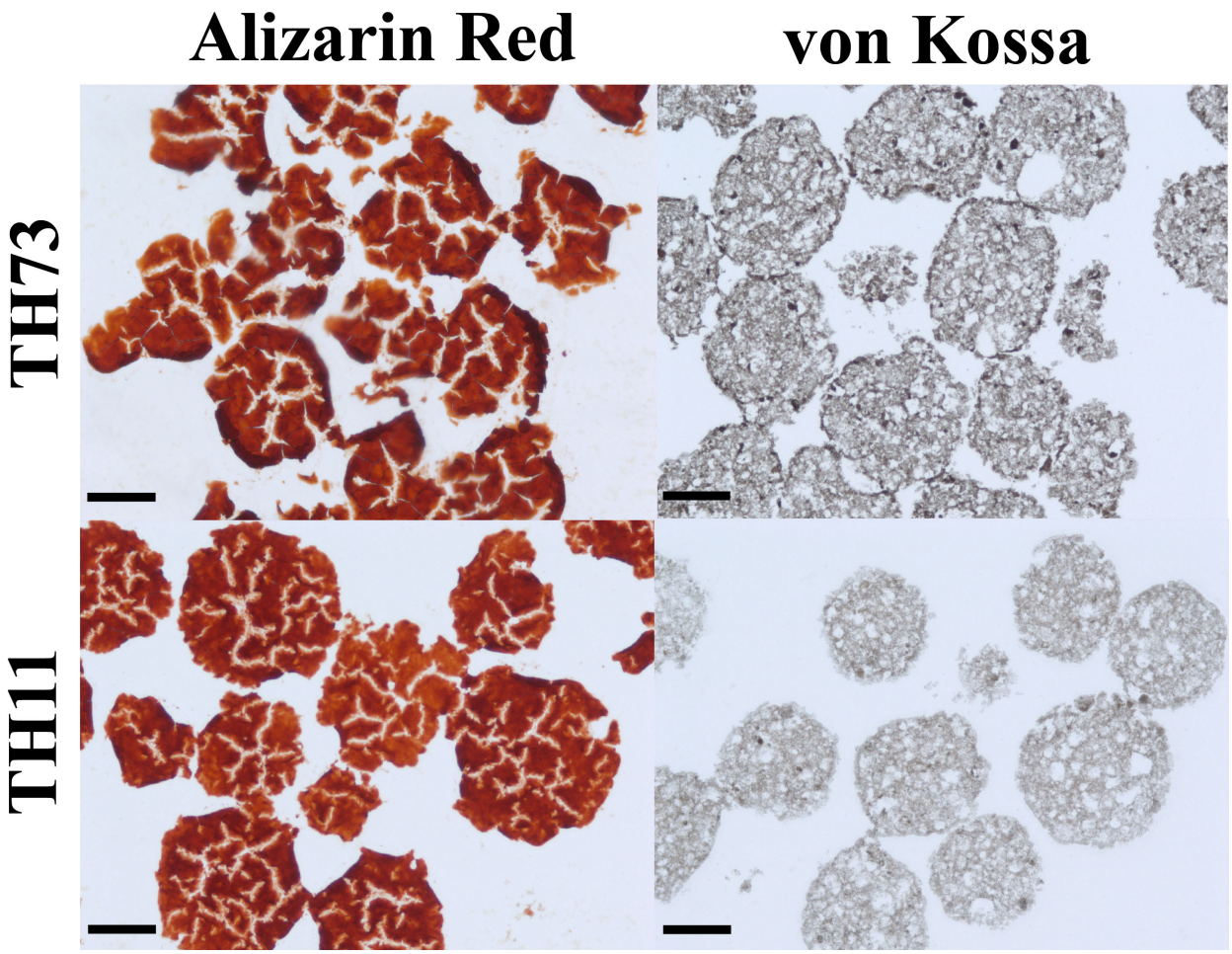

Figure 4.13: Alizarin Red and von Kossa staining images for acellular TCP/HAp 7:3 scaffolds and TCP/HAp 1:1 scaffolds at week 6

High staining intensities in the TCP/HAp groups indicate toward high mineral content remaining in these groups after 6 weeks. Scale bars: 100 μm.

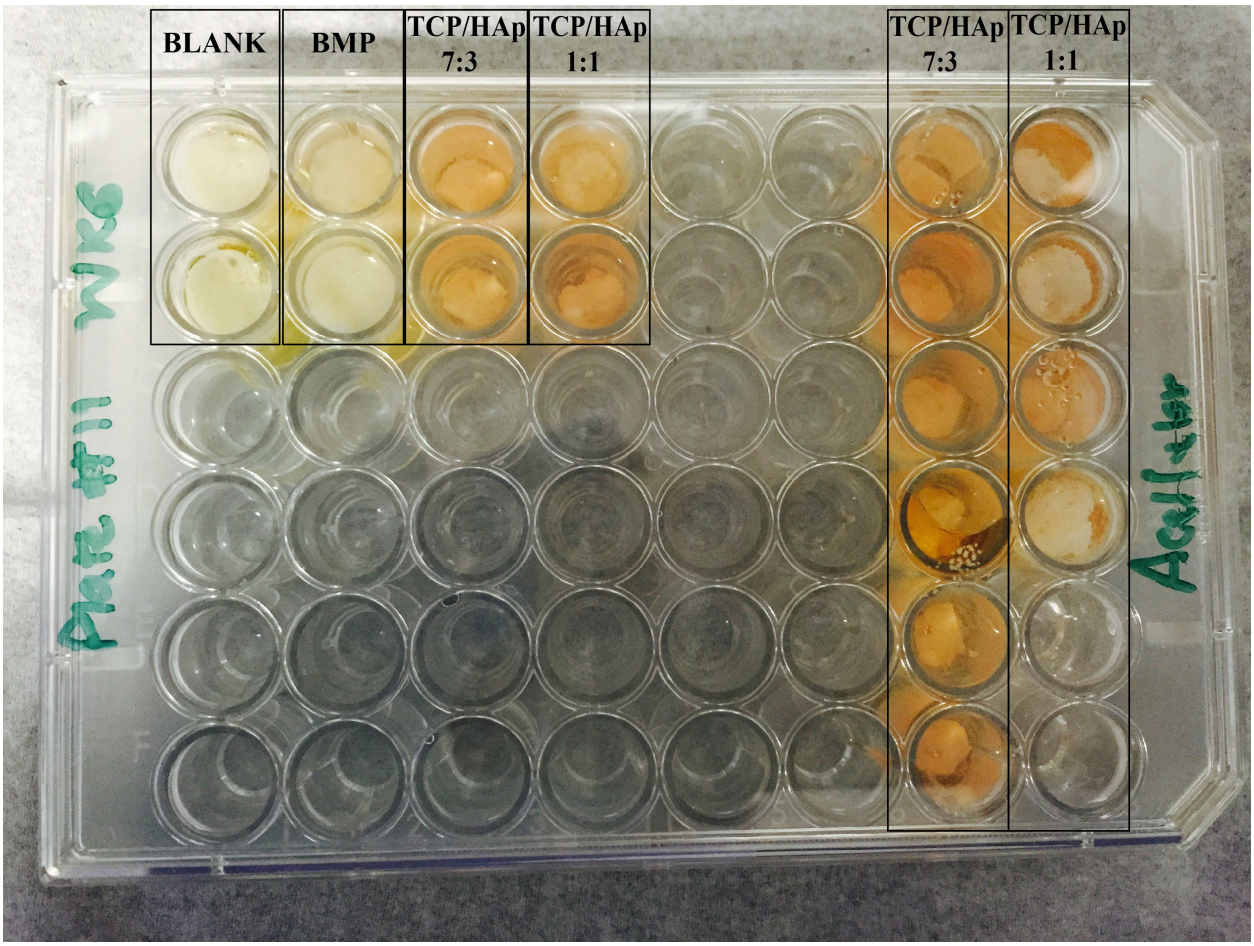

Figure 4.14 Image of acellular scaffolds in culture (week 4) depicting macroscopic changes in scaffold size and color changes in culture medium among different groups

The culture medium in the acellular BLANK and BMP scaffolds became acidic more rapidly than the medium in their TCP/HAp counterparts.

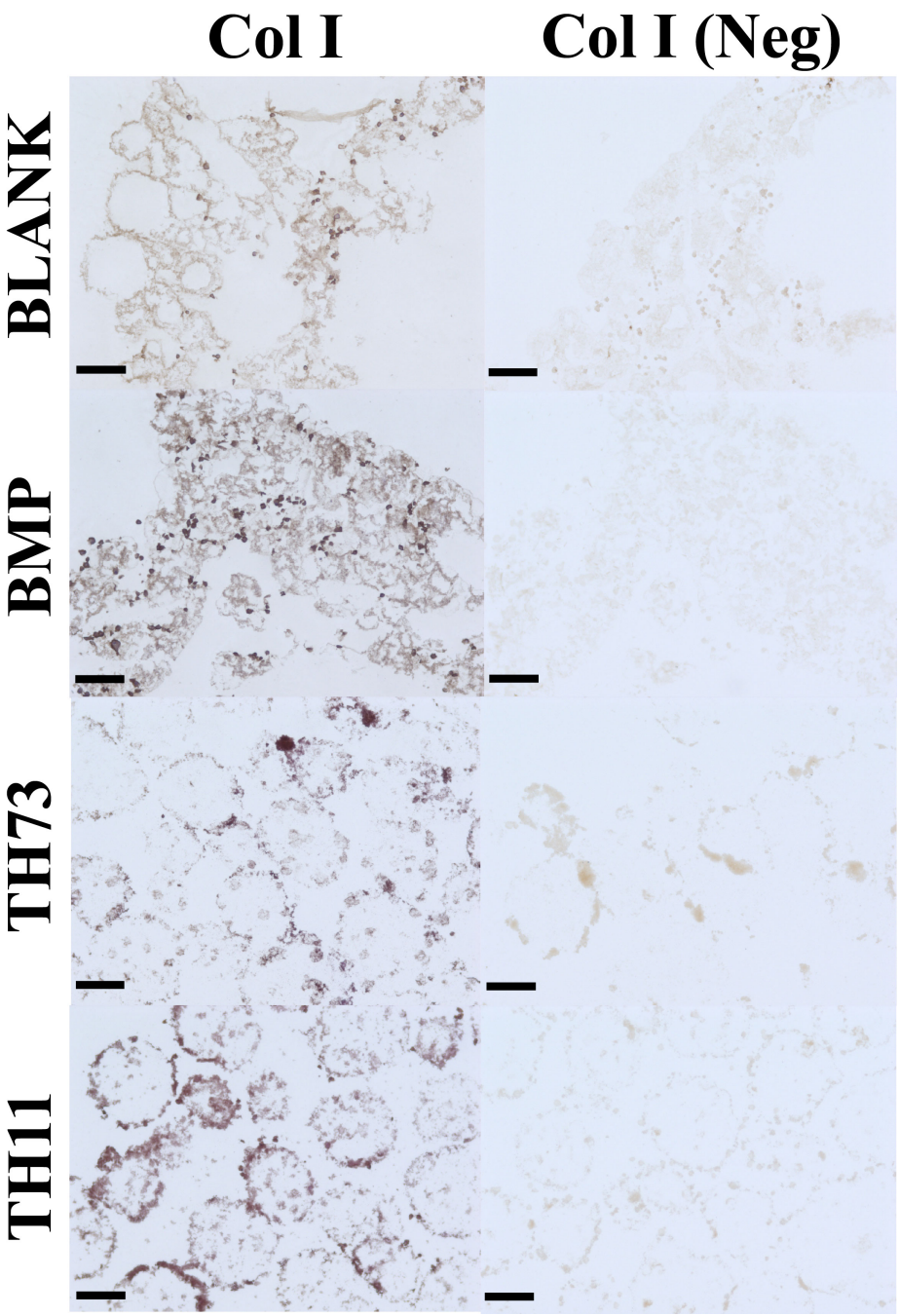

Figure 4.15: Immunohistochemical staining of microsphere-based constructs at week 6

BLANK, BMP, TH73 (TCP/HAp 7:3), and TH11 (TCP/HAp 1:1) scaffolds were stained for Collagen I (A-D). Images of negative controls (primary antibody omitted) are also shown (E-H). Collagen I staining was more intense in the BMP and TCP/HAp 1:1 groups than the staining in the BLANK group. Scale bars: 100 μm.

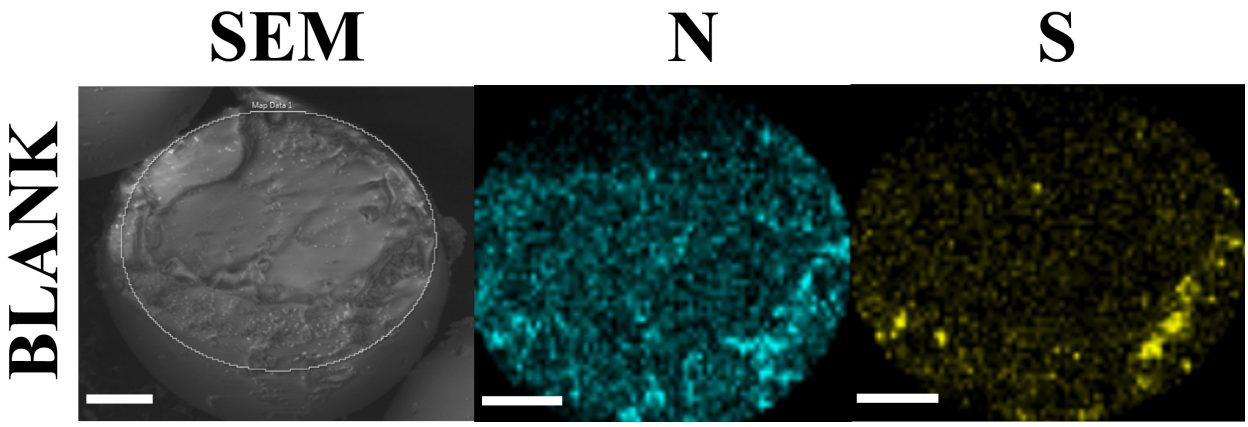

Figure 5.1: Scanning electron micrographs (left column) and energy dispersive spectral maps (center and right columns) of cryo-fractured BLANK microspheres for atomic nitrogen (N) and sulfur (S)

Both nitrogen and sulfur were essentially absent from the interior of the BLANK microspheres. Scale bars: 25 μm.

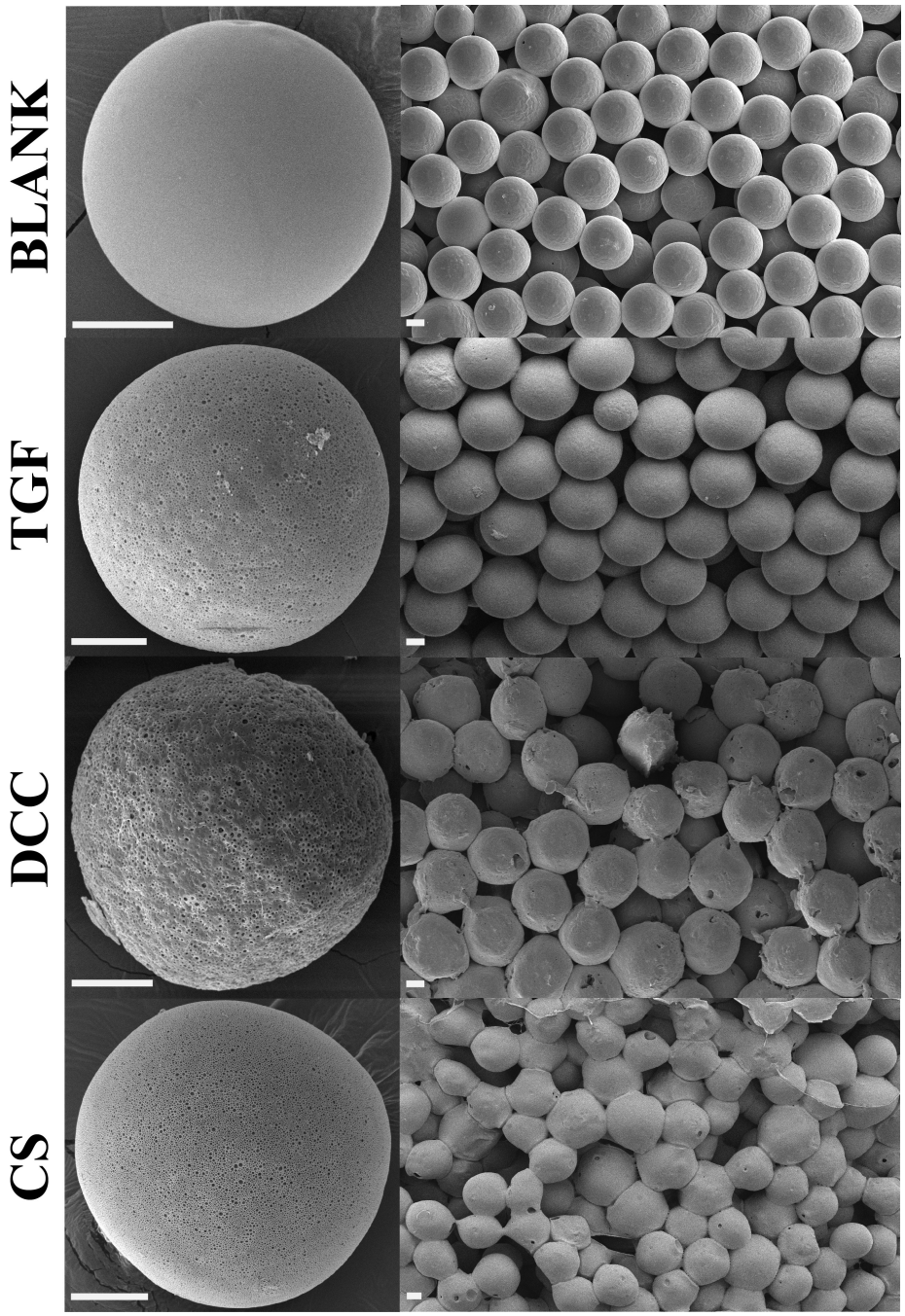

Figure 5.2: Scanning electron micrographs of microspheres (left column) and scaffolds (right column)

BLANK (PLGA-only), TGF (PLGA with TGF-β_3 encapsulated), DCC (PLGA with 30 wt% DCC), and CS (PLGA with 30 wt% CS) microspheres and scaffolds. The images reveal the distinct morphological features of the microspheres and scaffolds; note the porous nature of the surface of the TGF microspheres, rough surface of DCC microspheres, and relatively greater degree of sintering in the CS scaffolds. Scale bars: 50 μm.

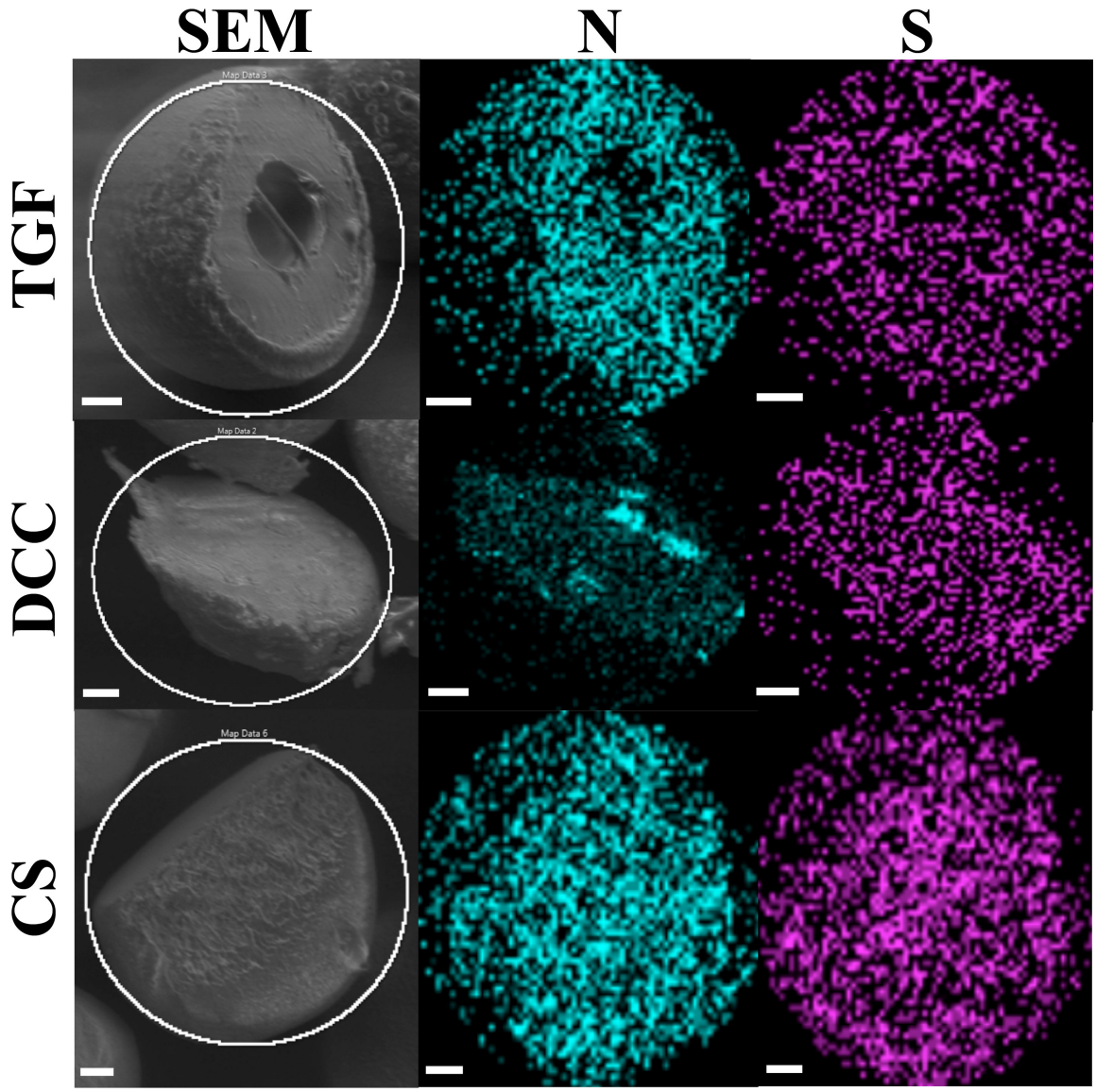

Figure 5.3: Scanning electron micrographs (left column) and energy dispersive spectral maps (center and right columns) of cryo-fractured microspheres for atomic nitrogen (N) and sulfur (S)

TGF (PLGA with TGF-β_3 encapsulated), DCC (PLGA with 30 wt% DCC), and CS (PLGA with 30 wt% CS) microspheres. Note the uniform distribution of nitrogen and sulfur in the TGF, DCC and CS microspheres. Scale bars: 25 μm.

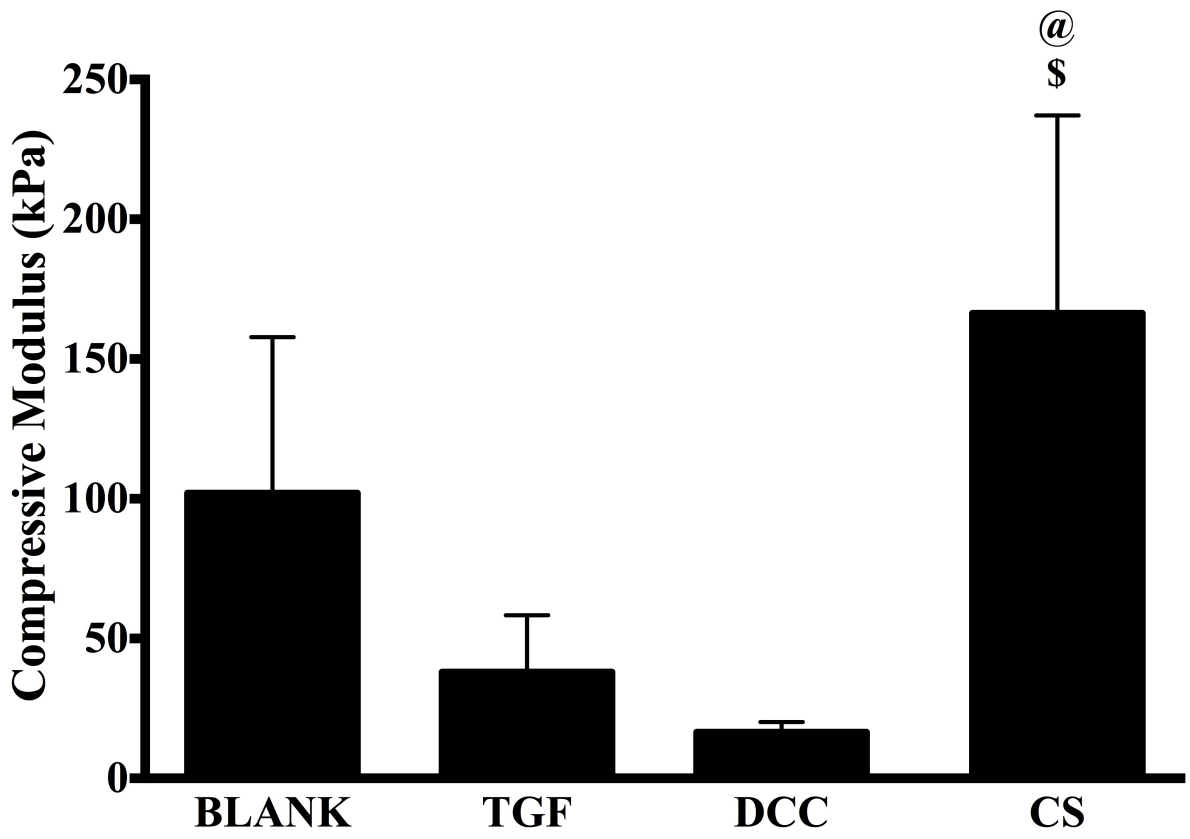

Figure 5.4: Average compressive moduli of elasticity of acellular microsphere-based scaffolds at week 0

All values are expressed as the average + standard deviation (n = 6). The CS group had a significantly higher modulus than the TGF and DCC groups. @significant difference from the TGF group and $significant difference from the DCC group ($p < 0.05$).

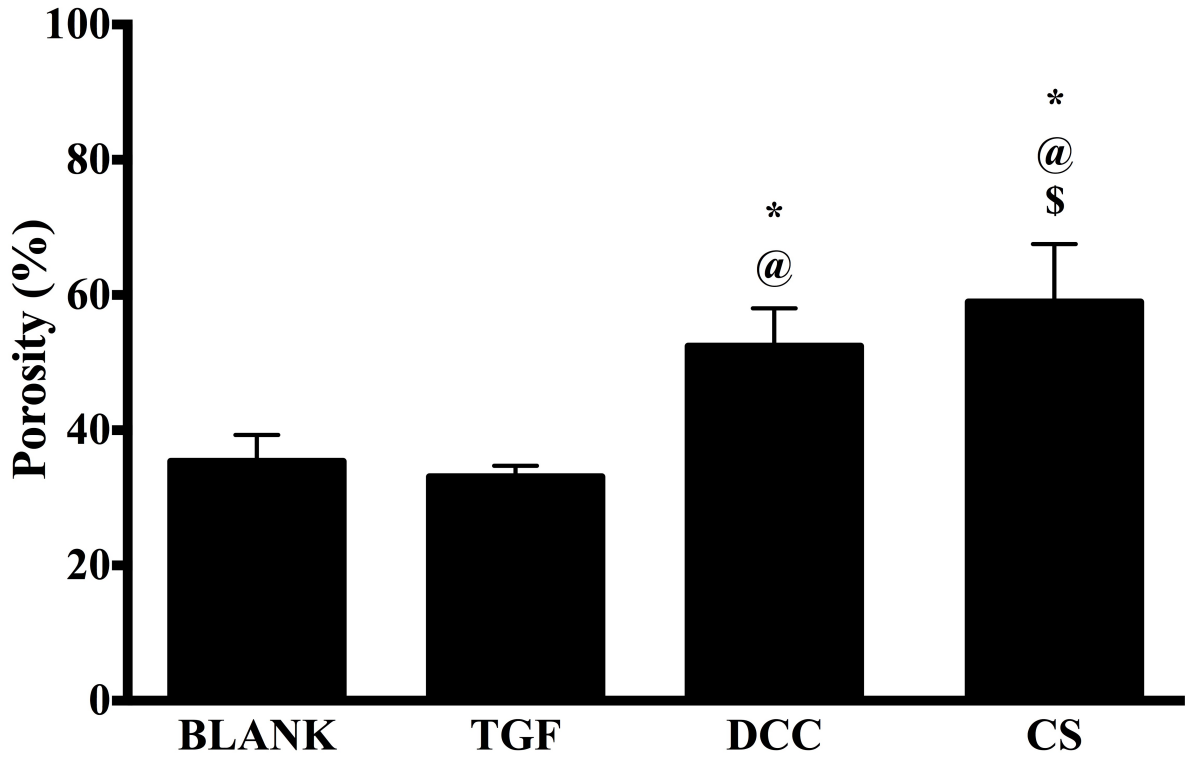

Figure 5.5: Average porosities of different scaffold groups

All values are expressed as the average + standard deviation (n = 6). Both the DCC and CS groups had higher porosities than the BLANK and TGF groups *significant difference from the BLANK group, @significant difference from the TGF group, and $significant difference from the DCC group ($p < 0.05$).

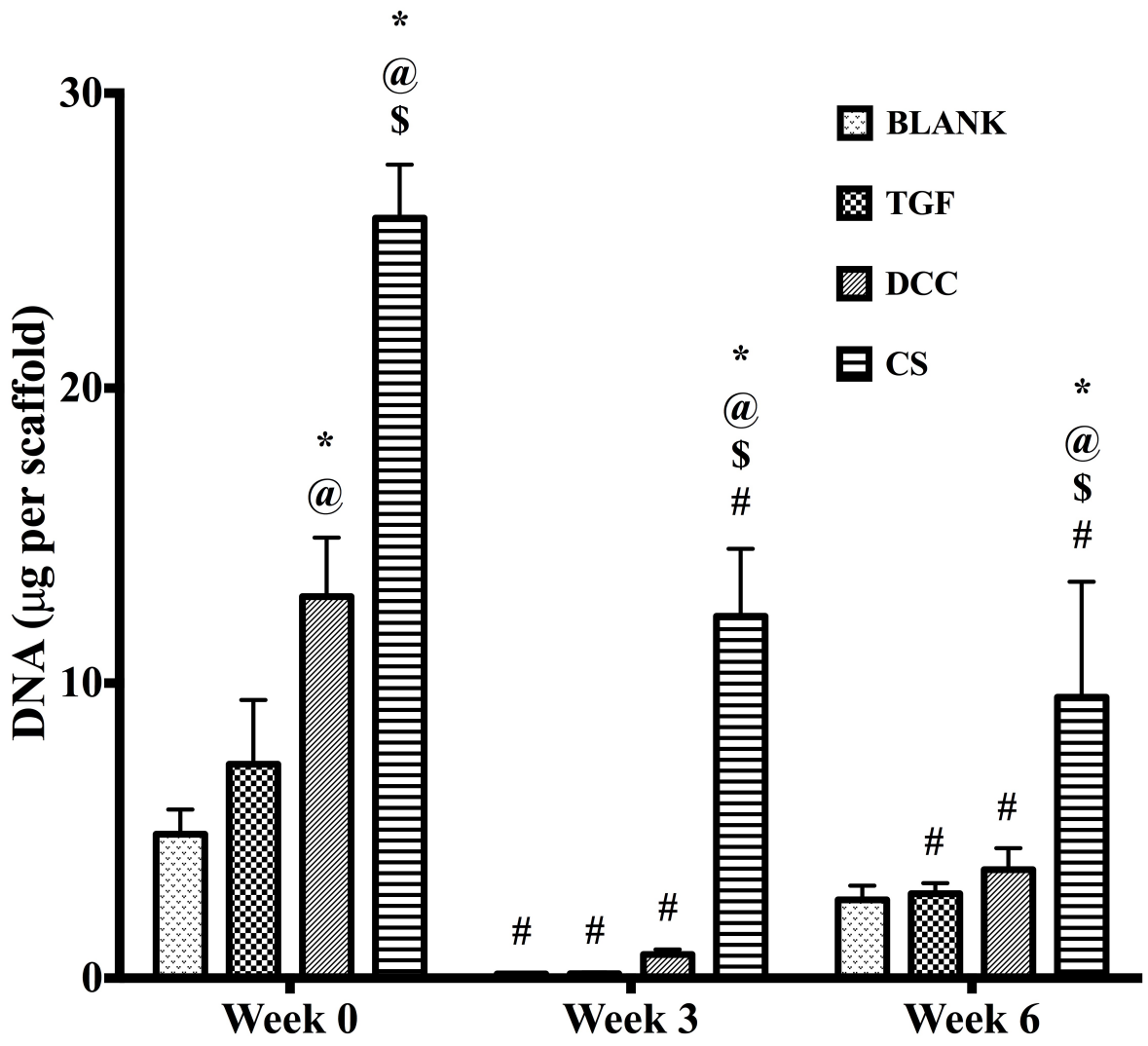

Figure 5.6: Total DNA content in different scaffold groups

All values are expressed as the average + standard deviation (n = 6). The CS group had the highest DNA content at all time points by at least a factor of 2. *significant difference from the BLANK group at same time point, @significant difference from the TGF group at same time point, $significant difference from the DCC group at same time point, and #significant difference from its value at week 0 ($p < 0.05$).

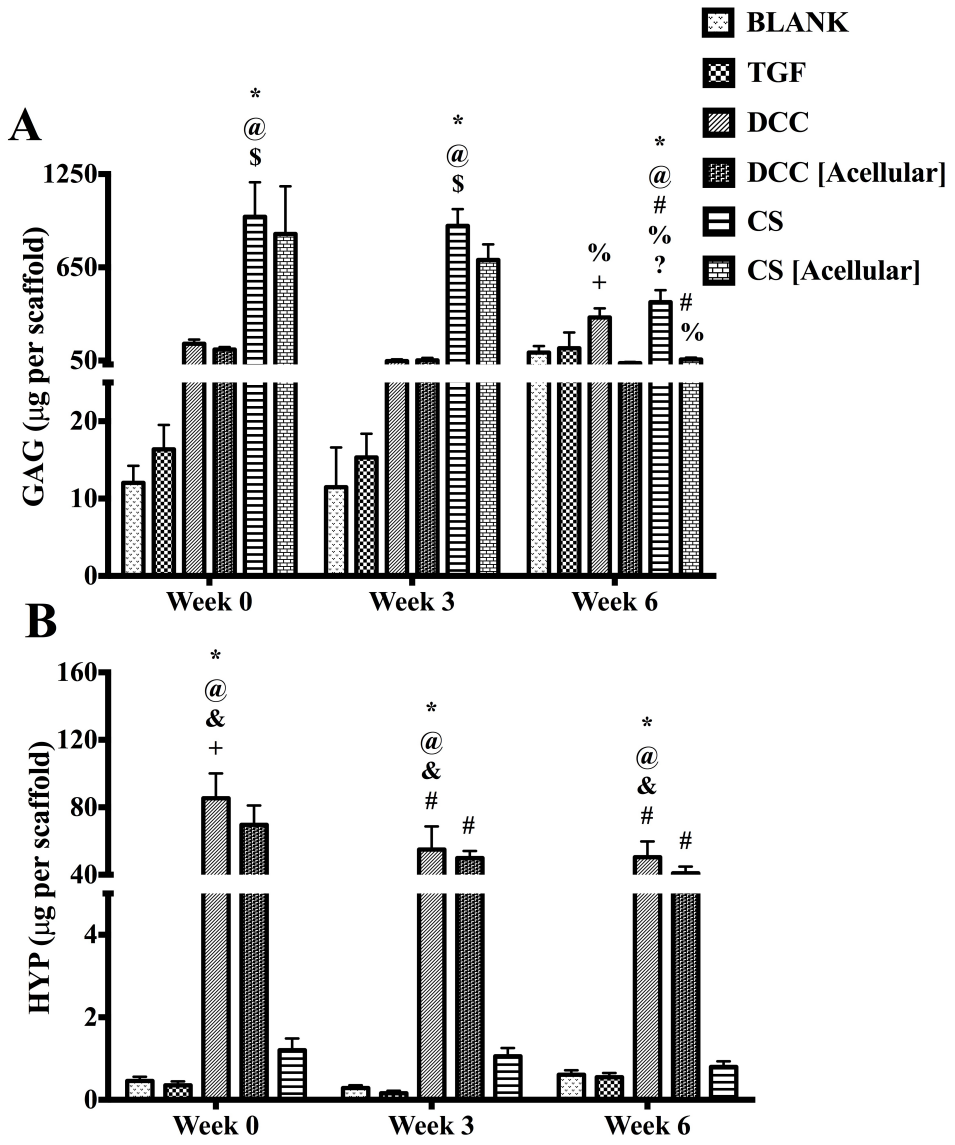

Figure 5.7: Total GAG content (A) and HYP content (B) in different scaffold groups

All values are expressed as the average + standard deviation (n = 6). The DCC and CS groups had significantly higher GAG content than their acellular counterparts at week 6. The DCC group at week 0 also had significantly higher HYP content than the DCC [Acellular] group. *significant difference from the BLANK group at same time point, @significant difference from the TGF group at same time point, $significant difference from the DCC group at same time point, +significant difference from the DCC [Acellular] group at same time point, ?significant difference from the CS [Acellular] group at same time point, #significant difference from its value at week 0, and %significant difference from its value at week 3 ($p < 0.05$).

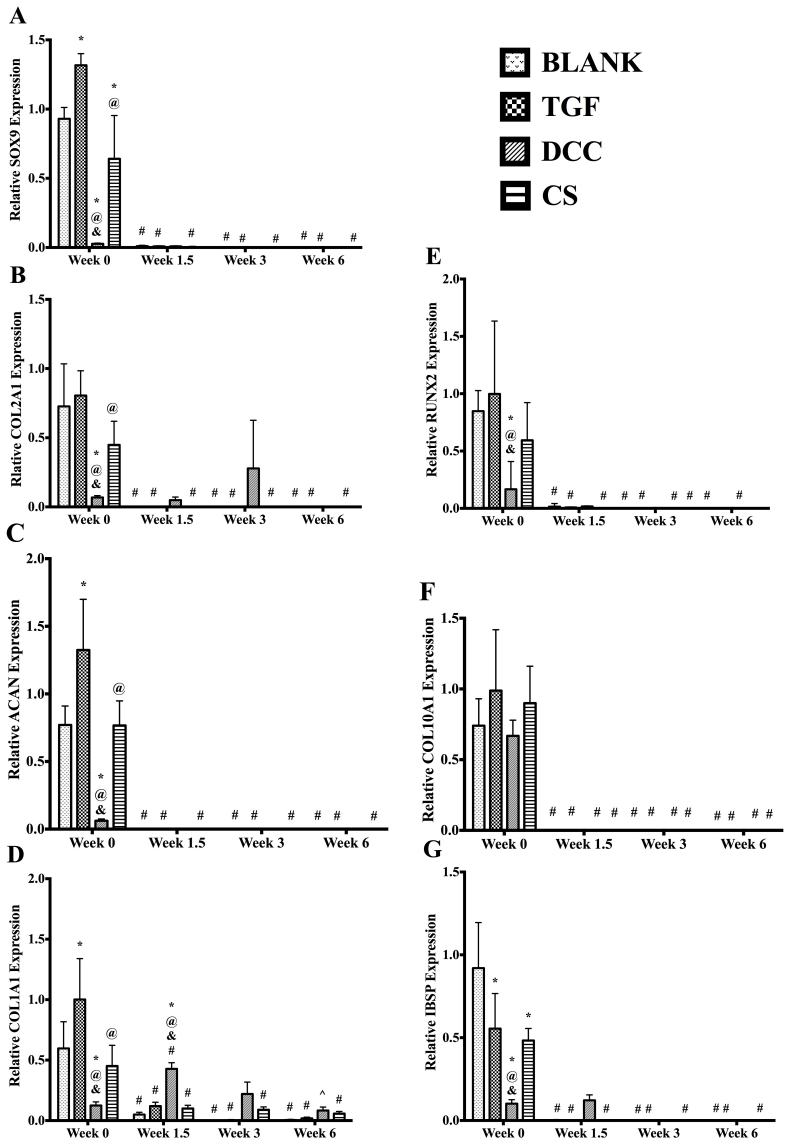

Figure 5.8: Relative gene expression. (A) SOX9 expression, (B) COL2A1 expression, (C) ACAN expression, (D) COL1A1 expression, (E) RUNX2 expression, (F) COL10A1 expression, and (G) IBSP expression

All values are expressed as the average + standard deviation (n = 6). The TGF positive control group had higher expression whereas the DCC group had lower expression of chondrogenic signals at week 0. *significant difference from the BLANK group at same time point, @significant difference from the TGF group at same time point, &significant difference from the CS group at same time point, #significant difference from its value at week 0, and ^significant difference from its value at week 1.5 ($p < 0.05$).

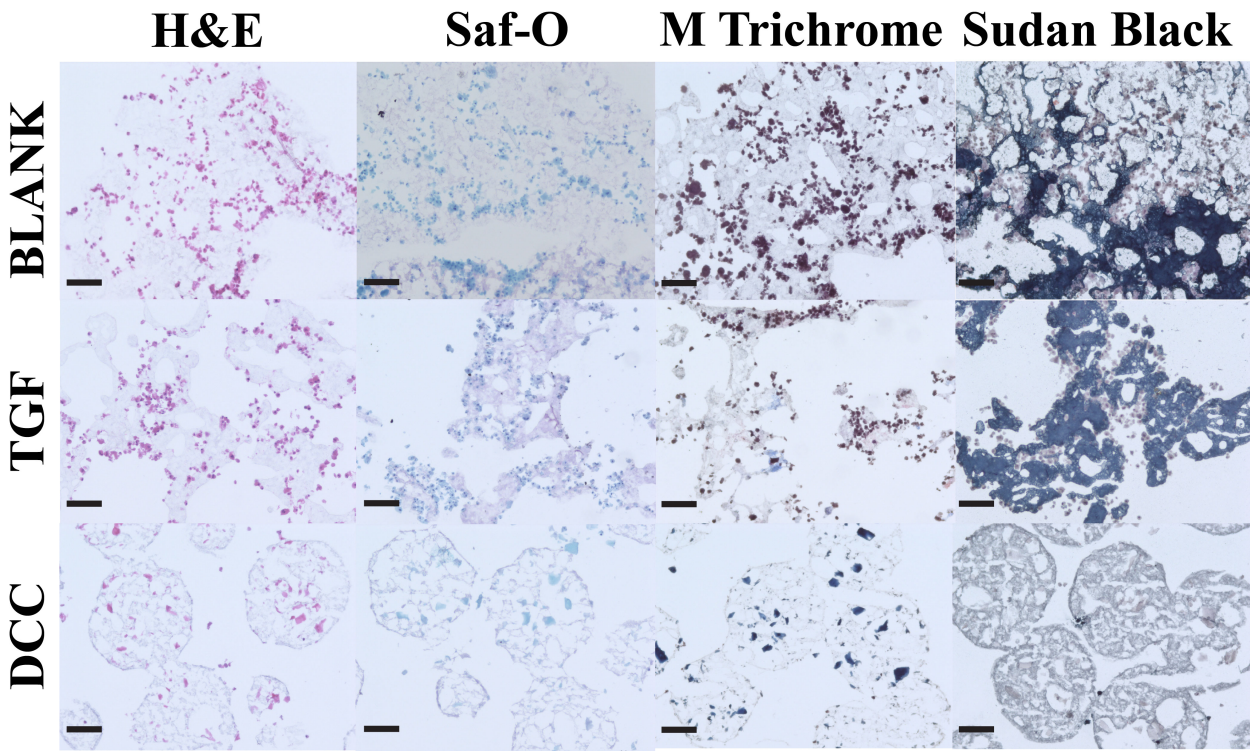

Figure 5.9: Histological staining images of cell-seeded microsphere-based constructs at week 6

BLANK, TGF, and DCC scaffolds were stained for H&E, Safranin-O, Masson's trichrome, and Sudan Black. No images could be obtained from the CS group as the sections washed off the slides during the staining process. The Sudan Black staining intensities for residual polymer were higher in the BLANK and TGF groups compared to the DCC group. Scale bars: 100 μm.

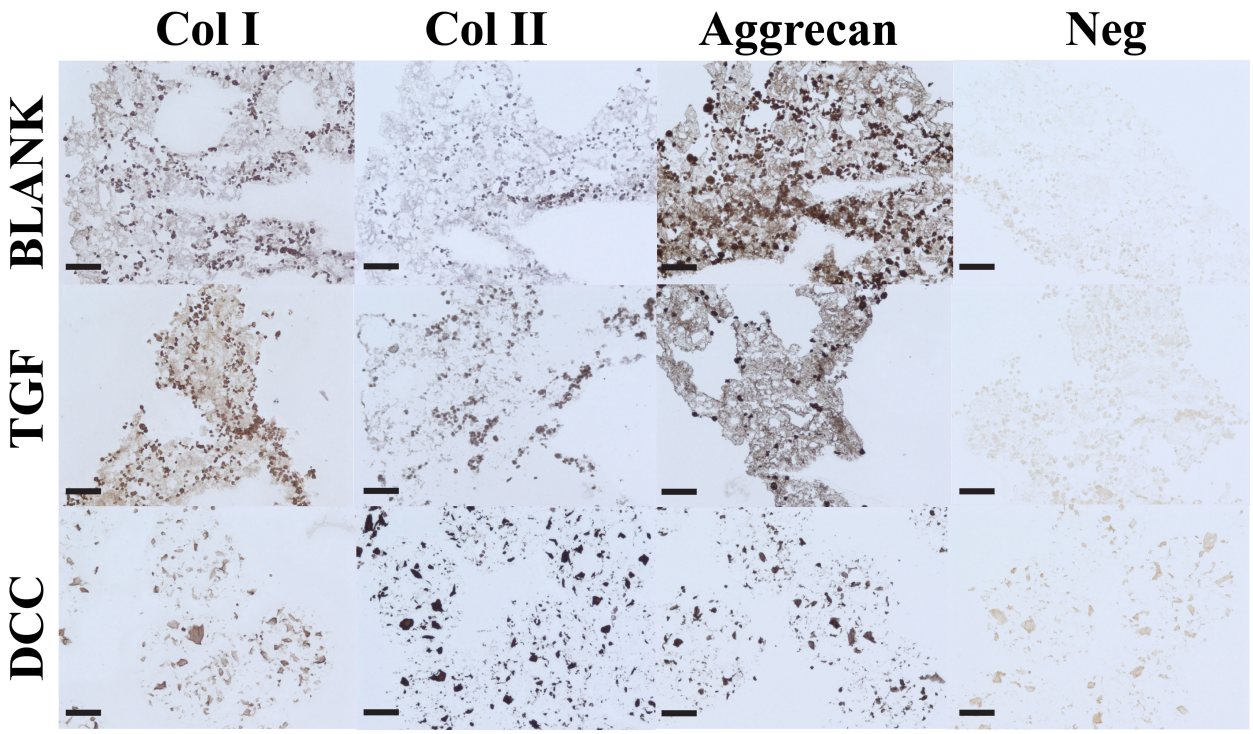

Figure 5.10: Immunohistochemical staining images of microsphere-based constructs at week 6

BLANK, TGF, and DCC were stained for collagen I, collagen II, and aggrecan. No images could be obtained from the CS group as the sections washed off from the slides during the staining process. The BLANK and the TGF group stained more intensely for aggrecan than the DCC group. Images of negative controls (primary antibody omitted) are also shown. Scale bars: 100 μm.

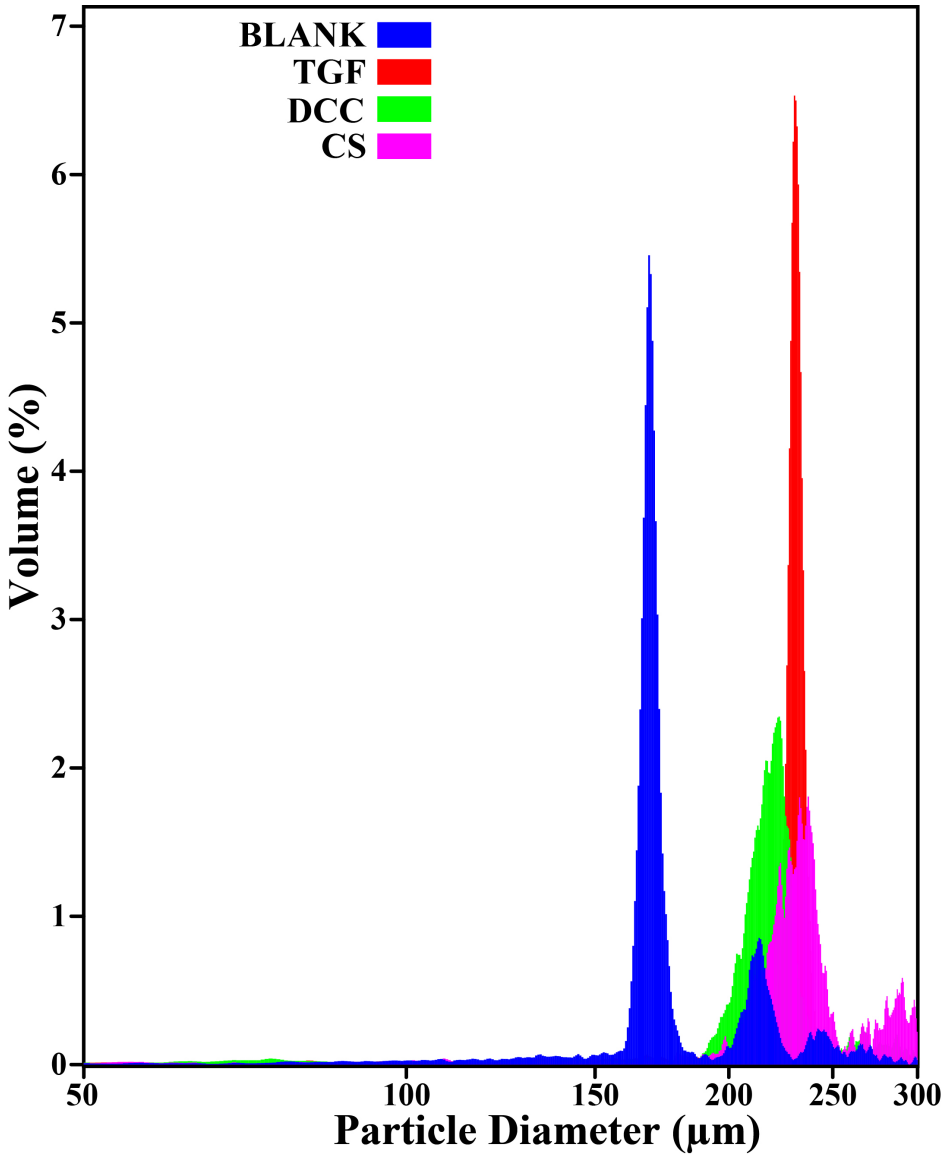

Figure 5.11: Size distribution graph for all four types of microspheres used in the study

All of the microspheres were uniform in size with average microsphere diameter ranging between 160-180 µm.

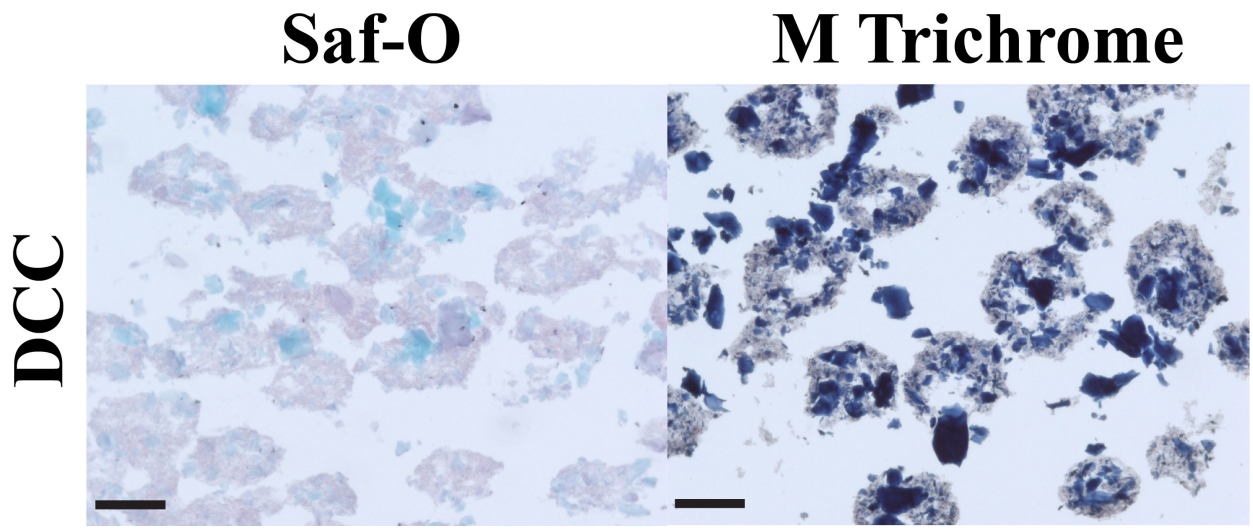

Figure 5.12: Safranin-O (A) and Masson's trichrome (B) staining images for acellular DCC scaffolds at week 6

Scale bar: 100 μm.

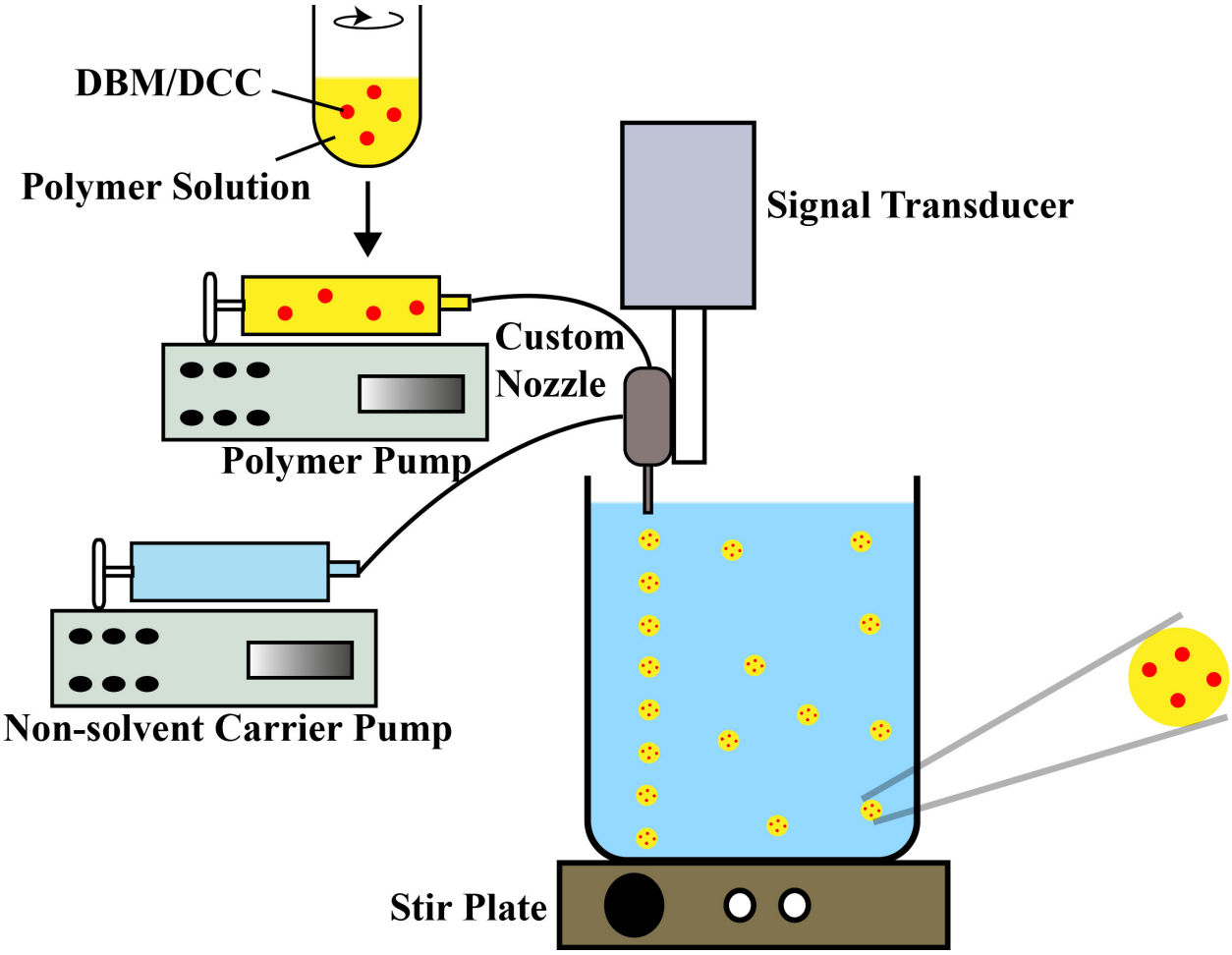

Figure 6.1: A schematic representation of microsphere fabrication process

Demineralized bone matrix (DBM) or decellularized cartilage (DCC) encapsulating poly(D,L-lactic-co-glycolic acid) (PLGA) microspheres were fabricating with a DBM/DCC loading of 10 wt%.

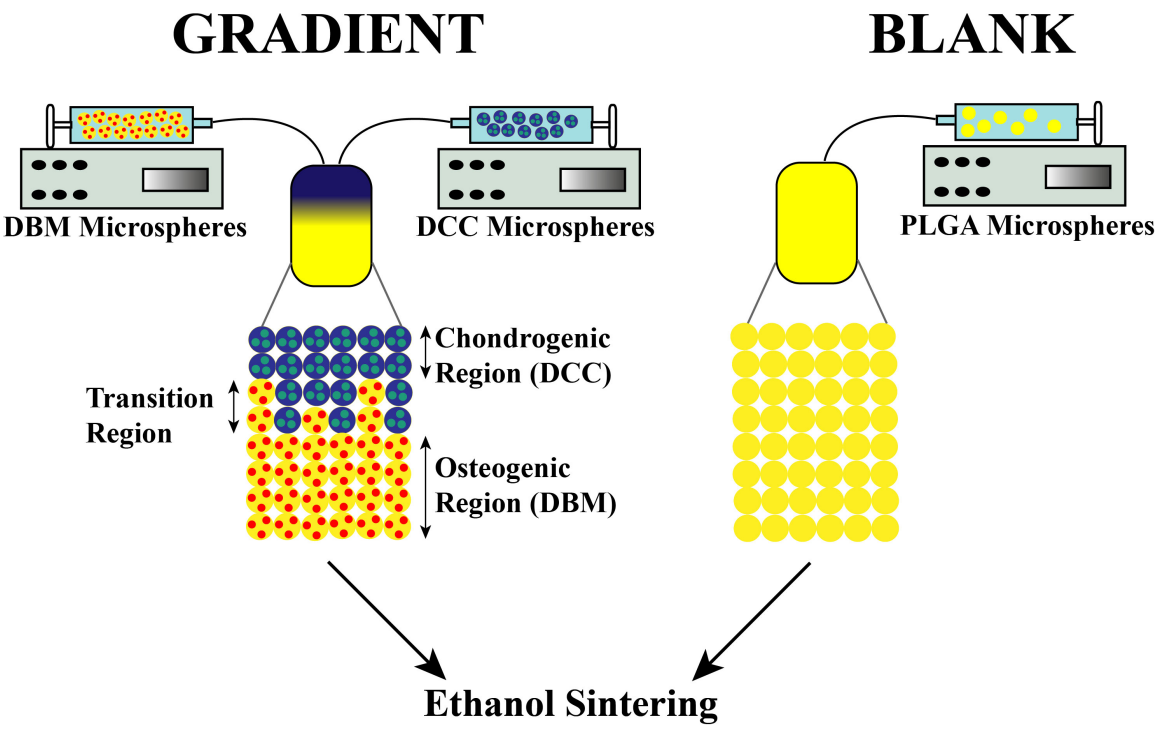

Figure 6.2: A schematic of scaffold fabrication process

Demineralized bone matrix (DBM) or decellularized cartilage (DCC) encapsulating poly(D,L-lactic-co-glycolic acid) (PLGA) microspheres were assembled to form continuously graded scaffolds containing opposing gradients of DCC and DBM.

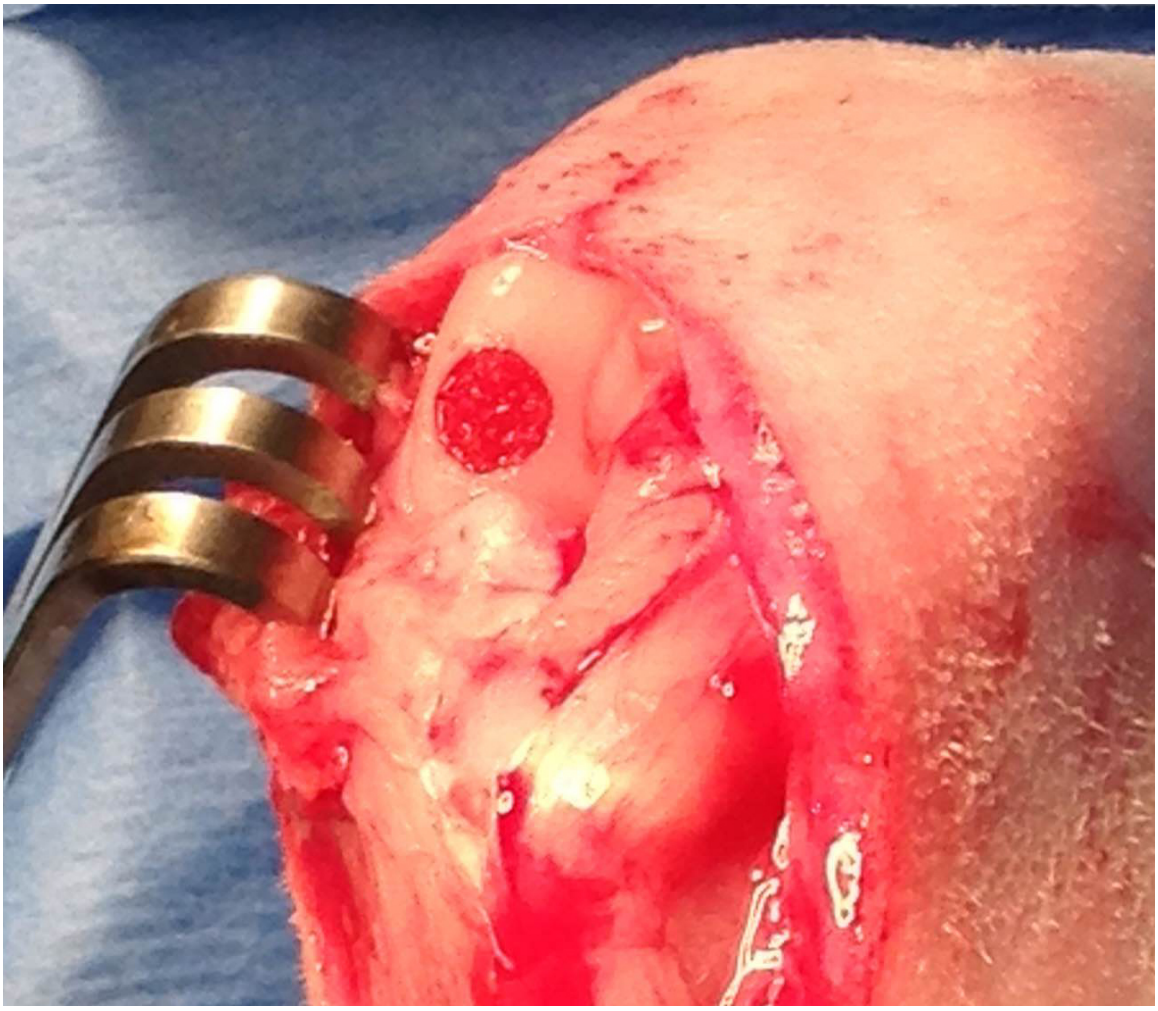

Figure 6.3: Implant placed in a defect in the medial femoral condyle (photo shows right knee)

Immediately after being placed into the defect, the implant was infiltrated by marrow.

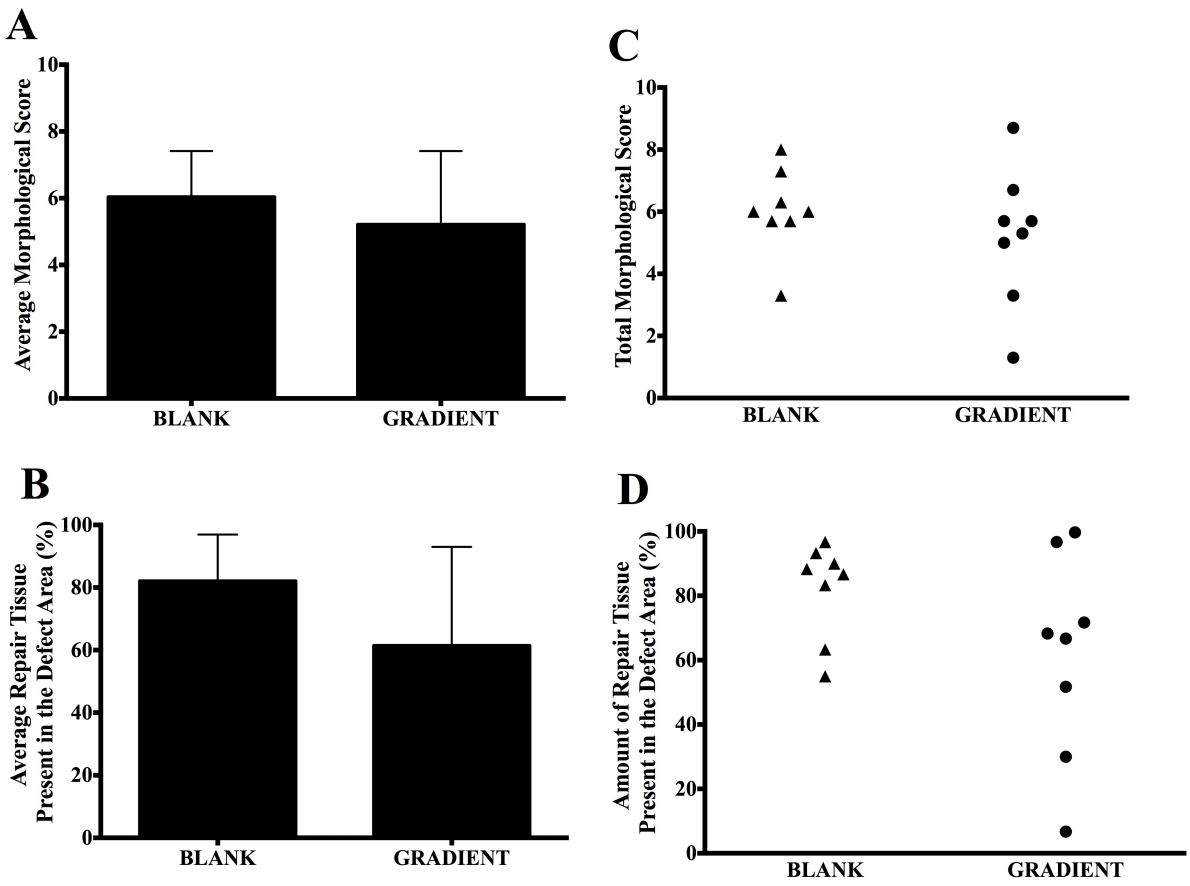

Figure 6.4: Gross morphological scores of retrieved joints 12 weeks post-implantation

(A) The average morphological score in the BLANK and GRADIENT groups, (B) the average percentage of repair tissue present at the defect site in the BLANK and GRADIENT groups, (C) the scatter plot showing total morphological score distribution in the BLANK and GRADIENT groups, and (D) the scatter plot showing amount of repair tissue present in the defect site in the PLGA and GRADIENT groups. All values are expressed as the average + standard deviation (n = 8). The maximum possible score was 10. No significant differences in gross morphological scores and amount of repair tissue present were observed between the two groups. The average morphological score in the BLANK group was 6.0 ± 0.5 with a highest score of 8.0, while the GRADIENT group average morphological score was 5.2 ± 0.8 with a highest score being 8.7 in the group.

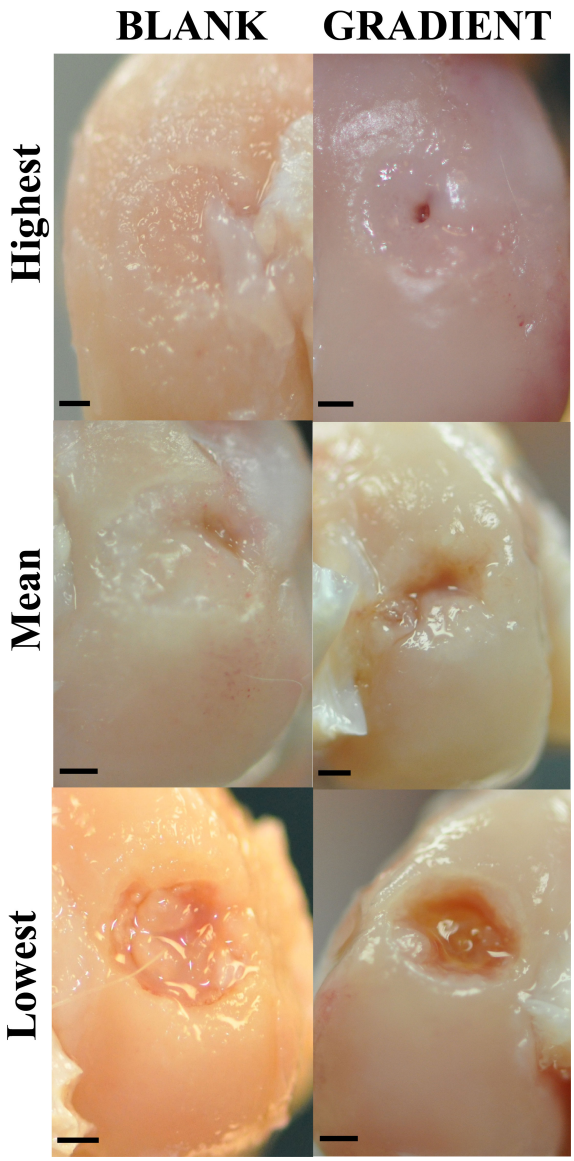

Figure 6.5: Representative images for gross morphology of the BLANK and GRADIENT groups at 12 weeks post-implantation

The top row represents images from the implants that received the highest morphological score (BLANK – 8, GRADIENT – 8.7). The middle row represents images from the implants that received the mean morphological score (BLANK – 6, GRADIENT – 5.2). The bottom row represents images from the implants that received the lowest morphological score (BLANK – 3.3, GRADIENT – 1.3). The BLANK group performed better in percent defect fill while the GRADIENT group performed better in edge integration with the native tissue. Scale bars: 1 mm.

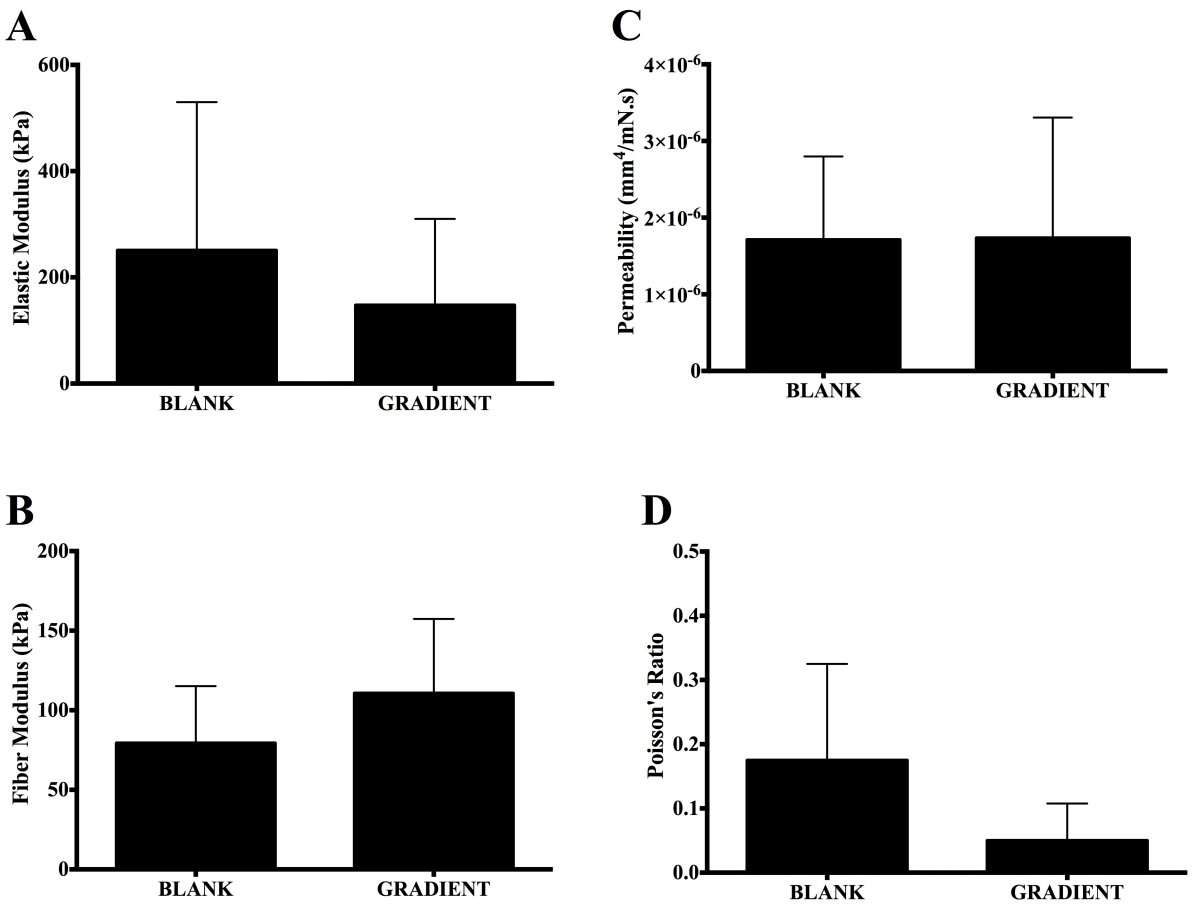

Figure 6.6: Mechanical testing results of repair tissue in the retrieved joints from the BLANK and GRADIENT groups at 12 weeks post-implantation

(A) Elastic modulus, (B) Fiber modulus, (C) Permeability, and (D) Poisson's ratio. All values are expressed as the average + standard deviation (n = 4). No significant differences in any of the four model parameter values were observed between the two groups. The Poisson's ratio for the BLANK group was 0.18 ± 0.08 and the GRADIENT group Poisson's ratio was 0.05 ± 0.03.

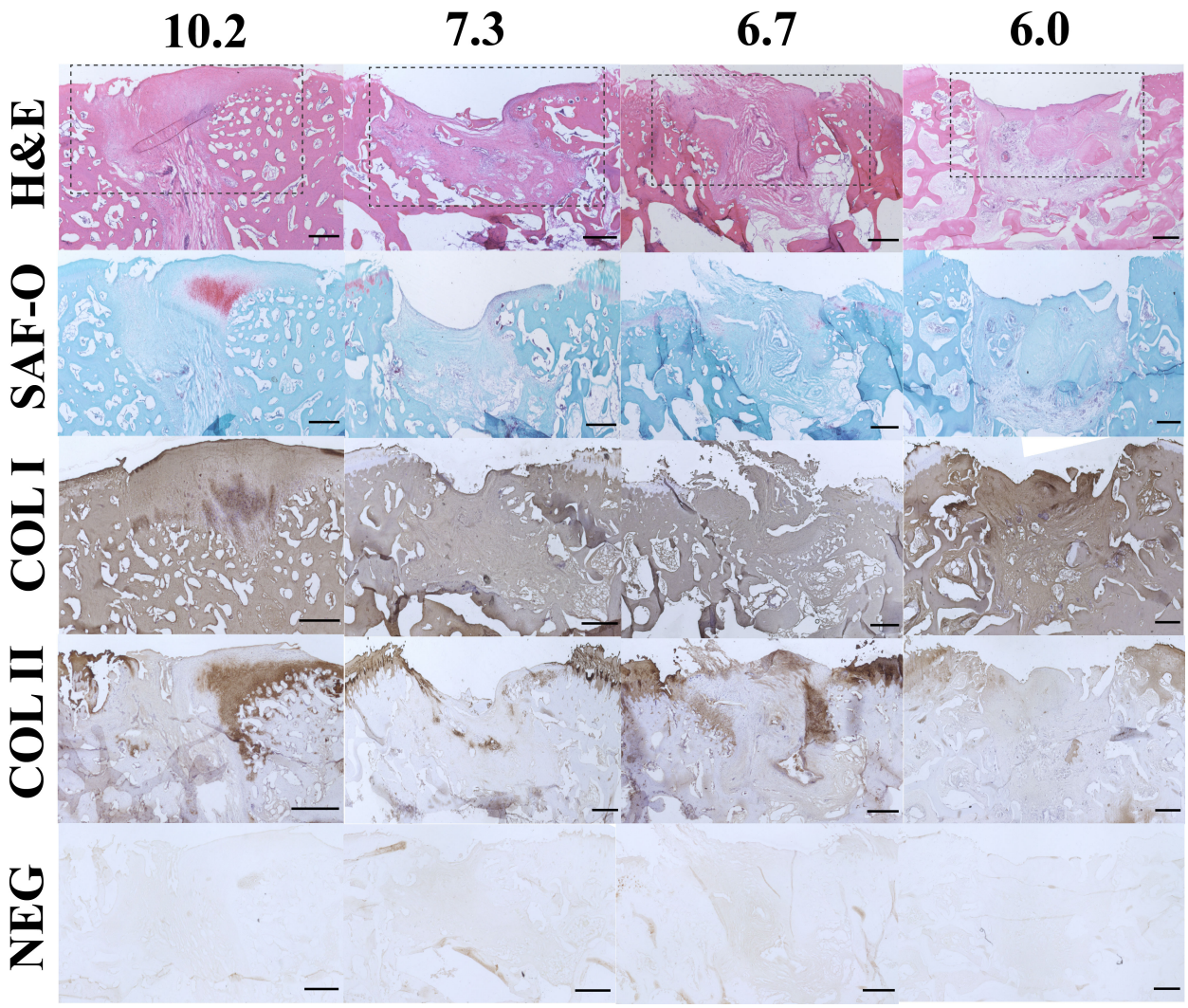

Figure 6.7: Histological and immunohistochemical (IHC) staining images for the BLANK implant along with their histological scores on top

First column represents images from the implant that received the highest histological score (10.2); second column represents images from the implant that received the second highest histological score (7.3); third column represents images from the implant that received the third highest histological score (6.7); and fourth column represents images from the implant that received the lowest score (6.0) in the BLANK group. The sections were stained for hematoxylin and eosin; safranin-O; collagen I; and collagen II. Negative controls for IHC were also run with the primary antibody omitted. The boxes in the top row outline the defect area. The regenerated tissue in the BLANK group was predominantly fibrous in nature with some evidence of cartilage repair and subchondral bone regeneration especially at the edges of the defect site. Scale bars: 500 μm.

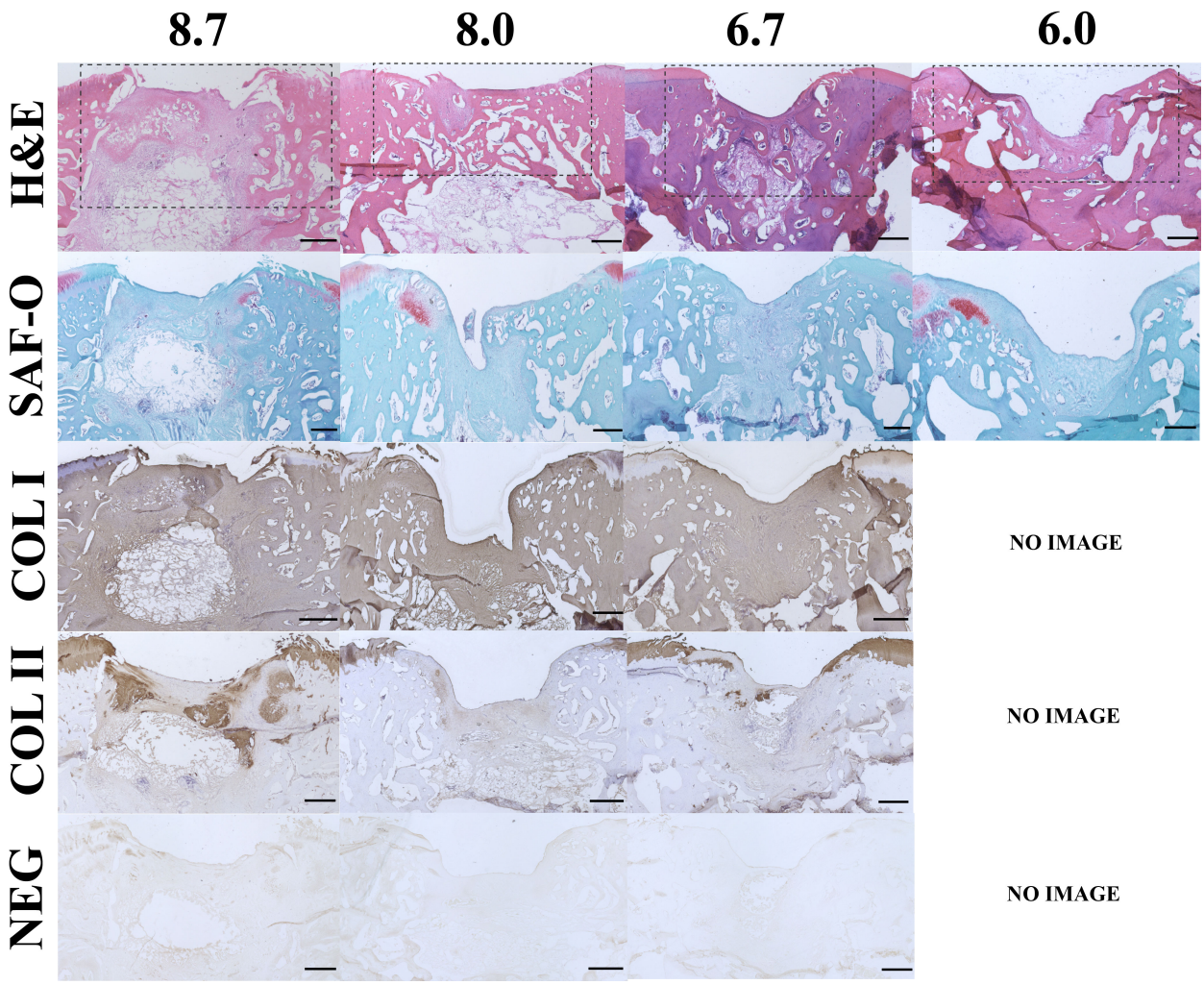

Figure 6.8: Histological and immunohistochemical (IHC) staining images for the GRADIENT implants along with their histological scores on top

First column represents images from the implant that received the highest histological score (8.7); second column represents images from the implant that received the second highest histological score (8.0); third column represents images from the implant that received the third highest histological score (6.7); and fourth column represents images from the implant that received the lowest score (6.0) in the GRADIENT group. The sections were stained for hematoxylin and eosin; safranin-O; collagen I; and collagen II. Negative controls for IHC were also run with the primary antibody omitted. The boxes in the top row outline the defect area. The repair tissue was predominantly fibrous in nature with some evidence of cartilage repair. The subchondral bone region consisted of void areas with minimal bone regeneration. Scale bars: 500 μm.

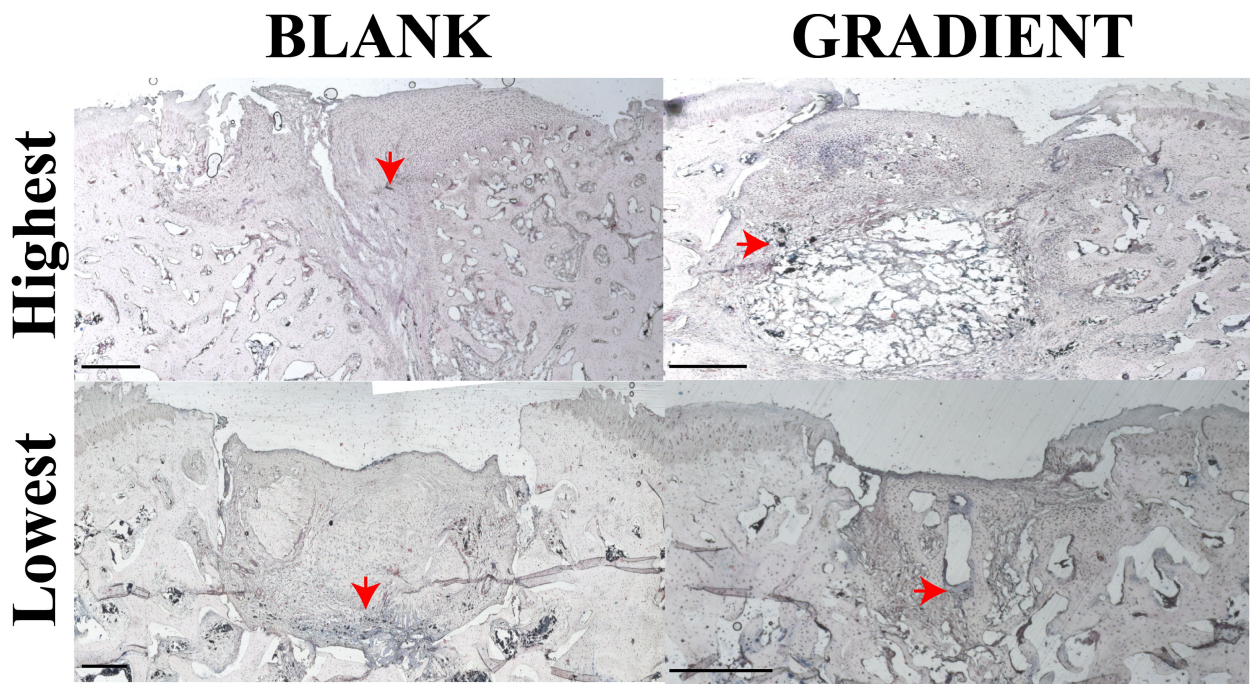

Figure 6.9: Sudan black staining images for the implants that received the highest and lowest histological scores in both the BLANK and GRADIENT groups

The defect sites in both of the groups demonstrated mild staining overall with a few dark-staining spots (arrows). Scale bars: 500 μm.

APPENDIX B: Tables

CHAPTER 1: No Tables

CHAPTER 2: Tables 2.1-2.2

CHAPTER 3: Tables 3.1-3.5

CHAPTER 4: Table 4.1

CHAPTER 5: Table 5.1

CHAPTER 6: Table 6.1-6.3

CHAPTER 7: No Tables

Table 2.1: Notable controlled release applications of microspheres in tissue engineering scaffolds

Reference	Microsphere Material	Encapsulated Factor	Scaffold Matrix	Application
Lee *et al.* [143, 144]	Chitosan	TGF-β_1	Collagen I and chitosan	CTE
Royce *et al.* [198]	PLGA	FGF-1	Fibrin	-
DeFail *et al.* [52]	PLGA	TGF-β_1	PEG	CTE
Wei *et al.* [248]	PLGA	PDGF-BB	PLLA	PTE
Basmanav *et al.* [15]	P_4VN & alginate	BMP-2 & BMP-7	PLGA	BTE
Jaklenec *et al.* [111]	PLGA	IGF-I & TGF-β_1	PLGA	CTE
Kempen *et al.* [129, 130]	PLGA	BMP-2	Gelatin & PPF	BTE
Lee *et al.* [147]	PLGA	bFGF	PCL	Smooth muscle regeneration
Bing *et al.* [148]	PLGA	BMP-2	PUR	BTE
Wang *et al.* [244]	PLGA & silk	BMP-2 & IGF-I	Alginate	OTE
Francis *et al.* [78]	P(3HB)	Gentamycin	Bioglass	BTE
Ju *et al.* [119]	PLGA	Dexamethasone	Collagen I	-
Liu *et al.* [153]	Ethyl cellulose	Ceftazidime	HA/PUR	BTE
Brown *et al.* [31]	PLGA	BMP-2	PUR	BTE
Howard *et al.* [133]	PLGA	Dibutyryl cyclic-AMP	Chitosan	NTE
Lee *et al.* [145, 146]	PLGA	BMP-2	PPF/DEF	BTE
Xufeng *et al.* [182]	Chitosan	BMP-2	nHAC/PLLA	BTE
Rooney *et al.* [197]	PLGA	Dibutyryl cyclic-AMP	OPF	NTE
Son *et al.* [219]	PLGA	Dexamethasone	HA	BTE
De Boer *et al.* [48]	PLGA	NGF & GDNF		NTE
Reyes *et al.* [194]	PLGA	PDGF, TGF-β_1 & VEGF	TCP	BTE
Soran *et al.* [220]	Alginate	BMP-6	Chitosan	PTE
Wang *et al.* [241]	Gelatin	BMP-2 & ALP	Gelatin	BTE
Lupu-Haber *et al.* [159]	PLGA	BMP-2	ZrO_2	BTE
Meng *et al.* [146]	P(3HB)	Tetracycline	Bioglass	BTE
Wang *et al.* [243]	Chitosan	ADM	PLGA	BTE

TGF-β_1, transforming growth factor-beta 1; CTE, cartilage tissue engineering; PLGA, poly(D, L-lactic-co-glycolic acid); FGF-1, fibroblast growth factor-1; PEG, poly(ethylene glycol); PDGF-BB, platelet-derived growth factor-BB; PLLA, poly(L-lactic acid); PTE, periodontal tissue engineering; P_4VN, poly(4-vinyl pyridine); BMP-2, bone morphogenic protein-2; BMP-7, bone morphogenic protein-7; BTE, bone tissue engineering; IGF-I, insulin growth factor-I; PPF, poly(propylene fumarate); bFGF basic fibroblast growth factor; PCL, polycaprolactone; PUR, polyurethane; OTE, osteochondral tissue engineering; P(3HB), poly(3-hydroxybutyrate); HA, hydroxyapatite; NTE, nerve tissue engineering; DEF, diethyl fumarate; nHAC, nanohydroxyapatite/collagen; OPF, oligo [(polyethylene glycol) fumarate]; NGF, nerve growth factor; GDNF, glial cell derived neurotropic factor; VEGF, vascular endothelial growth factor; BMP-6, bone morphogenic protein-6; ALP, alkaline phosphatase; ZrO_2, zirconium oxide; ADM, Adrenomedullin

Table 2.2 Notable applications of microsphere scaffolds (MSs) in tissue engineering

Reference	Microsphere Fabrication Method	Microsphere Material	Scaffold Type	Microsphere Sintering Method	Application	Encapsulated Factor	Cell Type	*In vitro /In vivo*
Borden *et al.* [25, 26]	SESE	PLAGA	Sintered	Heat	BTE	-	Osteoblasts and fibroblasts	*In vitro*
Jang *et al.* [112]	Cryopreparation	PLG	Sintered	Gas foaming	-	DNA		*In vitro*
Kofron *et al.* [137, 138]	SESE	PLAGA	Sintered	Heat	BTE	HA	Osteoblast-like (SaOS-2)	*In vitro*
Mercier *et al.* [166, 167]	ProLease	PLG	Injectable	-	CTE	$Mg(OH)_2$	Chondrocytes	*In vitro and In vivo*
Newman *et al.* [178]	DESE	PLGA	Injectable	-	NTE	RA	Embryonic (P-19)	*In vitro*
Barrias *et al.* [14]	Emulsion microgel fabrication	CTP	Injectable	-	BTE	-	BMSCs	*In vitro*
Kang *et al.* [121, 123-125]	SESE and DESE	PLGA	Injectable	-	CTE, ATE & BTE	-	Chondrocytes, adipocytes and osteoblasts	*In vitro and In vivo*
Kim *et al.* [135]	SESE	PLGA	Injectable	-	STE	-	Keratinocytes and dermal fibroblasts	*In vivo*
Habraken *et al.* [90, 91]	DESE	PLGA	Injectable	-	BTE	CaP	-	*In vitro and In vivo*
Jiang *et al.* [115-117]	SESE	PLAGA	Sintered	Heat	BTE	Chitosan	Osteoblast-like (MC3T3-E1)	*In vitro and In vivo*

Garkhal *et al.* [82]	SESE	PLCL	Injectable	-	-	-	Proximal kidney tubule & myoblasts	*In vitro*
Jabbarzadeh *et al.* [105-108]	SESE	PLAGA	Sintered	Heat	BTE	-	Endothelial cells, ADSCs	*In vitro*
Zhu *et al.* [261-263]	DESE & Emulsion microgel fabrication	PHBV & Gelatin	Injectable	-	LTE & VTE	bFGF & HGF	Hepatocyte-like (Hep3B) & hUCVECs	*In vitro*
Brown *et al.* [29, 30]	SESE	PLAGA & PPhos	Sintered	Solvent/ non-solvent	BTE	-	Preosteoblasts	*In vitro*
Chung *et al.* [42]	Emulsion gas foaming	PLGA	Injectable	-	CTE	-	Chondrocytes	*In vitro*
Cushnie *et al.* [46]	DESE	PLAGA	Sintered	Heat	BTE	HA	-	*In vitro*
Duan *et al.* [69, 70]	SESE	PHBV	Sintered	SLS	BTE	CaP	-	*In vitro*
Jaklenec *et al.* [109]	DESE	PLGA	Sintered	Solvent vapor	CTE	IGF-I & TGF-β_1	-	*In vitro*
Luciani *et al.* [158]	DESE	PCL	Sintered	Heat	-	BSA	-	*In vitro*
Nukavarapu *et al.* [184]	SESE	PPhos	Sintered	Solvent/ non-solvent	BTE	HA	Osteoblast	*In vitro*
Park *et al.* [187]	SESE	PLGA	Injectable	-	CTE	-	BMSCs	*In vitro*
Thorrez *et al.* [233]	DESE	PLG	Sintered	Gas foaming	MTE	-	Myoblasts	*In vitro and In vivo*
Valmikinathan *et al.* [239]	SESE	PLGA	Sintered	Heat	NTE	-	Schwann cells	*In vitro*
Zhou *et al.* [260]	SESE	PLLA	Sintered	SLS	BTE	HA	-	*In vitro*
Chesnutt *et al.* [39]	Emulsion microgel	Chitosan	Injectable	-	BTE	CaP	HEPM	*In vitro*

	fabrication							
Hong *et al.* [94]	SESE	PCL	Injectable	-	BTE	-	BMSCs	*In vitro*
Lv *et al.* [160]	SESE	PLAGA	Sintered	Heat	BTE	HA	BMSCs	*In vitro*
Nojedehian *et al.* [183]	DESE	PLGA	Injectable	-	NTE	RA	Embryonic	*In vitro*
Aronin *et al.* [190]	SESE & DESE	PLAGA	Sintered	Heat	BTE	-	-	*In vivo*
Dormer *et al.* [59, 60, 62, 64, 66]	PPF	PLGA	Sintered	Poor solvent	BTE & OTE	TGF-β_1, BMP-2, HA & TGF-β_3	BMSCs & UCMSCs	*In vitro and In vivo*
Liang *et al.* [151]	SESE	PLGA	Sintered	Heat	BTE	-	-	*In vivo*
Mittal *et al.* [168]	Emulsion gas foaming	PLGA	Injectable	-	-	-	Osteoblast-like (MG-63)	*In vitro*
Shi *et al.* [208]	SESE & DESE	PLGA	Sintered	Poor solvent	BTE	Dex, AA & GP	BMSCs	*In vitro*
Shin *et al.* [210]	SESE	PCL	Injectable	-	BTE	HA	BMSCs	*In vitro*
Singh *et al.* [213, 216]	PPF	PLGA	Sintered	Poor solvent & subcritical CO_2	ITE & CTE	$CaCO_3$ & TiO_2	UCMSCs	*In vitro*
Wang *et al.* [242]	SESE	PLGA	Sintered	Heat	BTE	-	Osteoblasts	*In vitro*
Wang *et al.* [246]	SESE	PLGA	Sintered	Heat	BTE	TiO_2	Osteoblasts	*In vitro*
Kumbar *et al.* [140]	SESE	CA, EC & PLAGA	Sintered	Solvent/non-solvent	BTE	-	Osteoblasts	*In vitro*
Mohan *et al.* [169, 171]	PPF	PLGA	Sintered	Poor solvent	OTE	TGF-β_1, BMP-2, HA, TGF-β_3, CS & BG	BMSCs	*In vitro and In vivo*

Watanabe *et al.* [247]	Emulsion microgel fabrication	Gelatin	Injectable	-	NTE	-	Fibroblasts	*In vitro and In vivo*
Amini *et al.* [4]	SESE	PLGA	Sintered	Heat	BTE	-	Osteoblasts	*In vitro*
Decaris *et al.* [51]	DESE	PLG	Sintered	Gas foaming	BTE	-	BMSCs	*In vitro*
Huang *et al.* [100]	Emulsion microgel fabrication	Gelatin	Injectable	-	STE	EGF	BMSCs	*In vivo*
Lakhkar *et al.* [142]	Flame spheroidization	TPG	Injectable	-	BTE	-	Osteoblast-like (MG-63)	*In vitro*
Liang *et al.* [149, 150]	DESE	PLGA	Injectable	-	CTE	Dex & bFGF	BMSCs	*In vitro*
Smith *et al.* [217]	Emulsion microgel fabrication	PEG	Injectable	-	CrTE	-	Cardiomyocytes	*In vitro*
Yu *et al.* [257]	Emulsion gas foaming	PLGA	Injectable	-	BTE	-	BMSCs	*In vivo*
Bhamidipati *et al.* [19]	PPF	PLGA & PCL	Sintered	Subcritical CO_2	BTE	-	BMSCs	*In vitro*
Chou *et al.* [41]	Emulsion gas foaming	PLGA	Injectable	-	LTE	-	Hepatocytes, HUVECs & BMSCs	*In vitro*
Clark *et al.* [44]	DESE	PLGA	Sintered	Heat	-	-	-	*In vitro*
Das *et al.* [47]	SESE	PLAGA	Sintered	Heat	BTE	FTY720	-	*In vitro and In vivo*
Ghanbar *et al.* [86]	TIPS	PLGA & PCL	Injectable	-	-	-	-	*In vitro*
Jeon *et al.* [114]	PPF	PLGA	Sintered	Subcritical CO_2	-	-	hUCMSCs	*In vitro*
Nguyen *et al.* [179]	Emulsion microgel	Chitosan	Sintered	Solvent	BTE	CaP	Osteoblast-like	*In vitro*

	fabrication						(Saos-2)	
Hu *et al.* [99]	SESE	PLGA	Injectable	-	BTE	HA	Osteoblast-like (OCT-1)	*In vitro*
Jin *et al.* [118]	SESE	PCL & PLDLA	Injectable	-	BTE	-	Preosteoblasts (MC3T3-E1)	*In vitro and In vivo*
Tahriri *et al.* [228]	SESE	PLGA	Sintered	Heat	BTE	FHA	Fibroblasts	*In vitro*
Xu *et al.* [255]	SESE	PLGA	Sintered	Heat	BTE	HMS	BMSCs	*In vitro*

SESE, single emulsion solvent evaporation; PLAGA, poly(lactide-co-glycolide); BTE, bone tissue engineering; PLG, poly(D,L-lactide-*co*-glycolide); HA, hydroxyapatite; CTE, cartilage tissue engineering; DESE, double emulsion solvent evaporation; PLGA, poly(D,L-lactic-*co*-glycolic acid); NTE, neural tissue engineering; RA, retinoic acid; CTP, calcium titanium phosphate; BMSCs, bone marrow stromal cells; ATE, adipose tissue engineering; STE, skin tissue engineering; CaP, calcium phosphate; PLCL, poly(L-lactide-co-e-caprolactone); PHBV, poly(3-hydroxybutyrate- co-3-hydroxyvalerate); LTE, liver tissue engineering; VTE, vascular tissue engineering; bFGF, basic fibroblast growth factor; HGF, hepatocyte growth factor; hUCVECs, human umbilical coed vein endothelial cells; PPhos, polyphosphazenes; IGF-I, insulin growth factor-I; TGF-β_1, transforming growth factor-beta 1; PCL, poly(ε-caprolactone); BSA, bovine serum albumin; MTE, muscle tissue engineering; PLLA, poly(L-lactide); HEPM, human embryonic palatal mesenchymal cells; PPF, precision particle fabrication; OTE, osteochondral tissue engineering; BMP-2, bone morphogenic protein; TGF-β_3, transforming growth factor-beta 3; UCMSCs, umbilical cord mesenchymal stromal cells; Dex, dexamethasone; AA, ascorbic acid; GP, β-glycerophosphate; ITE, interfacial tissue engineering; $CaCO_3$, calcium carbonate; TiO_2, titanium dioxide; CA, cellulose acetate; EC, ethyl cellulose; CS, chondroitin sulphate; BG, bioactive glass; EGF, epidermal growth factor; TPG, titanium

Table 3.1: GAG content measured over time in acellular scaffolds from the CS and GRADIENT groups

Group	GAG (µg/scaffold)		
	Week 0	**Week 3**	**Week 6**
CS	17.4 ± 9.4	15.9 ± 5.0	16.5 ± 3.8
GRADIENT	18.4 ± 23.9	9.3 ± 11.3	4.4 ± 2.5

All values are expressed as the average ± standard deviation (n = 3).

Table 3.2: Calcium content measured over time in acellular scaffolds from the TCP and GRADIENT groups

Group	Calcium (µg/scaffold)		
	Week 0	Week 3	Week 6
TCP	13.8 ± 19.3	3.3 ± 0.9	2.7 ± 2.5
GRADIENT	7.7 ± 3.7	6.9 ± 1.3	17.7 ± 6.5

All values are expressed as the average ± standard deviation (n = 3).

Table 3.3: Genes used for RT-qPCR analysis

Gene	Symbol	TaqMan Assay ID
Glyceraldehyde 3-phosphate dehydrogenase	GAPDH	Rn01775763_g1
SRY (sex determining region Y)-box 9	SOX9	Rn01751069_mH
Collagen type II	COL2A1	Rn01751069_mH
Aggrecan	ACAN	Rn00573424_m1
Collagen type I	COL1A1	Rn01463848_m1
Runt-related transcription factor 2	RUNX2	Rn01512298_m1
Bone gamma-carboxyglutamate protein	BGLAP	Rn00566386_g1
Secreted phosphoprotein 1	SPP1	Rn01449972_m1
Integrin-binding sialoprotein	IBSP	Rn00561414_m1

Table 3.4: Average porosities of different scaffold groups

Group	Average Porosity (%)
PLGA	21.0 ± 6.8
CS	49.6 ± 4.4*
TCP	21.6 ± 6.8
GRADIENT	18.4 ± 4.6

*significantly higher than the other three groups ($p < 0.05$)

Table 3.5: The dimensions of the constructs used for mechanical testing

Group	Week 0 (Acellular)		Week 6 (Cellular)	
	Diameter (mm)	Height (mm)	Diameter (mm)	Height (mm)
PLGA	4 ± 0	6.5 ± 0.7	4 ± 0	6.8 ± 0.3
CS	3.9 ± 0.1$^{\$}$	6.3 ± 0.9	5.7 ± 0.1$^{*\$}$	10 ± 1$^{*\$}$
TCP	4.1 ± 0.2	6.4 ± 0.2	3.8 ± 0.1*	6.3 ± 1.0
GRADIENT	4.1 ± 0.2	6.8 ± 0.2	4.4 ± 0.2$^{*\$}$	7.6 ± 0.5

All values are expressed as the average ± standard deviation (n = 3-5). *significant difference from its Week 0 value and $significant difference from PLGA group at that time point ($p < 0.05$).

Table 4.1: Genes used for RT-qPCR analysis

Gene	Symbol	TaqMan Assay ID
Glyceraldehyde 3-phosphate dehydrogenase	GAPDH	Rn01775763_g1
Collagen type I	COL1A1	Rn01463848_m1
Runt-related transcription factor 2	RUNX2	Rn01512298_m1
Bone gamma-carboxyglutamate protein	BGLAP	Rn00566386_g1
Integrin-binding sialoprotein	IBSP	Rn00561414_m1

Table 5.1: Genes used for RT-qPCR analysis

Gene	Symbol	TaqMan Assay ID
Glyceraldehyde 3-phosphate dehydrogenase	GAPDH	Rn01775763_g1
Collagen type I	COL1A1	Rn01463848_m1
Collagen type II	COL2A1	Rn01751069_mH
Collagen type X	COL10A1	Rn01408029_g1
Aggrecan	ACAN	Rn00573424_m1
SRY (sex determining region Y)-box 9	SOX-9	Rn01751069_mH
Runt-related transcription factor 2	RUNX2	Rn01512298_m1
Integrin-binding sialoprotein	IBSP	Rn00561414_m1

Table 6.1: List of implant received by each animal and the type of analysis performed for the implants

Animal ID	Left Knee	Right Knee	Time	Analysis
Rabbit 1	PLGA	GRADIENT	12 weeks	Morphology & Histology
Rabbit 2	PLGA	GRADIENT	12 weeks	Morphology & Histology
Rabbit 3	PLGA	GRADIENT	12 weeks	Morphology & Mechanical
Rabbit 4[a]	PLGA	GRADIENT	12 weeks	Euthanized prematurely
Rabbit 5	PLGA	GRADIENT	12 weeks	Morphology & Mechanical
Rabbit 6	GRADIENT	PLGA	12 weeks	Morphology & Histology
Rabbit 7	GRADIENT	PLGA	12 weeks	Morphology & Histology
Rabbit 8	GRADIENT	PLGA	12 weeks	Morphology & Mechanical
Rabbit 9	GRADIENT	PLGA	12 weeks	Morphology & Mechanical
Rabbit 10[b]	GRADIENT	PLGA	12 weeks	Euthanized prematurely

[a] Euthanized prematurely because of chronic lameness

[b] Euthanized prematurely because of causes unrelated to the implant

Table 6.2: Morphology scoring parameters for the regenerated tissue and associated numeric score

Repair tissue or implant present at the defect site	• Full – 2 • Partial – 1 • None – 0
Edge integration (new tissue relative to native cartilage)	• Full – 2 • Partial – 1 • None – 0
Smoothness of repair surface	• Smooth – 2 • Intermediate – 1 • Rough/Missing – 0
Cartilage surface degree of filling	• Flush – 2 • Slight depression – 1 Depressed/Overgrown – 0
Color of cartilage (opacity /translucency of repair tissue)	• Translucent – 2 • Opaque – 1 • Missing – 0
Amount of repair tissue relative to total area of defect	Estimated percentage present in defect

Table 6.3: Histology scoring parameters and associated numerical score

Cellular morphology	• Hyaline Cartilage – 4 • Mostly hyaline cartilage – 3 • Mixed hyaline and fibrocartilage – 2 • Mostly fibrocartilage – 1 • Some fibrocartilage and mostly nonchondrocytic cells – 0
Safranin-O staining	• Normal or nearly normal – 3 • Moderate – 2 • Slight – 1 • None – 0
Structural characteristics	• Normal – 2 • Slight disruption, including cysts – 1 • Severe disintegration, disruptions – 0
Thickness	• Similar to surrounding cartilage – 3 • Greater than surrounding cartilage – 2 • Less than surrounding cartilage – 1 • No cartilage – 0
Bonding	• Bonded at both ends of graft – 2 • Bonded at one end or partially at both ends – 1 • Not bonded – 0
Reconstruction of subchondral bone	• Normal or reduced subchondral bone reconstruction – 2 • Minimal subchondral bone reconstruction – 1 • No subchondral bone reconstruction – 0
Degenerative changes: graft	• Normal cellularity – 2

	• Slight hypocellularity -1 • Moderate hypocellularity or hypercellularity 0
Chondrocyte clustering	• No clusters – 2 • < 25% of the cells 1 • 25-100% of the cells – 0
Degenerative changes: adjacent cartilage	• Normal cellularity, no clusters, normal staining – 3 • Normal cellularity, mild clusters, moderate staining – 2 • Mild/moderate cellularity, moderate clusters, moderate hypocellularity, slight staining – 1 • Severe hypocellularity and degeneration, poor or no staining – 0
Strucutral integrity of regenerated cartilage	• Normal – 2 • Slight disruption, including cysts – 1 • Severe disintegration disruptions – 0
Inflammatory response in subchondral bone	• None/mild – 2 • Moderate – 1 • Severe – 0
Maximum possible score – 28	